Toward Canonical General Relativity in the Loop Gravity Phase Space

by

Jonathan Ziprick

A thesis
presented to the University of Waterloo
in fulfilment of the
thesis requirement for the degree of
Doctor of Philosophy
in
Physics

Waterloo, Ontario, Canada, 2013

Author's declaration

I hereby declare that I am the sole author of this thesis. This is a true copy of the thesis, including any required final revisions, as accepted by my examiners.

I understand that my thesis may be made electronically available to the public.

Abstract

The continuous, kinematical Hilbert space of loop quantum gravity is built upon a family of spaces $\mathcal{H}_\Gamma$, each associated to a different *graph* Γ, i.e. a network of interconnected one-dimensional links ℓ, embedded within a spatial geometry. The kinematics of loop quantum gravity are well-established, but difficult problems remain for the dynamics. There are two steps in getting to the quantum theory from the classical one: first, the embedded graphs are used to define a smearing of the continuous gravitational fields to obtain a holonomy h_ℓ and flux $\boldsymbol{X}_\ell$ for each link of the graph, giving a phase space P_Γ; second, this phase space is quantized to yield a finite dimensional Hilbert space $\mathcal{H}_\Gamma$. The intermediate classical theory in terms of P_Γ phase spaces remains largely unexplored, and here we endeavour to develop it. If we can find such a theory that is consistent with general relativity, then we will have a theory of gravity based upon finite-dimensional phase spaces that is nicely set up for quantization à la loop quantum gravity.

To begin, we first review the basic elements of the quantum theory before introducing the classical phase space structure. Within this framework we show that there is a one-to-one correspondence between the data on a graph and an equivalence class of continuous geometries. We find that a particular member of each class, the spinning geometry, makes a promising candidate as a gauge choice to represent the $(h_\ell, \boldsymbol{X}_\ell)$ data in the continuous theory, helping us to formulate a dynamics for the discrete theory. Considering all of the possible graphs, it is important to know how we can evolve from one phase space into another, and how the dynamics in P_Γ relates to the continuous evolution. There is a geometrical description of phase spaces where dynamics appears as a class of subspaces within a symplectic manifold. We use this picture to formulate a dynamics between P_Γ phase spaces, and demonstrate this process on a simple model that mimics the case of full gravity. Following this, we study a system of point particles in three-dimensional gravity which provides an illuminating demonstration of what we hope to accomplish for full gravity. We develop the classical theory of point particles and show that it can be described by an evolving triangulation where discrete bistellar flips can occur. From here we define the loop gravity theory and show that it agrees with the continuous theory, having two-to-two moves on the graph which mirror the bistellar flips in the triangulation. The results are promising for finding a dynamics for four-dimensional loop gravity, and if the full theory is developed further, we expect it will lead to a breakthrough in the quantum dynamics.

Acknowledgments

First and foremost I want to thank my advisors, Laurent Freidel and Lee Smolin, for teaching me about loop gravity and guiding my research. I have great respect for their visions of quantum gravity and it has been a pleasure to learn directly from them. I also thank my professor, Achim Kempf, for his professionalism and for being generous with his time outside of class. It has been a privilege to be a resident at the Perimeter institute and there have been many visitors and post-docs that I have interacted with during my time here. In particular I want to thank Seth Major, Leanardo Modesto, Eugenio Bianchi, Valentin Bonzom, Joseph Ben Geloun and Hal Haggard for providing answers to the various questions I have come to them with. And finally, I am grateful to my MSc advisor, Gabor Kunstatter, for continuing to take an interest in my well-being and for ongoing discussions about my current research.

Contents

List of Figures

List of Tables

Chapter 1

Introduction

In the last hundred years our understanding of nature has been radically altered by two revolutionary theories: general relativity and quantum mechanics. But this has been "the century of the incomplete revolution" [1] since we are yet unable to merge these ideas into a quantum theory of gravity. This is the challenge that physics in the twenty first century must face. The most direct methods have already been tried, so we must be creative in developing new approaches to this problem.

On the one hand we have general relativity, a purely classical description of gravity in terms of pseudo-Riemannian spacetime geometries. This theory has proven to be accurate at all macroscopic scales that are larger than a few millimeters. On the other hand we have quantum mechanics, describing the peculiar rules for interactions at microscopic scales. For gravity, one expects these quantum effects to become relevant only near the Planck scale $l_{\rm Pl} = 10^{-35}$m. Since one theory applies at large scales and the other at small scales, one of these can be safely ignored for most physical calculations, i.e. we can do classical calculations in curved spacetime and quantum calculations in flat spacetime. However, this is rather unsatisfactory if we are to have a unified understanding of the physical universe, and there are phenomena which we simply cannot describe without a quantum theory of gravity.

1.1 The need for quantum gravity

We do have some understanding of the interplay between gravity and quantum mechanics, and have developed certain semiclassical approximations to use for quantum field theory on curved space. For instance, we rely upon these methods to understand how the cosmic microwave background that we observe today results from quantum fluctuations of spacetime in the early universe. There are however situations where these methods do not suffice, and a full quantum theory of gravity is required [2, 3]:

> **Singularities:** Measurements of Hubble expansion and the cosmic microwave background support an inflationary cosmology, which implies the existence of an initial cosmological singularity [4]. Singularities have also been shown to form inside black holes, at least according to the classical rules of general relativity, under very general conditions [5].

These divergences represent an inadequacy of the classical theory for dealing with very large curvature. A quantum theory is required to describe these scenarios, which is expected to preclude such divergences by introducing a natural cut-off at small scales near the Planck length.

Hawking radiation: Black holes are known to lose mass through Hawking radiation [6]. The semiclassical derivation of this process breaks down for microscopic black holes, leaving the end state of evaporation unknown and bringing forth the information loss problem [7]. From the exterior of a black hole, one can only measure the mass, angular momentum and charge while all other knowledge about what went into the hole is veiled behind the event horizon. Hawking radiation is not believed to carry out information, so if a black hole evaporates by this process, where does the information go, and what is left behind?

Black hole entropy: The proportional relationship between black hole entropy and event horizon area was developed by Bekenstein [8] and Hawking [9]. Calculations based on this formulation give rise to enormous values for entropy, which is odd since high levels of entropy are usually associated with complex systems. Since black holes are relatively simple[1] objects, this suggests hidden degrees of freedom that might be explained by quantum mechanical effects.

Cosmological constant problem: If we naively choose an ultraviolet momentum cut-off of $1/l_{\mathrm{Pl}}$ resulting from quantum gravitational effects, we find the cosmological constant to differ from the experimental value by an embarrassing 120 orders of magnitude. This is quite probably the worst prediction in all of theoretical physics, and a quantum theory of gravity is expected to shed some light on this problem.

Unified field theory: Quantum theories have been developed for all non-gravitational interactions. If the four fundamental interactions are unified in the early universe, then it seems that gravity must behave according to quantum mechanics as well.

Inconsistency of semiclassical theories: Gravity is known to interact with all forms of energy via the Einstein equation:

$$R_{\mu\nu} - \frac{1}{2} R g_{\mu\nu} = 8\pi G T_{\mu\nu} \ .$$

Since the right hand side is fundamentally quantum mechanical, $T_{\mu\nu}$ can be taken as a quantum operator. However, trying to keep the right hand side of this equation classical by taking the expectation value of the stress-energy tensor is only useful for approximate solutions, and does not lead to a consistent full theory of quantum fields in curved spactime. It seems the only viable option is to treat spacetime geometry on the quantum mechanical level as well.

[1] The no-hair theorem conjectures that all black holes are characterized by only three properties: mass, electric charge and angular momentum.

These scenarios are at the fringes of known physics and may have little consequence for practical matters, but the philosophical tension these questions raise is of utmost importance. Without quantum gravity, physics is divided into two separate worlds, the big and the small. There will remain a fundamental flaw in our understanding of nature until we are able to bring these worlds together and find a quantum theory of gravity, the missing keystone that would interlock the disparate theories of general relativity and quantum mechanics. At the heart of this problem lie questions about the very nature of space, time and the creation of the universe. To learn about quantum gravity is to learn about some of the biggest philosophical questions that we face regarding our very existence.

Although many exceptionally talented people have pursued the quantization of gravity since the inception of general relativity and quantum mechanics, gravity remains the only fundamental interaction in nature lacking a consistent quantum description. Why is this such a formidable challenge? General relativity is a theory of geometry, and provides a description of the spacetime within which all of the other components of the universe exist. In developing quantum theories for the strong, weak and electromagnetic interactions, one assumes a fixed spacetime background. This takes gravity out of the picture since the Einstein equation implies that geometry is a dynamical entity, shaped and moved by matter, i.e. spacetime *is* the gravitational field. In quantizing gravity, we must quantize spacetime itself! This presents a very different and conceptually difficult challenge, with a potentially huge payoff. Since the dynamics of all physical interactions is played out on the background of spacetime, a theory of quantum gravity could lead to new discoveries over a wide range of physics research.

1.2 Loop quantum gravity

There are now many who work on the problem of quantum gravity from a variety of different angles. See the book [10] for a discussion of various approaches. String theory [11] and loop quantum gravity (LQG) [3, 12] are the two largest fields in terms of number of researchers, but there are several notable alternatives including causal dynamical triangulations [13], causal sets [14], noncommutative geometry [15] and asymptotic safety [16]. In this thesis we focus on LQG.

Loop quantum gravity is a modest and direct approach to quantum gravity. The goal is simply to take what we know about quantum field theory and apply it to general relativity. The theory is concerned only with gravity, and does not attempt to be a unified theory. It assumes a four-dimensional, Lorentzian spacetime, and does not require the introduction of so-far unobserved super-particles to make the theory consistent. Most of the other approaches listed above can be seen as 'bottom up' approaches which make an assumption of what the basic building blocks of space time are, e.g. strings, causal sets or four-simplices. Conversely, LQG is a 'top down' approach which begins on firm ground by starting from a Hamiltonian decomposition of the Einstein action. The introduction of loops, or in the modern treatment, spin networks, comes as a solution to the constraint equations, and the emergence of discrete geometry comes a result of the theory rather than an input.

There are many who believe that a necessary feature of quantum gravity is *background independence*, which means in practical terms that no background metric should be assumed

in developing the theory. See the article [17] for a philosophical discussion on this debate. Background independence is consistent with the idea that events can only be described in relation to other events, as opposed to the notion of an absolute space and time. LQG takes the stance that if one is attempting to give a general, quantum mechanical description of spacetime, then one cannot put into the theory any assumptions about the spacetime geometry.

A related feature of LQG is that it is non-perturbative. Perturbative theories introduce a fixed background spacetime as a reference and consider only small perturbation away from this background. Proponents of LQG tend to believe that a perturbative theory cannot yield a full theory of quantum gravity [18]. The rationale is that working around a fixed background is inadequate for dealing with regions of high curvature, as in the study of singularity formation (or avoidance). Perturbative theories assume spacetime to be smooth and obey classical symmetries down to arbitrarily small scales, but it may be necessary to relax these conditions at the Planck scale where the quantum properties of spacetime take form.

The principle of least action is a mathematical statement of nature's preference for maximal efficiency, and is a ubiquitous tool in physics. Beginning with an action, one can derive the equations of motion and gauge transformations for any classical system, and once the theory has been written in this form, a set of standard rules can be applied to obtain a first order (in $\hbar$) approximation to the quantum theory [19]. The canonical decomposition of the Einstein action was first done by Arnowitt, Deser and Misner [20] in 1962. Here the phase space is parameterized by a space metric q_{ab} and its conjugate momentum π^{ab}, so that gravity can be seen as spacelike hypersurfaces evolving in time. However, the quantization program of Dirac was never successfully applied due to the complicated nature of the Hamiltonian. Over two decades later, Ashtekar recast the theory in terms of new variables which simplify the Hamiltonian and make the theory look similar to an SU(2) Yang-Mills gauge theory. The fields parameterizing the phase space are the $\mathfrak{su}(2)$-valued Ashtekar-Barbero connection $\boldsymbol{A}$ [21], and its canonically conjugate 'electric' field $\boldsymbol{E} \in \mathfrak{su}(2)$, both being defined over spatial hypersurfaces foliating the spacetime manifold. This was the birth of LQG, the goal being a direct route to quantum gravity by applying a Dirac quantization to this more simple Hamiltonian for general relativity. Moreover, having the theory resemble a gauge theory allows for some useful tricks to be borrowed from lattice gauge theory.

As a first step toward construction of the quantum theory, one defines a smearing of the field variables $(\boldsymbol{A}(x), \boldsymbol{E}(x))$ in order to avoid bare delta function divergences. This is done by embedding within the spatial hypersurface an oriented graph Γ, i.e. a collection of oriented, one-dimensional curves (or links ℓ) which are joined at their endpoints. Given such an embedded graph, one can define on each link a holonomy $h_\ell \in \mathrm{SU}(2)$ as the path-ordered integral of the connection $\boldsymbol{A}(x)$ along the link. In order to smear the electric field $\boldsymbol{E}$, one chooses for each link ℓ a dual two-dimensional surface, where 'dual' means that the surface is pierced by the link at a single intersection point, and is not pierced by any other link. This duality implies that each link is dual to a unique two-surface. One then defines a flux $\boldsymbol{X}_\ell \in \mathfrak{su}(2)$ associated to the link ℓ as an integral of $\boldsymbol{E}$ over the two-surface dual to ℓ, which corresponds to the electric flux passing through the surface[2].

[2]Note there is an alternative approach where one takes the holonomy-flux variables associated to graphs as fundamental. The notion of a continuous spatial manifold is then seen as an emergent feature of the theory [22].

At the quantum level the smeared variables form the so-called holonomy-flux algebra [23], a cornerstone of the entire construction of LQG. Associated with this algebra and a given graph Γ is the so-called spin network Hilbert space $\mathcal{H}_\Gamma$. It captures only a finite number of degrees of freedom in the theory. One recovers the continuous kinematical Hilbert space by taking the projective limit[3] of spin network Hilbert spaces $\mathcal{H}_\Gamma$ associated to graphs.

In this construction, two very different procedures are realized at once. There is a discretization procedure in which the continuous fields are replaced by discrete holonomies and fluxes associated with graphs, and in the same stroke, these variables are promoted into quantum operators. The main idea we want to take advantage of is that the processes of discretization and quantization are totally independent. Here we shall disentangle these two steps so that we may study only the process of discretization using graphs, without delving into the quantization of the theory. This allows us to face the challenges stemming from the discretization alone, which are already difficult without the extra complications coming from quantization.

Given a graph Γ, we have a phase space $(h_\ell, X_\ell) \in T^*\mathrm{SU}(2)$ associated to each link ℓ. The phase space P_Γ of loop gravity on a graph is obtained as a direct product over the SU(2) cotangent bundles on each link. It is important to note that the spin network states and flux operators of the quantum theory can be developed from these phase spaces, so that P_Γ is the classical counterpart to the spin network Hilbert space $\mathcal{H}_\Gamma$. In light of this, we take the view that a study of classical general relativity in terms of holonomy-flux phase spaces is the next logical step to take once one has obtained the Hamiltonian in terms of the Ashtekar variables. Historically this is not the route that has been taken, and much is already well understood in the quantum theory. However, many issues remain in LQG, especially concerning dynamics, and we can learn a great deal from studying classical loop gravity.

Loop classical gravity provides a truncation of the gravitational degrees of freedom. The continuous phase space $\mathcal{P}$ for general relativity written in terms of fields $(\boldsymbol{A}(x), \boldsymbol{E}(x))$ is infinite-dimensional, and each point in this phase space represents a continuous spatial geometry. By smearing the field variables to define the holonomies and fluxes associated to an embedded graph, we are reducing the degrees of freedom to a finite number. Working with classical holonomies and fluxes allows us to shed some light on the types of geometry that can be represented by the holonomy-flux data on a graph. In this thesis we will use a certain symplectic reduction of the continuous phase space $\mathcal{P}$ to develop an isomorphism between the holonomy-flux phase space P_Γ and an equivalence class of continuous geometries.

Perhaps the greatest feature of classical loop gravity is that it allows us to address at the classical level one of the most challenging issues in LQG: dynamics. We will see that the geometries in terms of $(\boldsymbol{A}(x), \boldsymbol{E}(x))$ associated to a holonomy-flux phase space P_Γ provide a drastic simplification of the continuous Hamiltonian, which may allow us to express the classical dynamics of general relativity in terms of a collection of finite-dimensional phases spaces parametrized by holonomies and fluxes. The question is then: Can we capture the full dynamics of gravity in terms of the holonomy-flux phase spaces if we simultaneously consider *all* graphs? If there is a clear positive answer to this question at the classical level, then we would have a more complete starting point for the quantization of gravity with the only remaining issues being the treatment of quantization ambiguities in finite-dimensional systems.

[3]The 'projective limit' implies considering all possible graphs, see [24].

Furthermore we would have a clear picture of how the quantum theory should behave in the $\hbar \to 0$ limit.

This thesis is a start to a classical theory of loop gravity. It is self-contained and aims to be accessible to those not familiar with LQG. We tell the story beginning with the Einstein action, reviewing the ADM formalism in the next chapter. After this, we introduce the Ashtekar variables through a canonical transformation of the phase space. This helps to make clear the relationship between the Ashtekar variables and the well-known ADM phase space. In Chapter 3 we review the basic components of the quantum theory, constructing spin network states from the holonomies, and flux operators from the smeared electric field. We then take a step back from the quantum theory to introduce the loop gravity phase spaces P_Γ as the classical counterparts to spin network Hilbert spaces $\mathcal{H}_\Gamma$. Chapter 4 discusses in depth the continuous phase space $\mathcal{P}$ and the loop gravity phase space P_Γ. We prove an isomorphism between P_Γ and a symplectic reduction of $\mathcal{P}$, and discuss the classes of geometries described by the holonomies and fluxes in P_Γ. Chapter 5 goes deeper into describing a particular class of geometries which we call spinning geometries. These provide a beautiful geometrical representation of the holonomy-flux data associated to a graph, and allow us to develop a dynamics for P_Γ by relying upon this connection to the continuous theory. We work toward the dynamics in Chapter 6, studying the effects of reducing the continuous phase space to one of finite-dimension. It is interesting that point particles in 3d gravity give rise to spatial hypersurfaces that are the 2d analog of spinning geometries. We use the 3d point particle model as an example of what we hope to accomplish for the full theory of loop classical gravity. Finally, in Chapter 8 we give a summary of the thesis, discussing what we have achieved so far and what remains to be accomplished toward developing a canonical theory of general relativity in the loop gravity phase space.

Chapter 2

Hamiltonian formulation of general relativity

In this chapter we study canonical general relativity. We take the Einstein-Hilbert action as our starting point, and perform a Hamiltonian analysis along the lines first done by Arnowitt, Deser and Misner [20]. The ADM phase space variables are the space metric q_{ab} and its conjugate momentum π^{ab} where $a = 1, 2, 3$ label only the space coordinates. The space metric describes the intrinsic geometry of a spatial hypersurface while the momentum contains information about the extrinsic curvature, or how the hypersurface is embedded within the spacetime. In this framework, gravity appears as a dynamical three-geometry evolving in time.

Our goal is to arrive at a Hamiltonian written in terms of the Ashtekar variables. We do this in two steps, first making an intermediate canonical transformation to a phase space parameterized by the electric field E^a_i and its conjugate K^i_a, which turns out to be the extrinsic curvature itself. Here $i = 1, 2, 3$ is an $\mathfrak{su}(2)$ index labeling an internal flat space. The electric field, also called the 'densitized triad', is a tensor density composed out of the triad (also known as the frame field or dreibein), which contains the same information as the spatial metric. These variables possess an extra symmetry that is not present in the ADM variables, which we compensate by introducing the 'Gauss constraint'.

After establishing a Hamiltonian in terms of (E^a_i, K^i_a) we introduce the Ashtekar variables through another canonical transformation. This transformation keeps the electric field but exchanges the extrinsic curvature for a connection variable A^i_a, as in Yang-Mills theory. Having a theory of gravity which resembles a gauge theory proves exceedingly useful for quantization. We will also see a simplification in the scalar constraint (which generates dynamics), as compared to the way it is written in the ADM formulation. The endpoint of this chapter is to write a Hamiltonian theory for gravity in terms of the Ashtekar variables. The Ashtekar formulation of general relativity was the beginning of loop quantum gravity, and the point here is to demonstrate its connection to the ADM formulation.

2.1 ADM formulation

Consider a four-dimensional spacetime M endowed with a Lorentzian metric $g_{\alpha\beta}$ having the signature $(-,+,+,+)$. The Einstein-Hilbert action is:

$$\mathcal{A}[g_{\alpha\beta}] = \frac{1}{2}\int_M \Omega\tilde{R}, \tag{2.1}$$

in units where $c = 8\pi G = 1$. The volume element is $\Omega = d^4\tilde{x}\sqrt{|g|}$, $\tilde{R}$ is the Ricci scalar associated with $g_{\alpha\beta}$, g without indices represents the metric determinant and we are using the Greek alphabet to label spacetime coordinates $\alpha = 0, 1, 2, 3$.

2.1.1 Separating time and space

We assume the spacetime to be globally hyperbolic so that we can split the manifold into space and time components[1] so that $M = \mathbb{R} \times \Sigma$, where Σ is a fixed three-dimensional manifold of arbitrary topology. This implies the existence of Cauchy surfaces, i.e. a family of everywhere spacelike hypersurfaces connected to any point in M by a causal curve parameterized by a time function $t \in \mathbb{R}$, in accordance with deterministic physics. For every fixed t there is an embedding $\tilde{x}_t : \Sigma \to M$ defined by $\tilde{x}_t(x) := \tilde{x}(t, x^a)$ where x^a are local coordinates of Σ. We label each foliation $\Sigma_t := \tilde{x}_t(\Sigma)$. Since we do not choose a coordinate system this split remains completely arbitrary and the diffeomorphism invariance of general relativity remains intact.

We define n^α to be the unit vector that is normal to the hypersurfaces Σ_t. This vector satisfies:

$$n^\alpha n_\alpha = -1 \ , \tag{2.2}$$

$$g_{\mu\nu} n^\mu \tilde{x}^\nu_{,a} = 0 \ , \tag{2.3}$$

where $\tilde{x}^\nu_{,a} := \frac{\partial \tilde{x}^\nu(t,x)}{\partial x^a}$. The induced spatial metric or *first fundamental form* of Σ is:

$$q_{\alpha\beta} = g_{\alpha\beta} + n_\alpha n_\beta. \tag{2.4}$$

Note that the spatial metric is orthogonal to n^α, and that q^α_β (index order does not matter because of symmetry) is the projector onto Σ. The direction of time flow is given by:

$$t^\alpha := \frac{\partial \tilde{x}^\alpha(t,x)}{\partial t} =: \tilde{x}^\alpha_{,t} \ , \tag{2.5}$$

from which it follows that $t^\alpha \nabla_\alpha t = 1$. We decompose t^α as follows:

$$t^\alpha = N n^\alpha + N^\alpha \ , \tag{2.6}$$

where $N = -g_{\alpha\beta} t^\alpha n^\beta$ is the lapse function (taken to be positive definite so that time flows into the future) and $N^\alpha = q^\alpha_\beta t^\beta$ is the shift vector. The lapse function quantifies the portion of t^α that is orthogonal to Σ while the shift function is the tangential component. See fig. 2.1.

[1] A theorem by Geroch [25] proves that a globally hyperbolic manifold can always be decomposed in this way.

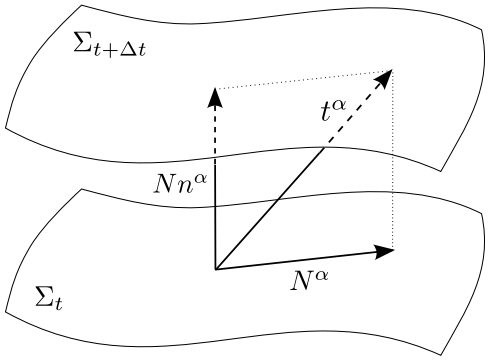

Figure 2.1: This image depicts portions of two neighbouring hypersurfaces, Σ_t and $\Sigma_{t+\Delta t}$, of the foliated spacetime. The time vector field and its components $t^\alpha = Nn^\alpha + \bar{N}^\alpha$ are shown to illustrate how a point on a hypersurface moves from one time slice to the next.

The flow of time throughout the manifold M is described by t^α. If we start at $t = 0$ at a point on the hypersurface Σ_0 and move forward to time t, we arrive at a unique point on the foliation Σ_t. We may view the dynamics as a time dependant, three-dimensional spatial manifold described by $q_{\alpha\beta}(t)$. Following this interpretation, we should be able to take $(q_{\alpha\beta}, N, N_\alpha)$ as our field variables in place of $g_{\alpha\beta}$. At first glance this seems to be an acceptable choice since it preserves the number of independent components (ten). Notice also that the inverse metric can be written as:

$$g^{\alpha\beta} = q^{\alpha\beta} - n^\alpha n^\beta = q^{\alpha\beta} - N^{-2}(t^\alpha - N^\alpha)(t^\beta - N^\beta). \tag{2.7}$$

Without reference to $g_{\alpha\beta}$, we can determine the contravariant form of $q_{\alpha\beta}$ by requiring $q^{\alpha\beta}q_{\beta\gamma}$ to be the identity operator on the tangent space of Σ, along with the condition that $q^{\alpha\beta}\nabla_\beta t = 0$. We can then find $N^\alpha = q^{\alpha\beta}N_\beta$. From the equation above we see that all the information in $g^{\alpha\beta}$ is contained in $(q_{\alpha\beta}, N, N_\alpha)$, and we are therefore able to use this as a complete set of field variables for vacuum gravity. We now set out to rewrite the action in terms of these variables.

We start by addressing the metric determinant present in the volume element. Separating out the time coordinate from the spatial ones, we write the line element:

$$\begin{aligned}
ds^2 &= g_{\mu\nu}(\tilde{x})d\tilde{x}^\mu \otimes d\tilde{x}^\nu \\
&= g_{\mu\nu}(t,x)[\tilde{x}^\mu_{,t}\mathrm{d}t + \tilde{x}^\mu_{,a}dx^a] \otimes [\tilde{x}^\nu_{,b}db + \tilde{x}^\nu_{,b}dx^b] \\
&= g_{\mu\nu}(t,x)[(Nn^\mu + N^\mu)\mathrm{d}t + \tilde{x}^\mu_{,a}dx^a] \otimes [(Nn^\nu + N^\nu)\mathrm{d}t + \tilde{x}^\nu_{,b}dx^b] \\
&= [q_{ab}(t,x)N^aN^b - N^2]\mathrm{d}t \otimes \mathrm{d}t + q_{ab}(t,x)N^b[\mathrm{d}t \otimes dx^a + dx^a \otimes \mathrm{d}t] + q_{ab}(t,x)dx^a \otimes dx^b \ .
\end{aligned}$$

Reading off the metric components of $g_{\mu\nu}$, we have in block form:

$$g_{\mu\nu} = \begin{pmatrix} q_{ab}N^aN^b - N^2 & q_{ab}N^b \\ q_{ab}N^b & q_{ab} \end{pmatrix} \ . \tag{2.8}$$

We can find the determinant using the following formula for block matrices:

$$\det \begin{pmatrix} A & B \\ C & D \end{pmatrix} = \det(D) \det\left(A - BD^{-1}C\right) \ . \tag{2.9}$$

The result is $|g| = N^2 q$ where no absolute value brackets are needed on the right hand side since q positive in our convention. This allows us to rewrite the invariant volume element:

$$\Omega = d^4\tilde{x}\sqrt{|g|} \to \mathrm{d}t\mathrm{d}^3x N\sqrt{q} \ . \tag{2.10}$$

Another important tensor on Σ is the extrinsic curvature, or *second fundamental form*, defined as:

$$K_{\alpha\beta} := q^\gamma_\alpha \nabla_\gamma n_\beta \ . \tag{2.11}$$

Note that $K_{\alpha\beta}$ is purely spatial, i.e. $n^\alpha K_{\alpha\beta} = n^\beta K_{\alpha\beta} = 0$ since $n^\alpha q^\beta_\alpha = 0$ and $n^\alpha \nabla_\beta n_\alpha = \frac{1}{2}\nabla_\beta n^\alpha n_\alpha = 0$. The extrinsic curvature will help us relate the four-dimensional Riemann tensor to the three-dimensional version. Looking further into the properties of $K_{\alpha\beta}$, we need the dual formulation of Frobenius' theorem [26]:

$$\xi_{[\alpha}\nabla_\beta \xi_{\gamma]} = 0 \ , \tag{2.12}$$

for any hypersurface orthogonal vector field ξ^α. Working with this for $n^\alpha = \xi^\alpha$ we find:

$$n^\gamma n_{[\alpha}\nabla_\beta n_{\gamma]} = -n_\alpha n^\gamma \nabla_\gamma n_\beta + n_\beta n^\gamma \nabla_\gamma n_\alpha - \nabla_\alpha n_\beta + \nabla_\beta n_\alpha = 0 \ . \tag{2.13}$$

Contracting again with $q^\alpha_\delta q^\beta_\varepsilon$, we find:

$$\begin{aligned} q^\alpha_\delta q^\beta_\varepsilon (\nabla_\beta n_\alpha - \nabla_\alpha n_\beta) &= 0 \\ \Rightarrow K_{\alpha\beta} &= K_{\beta\alpha} \ . \end{aligned} \tag{2.14}$$

So we see that the extrinsic curvature is symmetric allowing us to develop the following relation:

$$\begin{aligned} \pounds_n q_{\alpha\beta} &= n^\gamma \nabla_\gamma q_{\alpha\beta} + (g_{\gamma\beta} + n_\gamma n_\beta)\nabla_\alpha n^\gamma + (g_{\alpha\gamma} + n_\alpha n_\gamma)\nabla_\beta n^\gamma \\ &= n^\gamma \nabla_\gamma n_\alpha n_\beta + \nabla_\alpha n_\beta + \nabla_\beta n_\alpha \\ &= 2(\nabla_\alpha n_\beta + n_\alpha n^\gamma \nabla_\gamma n_\beta) \\ &= 2\nabla_\alpha n_\beta + 2(q^\gamma_\alpha - g^\gamma_\alpha)\nabla_\gamma n_\beta \\ &= 2K_{\alpha\beta} \ , \end{aligned}$$

where we used $n_\gamma \nabla_\alpha n^\gamma = 0$ to get the second line, and (2.13) was used to go from the second to third line. The second fundamental form can therefore be viewed as the rate of change of the spatial metric in the n^α-direction:

$$K_{\alpha\beta} = \frac{1}{2}\pounds_n q_{\alpha\beta} \ . \tag{2.15}$$

We can also relate the time derivative of the first fundamental form $\dot{q}_{\alpha\beta} := q^\gamma_\alpha q^\delta_\beta \pounds_t q_{\gamma\delta}$ to the extrinsic curvature:

$$\begin{aligned}
K_{\mu\nu} &= q^\alpha_\mu q^\beta_\nu K_{\alpha\beta} \\
&= \frac{1}{2} q^\alpha_\mu q^\beta_\nu (n^\gamma \nabla_\gamma q_{\alpha\beta} + q_{\gamma\beta}\nabla_\alpha n^\gamma + q_{\alpha\gamma}\nabla_\beta n^\gamma) \\
&= \frac{1}{2N} q^\alpha_\mu q^\beta_\nu (N n^\gamma \nabla_\gamma q_{\alpha\beta} + q_{\gamma\beta}\nabla_\alpha N n^\gamma + q_{\alpha\gamma}\nabla_\beta N n^\gamma) \\
&= \frac{1}{2N} q^\alpha_\mu q^\beta_\nu \pounds_{Nn} q_{\alpha\beta} \\
&= \frac{1}{2N} q^\alpha_\mu q^\beta_\nu (\pounds_t - \pounds_N) q_{\alpha\beta} \\
&= \frac{1}{2N} \left[\dot{q}_{\alpha\beta} - q^\alpha_\mu q^\beta_\nu (N^\gamma \nabla_\gamma q_{\alpha\beta} + q_{\gamma\beta}\nabla_\alpha n^\gamma + q_{\alpha\gamma}\nabla_\beta N^\gamma) \right] \\
&= \frac{1}{2N} \left[\dot{q}_{\alpha\beta} - q^\alpha_\mu q^\beta_\nu (N^\gamma \nabla_\gamma n_\alpha n_\beta + \nabla_\alpha N_\beta + \nabla_\beta N_\alpha + n_\gamma n_\beta \nabla_\alpha N^\gamma + n_\gamma n_\alpha \nabla_\beta N^\gamma) \right] \\
&= \frac{1}{2N} (\dot{q}_{\alpha\beta} - D_\mu N_\nu - D_\nu N_\mu) \ , \qquad (2.16)
\end{aligned}$$

where $n_\gamma N^\gamma = 0$ was used to cancel terms in the seventh line. We now have the extrinsic curvature in terms of our desired field variables.

The next part of the action we need to work on is the four-dimensional Ricci scalar $\tilde{R}(g_{\alpha\beta})$. In order to find the three-dimensional $R(q_{\alpha\beta})$, we need to define the covariant differential D acting on spatial tensors only. Using $\mathscr{T}(r,p)$ to represent a rank-r contravariant, rank-p covariant tensor, a well defined [26] derivative operator must:

i) be linear: For all $A, B \in \mathscr{T}(k,l)$ and $\alpha, \beta \in \mathbb{R}$,

$$\nabla(\alpha A + \beta B) = \alpha \nabla A + \beta \nabla B \ .$$

ii) be Leibnitz: For all $A \in \mathscr{T}(k,l)$ and $B \in \mathscr{T}(m,n)$,

$$\nabla(A \otimes B) = (\nabla A) \otimes B + A \otimes (\nabla B) \ .$$

iii) commute with contraction: For all $A \in \mathscr{T}(k,l)$,

$$\nabla_d (A^{a_1 \cdots c \cdots a_k}{}_{b_1 \cdots c \cdots b_l}) = \nabla_d A^{a_1 \cdots c \cdots a_k}{}_{b_1 \cdots c \cdots b_l} \ .$$

iv) be consistent with the notion of tangent vectors as directional derivatives on functions: For any function f and all $\xi \in \mathscr{T}(1,0)$,

$$\xi(f) = \xi^a \nabla_a f \ .$$

v) be torsion free[2]: For any function f,

$$\nabla_a \nabla_b f = \nabla_b \nabla_a f \ .$$

[2]If this last condition is not imposed, a derivative may still be well-defined provided there is an antisymmetric torsion tensor $J^a{}_{bc}$ such that $(\nabla_a \nabla_b - \nabla_b \nabla_a) f = -J^c{}_{ab} \nabla_c f$.

A covariant derivative has the additional property of metric compatibility, so we also require $D_\gamma q_{\alpha\beta} = 0$.

Proposition 2.1.1. *The following defines the unique covariant derivative associated with $q_{\alpha\beta}$:*

$$D_\gamma T^{\alpha_1\cdots\alpha_m}{}_{\beta_1\cdots\beta_n} = q^{\alpha_1}{}_{\delta_1}\cdots q_{\beta_1}{}^{\varepsilon_1} q_\gamma{}^\zeta \nabla_\zeta T^{\delta_1\cdots\delta_m}{}_{\varepsilon_1\cdots\varepsilon_n}. \tag{2.17}$$

Proof. We know that ∇ obeys the first four conditions, so it is easy to see that D obeys them as well. To show that this derivative is torsion free, we have:

$$\begin{aligned} D_\mu D_\nu f &= q^\beta_\mu q^\gamma_\nu \nabla_\beta q^\alpha_\gamma \nabla_\alpha f \\ &= q^\beta_\mu q^\alpha_\nu \nabla_\alpha \nabla_\beta f + q^\beta_\mu q^\gamma_\nu (\nabla_\beta q^\alpha_\gamma)(\nabla_\alpha f) \\ &= q^\beta_\mu q^\alpha_\nu \nabla_\alpha \nabla_\beta f + q^\beta_\mu q^\gamma_\nu [(\nabla_\beta n^\alpha) n_\gamma + n^\alpha (\nabla_\beta n_\gamma)](\nabla_\alpha f) \\ &= q^\beta_\mu q^\alpha_\nu \nabla_\alpha \nabla_\beta f + n^\alpha K_{\mu\gamma}(\nabla_\alpha f) \ , \end{aligned} \tag{2.18}$$

where the crossed out term is zero since $q^\gamma_\nu n_\gamma = 0$. Since (2.18) is symmetric, the torsion vanishes and condition V is satisfied. We also see that D is metric compatible:

$$D_\alpha q_{\beta\gamma} = q_\alpha{}^\delta q_\beta{}^\varepsilon q_\gamma{}^\zeta \nabla_\delta (g_{\varepsilon\zeta} + n_\varepsilon n_\zeta) = 0 \ , \tag{2.19}$$

using $\nabla_\delta g_{\varepsilon\zeta} = 0$ and $q_\beta{}^\varepsilon n_\varepsilon = 0$. Since D is metric compatible and torsion free, it is therefore the unique [26] covariant derivative associated with $q_{\alpha\beta}$. □

Now that we have defined this covariant derivative we can work on relating the four- and three-dimensional Riemann tensors. Considering a purely spatial covector u_α, the three-dimensional Riemann tensor is given by:

$$\begin{aligned} R_{\mu\nu\rho}{}^\sigma u_\sigma &:= 2D_{[\mu} D_{\nu]} u_\rho \\ &= 2q^\gamma_\rho q^\delta_{[\mu} q^\beta_{\nu]} \nabla_\delta q^\varepsilon_\beta q^\zeta_\gamma \nabla_\varepsilon u_\zeta \\ &= 2q^\zeta_\rho n^\varepsilon K_{[\mu\nu]} + 2q^\gamma_\rho q^\delta_{[\mu} q^\beta_{\nu]} (q^\varepsilon_\beta n^\zeta K_{\gamma\delta} + q^\varepsilon_\beta q^\zeta_\gamma \nabla_\delta) \nabla_\varepsilon u_\zeta \\ &= 2q^\gamma_\rho q^\delta_{[\mu} q^\beta_{\nu]} (-q^\varepsilon_\beta K_{\gamma\delta} u_\zeta \nabla_\varepsilon n^\zeta + q^\varepsilon_\beta q^\zeta_\gamma \nabla_\delta \nabla_\varepsilon u_\zeta) \\ &= 2(-K_{\rho[\mu} K^\zeta_{\nu]} + q^\varepsilon_\nu q^\zeta_\rho q^\delta_\mu \nabla_{[\delta} \nabla_{\varepsilon]}) u_\zeta \\ &= (-2K_{\rho[\mu} K^\eta_{\nu]} + q^\varepsilon_\nu q^\zeta_\rho q^\delta_\mu \tilde{R}^\eta_{\delta\varepsilon\zeta}) u_\eta \\ \Rightarrow R_{\mu\nu\rho\eta} &= -2K_{\rho[\mu} K_{\nu]\eta} + q^\delta_\mu q^\varepsilon_\nu q^\zeta_\rho q^\sigma_\eta \tilde{R}_{\delta\varepsilon\zeta\sigma} \ . \end{aligned} \tag{2.20}$$

where $\nabla_\varepsilon n^\zeta u_\zeta = 0$ and the symmetry of $K_{\mu\nu}$ was used in going from the third to fourth line. Contracting the last line to find the three-dimensional R in terms of the four-dimensional $\tilde{R}$:

$$\begin{aligned} R &= R_{\mu\nu\rho\sigma} q^{\mu\rho} q^{\nu\sigma} \\ &= K_{\mu\nu} K^{\mu\nu} - K^2 + q^{\mu\rho} q^{\nu\sigma} \tilde{R}_{\mu\nu\rho\sigma} \ , \end{aligned} \tag{2.21}$$

where $K := K^\alpha_\alpha$. Working on the $\tilde{R}_{\mu\nu\rho\sigma}$ term, we have:

$$\begin{aligned}
\tilde{R} &= \tilde{R}_{\mu\nu\rho\sigma} g^{\mu\rho} g^{\nu\sigma} \\
&= \tilde{R}_{\mu\nu\rho\sigma} (q^{\mu\rho} q^{\nu\sigma} - q^{\mu\rho} n^\nu n^\sigma - q^{\nu\sigma} n^\mu n^\rho + n^\mu n^\rho n^\nu n^\sigma) \\
&= \tilde{R}_{\mu\nu\rho\sigma} q^{\mu\rho} q^{\nu\sigma} - 2 q^{\mu\rho} n^\nu [\nabla_\mu, \nabla_\nu] n_\rho \\
&= \tilde{R}_{\mu\nu\rho\sigma} q^{\mu\rho} q^{\nu\sigma} - 2 n^\nu [\nabla_\mu, \nabla_\nu] n_\mu \ , \qquad (2.22)
\end{aligned}$$

where we have used the antisymmetry of $R_{\alpha\beta\gamma\delta}$. The second term of this last equation can be written as:

$$\begin{aligned}
n^\nu [\nabla_\mu, \nabla_\nu] n_\mu &= \nabla_\mu n^\nu \nabla_\nu n^\mu - (\nabla_\mu n^\nu)(\nabla_\nu n^\mu) - \nabla_\nu n^\nu \nabla_\mu n^\mu + (\nabla_\nu n^\nu)(\nabla_\mu n^\mu) \\
&= -K_{\mu\nu} K^{\mu\nu} + K^2 + \nabla_\mu (n^\nu \nabla_\nu n^\mu - n^\mu \nabla_\nu n^\nu) \ . \qquad (2.23)
\end{aligned}$$

Putting together (2.20–2.23) we obtain the *Codacci equation*:

$$\tilde{R} = R - K^2 + K_{\mu\nu} K^{\mu\nu} - 2\nabla_\mu (n^\nu \nabla_\nu n^\mu - n^\mu \nabla_\nu n^\nu) \ . \qquad (2.24)$$

Now that we have defined the necessary ingredients for writing the vacuum gravity action in terms of spatial tensors only, it is useful to pull back these quantities to Σ to develop our interpretation of this system as purely spatial objects evolving forward in time. Intuition tells us that we should be able to define D using a connection determined from q_{ab}, and the same follows for the curvature terms. Consider the pullback of $D_\alpha f$ for a function f:

$$\tilde{x}^\mu_{,a} D_\mu f = \tilde{x}^\mu_{,a} \partial_\mu f = \partial_a f =: D_a f \ . \qquad (2.25)$$

Now, for a purely spatial tensor $u_\alpha \in \mathscr{T}(0,1)$ we have:

$$\begin{aligned}
D_a u_b &= \tilde{x}^\mu_{,a} \tilde{x}^\nu_{,b} D_\mu u_\nu \\
&= \tilde{x}^\mu_{,a} \tilde{x}^\nu_{,b} \nabla_\mu u_\nu \\
&= \partial_a u_b - \tilde{x}^\mu_{,ab} u_\mu - u^c \Gamma_{\rho\mu\nu} \tilde{x}^\mu_{,a} \tilde{x}^\nu_{,b} \tilde{x}^\rho_{,c} \ . \qquad (2.26)
\end{aligned}$$

Working on the last term we find:

$$\begin{aligned}
\Gamma_{\rho\mu\nu} \tilde{x}^\mu_{,a} \tilde{x}^\nu_{,b} \tilde{x}^\rho_{,c} &= \frac{1}{2} \tilde{x}^\mu_{,a} \tilde{x}^\nu_{,b} \tilde{x}^\rho_{,c} (\partial_\mu g_{\nu\rho} + \partial_\nu g_{\mu\rho} - \partial_\rho g_{\mu\nu}) \\
&= \frac{1}{2} \big[\partial_a q_{bc} - g_{\nu\rho} (\tilde{x}^\rho_{,c} \tilde{x}^\nu_{,ab} + \tilde{x}^\nu_{,b} \tilde{x}^\rho_{,ac}) \\
&\quad + \partial_b q_{ac} - g_{\mu\rho} (\tilde{x}^\rho_{,c} \tilde{x}^\mu_{,ab} + \tilde{x}^\mu_{,a} \tilde{x}^\rho_{,bc}) \\
&\quad - \partial_c q_{ab} + g_{\mu\nu} (\tilde{x}^\nu_{,b} \tilde{x}^\mu_{,ac} + \tilde{x}^\mu_{,a} \tilde{x}^\nu_{,bc}) \ \big] \\
&= \Gamma_{cab} - g_{\mu\rho} \tilde{x}^\rho_{,c} \tilde{x}^\mu_{,ab} \ . \qquad (2.27)
\end{aligned}$$

Putting (2.27) back into (2.26), we have D expressed in terms of Christoffel symbols for $q_{ab}(x)$:

$$D_a u_b = \partial_a u_b - u^c \Gamma_{cab} \ . \qquad (2.28)$$

Note that wherever the coordinates are left unspecified, the use of roman lettered indices will correspond to (t, x) coordinates, and Greek lettered indices to $(\tilde{x})$. Now, any tensor can be written as a linear combination of tensor products of one-forms. By linearity and the Leibniz rule we have for a general tensor $W \in \mathscr{T}(0, n)$:

$$D_a W_{b_1 \cdots b_n} := \tilde{x}^{\mu}_{,a} \tilde{x}^{\nu_1}_{,b_1} \cdots \tilde{x}^{\nu^n}_{,b_n} D_\mu W_{\nu_1 \cdots \nu_n} \ . \tag{2.29}$$

Checking the definition of the Riemann tensor on Σ:

$$\begin{aligned} R_{abcd} &:= [D_a, D_b] u_c = \tilde{x}^{\mu}_{,a} \tilde{x}^{\nu}_{,b} \tilde{x}^{\rho}_{,c} [D_\mu, D_\nu] u_\rho \\ &= \tilde{x}^{\mu}_{,a} \tilde{x}^{\nu}_{,b} \tilde{x}^{\rho}_{,c} \tilde{x}^{\sigma}_{,d} R_{\mu\nu\rho\sigma} u^d \ , \end{aligned} \tag{2.30}$$

which is the result we anticipated: R_{abcd} is the same as the pullback of $R_{\mu\nu\rho\sigma}$. The Ricci tensor and scalar on Σ can be found by found by contracting (2.30) with q_{ab}.

Looking at the metrics, we see that q_{ab} is the pullback of $g_{\alpha\beta}$:

$$q_{ab}(t, x) := (\tilde{x}^{\mu}_{,a} \tilde{x}^{\nu}_{,b} q_{\mu\nu})(\tilde{x}) = \tilde{x}^{\mu}_{,a}(t, x) \tilde{x}^{\nu}_{,b}(t, x) g_{\mu\nu}(\tilde{x}) \tag{2.31}$$

using (2.3). For the second fundamental form we find:

$$K_{ab} := \tilde{x}^{\mu}_{,a} \tilde{x}^{\nu}_{,b} K_{\mu\nu} = \tilde{x}^{\mu}_{,a} \tilde{x}^{\nu}_{,b} \nabla_\mu n_\nu \ . \tag{2.32}$$

The lapse function is a scalar, so we simply have $N(t, x) = N(\tilde{x})$, while for the shift vector:

$$N^a := x^a_{,\mu} N^\mu \ , \tag{2.33}$$

where $\dfrac{\partial x^a}{\partial \tilde{x}^\mu} := x^a_{,\mu}$ and $x^a_{,\mu} \tilde{x}^\rho_a = \delta^\rho_\mu$. The scalars in the Lagrangian transform trivially in the pullback since contravariant and covariant indices transform inversely to each other:

$$K(t, x) = q^{ab} K_{ab} = q^{\mu\nu} x^a_{,\mu} x^b_\nu \tilde{x}^\rho_{,a} \tilde{x}^\sigma_{,b} K_{\rho\sigma} = q^{\mu\nu} K_{\mu\nu} = K(\tilde{x}) \ . \tag{2.34}$$

Similarly, we find:

$$K_{ab} K^{ab} = K_{\mu\nu} K^{\mu\nu} \ , \tag{2.35}$$

$$R(t, x) = R_{abcd} q^{ac} q^{bd} = R_{\mu\nu\rho\sigma} q^{\mu\rho} q^{\nu\sigma} \ . \tag{2.36}$$

Collecting all of these results, it is now possible to rewrite the action (2.1) in terms of a set of variables (q_{ab}, N, N_a) which are each defined on Σ:

$$\mathcal{A}[q_{ab}, N, N_a] = \int \mathrm{d}t \int \mathrm{d}^3 x N \sqrt{q} \left(R - K^2 + K_{ab} K^{ab} \right) \ , \tag{2.37}$$

where the pullback of (2.16) and (2.30) provide the extrinsic curvature and Ricci scalar in terms of q_{ab}, and the total divergence in (2.24) has been dropped since (by Stokes' theorem) it is a boundary term. Boundary terms will be dropped in this essay since they do not affect the equations of motion, and the total boundary term may be recovered after the Legendre transformation by making the variational principal well-defined. With all of the terms within the action pulled back to Σ, we henceforth use q_{ab} exclusively for raising and lowering indices. We are now prepared to derive the Hamiltonian.

2.1.2 Legendre transformation

Next we perform the Legendre transformation from the Lagrangian to the Hamiltonian. We begin by solving for the conjugate momenta and inverting these equations to yield expressions for the 'velocities' (time derivatives of the field variables). Several constraints arise that must be added to the Hamiltonian with corresponding Lagrange multipliers. The final task is to analyze these constraints, solve for the Lagrange multipliers and write down the Hamiltonian in reduced form.

The Lagrangian is easily read off from the action in the form (2.37). Solving for the conjugate momenta of N and N^a, we see that their are no time derivatives of these variables in the Lagrangian, so we find trivially that:

$$P := \frac{\delta L}{\delta \dot{N}} = 0 \; ; \tag{2.38}$$

$$P_a := \frac{\delta L}{\delta \dot{N}^a} = 0 \; . \tag{2.39}$$

These vanishing momenta present two primary constraints [19]:

$$C := P \approx 0 \; , \tag{2.40}$$

$$C_a := P_a \approx 0 \; , \tag{2.41}$$

where ≈ 0 means *weakly equal* to zero, i.e. these constraints may be set to zero only after all relevant Poisson brackets have been worked out (so that this information is maintained within the system of equations). Finding the non-trivial momentum:

$$\begin{aligned} \pi^{ab} &:= \frac{\delta L}{\delta \dot{q}_{ab}} \\ &= N\sqrt{q}\left(2K^{ab} + 2Kq^{ab}\right)\frac{\delta K_{ab}}{\delta \dot{q}_{ab}} \\ &= N\sqrt{q}\left(2K^{ab} + 2Kq^{ab}\right)\left(\frac{1}{2N}h^{ab}\right) \\ &= \sqrt{q}\left(K^{ab} - q^{ab}K\right) \; . \end{aligned} \tag{2.42}$$

The symmetry $\pi^{ab} = \pi^{ba}$ follows from the symmetry of K^{ab} and q^{ab}.

Because the momenta conjugate to N and N^a lead to constraints, we will not be able to solve for their velocities. Solving for $\dot{q}_{ab}$, we invert (2.42) to find:

$$K^{ab} = \frac{1}{\sqrt{q}}\left(\pi^{ab} - \frac{\pi}{2}q^{ab}\right) \; , \tag{2.43}$$

where $\pi = \pi^a_a$. We can now find $\dot{q}_{ab}$ with (2.16) and (2.43):

$$\dot{q}_{ab} = \frac{2N}{\sqrt{q}}\left(\pi_{ab} - \frac{\pi}{2}q_{ab}\right) + 2D_{(a}D_{b)} \; . \tag{2.44}$$

Using (2.44) to substitute for $\dot{q}_{ab}$ and adding in the constraints with Lagrange multipliers λ and λ^a, the resulting Hamiltonian density is:

$$\begin{aligned}
\mathscr{H} &:= \pi^{ab}\dot{q}_{ab} - \mathscr{L} + \lambda C + \lambda^a C_a \\
&= \pi^{ab}\left(\frac{2N}{\sqrt{q}}\pi_{ab} + 2D_{(a}D_{b)} - \frac{\pi N}{\sqrt{q}}q_{ab}\right) - N\sqrt{q}\left[R + \frac{1}{h}\left(\pi^{ab}\pi_{ab} - \frac{\pi^2}{2}\right)\right] + \lambda P + \lambda^a P_a \\
&= -N\sqrt{q}R + \frac{N}{\sqrt{q}}\left(\pi^{ab}\pi_{ab} - \frac{\pi^2}{2}\right) + 2\pi^{ab}D_a N_b + \lambda P + \lambda^a P_a \\
&= \left\{N\sqrt{q}\left[-R + \frac{\pi^{ab}\pi_{ab}}{q} - \frac{\pi^2}{2q}\right] - 2N_b D_a \pi^{ab}\right\} + \lambda P + \lambda^a P_a \ , \qquad (2.45)
\end{aligned}$$

where a boundary term was discarded on the last line.

We must ensure that the primary constraints remain zero throughout the evolution, i.e. we must have $\dot{C} = \dot{C}_a = 0$ (at least weakly, with the use of other constraints), which can give rise to secondary constraints. Taking the Poisson bracket of C with the Hamiltonian, we find the time derivative of the first constraint:

$$\dot{C} = \{P, H\} = \sqrt{q}\left[-R + \frac{\pi^{ab}\pi_{ab}}{q} - \frac{\pi^2}{2q}\right] \ . \qquad (2.46)$$

Now we have to enforce that this be zero, so we have a secondary constraint:

$$S(q_{ab}, \pi^{ab}) = \sqrt{q}\left(-R + \frac{\pi^{ab}\pi_{ab}}{q} - \frac{\pi^2}{2q}\right) \ , \qquad (2.47)$$

which is called the scalar constraint. Calculating $\dot{C}_a$ gives:

$$\dot{C}_a = \{P_a, H\} = -2q_{ac}D_b\pi^{bc}. \qquad (2.48)$$

We can keep the right hand side of the above Poisson bracket equal to zero on shell by including the following 'vector' constraint:

$$V^b(q_{ab}, \pi^{ab}) = -2D_a\left(\frac{\pi^{ab}}{\sqrt{q}}\right) \ . \qquad (2.49)$$

Now must also ensure that these remain zero on shell throughout the evolution, which can lead to further secondary constraints. This calculation is more complicated and requires integration by parts, so we must use smearing functions $f(t, x)$, which are positive definite and nowhere vanishing on M. We define the smeared constraints $S(f) := \int_\Sigma \mathrm{d}^3x f S$ and $V^b(f_b) := \int_\Sigma \mathrm{d}^3x f_b V^b$. Working out these Poisson brackets, we obtain [3]:

$$\{S(f), H\} = V^a(fN_{,a} - Nf_{,a}) - S(\pounds_N f) \approx 0 \ , \qquad (2.50)$$

$$\left\{V^b(f_b), H\right\} = S(\pounds_f N) - V^a(\pounds_N f_a) \approx 0 \ . \qquad (2.51)$$

Since both of these brackets are equal to a combination of the vector and scalar constraints, they vanish weakly and do not yield any further secondary constraints.

Looking at the constraint algebra, we notice that C and C^a have zero Poisson brackets with all constraints. Such constraints are called first class [19] and have unfixed Lagrange multipliers, so λ and λ^a are arbitrary functions. Now, the equations of motion for N and N^a are:

$$\dot{N} = \lambda \,, \tag{2.52}$$
$$\dot{N}^a = \lambda^a \,, \tag{2.53}$$

which means the trajectories of the lapse and shift functions are also arbitrary. Furthermore, the equations for $\dot{q}_{ab}$ and $\dot{\pi}^{ab}$ are completely unaffected by the $\lambda C + \lambda^a C_a$ term in the Hamiltonian. This implies that we may take N and N^a as Lagrange multipliers and eliminate the constraints C and C_a from the Hamiltonian.

We arrive at the ADM Hamiltonian:

$$H = \int \mathrm{d}^3x \left[N_b V^b + NS \right] \,. \tag{2.54}$$

This is a sum of constraints which is a general feature of theories without a fixed metric [18], and reflects the underlying diffeomorphism invariance of general relativity. Note that this Hamiltonian is consistent with vacuum Einstein gravity: the scalar constraint is equivalent to the time-time component of the Einstein equation, i.e. $G_{\alpha\beta} n^\alpha n^\beta = 0$, and the vector constraint is equivalent to the space-time component $G_{\beta\gamma} q^\beta_\alpha n^\gamma = 0$ [26].

The Hamiltonian is defined in terms of the spatial metric q_{ab} and the conjugate momentum π^{ab}. These variables parameterize a phase space with the Poisson algebra:

$$\left\{ q_{ab}(x), \pi^{cd}(y) \right\} = \delta^a_{(c} \delta^b_{d)} \delta(x,y) \,, \qquad \left\{ \pi^{ab}(x), \pi^{cd}(y) \right\} = \{ q_{ab}(x), q_{cd}(y) \} = 0 \,. \tag{2.55}$$

General relativity is cast in terms of three-geometries evolving in time, a beautiful and intuitive picture which makes for illuminating classical calculations. However, the scalar constraint is a complicated function of the spatial metric making the theory difficult to quantize. There are alternative Hamiltonian descriptions of general relativity which can be arrived at by making canonical transformations. The Ashtekar variables in particular are better-suited for quantization.

2.2 Ashtekar formulation

In this section we take the Hamiltonian derived above and perform a canonical transformation to rewrite it in terms of the Ashtekar variables. We present this as a two stage process by first transforming to an intermediate conjugate pair before introducing the Ashtekar variables in a final transformation.

2.2.1 First order gravity

General relativity in terms of a metric is referred to as the second order formulation in contrast to the first order formulation where one works in terms of a frame field and connection. The second order formulation possesses only one Lagrangian equation of motion, and the connection

can be defined in terms of the metric. On the other hand, the first order formulation now has two Lagrangian equations of motion, and the connection is *a priori* independent. In the Hamiltonian formulation, first order variables have more degrees of freedom than the second order variables. We will see that this is compensated by introducing additional constraints. Of course, one could simply take the curvature to be a function of the connection only and begin again at the Einstein action written as a function of the frame field and connection. However, we feel it is insightful to reach the Ashtekar formulation via the ADM formulation to make clear the similarities and differences between these two Hamiltonian theories for gravity.

In three-dimensions, we shall refer to the frame field as a triad e^i_a, a set of three one-forms at each point in space, where $i = 1, 2, 3$ are internal indices corresponding to local orthonormal coordinates. The inverse triad e^a_i satisfies $e^a_i e^i_b = \delta^a_b$ and $e^a_i e^j_a = \delta^j_i$, and the internal indices can be raised/lowered with the Kronecker delta. The spatial metric is written in terms of triads as:

$$q_{ab} = e^i_a e^j_b \delta_{ij} \ . \tag{2.56}$$

We assume the spatial metric to be non-degenerate and of Euclidean signature. Taking the determinant of both sides gives a positive definite value $q = e^2 > 0$ where $q := \det(q)$ and $e := \det(e)$. For the first of our new field variables we define the densitized triad:

$$E^a_i = \frac{1}{2} \operatorname{sgn}(e) \epsilon^{abc} \epsilon_{ijk} e^j_b e^k_c = \sqrt{q} e^a_i \ . \tag{2.57}$$

For future use, we note that the dreibein can be written in terms of the densitized triad:

$$e^i_a = \frac{1}{2} \frac{\epsilon_{abc} \epsilon^{ijk} E^b_j E^c_k}{\sqrt{|E|}}. \tag{2.58}$$

The densitized triad can be related to the inverse metric by:

$$\begin{aligned} E^a_i E^b_j \delta^{ij} &= q e^a_i e^b_j \delta^{ij} \\ &= q q^{ab} \ , \end{aligned} \tag{2.59}$$

and their determinants are related by:

$$\begin{aligned} E &:= \det(E^a_i) \\ &= q^{3/2} e^{-1} \\ \Rightarrow \sqrt{|E|} &= \sqrt{q} \ . \end{aligned} \tag{2.60}$$

As we show explicitly below, the second variable of the new canonical pair will be the extrinsic curvature. Using the triad, we can trade a spacetime index for an internal index of K_{ab} to define:

$$K^i_a := K_{ab} e^b_j \delta^{ij} = \frac{K_{ab} E^b_j \delta^{ij}}{\sqrt{|E|}} \ . \tag{2.61}$$

For now our goal is to rewrite the action in terms of (E^a_i, K^i_a). Notice that in (t, x) coordinates $\pounds_t = \frac{\partial}{\partial t}$, so that we have:

$$\dot{q} = q q^{ab} \dot{q}_{ab} = -q q_{ab} \dot{q}^{ab} \ . \tag{2.62}$$

Taking the time derivative of (2.59):

$$\begin{aligned} \dot{q}q^{ab} + q\dot{q}^{ab} &= (\dot{E}^a_i E^b_j + E^a_i \dot{E}^b_j)\delta^{ij} \\ qq_{ab}\dot{q}^{ab} &= 2\dot{E}^a_i E^i_a - 3\dot{q} \\ \dot{q} &= \dot{E}^a_i E^i_a \ , \end{aligned}$$

where (2.62) was used in getting to the third line. Substituting the third line back into the second yields:

$$\dot{q}^{ab} = \frac{1}{q}(2\dot{E}^a_i E^b_j \delta^{ij} - q^{ab}\dot{E}^c_k E^k_c) \ . \tag{2.63}$$

With the above equations we are now able to write the canonical term of the action using the variables (E^a_i, K^i_a) as follows:

$$\begin{aligned} \int_\Sigma \mathrm{d}^3x \pi^{ab}\dot{q}_{ab} &= \int_\sigma \mathrm{d}^3x - \pi_{ab}\dot{q}^{ab} \\ &= \int_\Sigma \mathrm{d}^3x - \sqrt{q}(K_{ab} - Kq_{ab})\frac{1}{q}(2\dot{E}^a_i E^b_j \delta^{ab} - q^{ab}\dot{E}^c_k E^k_c) \\ &= \int_\Sigma \mathrm{d}^3x - \frac{2}{\sqrt{q}} K_{ab}\dot{E}^a_i E^b_j \delta^{ij} \\ &= \int_\Sigma \mathrm{d}^3x 2E^a_i \dot{K}^i_a \ , \end{aligned} \tag{2.64}$$

where in the last line we integrated by parts and dropped the boundary term.

Next we work on rewriting the constraints. We have the following expressions for q_{ab} and π^{ab} in terms of (E^a_i, K^i_a):

$$q_{ab} = \frac{E^i_a E^j_b \delta_{ij}}{|E|} \ , \tag{2.65}$$

$$\pi^{ab} = \frac{2E^{ia}E^d_i K^j_{[d}\delta^b_{c]}E^c_j}{|E|} \ . \tag{2.66}$$

Substituting these expressions in (2.47) and (2.49), we are able to write:

$$S(E^a_i, K^i_a) = \frac{(K^l_a K^j_b - K^j_a K^l_b)E^a_j E^b_l}{\sqrt{|E|}} - \sqrt{|E|}R \tag{2.67}$$

$$V_a(E^b_i, K^i_b) = -2D_b\left(K^j_a E^b_j - \delta^b_a K^j_c E^c_j\right) \ . \tag{2.68}$$

Now, we are aiming to replace the six q_{ab} with nine E^a_i, so we must counter these extra degrees of freedom with additional constraints. The redundancy comes from the freedom to choose different local frames by acting on the internal indices with SU(2) rotations[3]. We account

[3]The theory does not distinguish between SO(3) and SU(2), so we choose to work with the more fundamental SU(2). This is the necessary choice if we want to include fermionic matter [27].

for the extra degrees of freedom by enforcing the symmetry $K_{[ab]} = 0$. To this end we introduce the Gauss constraint:

$$\begin{aligned} G_i(E^a_j, K^j_a) &= \epsilon^{bcd} e_{ib} K_{cd} \\ &= \epsilon^{bcd} e_{ib} e_{jc} K^i_d \\ &= e\epsilon_{ijk} e^{kd} K^i_d \\ &:= \epsilon_{ijk} E^{aj} K^k_a \ , \end{aligned} \tag{2.69}$$

where q_{ab} was written in terms of triads and the formula $ee^a_i \epsilon^{ijk} = \epsilon^{abc} e^j_b e^k_c$ was used to get from the second to third line.

The action can now be written as:

$$\mathcal{A}[E^a_i, K^i_a, N^a, N, \lambda^i] = \int \mathrm{d}t \int_{\Sigma_t} \mathrm{d}^3x \left[E^a_i \dot{K}^i_a - N^a V_a - NS - \lambda^i G_i \right] \ . \tag{2.70}$$

It remains to be shown that (E^a_i, K^i_a) form a canonical pair, i.e. that they obey:

$$\left\{ E^a_j(x), K^i_b(y) \right\} = \delta^a_b \delta^i_j \delta(x,y) \ , \qquad \left\{ E^a_i(x), E^b_j(y) \right\} = \left\{ K^i_a(x), K^j_b(y) \right\} = 0 \ . \tag{2.71}$$

We prove that this algebra holds by using these equations to calculate (2.55) in terms of the new variables. That is, we check that the Poisson algebra for (q_{ab}, π^{ab}) holds when we substitute for these variables in favour of (E^i_a, K^a_i) and use the equations in (2.71).

Since q_{ab} depends on E^i_a only we clearly have $\{q_{ab}(x), q_{cd}(y)\} = 0$. Looking at the Poisson bracket between two momenta we find:

$$\left\{ \pi^{ab}(x), \pi^{cd}(y) \right\} = -\left(\frac{e}{4} [q^{bc} G^{ad} + q^{bd} G^{ac} + q^{ac} G^{bd} + q^{ad} G^{bc}] \right)(x) \delta(x,y) \ , \tag{2.72}$$

where $G_{ab} := K^i_{[a} e^j_{b]} \delta_{ij}$ is a form of the constraint (2.69) and is therefore equal to zero on the constraint surface. Checking the last bracket we find as desired that:

$$\left\{ \pi^{ab}(x), q_{cd}(y) \right\} = \delta^a_{(c} \delta^b_{d)} \delta(x,y) \ . \tag{2.73}$$

This proves that $(E^a_i,\ K^i_a)$ are a canonical pair and completes our reformulation of the action in terms of these variables. We are now ready to introduce the Ashtekar variables.

2.2.2 Transformation to Ashtekar variables

In this section we perform a canonical transformation $(K^i_a, E^a_i) \to (A^i_a, E^a_i)$ into the *Ashtekar* variables, which casts the theory into the form of a Yang-Mills gauge theory. The notation is chosen so that E^a_i corresponds to the electric field, and A^i_a to the vector potential. Historically, the use of these variables has facilitated progress in the field by allowing for the implementation of techniques that have proven to be successful in Yang-Mills theory.

A^i_a is a connection, a generalization of the Christoffel symbols to something that can act on $\mathfrak{su}(2)$-valued tensors. Before introducing this variable, we will first define the triad-compatible 'spin connection'. For some function $f_i \in \mathfrak{su}(2)$, the covariant derivative acts as follows:

$$D_a f_i := \partial_a f_i + \Gamma_{ai}{}^j f_k \ , \tag{2.74}$$

Compatibility with the triad requires:

$$\begin{aligned} D_a e^i_b &= \partial_a e^i_b - \Gamma^c_{ab} e^i_c + \Gamma_{aij} e^j_b = 0 \qquad (2.75) \\ \Rightarrow \Gamma_{aij} &= -e^b_j(\partial_a e^i_b - \Gamma^c_{ab} e^i_c) \ . \qquad (2.76) \end{aligned}$$

The spin connection is also defined to commute with contraction. This tells us:

$$\begin{aligned} D_a \delta^i_j &= 0 \\ &= e^b_j D_a e^i_b + e^i_b D_a e^b_j \\ &= e^b_j(\partial_a e^i_b - \Gamma^c_{ab} e^i_c + \Gamma_{aik} e^k_b) + e^i_b(\partial_a e^b_j + \Gamma^b_{ac} e^c_j + \Gamma_{ajk} e^{kb}) \\ \Rightarrow \Gamma_{aij} &= -\Gamma_{aji} \ , \qquad (2.77) \end{aligned}$$

noting that terms cancel in the third line. This antisymmetry implies that the spin connection takes values in the $\mathfrak{su}(2)$-algebra. We define:

$$\Gamma^i_a := \frac{1}{2}\epsilon^{ijk}\Gamma_{aij} \ . \qquad (2.78)$$

The Christoffel symbols for D acting on tensorial indices can be defined in terms of tetrads:

$$\begin{aligned} \Gamma^c_{ab} &:= \frac{1}{2}q^{cd}(q_{db,a} + q_{ad,b} - q_{ab,d}) \\ &= e^c_j e^j_{(b,a)} + e^c_j e^{jd}\left(e_{kb} e^k_{[d,a]} + e_{ka} e^k_{[d,b]}\right) \ , \qquad (2.79) \end{aligned}$$

using the definition (2.56). Remembering that E^a_i has a density of $+1$ we find:

$$\begin{aligned} D_a E^b_i &= \partial_a E^b_i + \Gamma^k_{ai} E^b_k + \Gamma^b_{ac} E^c_i - \Gamma^c_{ca} E^b_i \\ &= \sqrt{E} D_a e^b_i + e^b_i\left(\partial_a\sqrt{E} - \Gamma^c_{ca}\sqrt{E}\right) \\ &= e^b_i(e e^c_k e^k_{c,a} - e\Gamma^c_{ca}) = 0 \ , \qquad (2.80) \end{aligned}$$

where the term on the second line is zero by (2.75) and the last line is found to be zero using (2.79). We see that compatibility of D with the triad extends to the densitized triad as well. Using the definition of Γ^i_a we can then write:

$$\begin{aligned} D_a E^a_i &= \partial_a E^a_i + \Gamma^k_{ai} E^a_k \\ &= \partial_a E^a_i + \epsilon_{ijk}\Gamma^j_a E^a_k = 0 \ . \qquad (2.81) \end{aligned}$$

Now with (2.76), (2.78) and (2.79) we can explicitly calculate a unique spin connection:

$$\begin{aligned} \Gamma^i_a &= -\frac{1}{2}\epsilon^{ijk} e^b_k(\partial_a e_{jb} - \Gamma^c_{ab} e_{jc}) \\ &= -\frac{1}{2}\epsilon^{ijk}\left(e^b_k \partial_a e_{jb} + e^b_k e_{jb,a} + e^b_k e_{ja,b} + e^b_k e^d_j e_{la} e^l_{d,b}\right) \\ &= \frac{1}{2}\epsilon^{ijk} e^b_k(e_{ja,b} - e_{jb,a} + e^c_i e_{la} e^l_{c,b}) \qquad (2.82) \\ &= \frac{1}{2}\epsilon^{ijk} E^b_k(E_{ja,b} - E_{jb,a} + E^c_i E_{la} E^l_{c,b}) + \frac{1}{4E}\epsilon^{ijk} E^b_k(E_{ja}E_{,b} - E_{jb}E_{,a}) \ . \qquad (2.83) \end{aligned}$$

We have shown in the last two lines that the spin connection can be written explicitly in terms of e^i_a or E^a_i.

Now, since $D_a E^a_i = 0$, we can add this to (2.69) to yield a constraint of the same form as the Gauss law of Yang-Mills theory:

$$\begin{aligned} G_i &= D_a E^a_i + \epsilon_{ijk} E^{aj} K^k_a \\ &= \partial_a E^a_i + \epsilon_{ijk}(\Gamma^j_a + K^j_a) E^a_k \\ &= \mathcal{D}_a E^a_i \ , \end{aligned} \tag{2.84}$$

where we have introduced a new connection to define $\mathcal{D}_a$:

$$A^j_a := \Gamma^j_a + \gamma K^j_a \ , \tag{2.85}$$

Recalling that adding a tensor to a connection yields another connection. The Immirzi parameter γ can be any non-zero real number [4]. A^i_a is the Ashtekar-Barbero connection, the new field variable we set out to derive.

Remarkably, the variables (A^i_a, E^b_j) form a conjugate pair. The Poisson bracket:

$$\left\{ E^a_i(x), E^b_j(y) \right\} = 0 \ , \tag{2.86}$$

remains unchanged, and since Γ^i_a is a function of E^a_i only we also see that:

$$\left\{ E^a_i(x), A^j_b(y) \right\} = \gamma \delta^a_b \delta^i_j \delta^3(x,y) \ . \tag{2.87}$$

The non-trivial exercise is proving the vanishing of:

$$\begin{aligned} \left\{ A^i_a(x), A^j_b(y) \right\} &= \gamma \left\{ \Gamma^i_a(x), K^j_b(y) \right\} + \gamma \left\{ K^i_a(x), \Gamma^j_b(y) \right\} \\ &= \gamma \left(\frac{\delta \Gamma^i_a(x)}{\delta E^b_j(y)} - \frac{\delta \Gamma^j_b(y)}{\delta E^a_i(x)} \right) \ . \end{aligned} \tag{2.88}$$

Notice that if we have a generating function F for Γ^i_a, e.g.:

$$\Gamma^i_a = \frac{\delta F}{\delta E^a_i(x)} \ , \tag{2.89}$$

then (2.88) is equal to:

$$\gamma \left(\frac{\delta^2 F}{\delta E^b_j(y) \delta E^a_i(x)} - \frac{\delta^2 F}{\delta E^a_i(x) \delta E^b_j(y)} \right) = 0 \ . \tag{2.90}$$

The above expression vanishes due to the symmetry of functional derivatives.

[4] Other conventions choose a complex γ which simplifies the constraints at the cost of requiring *reality conditions*.

A promising candidate for the generating function F is:

$$F = \int_\Sigma \mathrm{d}^3x E^a_i(x)\Gamma^i_a(x) \ . \tag{2.91}$$

In order to check if this generates the spin connection, we calculate the variation:

$$\delta F \ = \ \int \mathrm{d}^3x \left(\delta E^a_i(x)\Gamma^i_a(x) + E^a_i(x)\delta\Gamma^i_a(x)\right) . \tag{2.92}$$

Now, provided the second term on the right hand side is zero, we have our generating function. Using $\delta e^i_a e^b_i = \delta e^i_a e^a_j = 0$ repeatedly, we work on the term in question:

$$\begin{aligned}
E^a_i\delta\Gamma^i_a &= \frac{1}{2}\epsilon^{ijk}\,|e|\,e^a_i\delta[e^b_k(e_{ja,b} - e_{jb,a} + e^c_j e^l_a e_{lc,b})] \\
&= \frac{1}{2}\epsilon^{ijk}\,|e|\left[e^a_i\delta(e^b_k(e_{ja,b} - e_{jb,a})) - \delta(e^b_k e^c_j e_{ic,b}) - (\delta e^a_i)e^c_j e^l_a e^b_k e_{lc,b}\right] \\
&= \frac{1}{2}\epsilon^{ijk}\,|e|\left[e^a_i\delta(e^b_k(e_{ja,b} - e_{jb,a})) - \delta(e^b_k e^a_j e_{ia,b}) + (\delta e^l_a)e^a_i e^c_j e^b_k e_{lc,b}\right] \\
&= \frac{1}{2}\epsilon^{ijk}\,|e|\left[\delta(e^a_i e^b_k(e_{ja,b} - e_{jb,a}) - e^b_k e^a_j e_{ia,b}) + (\delta e^a_i)e^b_k(e^j_{a,b} - e_{jb,a}) + (\delta e^l_a)e^a_i e^c_j e^b_k e_{lc,b}\right] \\
&= \frac{1}{2}\epsilon^{ijk}\,|e|\left[\delta(e^b_k(e^a_j e_{ia,b} + e^a_i e_{ja,b}) - e^a_i e^b_k e_{jb,a}) + (\delta e^b_k)e^a_i e_{jb,a} + (\delta e^a_i)e^b_k e_{jb,a} + (\delta e^l_a)e^a_i e^c_j e^b_k e_{lc,b}\right] \\
&= -\frac{1}{2}\epsilon^{abc}\left[e_{jc}\delta e_{jb,a} - (\delta e^j_c)e_{jc,b}\right]\mathrm{sgn}(e) \\
&= -\frac{1}{2}\epsilon^{abc}\partial_a\left[(\delta e^j_b)e_{jc}\right]\mathrm{sgn}(e) \ .
\end{aligned} \tag{2.93}$$

This tedious calculation was carried out by carefully pulling terms into the variation, collecting terms and using symmetry. Also, the relations $e\epsilon^{ijk}e^b_j e^c_k = \epsilon^{abc}e^i_a$ and $e\epsilon^{ijk}e^a_i e^b_j e^c_k = \epsilon^{abc}$ were used in going from the fifth to sixth line. Note that the final line is a total divergence ($\mathrm{sgn}(e)$ is constant classically), so that we have:

$$\begin{aligned}
\int_\Sigma \mathrm{d}^3x E^q_i\delta\Gamma^i_a &= = -\frac{\mathrm{sgn}(e)}{2}\int_\Sigma \partial_a\left[\epsilon^{abc}(\delta e^j_b)e_{jc}\right] \\
&= -\frac{\mathrm{sgn}(e)}{2}\int_{\partial\Sigma} dS_a\epsilon^{abc}(\delta e^j_b)e_{jc} \ ,
\end{aligned} \tag{2.94}$$

where dS_a is an outward pointing element on the boundary $\partial\Sigma$. With the correct boundary term (see [3]) the right hand side of (2.94) vanishes, which implies that F is the generating potential for Γ^i_a. The right hand side of (2.88) is then seen to vanish in the form (2.90), and we arrive at the result:

$$\left\{A^i_a(x), A^j_b(y)\right\} = 0 \ . \tag{2.95}$$

This was the last item we needed to prove that (E^a_i, A^i_a) are a canonical pair.

We now rewrite the canonical term in (2.70):

$$\begin{aligned}\int_\Sigma \mathrm{d}^3x E^a_i(x)\dot{K}^i_a(x) &= \frac{1}{\gamma}\int_\Sigma \mathrm{d}^3x E^a_i(x)\left(\dot{A}^i_a(x)-\dot{\Gamma}^i_a(x)\right)\\ &= \frac{1}{\gamma}\int_\Sigma \mathrm{d}^3x\left(E^a_i(x)\dot{A}^i_a(x)+\frac{\mathrm{sgn}(e)}{2}\int_\Sigma \partial_a\left[\epsilon^{abc}(\dot{e}^j_b)e_{jc}\right]\right)\\ &= \frac{1}{\gamma}\int_\Sigma \mathrm{d}^3x E^a_i(x)\dot{A}^i_a(x)\ , \end{aligned} \tag{2.96}$$

where a calculation similar to (2.93) shows that $\int_\Sigma \mathrm{d}^3x E^a_i(x)\dot{\Gamma}^i_a(x)$ is a boundary term which we set to zero.

We will also need an expression for the curvature of the connection A^i_a. Introducing an arbitrary element $f^i \in \mathfrak{su}(2)$ we have:

$$\begin{aligned} F_{abik}f^k &:= [\mathcal{D}_a,\mathcal{D}_b]\,f_i\\ &= \partial_a\mathcal{D}_b f_i+\epsilon_{ijk}A^j_a\mathcal{D}_b f^k-\partial_b\mathcal{D}_a f_i-\epsilon_{ijk}A^j_b\mathcal{D}_a f^k\\ &= \epsilon_{ijk}\left[f^k(A^j_{b,a}-A^j_{a,b})+\epsilon^k{}_{lm}f^m(A^j_aA^l_b-A^j_bA^l_a)\right]\\ &= \epsilon_{ijk}f^k\left[2A^j_{[b,a]}+\epsilon^j{}_{lm}A^l_aA^m_b\right]. \end{aligned} \tag{2.97}$$

We can therefore write the curvature of the Ashtekar connection as:

$$F^j_{ab} = 2A^j_{[b,a]}+\epsilon^j{}_{kl}A^k_aA^l_b\ . \tag{2.98}$$

In terms of (E^a_i,A^i_a) the constraints become:

$$V_b(E^a_i,A^i_a) = E^a_iF^i_{ab}-(1+\gamma^2)K^i_aG_i\ , \tag{2.99}$$

$$S(E^a_i,A^i_a) = \frac{E^a_iE^b_j}{\sqrt{E}}\left(\epsilon^{ij}{}_kF^k_{ab}-2(1+\gamma^2)K^i_{[a}K^j_{b]}\right)\ , \tag{2.100}$$

$$G_i(E^a_j,A^i_a) = \mathcal{D}_aE^a_i\ , \tag{2.101}$$

where it is understood that $\gamma K^i_a = A^i_a-\Gamma^i_a$. Finally, the action in terms of the Ashtekar variables is:

$$\mathcal{A}[E^a_i,A^i_a,N_a,N,\lambda^i] = \frac{1}{\gamma}\int \mathrm{d}t\int_{\Sigma_t}\mathrm{d}^3x\left[E^a_i\dot{A}^i_a-N^aV_a-NS-\lambda^iG_i\right]\ . \tag{2.102}$$

This action contains all the information of the vacuum Einstein equations and the ADM Hamiltonian formulation, but suggests a new geometric interpretation of the dynamics. A^i_a provides a definition of parallel transport for SU(2) spinors and E^a_i encodes the full background independent geometry of Σ. If one takes the connection as the configuration variables, the dynamics of gravity is the evolution of the connection A^i_a on a three-dimensional manifold whose intrinsic geometry is described by E^a_i.

Notice the scalar constraint is more simple in terms of the Ashtekar variables (2.100) than it is in terms of the ADM variables (2.47). Up to the density weight factor of $1/\sqrt{E}$, the scalar

constraint is now a polynomial. There is a well-known way of dealing with this term, often referred to as the 'Thiemann trick' [28], where one replaces the $1/\sqrt{E}$ by a Poisson bracket that is easier to manage. Another option sometimes discussed is to absorb the density weight into the lapse function.

We can learn more about these variables by studying the gauge transformations generated by the constraints [5]. The scalar constraint encodes the time evolution of E^a_i and A^i_a. The parameter t has no physical relevance and one can arbitrarily choose a new time coordinate (or a new foliation) without changing the underlying physics, i.e. the redefinition of t is pure gauge so the constraint which generates dynamics is a constraint.

Explicitly calculating the infinitesimal transformations generated by the smeared Gauss constraint $G_i(\lambda^i)$, we have:

$$\begin{aligned}
\delta_G A^i_a(x) &= \left\{A^i_a(x), G_i\left(\lambda^i(y)\right)\right\} \\
&= \frac{1}{\gamma}\int_\Sigma \mathrm{d}^3y \lambda^j(y)\left\{A^i_a(x), \partial_b E^b_j(y) + \epsilon_{jk}{}^l A^k_b(y) E^b_l(y)\right\} \\
&= -\int_\Sigma \mathrm{d}^3y \left(\partial_a \lambda^i(y) + \epsilon^i{}_{jk} A^j_a(y)\lambda^k(y)\right) \\
&= -\mathcal{D}_a\lambda^i(x)\ ; \qquad (2.103) \\
\delta_G E^a_i(x) &= \left\{E^a_i(x), G_i(\lambda^i(y))\right\} \\
&= \frac{1}{\gamma}\int_\Sigma \mathrm{d}^3y \lambda^j(y)\epsilon_{jk}{}^l E^b_l(y)\left\{E^a_i(x), A^k_b(y)\right\} \\
&= \epsilon_i{}^j{}_k E^a_j(x)\lambda^k(x)\ . \qquad (2.104)
\end{aligned}$$

These gauge transformations must hold for arbitrary λ^i.

In order to express the finite transformations, we introduce a basis of $\mathfrak{su}(2)$ generators $\boldsymbol{\tau}^i$ that are equivalent to $-i/2$ times the Pauli matrices. We shall express elements of the $\mathfrak{su}(2)$ algebra using a bold font so that $\boldsymbol{A}_a = A^i_a\boldsymbol{\tau}_i$ and $\boldsymbol{E}^a = E^a_i\boldsymbol{\tau}^i$. Now, for some group element $g \in \mathrm{SU}(2)$ we can write the finite transformations as:

$$g \triangleright \boldsymbol{A}_a = g\boldsymbol{A}_\mu g^{-1} + g\partial_a g^{-1}\ , \qquad g \triangleright \boldsymbol{E}^a = g\boldsymbol{E}^a g^{-1}\ . \qquad (2.105)$$

As in Yang-Mills theory, one sees that the Gauss constraint encodes the SU(2)-gauge invariance of the theory.

Looking at the vector constraint, we find [27]:

$$\delta_V A^i_a = \pounds_N A^i_a\ , \qquad \delta_V E^a_i = \pounds_N E^a_i\ . \qquad (2.106)$$

Exponentiating this gauge transformation leads to finite diffeomorphisms on Σ which, along with refoliation-invariance, preserves the diffeomorphism invariance of general relativity.

We have arrived at a Hamiltonian formulation for general relativity in terms of the Ashtekar variables, which presents gravity as a theory with similarities to an SU(2) gauge theory. The

[5] The constraints are first class since they can be shown to each have vanishing Poisson brackets (weakly) with all of the other constraints [3]. First class constraints are the generators of gauge transformations [19].

variables are an electric field and a connection, and there is a Gauss constraint which enforces invariance of physical quantities under SU(2) gauge transformations. This constraint implies that if one integrates the electric field over a surface, the amount of electric flux flow through the surface is determined entirely by a boundary integral around the surface. We will see in the next section that the Gauss constraint allows for the use of Wilson loops as gauge-invariant objects, which in turn leads to the development of spin networks as the physical states of the quantum theory. Another key feature is the simplification of the scalar constraint which plays the important role of generating dynamics. In the ADM formulation, the scalar constraint is a complicated expression of q_{ab} and π^{ab} containing inverse powers of the metric determinant. In terms of Ashtekar variables, we can express the scalar constraint as a polynomial of the phase space variables, up to a multiplicative factor of $1/\sqrt{E}$, and there are techniques for handling such an overall density weight. The development of this Hamiltonian was an exciting step for those working to quantize general relativity, and was the beginning of what came to be known as loop quantum gravity.

The Ashtekar formulation is rigourously defined and well-understood. This is what we take as the starting point for the new ideas presented in this thesis. Historically the next step was to go into the quantum theory. Our point of view however is to proceed more cautiously, taking a step back from the quantization to first introduce new phase space variables which are well suited for quantization later on. By studying more carefully the loop gravity phase space, we aim to develop a classical theory which agrees with general relativity and can be readily quantized à la loop quantum gravity. In this way, the theory of classical loop gravity is designed to bridge general relativity with loop quantum gravity, so that a direct correspondence with general relativity is built into the quantum theory by construction.

Chapter 3

Elements of loop gravity

One of the main features of the Ashtekar formulation of general relativity is that it very closely resembles a gauge theory, being written in terms of an electric field and a connection that are subject to a Gauss constraint. This makes it possible to adapt for loop gravity techniques that have worked in other gauge theories. Of particular interest is lattice gauge theory, where one defines a regular lattice composed of links ℓ that all have the same length a. On each link one defines a group element, permitting a discretization of the Yang-Mills action to be written in terms of Wilson loops [29] composed from these group elements. Refining the lattice increases the degrees of freedom, and the continuous theory is recovered in the limit that $a \to 0$.

Loop gravity possesses a construction that is analogous to lattice gauge theory [30] but with an important difference. If one wants to define a background independent theory, then one cannot specify a length for the links in order to define a regular lattice. This is geometrical information that must come out as a result of the theory rather than being input from the start. Instead of regular lattices then, loop gravity employs a generalization of this concept which we call *oriented graphs*. An oriented graph (or simply 'graph' hereafter) is an *irregular* lattice, composed of arbitrarily shaped links, each possessing an orientation, which are joined with other links at their endpoints. See fig. 3.1 for an example. Each link ℓ is assigned a group element $h_\ell \in \mathrm{SU}(2)$ called a holonomy, and one can compose Wilson loops from these group elements. In fact the first solutions to the kinematical constraints were written in terms of loops rather than graphs, which is the origin of the name 'loop' gravity. The loop representation [31] was found soon after the Ashtekar formulation and generated a lot of excitement in the field, since the kinematical constraints for a quantum theory of gravity had been solved. Using the Mandelstam identities, one can show that the holonomy data on a graph is equivalent to a sum over sets of loops [32]. Since the graph representation is more convenient for working with this is used in the modern treatment. Recovering general relativity in some limit is a more difficult task than in lattice gauge theory since one can no longer simply take the $a \to 0$ limit. However, this is another success of the theory as one does recover the continuous theory in an appropriate limit, called the *projective* limit [24] which we describe in more detail below. The beauty of this approach, as we shall see, is that one obtains the continuous theory without reference to any background structure.

To any given graph Γ, there is an associated Hilbert space $\mathcal{H}_\Gamma$ in the quantum theory.

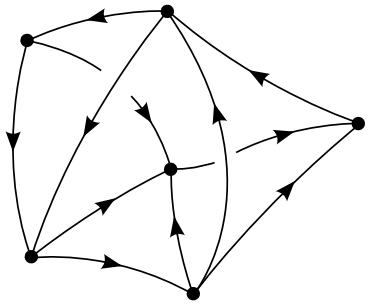

Figure 3.1: An example of a three-dimensional graph. Each link is drawn with an orientation, and intersections between links occur only at the nodes.

Spin network states constructed from the holonomies associated to the links form a basis of states for $\mathcal{H}_\Gamma$ that is orthogonal under the inner product defined by the Ashtekar-Lewandowski measure [33]. The basic operators are the flux $\hat{X}(S)$ which measures the flux of the electric field through a surface S, and a holonomy operator $\hat{h}_\ell$ which acts to add the link ℓ to the graph and generates a new spin network state which belongs to a different Hilbert space $\mathcal{H}_{\Gamma'}$ associated to some other graph $\Gamma' = \Gamma \bigcup \ell$. Geometrical operators such as the area [34], volume [35], and length operator [36] are constructed from the flux operator $\hat{X}(S)$.

In this chapter we review the basic elements of loop quantum gravity, establishing a basis of states and an inner product for the Hilbert space $\mathcal{H}_\Gamma$ associated to a graph Γ. We describe the projective limit of these Hilbert spaces and explain how the continuous kinematical Hilbert space $\mathcal{H}_{\text{kin}}$ is obtained. We define spin network states which give a basis for the gauge invariant Hilbert space $\mathcal{H}^G_{\text{kin}}$ that is orthogonal under the inner product. The diffeomorphism invariant Hilbert space $\mathcal{H}^D_{\text{kin}}$ is spanned by equivalence classes of spin network states related by diffeomorphisms acting on the graphs. We then define the holonomy and flux operators which are well-defined on $\mathcal{H}_{\text{kin}}$, and construct the area and volume operators from the flux operators. After this overview of the quantum theory, we use this framework to motivate a phase space P_Γ from which the quantum Hilbert spaces $\mathcal{H}_\Gamma$ can be constructed. The phase space P_Γ is associated to a graph Γ and has a pair of variables assigned to each link: a flux $\boldsymbol{X}_\ell \in \mathfrak{su}(2)$ and a holonomy $h_\ell \in \text{SU}(2)$. The spin network basis states of $\mathcal{H}_\Gamma$, as well as the operators $\hat{X}(S)$ and $\hat{h}_\ell$ are obtained upon quantization of P_Γ. Having a classical phase space to work with allows us to better understand the relationship between loop gravity and general relativity, and developing this relationship is the main focus of this thesis.

3.1 Wilson loops

Let us start by reviewing the SU(2) formalism of parallel transport using holonomies. Consider a path $\ell : [0,1] \to \Sigma$ sending the parameter $s \in [0,1] \to x^a(s)$, defining a one-dimensional curve in a spatial hypersurface. The holonomy which defines parallel transport along ℓ is a group

element $h_\ell \in \mathrm{SU}(2)$ that solves the ordinary differential equation:

$$\frac{d}{ds} h_\ell[\boldsymbol{A}, s] + \frac{\partial x^a}{\partial s} A_a h_\ell[\boldsymbol{A}, s] = 0 \ . \tag{3.1}$$

With the boundary condition $h_\ell[\boldsymbol{A}, 0] = \mathbb{1}$, the solution is given by the path ordered integral:

$$\begin{aligned} h_\ell[\boldsymbol{A}] &= \overrightarrow{\exp}\left(- \int_\ell \frac{\partial x^a}{\partial s} \boldsymbol{A}_a \right) & (3.2) \\ &= \sum_{n=0}^{\infty} \int_0^1 ds_1 \int_0^{s_1} ds_2 \cdots \int_0^{s_{n-1}} ds_n \frac{\partial x^{a_1}}{\partial s_1} \cdots \frac{\partial x^{a_n}}{\partial s_n} A_{a_1}(s_1) \cdots A_{a_n}(s_n) \ , & (3.3) \end{aligned}$$

where we use the notation $h_\ell[\boldsymbol{A}] \equiv h_\ell[\boldsymbol{A}, 1]$.

From this definition, several key properties of the holonomy are apparent:

i) The holonomy is independent of the parametrization of ℓ.

ii) The holonomy is a representation of the groupoid of oriented paths. The identity is given by a single point. If we define two paths ℓ_1 and ℓ_2, with the second path beginning where the first path ends, we define $\ell = \ell_1 \cdot \ell_2$ and have:

$$h_\ell[\boldsymbol{A}] = h_{\ell_1}[\boldsymbol{A}] h_{\ell_2}[\boldsymbol{A}] \ . \tag{3.4}$$

This property makes the holonomy well-defined even if there are a finite set of points where the path is non-differentiable, since one can always split the path in to differentiable components. The inverse is given by

$$h_\ell^{-1}[\boldsymbol{A}] = h_{\ell^{-1}}[\boldsymbol{A}] \ , \tag{3.5}$$

which is the same as reversing the orientation of the path.

iii) Under an SU(2) gauge transformation of the connection parameterized by a field $g(x) \in \mathrm{SU}(2)$, the holonomy transforms as:

$$h'_\ell[\boldsymbol{A}] = g_{s(\ell)} h_\ell[\boldsymbol{A}] g^{-1}_{t(\ell)} \ , \tag{3.6}$$

where $s(\ell)$ denotes the start of the link and $t(\ell)$ denotes the terminal end of the link.

The fact that the gauge transformation of the holonomy depends upon the field $g(x)$ only at the endpoints of the link makes holonomies well suited for constructing SU(2)-gauge invariant states. The most simple gauge invariant object we can form is the Wilson loop. A loop is a path $\ell_\circ$ such that the starting and terminal ends are identified $s(\ell_\circ) = t(\ell_\circ)$, and a Wilson loop is defined as the trace of the holonomy around this loop:

$$W_{\ell_\circ} = \mathrm{Tr} h_{\ell_\circ}. \tag{3.7}$$

This object is clearly SU(2)-gauge invariant:

$$W'_{\ell_\circ} = \mathrm{Tr}\left(g_{s(\ell)} h_{\ell_\circ} g^{-1}_{t(\ell)} \right) = \mathrm{Tr} h_{\ell_\circ} = W_{\ell_\circ} \ , \tag{3.8}$$

using the cyclic property of the trace and the fact that $s(\ell) = t(\ell)$ for a loop. Gauge-invariance implies that the choice of base-point for the loop does not affect the value of the Wilson loop, since a new choice of base-point for the holonomy is of the same form as a gauge transformation. Calling the new base-point p' and the old base point p, consider a path P that takes us from p' to p. The holonomy around the loop becomes $h_P h_{\ell_\circ} h_P^{-1}$, and the component which depends upon the path P gets traced out as in (3.8).

3.2 Kinematical Hilbert space $\mathcal{H}_{\mathbf{kin}}$

Wilson loops are one example of more general objects called *cylindrical* functions which are built upon oriented graphs. An oriented graph Γ is a set of links ℓ, each having an orientation and connected with other links at the endpoints, called nodes n. A node at the intersection of three links is called 'tri-valent', and we can generally have nodes of any valency greater then or equal to three[1]. A loop is the most basic graph and consists of a single link and no nodes. On each link of a graph we associate a holonomy h_ℓ. Cylindrical functions $\psi_{\Gamma,f}$ are labeled by a graph Γ and a function of the associated group elements $f : \mathrm{SU}(2)^{|\ell_\Gamma|} \to \mathbb{C}$ where $|\ell_\Gamma|$ is the number of links in the graph. For example, the function f of a Wilson loop is the trace. More generally though, f can be any function of the group elements associated to the links of a graph, and is not necessarily gauge invariant.

We denote the space of cylindrical functions associated to the graph Γ as Cyl_Γ. These functions form a basis of the kinematical Hilbert space associated to a graph $\mathcal{H}_\Gamma$. The inner product for this Hilbert space is constructed from a Haar measure for each link of the graph. The normalized SU(2) Haar measure $\mathrm{d}g$ is defined as the unique measure which satisfies the following properties:

$$\int_{\mathrm{SU}(2)} \mathrm{d}g = 1, \qquad \mathrm{d}g = \mathrm{d}(gh) = \mathrm{d}(hg) = \mathrm{d}g^{-1}, \qquad \forall\ g, h \in \mathrm{SU}(2). \tag{3.9}$$

An important property of the Haar measure is the orthogonality relation for matrix elements $\overset{j}{\Pi}(g)^m{}_{m'}$ of an element of SU(2) belonging to the spin-j representation:

$$\int_{\mathrm{SU}(2)} \mathrm{d}g\, \overset{j}{\Pi}(g)^m{}_{m'} \overset{k}{\Pi}(g)^n{}_{n'} = \frac{1}{2j+1} \delta^{jk} \delta^{mn} \delta_{m'n'}. \tag{3.10}$$

This shows us that different representations of the same group element are orthogonal, and that different matrix elements of the same representation are orthogonal.

The Ashtekar-Lewandowski measure is constructed by taking the product of Haar measures associated to links:

$$\mathrm{d}\mu_\Gamma = \prod_{\ell \in \Gamma} \mathrm{d}h_\ell. \tag{3.11}$$

This allows us to define an inner product for cylindrical functions on a given graph:

$$\mu_\Gamma \left(\psi_{\Gamma,f}, \psi'_{\Gamma,f'} \right) := \int_\Gamma \mathrm{d}\mu_\Gamma\, \overline{\psi}_{\Gamma,f}\, \psi'_{\Gamma,f'}. \tag{3.12}$$

[1] We exclude the case of a bi-valent node because these can be removed by the property of the holonomy (3.4).

The inner product vanishes if any group elements in ψ are in different representations than the group elements in ψ' on the same link. This inner product is very similar to that of lattice gauge theory, but here the background independence of the theory is evident as the links are not part of a regular lattice. We note also that the Ashtekar-Lewandowski measure gives a faithful representation of SU(2) since the normalization:

$$\int_\Gamma \mathrm{d}\mu_\Gamma \, \overline{\psi}_{\Gamma,f} \, \psi_{\Gamma,f} \geq 0, \tag{3.13}$$

is positive definite and equal to zero only when $\psi_{\Gamma,f} = 0$.

The orthogonality relation (3.10) tells us that cylindrical functions which carry a different set of representations j_ℓ of the group elements h_ℓ are orthogonal. The space of cylindrical functions which are square integral under the Ashtekar-Lewandowski measure define a basis for the kinematical Hilbert space $\mathcal{H}_\Gamma$. This is a useful basis to work with, but it is not orthogonal. To find an orthonormal basis, one observes that a generic cylindrical function can be written in terms of matrix elements of representations associated to the links [27], which follows from the Peter-Weyl theorem. This implies that an orthogonal basis is composed of products of matrix elements in the representations associated to the links, i.e. $\prod_{\ell\in\Gamma} \overset{j_l}{\Pi}(h_\ell)^{m_\ell}{}_{m'_\ell}$.

With a basis and an inner product, we now have the graph Hilbert space $\mathcal{H}_\Gamma = L^2[\mathrm{SU}(2)^{|\ell_\Gamma|}]$, built upon square integral functions of (representations of) group elements h_ℓ under the measure $\mathrm{d}\mu_\Gamma$. Now, these Hilbert spaces are finite-dimensional but we need an infinite-dimensional Hilbert space if we want to describe a continuous quantum theory for general relativity. In order to address this issue we need to consider the infinite number of graphs that can be defined, each with an associated space of cylindrical functions Cyl_Γ. To define a basis for the continuous Hilbert space, we need to use the union all these spaces associated to graphs:

$$\mathrm{Cyl} := \bigcup_\Gamma \mathrm{Cyl}_\Gamma. \tag{3.14}$$

This space provides us with a set of states for the continuous Hilbert space $\mathcal{H}_{\mathrm{kin}}$, but we still need an inner product since our previous definition applies only to a single graph. Given two cylindrical functions associated to graphs Γ, Γ', one can define a larger graph as the union $\Gamma'' = \Gamma \bigcup \Gamma'$. Under the inclusion map, the functions f and f' associated to the graphs Γ and Γ' are well-defined on the larger graph Γ''. We then have a well-defined inner product for any two cylindrical functions in the space Cyl:

$$\mu(\psi_{\Gamma,f}, \psi'_{\Gamma',f'}) := \int_{\Gamma''} \mathrm{d}\mu_{\Gamma''} \, \overline{\psi}_{\Gamma,f} \, \psi'_{\Gamma',f'}. \tag{3.15}$$

As in the inner product (3.12), the result here is zero if either the representations are different between the two cylindrical functions. There is an important case to consider. Suppose we have $\Gamma' = \Gamma \bigcup \ell$, so that the graph Γ' is obtained by adding the link ℓ to Γ and $\Gamma \bigcup \Gamma' = \Gamma'$. The function f' may then be dependent upon a non-trivial representation of a group element h_ℓ, labeled by some non-zero spin number j_ℓ. Since this link does not exist in Γ, the Haar measure integral associated to the link ℓ in the inner product yields zero, making the overall inner product vanish.

The set of all graphs possesses a partial ordering: A graph Γ' is said to be larger than another graph Γ if Γ' possesses all the links of Γ in addition to other links. For example, when we have a graph composed by the union of two other graphs $\Gamma'' = \Gamma' \bigcup \Gamma$, the partial ordering is $\Gamma'' \geq \Gamma$ and $\Gamma'' \geq \Gamma'$, while no statement can be made about an ordering of Γ in relation to Γ'. This implies that the Hilbert spaces $\mathcal{H}_\Gamma$ and $\mathcal{H}_{\Gamma'}$ are each subspaces of $\mathcal{H}_{\Gamma''}$. Taking all graphs into consideration, we refer to this nested structure of Hilbert spaces as a *projective family*. Now, one can define a precise sequence of ever-larger graphs, and the 'large graph' limit of this sequence is the projective limit. It has been shown that the continuous Hilbert space $\mathcal{H}_{\rm kin}$ is obtained in the *projective limit* [24] of this sequence of graph Hilbert spaces. It is remarkable that we can obtain a continuous Hilbert space for gravity without reference to any background structure.

3.3 Gauge invariant Hilbert space $\mathcal{H}^G_{\rm kin}$

Now, we introduced Wilson loops above as functions of the holonomies which are invariant under SU(2) gauge transformations. The space of functions Cyl_Γ is not gauge invariant, but we can define a gauge invariant subset called spin network functions $\psi_{\Gamma,j_l,\iota_n}$. These require a spin-label j_ℓ (a positive half-integer) associated to each link, and an SU(2)-gauge invariant tensor ι_n called an *intertwiners* at each node. Before we define intertwiners, let us briefly review some necessary aspects of SU(2) spinors.

The fundamental representation of SU(2) is defined by the natural action of the elements on $\mathbb{C}^2$. The representation space is therefore the space of complex vectors with two components, called spinors:

$$\chi^A = \begin{pmatrix} \chi^0 \\ \chi^1 \end{pmatrix} \ , \tag{3.16}$$

where we have used upper case Latin letters for spinor indices. The only invariant under the action of SU(2) is the antisymmetric tensor:

$$\epsilon^{AB} = g^A{}_C g^B{}_D \epsilon^{CD}, \tag{3.17}$$

where $g_A{}^B \in \mathrm{SU}(2)$ is the inverse of $g^A{}_B$. Spinor indices are raised and lowered using the antisymmetric tensor.

Consider the space of completely symmetric spinors with n indices, and notice that this space transforms into itself when acted on by n elements $g \in \mathrm{SU}(2)$:

$$\chi^{A_1 \cdots A_n} \to g^{A_1}{}_{B_1} \cdots g^{A_n}{}_{B_n} \chi^{B_1 \cdots B_n} \ , \tag{3.18}$$

implying that this space is a representation of SU(2). This representation is irreducible, has dimension $2j+1$ (where $j = n/2$) and is called the spin-j representation.

When two spinors are combined in a tensor product, the result can be decomposed into irreducible subspaces. As a first example, consider the tensor product of two $j = 1/2$ spinors:

$$(\chi \otimes \phi)^{AB} = \chi^A \phi^B \ . \tag{3.19}$$

This defines a reducible representation on the space of two index spinors χ^{AB}. Any two index spinor can be decomposed into its symmetric and antisymmetric parts using the invariant tensor ϵ^{AB} as follows:

$$\chi^{AB} = \chi_0 \epsilon^{AB} + \chi_1^{(AB)}, \qquad \chi_0 = \frac{1}{2}\epsilon_{AB}\chi^{AB}. \tag{3.20}$$

This decomposition is invariant because of the invariance of ϵ^{AB}. The scalar χ_0 forms a one-dimensional subspace defining the trivial representation $j = 0$, and the symmetric part is a three-dimensional subspace defining the $j = 1$ representation. Therefore, the tensor product of two spin-1/2 representations is the direct sum of a spin-0 and a spin-1 representation:

$$\mathcal{V}_{1/2} \otimes \mathcal{V}_{1/2} = \mathcal{V}_0 \oplus \mathcal{V}_1 \ . \tag{3.21}$$

With this example, we can better understand how to decompose the tensor product of two spinors with arbitrary spins j_1 and j_2. The subspace of highest dimension is obtained by symmetrizing all of the indices, giving us the spin-(j_1+j_2) representation. Alternatively, we can use an ϵ^{AB} to contract one index from each spinor and symmetrize the remaining $2(j_1+j_2-1)$ indices. The maximum number of ϵ^{AB}'s that we can use is the smallest of $2j_1$ and $2j_2$. Let's say $j_1 > j_2$, so that the maximum number of ϵ^{AB} tensors we can contract with is given by $2j_2$, and this yields the subspace of smallest dimension, the $|j_1 - j_2|$ representation. From this discussion we see that the general decomposition of the tensor product between two spinor representation spaces is:

$$\mathcal{V}_{j_1} \otimes \mathcal{V}_{j_2} = \mathcal{V}_{|j_1-j_2|} \oplus \mathcal{V}_{|j_1-j_2|+1} \oplus \cdots \oplus \mathcal{V}_{j_1+j_2} \ . \tag{3.22}$$

From the above equation (3.22), notice that each irreducible subspace j_3 appears in the decomposition of the product of two representations at most once, and this occurs only if:

$$j_1 + j_2 + j_3 \qquad \text{is an integer ;} \tag{3.23}$$

$$|j_1 - j_2| \leq j_3 \leq (j_1 + j_2) \ . \tag{3.24}$$

These are the Clebsch-Gordon conditions. An equivalent statement of these conditions is that there exist three non-negative integers a, b, c such that:

$$2j_1 = a + c \ ; \qquad 2j_2 = a + b \ ; \qquad 2j_3 = b + c \ . \tag{3.25}$$

Now, the most elementary node on a graph lies at the intersection of three links, i.e. a tri-valent node. Each link carries it's own representation defined by the spin numbers j_1, j_2 and j_3. The tensor product between these three representation spaces can be decomposed into a direct sum between irreducible subspaces, and from the above discussion we can see that the decomposition will contain the trivial representation if and only if the Clebsch-Gordon conditions are satisfied. The tensor product of three representations yields a tensor with $2(j_1 + j_2 + j_3)$ indices, symmetric in the first $2j_1$ indices, the next $2j_2$ indices and the last $2j_3$ indices. The intertwiner is the unique tensor (up to scaling) given by combinations of ϵ^{AB} that has this symmetry. It is formed by combining a tensors ϵ^{AB}, b tensors ϵ^{BC} and c tensors ϵ^{CA}:

$$\begin{aligned} \iota^{(A_1\cdots A_{2j_1})(B_1\cdots B_{2j_2})(C_1\cdots C_{2j_3})} = \quad & K\epsilon^{A_1B_1}\cdots\epsilon^{A_aB_a} \\ & \epsilon^{B_{a+1}C_1}\cdots\epsilon^{B_{a+b}C_b} \\ & \epsilon^{C_{b+1}A_{a+1}}\cdots\epsilon^{C_{b+c}A_{a+c}}, \end{aligned} \tag{3.26}$$

where K is a normalization factor. Under a gauge transformation, the holonomies associated to each link pick up an SU(2) element at each node. These elements arising from the gauge transformation can be absorbed into the intertwiners due to their invariance properties, and this will allow us to construct gauge invariant functions of the holonomies.

Working in the fundamental representation with indices $A = 1, 2$ has been convenient for introducing the intertwiners, but a more convenient notation for what follows is to use the j, m labels for spinors, where m is an index running from $-j$ to j. The intertwiner for a tri-valent node can then be written as a Wigner-3j symbol:

$$\iota^{m_1 m_2 m_3} = K \begin{Bmatrix} j_1 & j_2 & j_3 \\ m_1 & m_2 & m_3 \end{Bmatrix} \tag{3.27}$$

The normalization factor is chosen so that $\iota^{m_1 m_2 m_3} v_{m_1 m_2 m_3} = 1$, which selects a unique intertwiner in the case when three links meet at the node. For example, if we take $j_1 = 1$ and $j_2 = j_3 = 1/2$, the intertwiner is obtained from the Pauli matrices:

$$(\sigma_{m_1})^{m_2}{}_{m_3} = \left\{ \begin{pmatrix} 0 & 1 \\ 1 & 0 \end{pmatrix}, \begin{pmatrix} 0 & -i \\ i & 0 \end{pmatrix}, \begin{pmatrix} 1 & 0 \\ 0 & -1 \end{pmatrix} \right\} , \tag{3.28}$$

where here $m_1 = 1, 2, 3$ counts the three matrices, and m_2, m_3 label the row and column of each matrix. This set of matrix elements is almost the intertwiner, but we need to normalize and raise two of the indices to obtain:

$$\iota^{m_1 m_2 m_3} = \frac{1}{\sqrt{6}} (\sigma_{m_1'})^{m_2}{}_{m_3'} \delta^{m_1' m_1} \epsilon^{m_3' m_3}. \tag{3.29}$$

One can check that this intertwiner is gauge invariant, satisfying the following equation:

$$\overset{1}{\Pi}(g)^{m_1}{}_{m_1'} \overset{1/2}{\Pi}(g)^{m_2}{}_{m_2'} \overset{1/2}{\Pi}(g)^{m_3}{}_{m_3'} \left(\sigma^{m_1'}\right)^{m_2' m_3'} = (\sigma^{m_1})^{m_2 m_3} \ . \tag{3.30}$$

In general, a node may lie at the intersection of any number of links greater than or equal to three. In order to construct a 4-valent intertwiner, one sums over the tri-valent intertwiners as follows:

$$\iota_j^{m_1 m_2 m_3 m_4} = v^{m_1 m_2 m} v_m{}^{m_3 m_4} \ , \tag{3.31}$$

where the index $m = -j, j+1, \cdots, j$ corresponds to a choice of the spin-j representation, which must be one of the representations satisfying the Clebsch-Gordon conditions with both pairs (m_1, m_2) and (m_3, m_4) separately. Each such choice of j yields a different intertwiner, and the set of intertwiners for all of these j values spans an orthonormal basis. Notice also that we could choose different pairings to define the Clebsch-Gordon conditions that the choices for j must satisfy. A different choice of pairings yields a different basis of four-valent intertwiners, for example:

$$w_j^{m_1 m_2 m_3 m_4} = v^{m_1 m_3 m} v_m{}^{m_2 m_4} \ . \tag{3.32}$$

Each index of the tri-valent intertwiners labeled v on the right hand sides of (3.31) and (3.32) is associated to a link on the graph, and the link which holds the choice for j described above

Figure 3.2: Two of the three choices for the 4-valent intertwiner; (a) corresponds to $\iota_j^{m_1m_2m_3m_4} = v^{m_1m_2m}v_m{}^{m_3m_4}$; (b) corresponds to $w_j^{m_1m_2m_3m_4} = v^{m_1m_3m}v_m{}^{m_2m_4}$. The link labeled j in each figure represents the indices m which get summed over.

is drawn as a 'virtual' link, connecting the two tri-valent intertwiners to form a four-valent one. See fig. 3.2 for a graphical representation of these two choices of intertwiner bases. The two bases are related by the following equation:

$$\iota_j = \sum_k (2k+1) \begin{Bmatrix} j_1 & j_2 & j \\ j_3 & j_4 & k \end{Bmatrix} w_k \tag{3.33}$$

We can of course create higher valence intertwiners by combining lower valence intertwiners. For instance, a five-valent intertwiner is constructed from a four-valent and a tri-valent intertwiner. In general, a d-valent intertwiner is constructed from $d-2$ tri-valent intertwiners as follows:

$$\iota_{k_1\cdots k_{d-3}}^{m_1\cdots m_d} := v^{m_1m_2n_1}v_{n_1}{}^{m_3n_2}\cdots v_{n_{d-3}}{}^{m_{d-1}m_d}, \tag{3.34}$$

where the k labels in the subscript of ι on the left hand side denote choices of basis for which to sum over in combining the tri-valent indices on the right hand side.

With a definition of intertwiners, we now have the necessary tools to define gauge invariant functions of the holonomies associated to graphs Γ. Recall that on each link ℓ of a graph, we have a holonomy $h_\ell \in \mathrm{SU}(2)$ taken to be in the spin-j_ℓ representation. We write these representation matrices as:

$$\overset{j}{\Pi}_{mm'}(h_\ell) \qquad \text{where} \quad m, m' = -j, -j+1, \cdots, j\ . \tag{3.35}$$

At each node n of the graph, we assign an intertwiner ι_n defined to be invariant in the tensor product of representations associated to the links which meet at the node. A spin network state is a cylindrical function defined by this data, $(\Gamma, j_\ell, \iota_\mathsf{n})\ \forall\ \ell, \mathsf{n} \in \Gamma$, and a function f which contracts all of the indices associated to the intertwiners and holonomy representations. To see how this contraction works, consider the theta graph $\Gamma = \theta$ of fig. (3.3) and take $j_1 = 1$, $j_2 = j_3 = 1/2$. Using the trivalent intertwiners defined in (3.29), we write this spin network state as:

$$\psi_{\theta, j_\ell, \iota_\mathsf{n}} = K\,(\sigma_{m_1})_{m_2m_3}\,\overset{1}{\Pi}{}^{m_1}{}_{m_1'}\,\overset{1/2}{\Pi}{}^{m_2}{}_{m_2'}\,\overset{1/2}{\Pi}{}^{m_3}{}_{m_3'}\left(\sigma^{m_1'}\right)^{m_2'm_3'}\ , \tag{3.36}$$

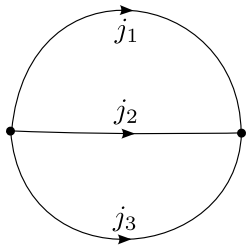

Figure 3.3: The 'theta' graph, showing labeled links with a choice of orientation.

where the factor K is a normalization constant. Indices on the holonomy representations are placed 'up' where the link is directed outward from a node, and 'down' where the link comes into the node. Is this function of the holonomies invariant under gauge transformations? Under a gauge transformations, each of the three holonomies picks up an SU(2) element at each node. Let us say that one node is at point p and the other is at q. Considering (3.6) and (3.30), we see that this cylindrical function is invariant under a gauge transformation parameterized by a function $g \in \mathrm{SU}(2)$:

$$\begin{aligned}
g \triangleright \psi_{\theta,j_\ell,\iota_\mathsf{n}} &= K\,(\sigma_{m_1})_{m_2 m_3} \left[g(p)^{m_1}{}_{m_1'} \overset{1}{\Pi}{}^{m_1'}{}_{n_1'} g(q)^{n_1'}{}_{n_1} \right] \times \\
&\quad \left[g(p)^{m_2}{}_{m_2'} \overset{1/2}{\Pi}{}^{m_2'}{}_{n_2'} g(q)^{n_2'}{}_{n_2} \right] \left[g(p)^{m_3}{}_{m_3'} \overset{1/2}{\Pi}{}^{m_3'}{}_{n_3'} g(q)^{n_3'}{}_{n_3} \right] (\sigma^{n_1})^{n_2 n_3} \\
&= K \left[(\sigma_{m_1})_{m_2 m_3}\, g(p)^{m_1}{}_{m_1'} g(p)^{m_2}{}_{m_2'} g(p)^{m_3}{}_{m_3'} \right] \times \\
&\quad \overset{1}{\Pi}{}^{m_1'}{}_{n_1'} \overset{1/2}{\Pi}{}^{m_2'}{}_{n_2'} \overset{1/2}{\Pi}{}^{m_3'}{}_{n_3'} \left[g(q)^{n_1'}{}_{n_1} g(q)^{n_2'}{}_{n_2} g(q)^{n_3'}{}_{n_3} (\sigma^{n_1})^{n_2 n_3} \right] \\
&= K\,(\sigma_{m_1})_{m_2 m_3} \overset{1}{\Pi}{}^{m_1}{}_{n_1} \overset{1/2}{\Pi}{}^{m_2}{}_{n_2} \overset{1/2}{\Pi}{}^{m_3}{}_{n_3} (\sigma^{n_1})^{n_2 n_3} \\
&= \psi_{\theta,j_\ell,\iota_\mathsf{n}} \ . \qquad (3.37)
\end{aligned}$$

The gauge transformation is absorbed into the intertwiners, as is the case for any spin network function.

On a general graph one defines a spin network function of the holonomies, or equivalently a functional of the connection, as:

$$\psi_{\Gamma,j_\ell,\iota_\mathsf{n}}[\boldsymbol{A}] := \left(\bigotimes_{\iota \subset \Gamma} \iota \right) \bullet \left(\bigotimes_{\ell \subset \Gamma} \overset{j_\ell}{\Pi}(h_\ell[\boldsymbol{A}]) \right) \ , \qquad (3.38)$$

where the $\bullet$ denotes contraction over all indices between holonomy representations and intertwiners, as done in the example (3.36). These functions are invariant (classically) under gauge transformations generated by the Gauss constraint, and this invariance carries over to the quantum theory, i.e. spin network states solve the quantum Gauss constraint.

Spin network functions satisfy the condition of *cylindrical consistency*: For two graphs $\Gamma > \Gamma'$ a cylindrically consistent function is one that satisfies $\psi_{\Gamma,j_\ell,\iota_\mathsf{n}} = \psi_{\Gamma',j_{\ell'},\iota_{\mathsf{n}'}}$, where the

labels $(j_\ell, \iota_{\mathsf{n}})$ are mapped by inclusion into the larger set $(j_{\ell'}, \iota_{\mathsf{n}'})$. The links $\ell'' \in \Gamma \setminus \Gamma'$ are labeled with $j_{\ell''} = 0$. For example, a spin network function defined on a graph Γ' is unchanged if one adds some links ℓ'' to Γ' and labels with spin numbers $j_{\ell''} = 0$. Note that the space of intertwiners between spin-0 representations is zero-dimensional so there are no new intertwiners to label on the nodes $\mathsf{n}'' \in \Gamma \setminus \Gamma'$. Cylindrical consistency ensures that the inner product (3.15) is well defined on spin network states $\psi_{\Gamma, j_\ell, \iota_{\mathsf{n}}} \in \mathrm{Cyl}$. With this inner product, the spin network states span the gauge-invariant kinematical Hilbert space associated to a graph $\mathcal{H}^G_\Gamma$, and the gauge-invariant continuous Hilbert space $\mathcal{H}^G_{\mathrm{kin}}$ is obtained in the projective limit.

3.4 Diffeomorphism invariant Hilbert space $\mathcal{H}^D_{\mathbf{kin}}$

In the previous section we found the gauge invariant kinematical Hilbert space to be a subset $\mathcal{H}^G_{\mathrm{kin}} \subset \mathcal{H}_{\mathrm{kin}}$. We were able to do this because the orbit of the Gauss constraint is compact. However, the orbit of the vector constraint which generates diffeomorphisms is not compact, and we must look for diffeomorphism invariant states in the dual space Cyl^*, that is, the space of linear functions from Cyl to $\mathbb{C}$ which includes distributions. This structure is called a Gelfand triple $\mathrm{Cyl} \subset \mathcal{H}_{\mathrm{kin}} \subset \mathrm{Cyl}^*$ and occurs in the quantization of any theory with non-compact gauge orbits.

Let us denote by $\hat{U}(\phi)$ the operator which generates a spatial diffeomorphism $\phi \in \mathrm{Diff}(\Sigma)$ that is connected to the identity. The action on a cylindrical function is:

$$\hat{U}(\phi)|\psi_{\Gamma,f}\rangle = |\psi_{\phi^{-1}\Gamma,f}\rangle. \tag{3.39}$$

Using this we define the diffeomorphism-invariant state as:

$$([\psi_{\Gamma,f}]| := \sum_{\phi \in \mathrm{Diff}(\Sigma)} \langle \psi_{\Gamma,f}]|\hat{U}(\phi) = \sum_{\phi \in \mathrm{Diff}(\Sigma)} \langle \psi_{\phi\Gamma,f}]|. \tag{3.40}$$

The brackets $([\psi_{\Gamma,f}]|$ denote an equivalence class of cylindrical functions related by diffeomorphisms. We can see that these are diffeomorphism invariant since $([\psi_{\Gamma,f}]|\,\hat{U}(\phi') = ([\psi_{\Gamma,f}]|$. The action on a state in Cyl is:

$$([\psi_{\Gamma,f}]|\,\psi_{\Gamma',f'}\rangle = \sum_{\phi \in \mathrm{Diff}(\Sigma)} \langle \psi_{\phi\Gamma,f}|\psi_{\Gamma',f'}\rangle =: \langle \psi_{\phi\Gamma,f}|\psi_{\Gamma',f'}\rangle_{\mathrm{Diff}}, \tag{3.41}$$

which defines the diffeomorphism invariant inner product. The sum over all diffeomorphisms is rather large, but due to the orthogonality of spin network states only a finite number of terms contribute. This is because a diffeomorphism shifts the links of a graph, and the inner product is non-zero only when all of the links on each graph describe the same curves in Σ, as discussed below the definition of the inner product in (3.15). Notice this is not the same as requiring the graphs to be the same, since if there is a discrete symmetry to the graph, it is possible to shift the whole graph by a diffeomorphism so that it lies on top of its pre-image. But this is a discrete operation which can only apply a finite number of times, so the number of terms in the sum is always finite.

One can define diffeomorphism-invariant states also within the gauge-invariant space of cylindrical functions to obtain a Hilbert space $\mathcal{H}^{G,D}_{\rm kin}$, spanned by equivalence classes of spin network states under diffeomorphisms. This basis of states is represented by so-called s-knots, which are labeled by a sort of 'floating' graph, not embedded within any geometry. The s-knots carry information about which links exist and how they are interconnected at nodes, as well as the spin-labels j_ℓ on the links and intertwiner labels ι_{n} on the nodes. They are defined according to their knotting class as in knot theory [37], since a graph with knots cannot be deformed into a graph with different knots by a diffeomorphism connected to the identity. Note that there is no information in an s-knot about how the graph is embedded in a geometry, since this information disappears when forming the equivalence class.

3.5 Operators

Let us now turn to the operators which act upon the Hilbert space $\mathcal{H}_{\rm kin}$, spanned by the space of cylindrical functions associated to the graphs. In the quantum theory one takes the holonomies rather than the connection $\boldsymbol{A}$ to be the fundamental configuration variables. A set of holonomies associated to a graph are sometimes referred to as generalized connection. As an operator, holonomies $\hat{h}^\ell$ act simply by multiplication, adding the link ℓ and a representation of the holonomy h_ℓ to the state, forming a new state based on a new graph[2]. This action is well defined also in the gauge invariant Hilbert space $\mathcal{H}^G_{\rm kin}$, so long as the new graph supports a gauge-invariant cylindrical function. In fact, any spin network makes a well defined operator in $\mathcal{H}^G_{\rm kin}$.

The operator which measures the electric field $\hat{E}^a_i$ takes more work to define. Since the kinematical states are given by cylindrical functions, we need to find the action of $\hat{E}^a_i$ on holonomies. This action descends from the classical Poisson bracket:

$$\{E^a_i(x), h_\ell[\boldsymbol{A}]\} = \mp\gamma \int_\ell \mathrm{d}s\, \frac{\partial x^a}{\partial s}\delta^3\left(x, \ell(s)\right)\, h_{\ell_1}\boldsymbol{\tau}_i h_{\ell_2}, \tag{3.42}$$

which splits the link into to $\ell \to \ell_1 \circ \ell_2$ and inserts a generator $\boldsymbol{\tau}_i$ of $\mathfrak{su}(2)$ at the point x of intersection. The sign is negative when the link and surface possess the same orientation, and positive when the are oriented opposite to each other. This result can be obtained by applying the Poisson bracket $\left\{E^i_a(x), A^j_b(y)\right\}$ to the definition of the holonomy given in (3.3). When the electric field acts on a representation of the holonomy, the algebra element $\boldsymbol{\tau}_i$ is taken to be in the spin-j_ℓ representation.

The Poisson bracket (3.42) shows us that a naive quantization of the electric field would lead to bare delta functions. The integral in (3.42) is along a one-dimensional link, but we need to integrate over all three spatial dimensions in order to satiate the delta function. Notice the connection is a one-form, so it is naturally integrated along a one-dimensional curve. The electric field is a rank-1 contravariant tensor, but it's Hodge dual is a two-form:

$$E^i_{ab} = \epsilon_{abc}\delta^{ij}E^c_j. \tag{3.43}$$

[2]This works to remove links as well, for one could then act with $\widehat{h^{-1}}_\ell$ to remove the link.

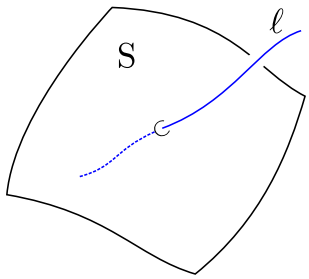

Figure 3.4: A link ℓ which transversely intersects a two-surface S.

This two-form can be naturally integrated over a two-dimensional surface, which is what we need to deal with the delta function. Integrating the electric field over a two-surface S we obtain:

$$\boldsymbol{X}(S) = \int_S \epsilon_{abc} \boldsymbol{E}^a \, \mathrm{d}x^b \, \mathrm{d}x^c. \tag{3.44}$$

This is referred to as the 'flux' since it is a measure of the electric field flowing through the surface S, analogous to the flux in electromagnetism.

There is somewhat of a mystery concerning the flux, which we shall address this in the next chapter. Consider a surface S which is punctured by a single link ℓ as shown in fig. 3.4. If one takes the limit of the surface approaching the start of the link, one finds the following Poisson brackets by direct calculation:

$$\{h_\ell, h_{\ell'}\} = 0, \qquad \left\{X^i(S), h_\ell\right\} = -\boldsymbol{\tau}^i h_\ell. \tag{3.45}$$

Naively, one expects from the definition (3.44) to find that the fluxes commute, but this does not satisfy the Jacobi identity:

$$\{\{\boldsymbol{X}(S), \boldsymbol{X}(S)\}, h_\ell\} + \{\{\boldsymbol{X}(S), h_\ell\}, \boldsymbol{X}(S)\} + \{\{h_\ell, \boldsymbol{X}(S)\}, \boldsymbol{X}(S)\} = 0. \tag{3.46}$$

To satisfy this equation, one finds that the fluxes do not commute:

$$\left\{X^i(S), X^j(S)\right\} = \epsilon^{ij}{}_k X^k(S). \tag{3.47}$$

This is taken to be the definition of the Poisson bracket between fluxes and descends to the quantum commutator algebra. These Poisson brackets define the Poisson algebra of the cotangent space $T^*(\mathrm{SU}(2))$, given by an algebra element $\boldsymbol{X} \in \mathfrak{su}(2)$ and a group element $h_\ell \in \mathrm{SU}(2)$.

Let us consider again a link ℓ which possesses a single, transverse intersection with the surface S, but here we take the intersection to be in the interior of the link. Upon quantization, we see from (3.42) that the flux associated to S acts on the holonomy h_ℓ as follows:

$$\hat{X}^i(S) h_\ell[\boldsymbol{A}] = \mp \gamma h_{\ell_1} \boldsymbol{\tau}_i h_{\ell_2}, \tag{3.48}$$

where the sign is negative when the link and surface possess the same orientation, and positive when the are oriented opposite to each other. Notice the dependence on the Immirzi parameter

γ. This is a self-adjoint operator on the space $\mathcal{H}_\Gamma$. If the link and surface possess multiple intersections, one can split the curve into components to analyze each intersection separately. The case where a portion of the link ℓ runs within the two-surface S can also be treated, as in [23] for instance.

The flux operator is the basic building block of the geometrical operators of loop quantum gravity. In order to define an area operator, first consider the action of the 'squared' flux operator:

$$\hat{\boldsymbol{X}}^i(S)\hat{\boldsymbol{X}}_i(S)h_\ell = \gamma^2 j_\ell(j_\ell+1)h_\ell, \tag{3.49}$$

where $\boldsymbol{\tau}^i\boldsymbol{\tau}_i = j_\ell(j_\ell+1)$ is the Casimir[3] of the spin-j representation of SU(2). Notice the squared flux is gauge-invariant and therefore gives a well-defined operator on $\mathcal{H}^G_{\text{kin}}$. Also notice the term on the right hand side is positive definite, so that the square root is well defined.

Now, the classical function $\boldsymbol{X}^i(S)\boldsymbol{X}^i(S)$ is the Riemannian definition of the squared area of the surface S. Since the quantum version is a positive definite operator, we are able to act with each $\hat{\boldsymbol{X}}^i(S)$ and take the square root to define an area operator in $\mathcal{H}^G_{\text{kin}}$. However, when acting on a spin network, we will generally obtain multiple intersections between the links and the surface S which leads to generators of $\mathfrak{su}(2)$ being contracted at different points, and causing problems for this definition. The way around this is to use a regularization procedure, decomposing the surface S into N two-cells and then taking the limit of $N \to \infty$. Labeling each two-cell S_c, we define the area operator as:

$$\hat{A}(S) := \lim_{N\to\infty} \sum_{c=1}^{N} \sqrt{\hat{X}(S_c)^i \hat{X}(S_c)^i}. \tag{3.50}$$

In practice, this operator is well defined once there is one intersection per cell which occurs for some finite N. When acting on a spin network state we get a finite number of contributions coming from the cells which contain an intersection (or puncture P) between the links of the spin network and the surface. Restoring units, the result is:

$$\hat{A}(S)|\psi_{\Gamma,j_\ell,\iota_n}\rangle = 8\pi\gamma l^2_{\text{Pl}} \sum_P \sqrt{j_P(j_P+1)}|\psi_{\Gamma,j_\ell,\iota_n}\rangle, \tag{3.51}$$

where l_{Pl} is the Planck length. This tells us that spin network states are eigenstates of the area operator! Notice also that there is a minimum non-zero eigenvalue in the spectrum. With additional care, one can treat the so called 'degenerate sector' which considers the possibility of links which run within the surface S. See [34] for further details.

A volume operator for a three-dimensional region R can be defined from the quantization of the classical expression:

$$V(R) = \int_R \mathrm{d}^3x \sqrt{\frac{1}{3!}\left|\epsilon_{abc}\epsilon^{ijk}E^a_i E^b_j E^c_k\right|}. \tag{3.52}$$

[3]Note that other Casimirs exist in the literature [38]. Of particular interest are $(j_\ell + \frac{1}{2})^2$ and j_ℓ^2 which lead to equally spaced spectra for the area operator.

We give a sketch of this operator, and refer the reader to [35] for more details. We again use a regularization procedure, decomposing the region R into N three-cells R_c so that we may define the operator using a refinement limit:

$$\hat{V}(R) = \lim_{N\to\infty} \sum_{c=1}^{N} \sqrt{\frac{1}{3!} \left| \epsilon^{ijk} \hat{X}^i(\partial R_c) \hat{X}^j(\partial R_c) \hat{X}^k(\partial R_c) \right|}, \tag{3.53}$$

where ∂R_c is the boundary of the cell R_c. Similarly to the area operator, the previous expression is well defined once the decomposition is fine enough to have at most one node per cell, which happens generically for some finite number N of cells. It turns out that we get a contribution from each cell that contains a node n of valence greater than three. A tri-valent node gives a contribution of zero, and is analogous to the volume of a region bounded by three flat faces. One needs at least four flat faces (a tetrahedron) to bound a region of non-zero volume. There are is an alternative to this volume operator which uses this idea that a d-valent node corresponds to a flat, convex polyhedron with d faces. See [39] for more on this approach.

Using the volume operator and an appropriate regularization scheme, it is possible to give a definition of the scalar constraint which solves:

$$\hat{S}(N)|\psi_{\Gamma,j_\ell,\iota_\mathsf{n}}\rangle = 0. \tag{3.54}$$

This is the program developed by Thiemann and is presented in his book [3]. The resulting picture of dynamics is that the operator $\hat{S}(N)$ adds links around each node of a spin network state, creating a sum over spin networks with these 'dressed' nodes. However, since each node is dressed independently of the others, this formulation does not seem to provide any means to describe the propagation of gravitons [40]. A more recent idea to obtain a dynamical theory has been to use a Lagrangian formulation for quantum gravity built upon the kinematical spin network states. This is the spin foam approach, which aims to calculate transition amplitudes between spin network states in the spirit of Feynman diagrams. See [12] and also [41] for an introduction to spin foams.

3.6 Loop gravity phase space

The theory we have presented so far in this chapter provides an appealing description of a quantum theory of gravity. The Hilbert spaces are well-defined and provide a rather elegant description of quantum geometry built upon graphs. The quantized gravitational field is represented by operators which measure discrete values for areas, volumes and lengths. However, the theory is not yet complete as much work remains in developing the dynamics, and also in finding a complete set of physical observables. Another issue is that given the lack of experimental evidence to guide us, how will we know if a theory is correct once it is complete? It seems the best way to do this is to check whether the theory agrees with general relativity in the appropriate limit. This is a tricky task, since we are using a projective limit to reach the continuous theory, but in practice we work with Hilbert spaces associate to graphs. This implies that we must take both the classical $\hbar \to 0$ limit as well as a continuous limit in order to make the comparison. This is an active area of research, with most of the focus being to

study the spin foam action in order to obtain the Regge action [42], which is known to describe general relativity in the proper limit.

Here we are making a distinction between *discretization* and *quantization*, where in other contexts such as audio signal processing, these words are used interchangeably. A common feature amoung quantum theories is that spectra which are classically continuous become discrete upon quantization, as is the case for example in the energy spectrum of a harmonic oscillator, but this *is not* the type of discreteness we are referring to. In this thesis we are contrasting a discrete phase space, written in terms of a *finite* number of variables, with a continuous phase space written in terms of continuous fields with *infinite* degrees of freedom. Such a discrete phase space can be obtained by putting a continuous theory on a lattice. Both of the phase spaces are classical, but one is discrete and the other is continuous. On top of a classical phase space, one can build a quantum theory by promoting the phase space variables to operators on a suitable Hilbert space. This quantization is a separate issue, not related to the discretization.

The approach we present now is to take a step back from the quantization, in order to develop a set of discrete, classical phase spaces which can be easily quantized to yield the quantum theory. The Hilbert space associated to a graph $\mathcal{H}_\Gamma$ represents a truncation of the full Hilbert space $\mathcal{H}_{\rm kin}$ to a finite number of degrees of freedom. What we would like to emphasize here is that spin network Hilbert spaces can be obtained as the quantization of finite-dimensional phase spaces associated to embedded oriented graphs Γ. Each of these truncated phase spaces are spanned by a finite number of holonomies and fluxes which reproduce the Poisson algebra of $T^*\mathrm{SU}(2)$. This fact has already been recognized in the literature [43] and is at the basis of most of the recent semi-classical analyses of LQG [44, 45, 46]. Our main point is that the process of truncating the theory to a finite number of degrees of freedom and the process of quantizing this truncated theory are separate issues which can be studied individually. Here we would like to use that the continuous kinematical phase space $\mathcal{P}$ can be obtained in the projective limit of phase spaces P_Γ associated to embedded oriented graphs [47]. In particular, we would like to understand the relationship between these finite-dimensional phase spaces P_Γ and the continuous phase space variables, and the nature of the truncation.

In the quantum field theory of massive particles one defines the theory within a truncation scheme, restricting first the definition of asymptotic states to a finite number of particles, then defining the amplitudes recursively between an arbitrary number of in and out particle states. What this truncation achieves is the possibility to organize the theory in terms of Fock states so that we can deal with finite-dimensional Hilbert spaces at each energy level. It also emphasizes a basis of states that possesses a strong classical interpretation: the particle. This truncation is very different from an approximation scheme such as a discretization. It is not supposed to be an approximate description of a continuum theory that needs some continuum limit. It is supposed to be an *exact* description of the continuum theory restricted to a particularly convenient and finite basis of states. The full theory lies in the knowledge of all amplitudes, not in some continuum limit. There are some limiting procedures to be taken which are associated with the reorganization of coupling constants, following from the existence of naive divergences. These divergences are in some sense welcome since they give us strong clues about spacetime locality.

Interestingly, loop quantum gravity and spin foams possess the same set of ingredients. In

loop quantum gravity, a truncation is needed in order to define the kinematical Hilbert space. One truncates the theory by looking first at spin networks states that are supported on a *finite* graph Γ embedded in space. Then one shows that this leads to finite dimensional Hilbert spaces and discrete spectra. Spin foams aim at computing all possible amplitudes between such states supported on finite graphs. Also, there exists interesting naive divergences in these amplitudes. These divergences should be welcome and renormalized; they have been recognized to be related to the existence of spacetime diffeomorphism symmetry [48].

Let us emphasize that this point of view is key to understanding the program that we are advocating here. If one thinks of loop gravity as a truncation rather than a discretization (or approximation), one should not try to take a naive continuum limit of it. One should instead find a proper way to understand and deal with the reorganization of infinities, and understand the intertwining of these infinities with spacetime diffeomorphism.

It is important to understand the classical nature of the truncation in order to decide whether loop gravity should be treated as a truncation or as a discretization. In the field theory case, the truncation is associated with particles and can be expressed in terms of classical field configurations with compact topology. Therefore, the central question we want to investigate here, is whether it is possible to assign to the loop gravity truncation a classical meaning in terms of acceptable three-geometries. Loop gravity is after all a theory of quantum gravity, based on the quantization of a phase space which is interpreted as the cotangent bundle over the space of three-geometries. So the question is whether we can understand the truncated phase space P_Γ to be associated with a classical, albeit discrete, geometry.

In [47] it has been shown how, for a given graph Γ, the graph phase space P_Γ can be obtained from the continuous phase space, and carries the Poisson structure of finite direct products of SU(2) cotangent bundles. It has furthermore been shown how the regulator corresponding to the graph can be removed, thereby defining a continuum limit (via a suitable projective sequence) which contains the original infinite-dimensional continuous phase space. In the present chapter we will recall some elements of this construction like the definition of the discrete phase spaces, and will push this program forward in subsequent chapters toward the goal of understanding gravity in terms of the phase spaces P_Γ.

The kinematical phase space P_Γ associated with a graph is isomorphic to a direct product for each link of SU(2) cotangent bundles[4]:

$$P_\Gamma \equiv \underset{\ell}{\times} T^*\mathrm{SU}(2)_\ell. \tag{3.55}$$

Explicitly, this phase space is labeled by couples $(h_\ell, X_\ell) \in \mathrm{SU}(2) \times \mathfrak{su}(2)$ of Lie group and Lie algebra elements for each link $\ell \in \Gamma$. This data depends on a choice of orientation for each link, and under an orientation reversal ($\ell \to \ell^{-1}$) we have:

$$h_{l^{-1}} = h_\ell^{-1}, \qquad\qquad X_{\ell^{-1}} = -h_\ell^{-1} X_\ell h_\ell. \tag{3.56}$$

Since we have chosen here to trivialize $T^*\mathrm{SU}(2)$ with right-invariant vector fields, this last relation means that under orientation reversal of the link we obtain the left-invariant ones. The

[4]Given a Lie group G, the group action on itself by left (or right) multiplication can be used to obtain an isomorphism of vector fields with the Lie algebra $\mathfrak{g}$, and to trivialize the cotangent bundle as $T^*G = G \times \mathfrak{g}^*$ [49].

variables (h_ℓ, X_ℓ) satisfy the Poisson algebra:

$$\left\{\boldsymbol{X}^i_\ell, \boldsymbol{X}^j_{\ell'}\right\} = \delta_{\ell\ell'}\epsilon^{ij}{}_k \boldsymbol{X}^k_\ell, \qquad \left\{\boldsymbol{X}^i_\ell, h_{\ell'}\right\} = -\delta_{\ell\ell'}\boldsymbol{\tau}^i h_\ell + \delta_{\ell\ell'^{-1}}\boldsymbol{\tau}^i h_\ell^{-1}, \qquad \left\{h_\ell, h_{\ell'}\right\} = 0, \quad (3.57)$$

As shown in [50, 51], the symplectic potential and symplectic two-form for this Poisson structure are given respectively by:

$$\Omega_\Gamma = \sum_\ell \mathrm{Tr}\left(X_\ell \delta h_\ell h_\ell^{-1}\right), \qquad \omega_\Gamma = -\mathrm{d}\Omega_\Gamma. \quad (3.58)$$

This is consistent with the Poisson algebra we presented above in defining the action of flux operators.

On the spin network phase space P_Γ, we can define the action of the gauge group $G_\Gamma \equiv \mathrm{SU}(2)^{|\mathsf{n}_\Gamma|}$ at the nodes n_Γ of the graph. Given an element $g_\mathsf{n} \in \mathrm{SU}(2)$, finite gauge transformations are given by:

$$g_\mathsf{n} \triangleright h_\ell = g_{s(\ell)} h_\ell g_{t(\ell)}^{-1}, \qquad g_\mathsf{n} \triangleright X_\ell = g_{s(\ell)} X_\ell g_{s(\ell)}^{-1}, \quad (3.59)$$

where $s(\ell)$ (resp. $t(\ell)$) denotes the starting (resp. terminal) node of ℓ. This action on the variables h_ℓ and X_ℓ is generated at each node by the Hamiltonian:

$$G_\mathsf{n} \equiv \sum_{\ell \ni \mathsf{n}} X_\ell = \sum_{\ell | s(\ell) = \mathsf{n}} X_\ell + \sum_{\ell | t(\ell) = \mathsf{n}} X_{\ell^{-1}}, \quad (3.60)$$

which can be understood as a discrete Gauss constraint. Since this action is Hamiltonian, we can define the gauge-invariant phase space:

$$P_\Gamma^G = \underset{\ell}{\times} T^*\mathrm{SU}(2)_\ell /\!\!/ \mathrm{SU}(2)^{|\mathsf{n}_\Gamma|} = G_\mathsf{n}^{-1}(0)/\mathrm{SU}(2)^{|\mathsf{n}_\Gamma|}, \quad (3.61)$$

by symplectic reduction where $|\mathsf{n}_\Gamma|$ is the number of nodes in the graph. The double quotient means to impose the Gauss constraint at each node n and divide out the action of the SU(2) gauge transformation (3.59) that it generates, i.e. to identify values of the parameters which are related by SU(2)-gauge tansformations.

This establishes a classical phase space P_Γ and a discrete Gauss constraint associated to a graph, amenable to quantization à la loop quantum gravity. Clearly the holonomies we define are the same as those of the traditional quantum theory and correspond to the holonomy operators upon quantization. Furthermore, by introducing intertwiners at the nodes of the graph, one can define the (gauge invariant) spin network states which form a basis of $\mathcal{H}^G_\Gamma$ and $\mathcal{H}^G_{\mathrm{kin}}$ in the projective limit. The flux has the appropriate Poisson algebra to yield a set of flux operators, from which the geometric operators can be constructed. A new feature here is that we now have a unique flux for each link of the graph. We will see in the next chapter that this implies a set of two-surfaces (or faces f_ℓ) are defined so that there is a one-to-one correspondence between links and faces. This leads to a well-defined notion of three-cells, and we anticipate that this extra structure will allow for a cleaner derivation of geometric operators upon quantization, without the need for regularization. The existence of well-defined surfaces for the flux operators is required for making sense of the classical limit of (the expectation value) of flux operators, since these require the specification of two-surfaces. We will give a detailed description of the duality between the links ℓ of graph and these faces f_ℓ in the next chapter.

Chapter 4

Relating the discrete and continuous phase spaces

The question we address in this chapter is: What is the relationship between the continuous phase space given by the Ashtekar variables $(\boldsymbol{A}, \boldsymbol{E}) \in \mathcal{P}$, and the spin network phase space in terms of holonomies and fluxes $(h_\ell, \boldsymbol{X}_\ell) \in P_\Gamma$? More precisely, is it possible to reconstruct from the discrete set of holonomy-flux data in P_Γ, a point in the continuous phase space $\mathcal{P}$? What we need in order to describe the relationship between the discrete and continuous data is a map from the continuous to the discrete phase space. We can then study its kernel and see to what extent it can be inverted.

There is some previous work in this direction which has lead to the development of twisted geometries [52]. In this paper it was shown that the truncated loop gravity phase space P_Γ possesses a natural geometrical interpretation in terms of discrete geometries. This phase space was shown to be understood as the gluing of convex polyhedra [53, 39] along their faces, leading to a piecewise-linear-flat[1] but discontinuous geometry. The relationship between twisted geometries and twistors has also been developed [54, 55]. Recently an important development [56] showed that twisted geometries admit a torsionless connection. This shows that twisted geometries are a natural generalization of Regge geometries. As a confirmation, the analog of the Regge action for twisted geometries have been found [57] and shown to appear in the asymptotics of 15j-symbols.

Despite the success of this approach, one drawback lies in the fact that the geometries obtained are discontinuous across the faces of the polyhedra. Indeed, the shape of each face appears differently from the perspective of each polyhedron that shares it, and it is therefore not possible to assign a common length to the links of this geometry. This is in sharp contrast with a Regge geometry where link lengths agree along faces that are glued together. This is an issue if one wants to have a well defined notion of frame fields, and it has motivated some authors to impose on the twisted geometries the Regge constraints [58]. However, by doing so we lose the link with the loop gravity phase space, the discreteness of geometrical observables and the power of spin foam quantization.

[1] Here 'flat' implies that the metric associated to each polyhedron is flat, while 'linear' refers to the fact that gluing maps have to be linear which implies the flatness of the induced metric on each face.

Twisted geometries give a very intuitive picture in terms of polyhedra-shaped cells, but the discontinuous nature of the overall three-geometry does not coincide with the types of geometries we usually require for a theory of gravity. Here we will develop a more general relationship between the discrete holonomy-flux phase space P_Γ and the continuous phase space $\mathcal{P}$ parametrized by the Ashtekar field variables. In [59], it was shown that the spin network Hilbert space can be identified with the state space of a topological theory on a flat manifold with defects. Our analysis in this chapter, which closely follows that of [60], makes the same type of identification at the classical level and emphasizes the fact that the frame field determines only an equivalence class of geometries. The idea that the discrete data labels only an equivalence class of geometries has already been advocated in [43] on a general basis. Our approach gives a precise understanding of which set or equivalence class of continuous geometries is represented by the discrete geometrical data.

4.1 Symplectic reduction

The configuration space of the continuous theory is the space $\mathcal{A}$ of smooth connections on Σ. The phase space is the cotangent bundle $\mathcal{P} \equiv T^*\mathcal{A}$, and carries a natural symplectic potential. In this chapter we shall work exclusively with the two-form $\boldsymbol{E}^i_{ab}$ which is related to the vector field $\boldsymbol{E}^a_i$ through:

$$E_{ab\,i} \equiv \epsilon_{abc}\tilde{E}^c_i, \qquad E_i \equiv E_{ab\,i}\mathrm{d}x^a \wedge \mathrm{d}x^b, \qquad \boldsymbol{E} \equiv E_{ab\,i}\boldsymbol{\tau}^i, \tag{4.1}$$

where we are using a bold font for elements of $\mathfrak{su}(2)$. The symplectic potential of the cotangent bundle is given by:

$$\Omega = \int_\Sigma E_i \wedge \delta A^i = \int_\Sigma \mathrm{Tr}\left(\boldsymbol{E} \wedge \delta \boldsymbol{A}\right), \tag{4.2}$$

where we denote by Tr the natural metric on $\mathfrak{su}(2)$ which is invariant under the adjoint action $\mathrm{Ad}_{\mathrm{SU}(2)}$ of the group. The phase space $\mathcal{P}$ also carries an action of the gauge group SU(2) and of spatial diffeomorphisms. In fact, since $\mathcal{P}$ is 18-dimensional at each point of Σ, the (first class) constraints of the canonical theory have to be taken into account in order to obtain the physical phase space with 4 degrees of freedom at each point. This can be achieved through the process of symplectic (or Hamiltonian) reduction, which we now describe.

Let P be a symplectic manifold, which is seen as the classical phase space of the theory of interest, and G a group of transformations. Suppose that the infinitesimal group transformations are generated via Poisson bracket by a constraint C. Then the Marsden-Weinstein theorem [61, 62, 63] ensures that the symplectic reduction of P by the group G, denoted by the double quotient $P/\!\!/G$, is still a symplectic manifold and carries a unique symplectic form. The reduced phase space is given by imposing the constraints and dividing the constraint surface by the action of gauge transformations. This is written as:

$$P/\!\!/G \equiv C^{-1}(0)/G. \tag{4.3}$$

The double quotient means to find a subclass of the phase space variables which satisfy the constraint C, and from these form equivalence classes defined by the gauge transformations.

For notational simplicity, below we will denote the group of transformations G and the associated constraint C with the same letters. Note that the Marsden-Weinstein theorem is proven in general for finite-dimensional phase spaces, but these methods are commonly extended to infinite-dimensional phase spaces. See [64] for a symplectic reduction of $\mathcal{P} \equiv T^*\mathcal{A}$, and the first two chapters of [19] for a description of this method as commonly employed in physics in the study of a Hamiltonian theory with constraints.

We can apply this to the phase space of four-dimensional gravity described in Chapter 2, where the physical phase space is obtained from the kinematical (unconstrained) phase space $\mathcal{P}$ by performing three symplectic reductions. The first one is defined with respect to the group of SU(2) gauge transformations, the Gauss constraint. Since the action of this gauge group on $\mathcal{P}$ is 'Hamiltonian', we can define the gauge-invariant phase space $T^*\mathcal{A}/\!\!/G$. More precisely, the Hamiltonian generating these transformations is the smeared Gauss constraint:

$$G(\boldsymbol{\lambda}) = \int_\Sigma \lambda^i (\mathrm{d}_A \boldsymbol{E})_i = 0, \tag{4.4}$$

where d_A denotes the covariant differential and $\boldsymbol{\lambda}$ is a Lie algebra-valued Lagrange multiplier. Its infinitesimal action on the phase space variables is given by:

$$\delta^G_{\boldsymbol{\lambda}} \boldsymbol{A} = \big\{\boldsymbol{A}, G(\boldsymbol{\lambda})\big\} = \mathrm{d}_A \boldsymbol{\lambda}, \qquad\qquad \delta^G_{\boldsymbol{\lambda}} \boldsymbol{E} = \big\{\boldsymbol{E}, G(\boldsymbol{\lambda})\big\} = [\boldsymbol{E}, \boldsymbol{\lambda}]. \tag{4.5}$$

The other relevant symplectic reduction is defined with respect to the group of spatial diffeomorphisms, and enables one to construct the diffeomorphism-invariant phase space $T^*\mathcal{A}/\!\!/\big(G \times \mathrm{Diff}(\Sigma)\big)$. Here, the action of the group of diffeomorphisms on the phase space variables generated by the vector constraint is given by:

$$\delta^V_\xi \boldsymbol{A} = \big\{\boldsymbol{A}, V(\xi)\big\} = \mathcal{L}_\xi \boldsymbol{A}, \qquad\qquad \delta^V_\xi \boldsymbol{E} = \big\{\boldsymbol{E}, V(\xi)\big\} = \mathcal{L}_\xi \boldsymbol{E}, \tag{4.6}$$

where $\mathcal{L}_\xi$ is the Lie derivative along the shift vector field ξ^a. Finally, the physical phase space can be obtained from the gauge and diffeomorphism-invariant phase space by performing a symplectic reduction with respect to the scalar constraint. The latter is given by:

$$S(N) = \int_\Sigma N E^a_i E^b_j 2\sqrt{\det(E^a_i)}\left(\epsilon^{ij}{}_k F^k_{ab} - 2(\gamma^2 - \sigma) K^i_{[a} K^j_{b]}\right) = 0, \tag{4.7}$$

where the smearing variable is the lapse function N, and $\sigma = \mp 1$ in Lorentzian or Riemannian signature respectively. Notice that for a (anti) 'self-dual' connection ($\gamma = \pm i$ in the Lorentzian case, or ± 1 in the Riemannian case) the second term vanishes and the constraint simplifies greatly.

4.2 From continuous to discrete data

Let us now develop the map from the continuous fields $(\boldsymbol{A}, \boldsymbol{E})$ to a discrete set of holonomies and fluxes $(h_\ell, \boldsymbol{X}_\ell)$ associated to a graph Γ. In order to construct the discrete data, let us first choose an embedded graph Γ within the spatial manifold Σ. Given this embedded graph, it is well understood in the discrete picture that the group elements h_ℓ represent holonomies of

the Ashtekar-Barbero connection A_a^i along links ℓ. It is necessary to work with such objects because an important step toward the quantization of the canonical theory is the smearing of the Poisson algebra. Since the connection A_a^i is a one-form, it is natural to smear it along paths ℓ. Now we could just take the integral of $\boldsymbol{A}$ along ℓ as a smearing but this will not respect the gauge transformations. What is needed is a smearing that does intertwine the notion of continuous and discrete gauge transformations. It is well known that this is given by the notion of parallel transport along ℓ, encoded in the holonomy we defined in the previous chapter:

$$h_\ell[\boldsymbol{A}] \equiv \overrightarrow{\exp} \int_\ell \boldsymbol{A} = \overrightarrow{\exp} \int_\ell A_a^i \dot{\ell}^a \boldsymbol{\tau}_i = \overrightarrow{\exp} \int_{s(\ell)}^{t(\ell)} A_a^i \dot{\ell}^a \boldsymbol{\tau}_i, \tag{4.8}$$

where $\dot{\ell}^a$ denotes the tangent vector to the path and $\overrightarrow{\exp}$ denotes the path-ordered exponential.

Let us recall the fundamental properties of the holonomy functional. The holonomy is invariant under reparametrizations of the path ℓ, and the holonomy of a path corresponding to a single point is the identity. If we consider the composition $\ell = \ell_1 \circ \ell_2$ of two paths which are such that $s(\ell_2) = t(\ell_1)$, the holonomy satisfies:

$$h_\ell = h_{\ell_1} h_{\ell_2}. \tag{4.9}$$

If we reverse the orientation of a path, we have:

$$h_{l^{-1}} = h_\ell^{-1}. \tag{4.10}$$

These properties come from the fact that the holonomy is a representation of the groupoid of oriented paths [65]. Under SU(2) gauge transformations, the holonomy transforms as:

$$g \triangleright h_\ell = g_{s(\ell)} h_\ell g_{t(\ell)}^{-1}, \tag{4.11}$$

which shows that the finite gauge transformation $g \triangleright \boldsymbol{A} = g\boldsymbol{A}g^{-1} + g\mathrm{d}g^{-1}$ of the connection becomes a discrete gauge symmetry acting on the nodes defining the boundary of the link ℓ. Finally, under the action of a diffeomorphism $\Phi \in \mathrm{Diff}(\Sigma)$, the holonomy transforms as:

$$h_\ell(\Phi^* \boldsymbol{A}) = h_{\Phi^{-1}(\ell)}[\boldsymbol{A}]. \tag{4.12}$$

The exact meaning of "momentum" variable $\boldsymbol{X}_\ell$ is less clear. Roughly speaking, we usually build a flux operator by smearing the field $\boldsymbol{E}_i^a$ along a surface f_ℓ dual to an link ℓ [3]. But if one wants this integrated flux to have a covariant behavior under gauge transformations, it is essential for the integration along f_ℓ to involve some notion of parallel transport. Indeed, the naive definition given in the Chapter 3 is the traditional definition:

$$\bar{\boldsymbol{X}}_\ell(E) = \int_{\mathsf{f}_\ell} \boldsymbol{E}(x), \tag{4.13}$$

but this is not covariant under gauge transformations, i.e.

$$\bar{\boldsymbol{X}}_\ell(g \triangleright \boldsymbol{E}) = \bar{\boldsymbol{X}}_\ell \left(g\boldsymbol{E}g^{-1}\right) \neq g_{s(\ell)} \bar{\boldsymbol{X}}_\ell(\boldsymbol{E}) g_{s(\ell)}^{-1}. \tag{4.14}$$

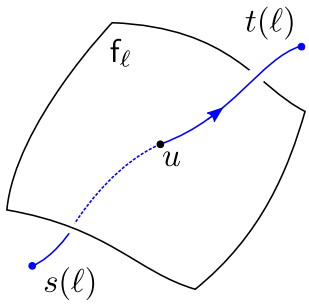

Figure 4.1: A link ℓ (in blue) which transversely intersects the dual face f_ℓ (in black) at the point u, shown as a filled black circle. The start $s(\ell)$ and terminal $t(\ell)$ ends of the link are shown as filled blue circles.

This is an important point which has often been ignored in the LQG literature, the only noticeable exceptions being [47, 66, 67], and more recently [52, 68]. For the holonomy, the only reason we consider the parallel transport operator instead of the simple integral of $\boldsymbol{A}$ along ℓ is to have a discretization covariant under gauge transformation. It is as important to preserve this covariance for the flux as it is for the holonomy. Another drawback is that the non-covariant definition of the flux does not produce the Poisson algebra given in (3.57), unless the intersection $\mathsf{f}_\ell \cap \ell$ between face and link is at the start point $s(\ell)$ or terminal point $t(\ell)$ of the link. If we consider a face that intersects somewhere in the middle of the link, i.e. write the link as $\ell = \ell_1 \circ \ell_2$ and have the intersection $\mathsf{f}_\ell \cap \ell = s(\ell_2) = t(\ell_1)$, then we have:

$$\left\{\bar{X}^i_\ell, h_{\ell'}\right\} = -\delta_{\ell\ell'} h_{\ell_1} \boldsymbol{\tau}^i h_{\ell_2} + \delta_{\ell\ell'^{-1}} h^{-1}_{\ell_1} \boldsymbol{\tau}^i h^{-1}_{\ell_2}, \tag{4.15}$$

which splits the holonomy in two.

The way around this problem is to define a flux operator which also depends on the connection through its holonomy, as first introduced in the paper [66]. Given an oriented link $\ell \in \Gamma$ and a point u on this link, we choose a surface f_ℓ intersecting ℓ transversely at $u = \mathsf{f}_\ell \cap \ell$ as shown in fig. 4.1. We also choose a set of paths π_ℓ assigning to any point $x \in \mathsf{f}_\ell$ a unique path π_ℓ going from the source $s(\ell)$ to x. Such a path starts at the source node of the link ℓ, goes along ℓ until it reaches the intersection point $u = \mathsf{f}_\ell \cap \ell$, and then goes from u to any point $x \in \mathsf{f}_\ell$ while staying tangential to the surface f_ℓ. More precisely, we have $\pi_\ell : \mathsf{f}_\ell \times [0,1] \longrightarrow \Sigma$ such that $\pi_\ell(x,0) = s(\ell)$ and $\pi_\ell(x,1) = x$. With the set of data $(\mathsf{f}_\ell, \pi_\ell)$, one can define the flux:

$$\boldsymbol{X}_{(\mathsf{f}_\ell,\pi_\ell)}[\boldsymbol{A}, \boldsymbol{E}] \equiv \int_{\mathsf{f}_\ell} h_{\pi_\ell}(x) \boldsymbol{E}(x) h_{\pi_\ell}(x)^{-1}, \tag{4.16}$$

where:

$$h_{\pi_\ell}(x) \equiv \overrightarrow{\exp} \int_{s(\ell)}^{x} \boldsymbol{A}. \tag{4.17}$$

Notice that by definition, the source of the path π_ℓ is $s(\ell)$, and its target is the point $x \in \mathsf{f}_\ell$. Therefore, under the gauge transformations:

$$g \triangleright \boldsymbol{E}(x) = g(x) \boldsymbol{E}(x) g(x)^{-1}, \qquad g \triangleright h_{\pi_\ell}(x) = g_{s(\ell)} h_{\pi_\ell}(x) g(x)^{-1}, \tag{4.18}$$

the flux operator becomes:

$$\boldsymbol{X}_{(\mathsf{f}_\ell,\pi_\ell)}(g \triangleright \boldsymbol{A}, g \triangleright \boldsymbol{E}) = g_{s(\ell)} \boldsymbol{X}_{(\mathsf{f}_\ell,\pi_\ell)}(\boldsymbol{A}, \boldsymbol{E}) g_{s(\ell)}^{-1}, \tag{4.19}$$

which is in agreement with (3.59). The existence of a covariant transformation property is one of the main justifications for introducing the extra holonomy dependance in the definition of the flux operator. With the definition (4.16), the flux operator intertwines the continuous and discrete actions of the gauge group.

From the definition of the paths π_ℓ we see that reversing the orientation of the link gives a system of paths beginning at $t(\ell)$ and ending at a point $x \in \mathsf{f}_\ell$, i.e. $\pi_{\ell^{-1}}(x,0) = t(\ell)$ and $\pi_{\ell^{-1}}(x,1) = x$. This implies that $\pi_{\ell^{-1}} = \ell^{-1} \circ \pi_\ell$, and therefore:

$$h_{\pi_{\ell^{-1}}}(x) = h_\ell^{-1} h_{\pi_\ell}(x). \tag{4.20}$$

Moreover, the surface f_ℓ possesses a reverse orientation $\mathsf{f}_{\ell^{-1}} = -\mathsf{f}_\ell$, and thus we have:

$$\boldsymbol{X}_{\left(\mathsf{f}_{\ell^{-1}},\pi_{\ell^{-1}}\right)} = -h_\ell^{-1} \boldsymbol{X}_{(\mathsf{f}_\ell,\pi_\ell)} h_\ell, \tag{4.21}$$

which proves that our mapping is consistent with (3.56). Notice also that any two fluxes that differ only by the choice of surfaces are in the commutant of the holonomy algebra:

$$\left\{ X_{(\mathsf{f}'_\ell,\pi'_\ell)} - X_{(\mathsf{f}_\ell,\pi_\ell)}, h_\ell \right\} = 0, \tag{4.22}$$

where π_ℓ and π'_ℓ each follow the link until the intersection points with their respective surfaces as defined above. An important feature of the mapping that we have described is that it reproduces the Poisson algebra (3.57), specifically the Poisson bracket between flux and holonomy. To show this, let us use the notation $R(h_{\pi_\ell})^i_j E^j \equiv (h_{\pi_\ell} \boldsymbol{E} h_{\pi_\ell}^{-1})^i$ in writing the flux. In the case where the flux and holonomy are associated to the same link and have the same orientation, we have:

$$\begin{aligned}
\left\{ X^i_{(\mathsf{f}_\ell,\pi_\ell)}(\boldsymbol{A}, \boldsymbol{E}), h_e[\boldsymbol{A}] \right\} &= \int_{\mathsf{f}_\ell} R(h_{\pi_\ell})^i_j \left\{ E^j, h_\ell[\boldsymbol{A}] \right\} \\
&= -R(h_{\ell_1})^i_j h_{\ell_1} \boldsymbol{\tau}^j h_{\ell_2} \\
&= -h_{\ell_1} h_{\ell_1}^{-1} \boldsymbol{\tau}^i h_{\ell_1} h_{\ell_2} \\
&= -\boldsymbol{\tau}^i h_\ell,
\end{aligned} \tag{4.23}$$

where we are using the same notation as above when splitting the link into ℓ_1 and ℓ_2 at the point of intersection, and we have $h_{\pi_\ell} = h_{\ell_1}$ at the only point contributing to the integral in the first line. Also notice that the SU(2) rotation $R(h_{\pi_\ell})^i_j$ acts on the basis elements $\boldsymbol{\tau}^i$ inversely to the way it acts on $\boldsymbol{E}^i$. A similar calculation with the inverse holonomy yields the second term shown in (3.57).

Finally, we know that the requirement of consistency with the Jacobi identity imposes that the fluxes do not commute among each other as shown in Chapter 3. This property, which seems inconsistent if $\boldsymbol{X}_\ell$ depends purely on the (commuting) densitized triad field, is perfectly understandable if the flux depends also on the connection, and provides a natural explanation to the "mystery" behind the non-commutativity of the fluxes [69]. This is consistent with the

understanding of the spin network phase space in terms of twisted geometries [52], where it appears clearly that the flux operators also contain information about the holonomies, and cannot be thought of as being purely geometrical. In other words, the flux operators are not commuting because they capture information not only about the intrinsic geometry, but also about the extrinsic curvature.

The map that we have described depends on three types of data. It depends on a choice of embedded graph Γ defining a network of links ℓ in Σ, a choice of surface f_ℓ transverse to each link ℓ at u, and a choice of paths π_ℓ going from each $s(\ell)$ to a point $x \in \mathsf{f}_\ell$. Once this data is given, we can construct a map:

$$\begin{array}{rccl} I: & \mathcal{P} & \longrightarrow & P_\Gamma \\ & (\boldsymbol{A}, \boldsymbol{E}) & \longmapsto & \big(h_\ell[\boldsymbol{A}], X_{(\mathsf{f}_\ell,\pi_\ell)}(\boldsymbol{A}, \boldsymbol{E})\big)\,, \end{array} \tag{4.24}$$

which has the key property of intertwining gauge transformations on the continuous and discrete phase spaces, is compatible with the orientation reversal of the links, and respects the Poisson structure of $T^*\mathrm{SU}(2)$.

4.3 From discrete to continuous data

Now we would like to investigate to what extent it is possible to invert the map from continuous to discrete data $I : \mathcal{P} \longrightarrow P_\Gamma$. In other words, to what extent does the discrete data determine the continuous data? Can we reconstruct a unique representative of the continuous data starting from the discrete one, or describe a specific equivalence class?

At first sight, this seems like an impossible task since the flux is not uniquely defined by the electric field $\boldsymbol{E}$. There are several ambiguities in its definition. There are many possible choices of surfaces f_ℓ that are transverse to the link ℓ, and also many possible paths that one can choose on f_ℓ. Different choices lead to different mappings from the continuous data to the discrete data. This means that giving a flux $\boldsymbol{X}_{(\mathsf{f}_\ell,\pi_\ell)}$ (which we will call $\boldsymbol{X}_\ell$ for simplicity) does not allow one to reconstruct a continuous field $\boldsymbol{E}$, which constitutes a fundamental ambiguity. This state of affairs is fine if one treats the discrete data as some approximate description of continuous geometry which only takes physical meaning in some continuous limit. This is the usual point of view [43], and it implies that operators expressed in terms of the fluxes $\boldsymbol{X}_\ell$ do not have a sharp semi-classical geometric interpretation.

In this work we would like to be more ambitious and interpret the discrete data as potential initial value data for the continuous theory of gravity. The challenge is to show that one can reconstruct continuous fields $(\boldsymbol{A}, \boldsymbol{E})$ explicitly from the knowledge of an embedded graph and the associated discrete data $(h_\ell, \boldsymbol{X}_\ell)$. How can this be possible in light of all the ambiguities that we have listed above? In order to make some progress in this direction, let us first remark that there are configurations of fields for which the ambiguities disappear. This is the case in particular for a flat connection.

Suppose that we focus on a region c_n of simple topology (isomorphic to a three-ball) around a node $\mathsf{n} \in c_\mathsf{n}$, and that in this region the connection $\boldsymbol{A}$ is flat. In this case, the expression (4.16) for the flux becomes independent of the system of paths π_ℓ, since the flatness of the connection

implies that there exists an SU(2) element $a(x)$ such that $\boldsymbol{A} = a\mathrm{d}a^{-1}$ and $h_{\pi_\ell}(x) = a(v)a(x)^{-1}$. Indeed, we have

$$\boldsymbol{X}_{(\mathsf{f}_\ell,\pi_\ell)} = \boldsymbol{X}_\ell = a(\mathsf{n})\left(\int_{\mathsf{f}_\ell} a(x)^{-1}\boldsymbol{E}(x)a(x)\right)a(\mathsf{n})^{-1}, \tag{4.25}$$

and the dependence on the system of paths has disappeared. Moreover, one can see that the Gauss law expresses the fact that $X^i_{\mathsf{f}_\ell} = X^i_{\mathsf{f}'_\ell}$, for if f_ℓ and f'_ℓ have the same oriented boundary, their union encloses a volume and we have that:

$$0 = \int_{c_\mathsf{n}} a(x)^{-1}\mathrm{d}_A\boldsymbol{E}(x)a(x) = \int_{c_\mathsf{n}} \mathrm{d}\left(a(x)^{-1}\boldsymbol{E}(x)a(x)\right) = a(\mathsf{n})^{-1}\left(\boldsymbol{X}_{\mathsf{f}_\ell} - \boldsymbol{X}_{\mathsf{f}'_\ell}\right)a(\mathsf{n}). \tag{4.26}$$

In the next section, we are going to make this statement more precise, and study the case of a partially flat connection.

4.3.1 Partially flat connection

In this section, we formulate and prove the equivalence between the continuous phase space of partially flat geometries and the discrete spin network phase space. In order to do so, we first need to introduce some notions of topology.

An important geometrical construct that we rely upon is a CW complex[2] [70], a rather general way of gluing together cells to form a cell complex. A CW complex Δ of dimension n can be decomposed in terms its i-skeleton Δ_i, $i = 0, \cdots, n$. Δ_i is defined recursively by gluing a disjoint union of dimension i open balls $\mathring{B}_i$, to Δ_{i-1}. In the following we denote by $c_i \approx \mathring{B}_i$ the open cells of dimension i. We denote by $\bar{c}_i$ the closure of c_i and by $\partial c_i = \bar{c}_i \backslash c_i$ its boundary. We have that $\partial c_i \approx S^{i-1}$.

Let us now be more precise about the definition of the i-skeleton Δ_i. Suppose that the $(i-1)$-skeleton Δ_{i-1} is given. We introduce *gluing maps* s^i and define Δ_i by gluing i-dimensional cells to Δ_{i-1}:

$$s^i : \partial c_i \to \Delta_{i-1}, \qquad \Delta_i \equiv \left(\Delta_{i-1} \coprod_{c_i} c_i\right) / \sim, \tag{4.27}$$

where the quotient by $\sim$ denotes the identification provided by the gluing maps: given $x \in \partial c_i$, $y \in \Delta_{i-1}$ we say that $x \sim y$ if $s^i(x) = y$. This formula means that we obtain Δ_i by quotienting the disjoint union of Δ_{i-1} and c_i by the identification relation provided by the gluing maps s^i. In this way we can start with a set of points Δ_0 and build up to dimension i recursively. Note that $\bar{c}_i$ is itself included in Δ_i and under this inclusion it becomes itself an *elementary* cell complex whose boundary can be decomposed into cells of different dimensions.

Since we are interested specifically in dimension 3 we will denote the three-dimensional open cells by c, the two-dimensional open cells (called faces) by f, the one-dimensional open cells (called edges) by e, and the zero dimensional cells (the vertices) by v. In the following

[2]The 'C' is for closure-finite and the 'W' is for weak topology.

$(c, \mathsf{f}, \mathsf{e})$ always denote open cells, their closure is denoted by $(\bar{c}, \bar{\mathsf{f}}, \bar{\mathsf{e}})$ and their boundary is $\partial c = \bar{c} \backslash c$.

A CW complex can be a very general object. Here we are going to study a subclass of CW complexes that we call regular (see [71] for a related discussion in the piecewise linear context).

Definition 4.3.1. A regular three-dimensional cellular space Δ is a collection of three-dimensional cells c, glued together. We demand that:
1) The closure of each cell is diffeomorphic to a convex polyhedra $P_c \subset \mathbb{R}^3$; the diffeomorphism is denoted $\psi_c : \bar{c} \to P_c$. We denote by $(\mathsf{f}_c, \mathsf{e}_c, \mathsf{v}_c) \subset \partial c$, the inverse images of (respectively) the faces, edges and vertices of the boundary of P_c.
2) There exist invertible gluing maps for the unique pair of cells that are glued along f:

$$s_{cc'} : \quad \bar{\mathsf{f}}_c \to \bar{\mathsf{f}}_{c'}. \tag{4.28}$$

Moreover the restriction of these maps to the boundary of the face $\partial \mathsf{f}_c$ are invertible maps onto $\partial \mathsf{f}_{c'}$. The three-dimensional cell complex is defined as the quotient space $\sqcup_c c/\sim$ where $x \in \bar{f}_c$ is equivalent to $y \in \bar{\mathsf{f}}_{c'}$ when $s_{cc'}(x) = y$. Where cells are glued together, each face is identified with a single other face that it is glued to, and multiple edges are mapped to each other and identified under the gluing maps. These identifications allow us to have consistent definitions of the two-skeleton Δ_2 and one-skeleton Δ_1.

Notice that the n-skeleton of a cellular space is also a cellular space, and in particular, the one-skeleton $\Delta_1 \equiv \Gamma^*$ of a cellular space is a graph. The one-skeleton Γ^* is not however the graph Γ upon which the holonomies and fluxes are defined. There is a duality relationship between the graphs (Γ, Γ^*) which we now define.

Definition 4.3.2. A regular, three-dimensional cellular space Δ is said to be dual to the graph Γ if there is a one-to-one correspondence $\mathsf{n} \longmapsto c_{\mathsf{n}}$ between nodes of Γ and three-cells of Δ, and a one-to-one correspondence $\ell \longmapsto \mathsf{f}_\ell$ between links of Γ and two-cells of Δ, such that:

i) There is a unique node n inside each three-cell c_{n}.

ii) The two-cells f_ℓ intersect Γ transversally at one point only, and the intersection belongs to the interior of the link ℓ of Γ.

In other words, a cellular space dual to Γ is such that each node of Γ is dual to a three-cell, and each link of Γ is dual to a two-cell. Each link ℓ is a path between two nodes, starting at the unique node $n \in c_{\mathsf{n}}$ and ending at the node $\mathsf{n}' \in c'_{\mathsf{n}'}$, and the inverse is denoted ℓ^{-1}. The the point of intersection between the link and face $x = \ell \cap \mathsf{f}_{cc'}$ is mapped to the point of intersection as seen in the neighbouring cell $y = \ell \cap f_{c'c}$ under the gluing maps, i.e. $y = s_{cc'}(x)$. See fig. 4.2.

Now let us consider a pair (Γ, Γ^*) of graphs.

Definition 4.3.3. We say that an embedded graph Γ is dual to the graph Γ^* (and vice versa), or that (Γ, Γ^*) forms a pair of dual graphs, if there exists a graph Γ dual to a cellular space Δ whose one-skeleton Δ_1 is Γ^*.

Notice that if we take any diffeomorphism which is *connected to the identity*, then the duality between $(\Gamma, \Gamma^*))$ is preserved. Given any cellular space Δ, there are many ways to embed a dual graph.

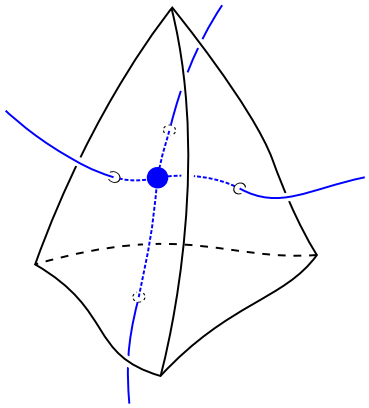

Figure 4.2: A single cell c of a CW complex and its dual node n in a graph Γ. The faces f and edges e in the cell boundary are shown in black. In blue we have shown the node n embedded within the cell, with a link ℓ piercing each face.

From now on, we consider that (Γ, Γ^*) is a pair of dual embedded graphs, and we denote by Δ the cellular space dual to Γ with a one-skeleton Δ_1 given by Γ^*. We take our three-geometry Σ to be the cellular space Δ. Given such a pair of dual graphs, we are going to construct a certain phase space $\mathcal{P}_{\Gamma,\Gamma^*}$, and prove that it is the continuous analogue of the discrete spin network phase space P_Γ. In fact, we are going to show that there is a symplectomorphism between $\mathcal{P}_{\Gamma,\Gamma^*}$ and P_Γ.

4.3.2 The reduced phase space $\mathcal{P}_{\Gamma,\Gamma^*}$

To define the reduced phase space $\mathcal{P}_{\Gamma,\Gamma^*}$, we first construct a group $\mathcal{F}_{\Gamma^*} \times G_\Gamma$ of gauge transformations acting on $\mathcal{P}$. For this, let us consider an infinite-dimensional Abelian group of transformations $\mathcal{F}_{\Gamma^*}$ parametrized by Lie algebra-valued one-forms $\phi^i \in \Omega^1\big(\Sigma, \mathfrak{su}(2)\big)$ which have the property that they vanish on Γ^*:

$$\phi^i(x) = 0, \qquad \forall\, x \in \Gamma^*. \tag{4.29}$$

This group action is Hamiltonian and generated by the curvature constraint:

$$\mathcal{F}_{\Gamma^*}(\phi) = \int_\Sigma \phi_i \wedge F^i[\boldsymbol{A}], \tag{4.30}$$

whose action on the continuous phase space $\mathcal{P}$ is given by:

$$\delta_\phi^{\mathcal{F}_{\Gamma^*}} \boldsymbol{A} = \big\{\boldsymbol{A}, \mathcal{F}_{\Gamma^*}(\boldsymbol{\phi})\big\} = 0, \qquad \delta_\phi^{\mathcal{F}_{\Gamma^*}} \boldsymbol{E} = \big\{\boldsymbol{E}, \mathcal{F}_{\Gamma^*}(\boldsymbol{\phi})\big\} = \mathrm{d}_A \boldsymbol{\phi}. \tag{4.31}$$

This constraint enforces the flatness of the connection outside of the one-skeleton graph Γ^*. See The second group, G_Γ, is the group of gauge transformations parametrized by Lie algebra-valued functions $\lambda^i \in \Omega^0\big(\Sigma, \mathfrak{su}(2)\big)$ which have the property that they vanish on the nodes of

Γ:

$$\lambda^i(x) = 0, \qquad \forall\, x \in \mathsf{n}_\Gamma. \tag{4.32}$$

This group action is also Hamiltonian. It is generated by the smeared Gauss constraint:

$$G_\Gamma(\boldsymbol{\lambda}) = \int_\Sigma \lambda^i (\mathrm{d}_A \boldsymbol{E})_i, \tag{4.33}$$

whose infinitesimal action on the phase space variables is given by:

$$\delta_\lambda^{G_\Gamma} \boldsymbol{A} = \big\{\boldsymbol{A}, G_\Gamma(\boldsymbol{\lambda})\big\} = \mathrm{d}_A \boldsymbol{\lambda}, \qquad \delta_\lambda^{G_\Gamma} \boldsymbol{E} = \big\{\boldsymbol{E}, G_\Gamma(\boldsymbol{\lambda})\big\} = [\boldsymbol{E}, \boldsymbol{\lambda}]. \tag{4.34}$$

From the various Poisson brackets:

$$\big\{G_\Gamma(\boldsymbol{\lambda}), G_\Gamma(\boldsymbol{\lambda}')\big\} = G_\Gamma([\boldsymbol{\lambda}, \boldsymbol{\lambda}']), \tag{4.35a}$$

$$\big\{G_\Gamma(\boldsymbol{\lambda}), \mathcal{F}_{\Gamma^*}(\boldsymbol{\phi})\big\} = \mathcal{F}_{\Gamma^*}([\boldsymbol{\lambda}, \boldsymbol{\phi}]), \tag{4.35b}$$

$$\big\{\mathcal{F}_{\Gamma^*}(\boldsymbol{\phi}), \mathcal{F}_{\Gamma^*}(\boldsymbol{\phi}')\big\} = 0, \tag{4.35c}$$

we see that the Hamiltonians (4.30) and (4.33) form a first class algebra.

We are interested in the phase space obtained from $\mathcal{P}$ by symplectic reduction with respect to $\mathcal{F}_{\Gamma^*}$ and G_Γ, which we denote by:

$$\mathcal{P}_{\Gamma,\Gamma^*} \equiv T^*\mathcal{A} /\!\!/ \big(\mathcal{F}_{\Gamma^*} \times G_\Gamma\big) = \mathcal{C} / \big(\mathcal{F}_{\Gamma^*} \times G_\Gamma\big), \tag{4.36}$$

where:

$$\mathcal{C} \equiv \big\{(\boldsymbol{A}, \boldsymbol{E}) \in T^*\mathcal{A} | F[\boldsymbol{A}](x) = \mathrm{d}_A E(y) = 0,\, \forall\, x \in \Sigma\backslash\Gamma^*,\, \forall\, y \in \Sigma\backslash V_\Gamma\big\} \tag{4.37}$$

is the constrained space. This is the infinite-dimensional space of flat SU(2) connections on $\tilde{\Sigma} \equiv \Sigma\backslash\Gamma^*$, and fluxes satisfying the Gauss law outside of V_Γ. Once we divide this constrained space by the action of the two gauge groups introduced above, we obtain the finite-dimensional orbit space $\mathcal{P}_{\Gamma,\Gamma^*}$ [64]. We are going to prove that $\mathcal{P}_{\Gamma,\Gamma^*}$ is the continuous analogue of the discrete spin network phase space P_Γ.

Explicitly, the space $\tilde{\Sigma}$ can be written as:

$$\tilde{\Sigma} = \bigcup_{\mathsf{n}} c_{\mathsf{n}} \bigcup_{\ell} \mathsf{f}_\ell, \tag{4.38}$$

where c_{n} are three-dimensional open cells labeled by the nodes $\mathsf{n} \in \Gamma$, and f_ℓ are two-dimensional open cells labeled by the links $\ell \in \Gamma$. We would like to solve the curvature constraint $\boldsymbol{F}[\boldsymbol{A}] = \mathrm{d}_A \boldsymbol{A} = 0$ on $\tilde{\Sigma}$ and the Gauss constraint $\mathrm{d}_A \boldsymbol{E} = 0$ on $\Sigma\backslash\mathsf{n}_\Gamma$. We start by solving them for each three-dimensional cell c_{n}.

To solve the curvature constraint, let us define on a three-cell c_{n} a group-valued map $a_{\mathsf{n}}(x) : c_{\mathsf{n}} \longrightarrow \mathrm{SU}(2)$ as the path-ordered exponential:

$$a_{\mathsf{n}}(x) \equiv \overrightarrow{\exp} \int_x^v \boldsymbol{A}, \tag{4.39}$$

where the integration can be taken over any arbitrary path from the point $x \in c_{\mathsf{n}}$ to the node n because the connection is flat and c_{n} is simply connected. By construction, this map is such that $a_{\mathsf{n}}(v) = \mathrm{id}$. This allows us to reconstruct on c_{n} the flat connection $\boldsymbol{A}$ as:

$$\boldsymbol{A}(x) = a_{\mathsf{n}}(x)\mathrm{d}a_{\mathsf{n}}^{-1}(x). \tag{4.40}$$

The second constraint to satisfy is the Gauss law outside of the node n which lies inside the cell c_{n}. Because the connection is flat, the covariant derivative of the electric field $\boldsymbol{E}$ can be written as:

$$\mathrm{d}_A\boldsymbol{E} = dE + \left[a_{\mathsf{n}}\mathrm{d}a_{\mathsf{n}}^{-1}, \boldsymbol{E}\right] = a_{\mathsf{n}}\mathrm{d}\left(a_{\mathsf{n}}^{-1}\boldsymbol{E}a_{\mathsf{n}}\right)a_{\mathsf{n}}^{-1} = a_{\mathsf{n}}\mathrm{d}\boldsymbol{X}_{\mathsf{n}}a_{\mathsf{n}}^{-1}, \tag{4.41}$$

where we have introduced the Lie algebra-valued two-form field:

$$\boldsymbol{X}_{\mathsf{n}}(x) \equiv a_{\mathsf{n}}(x)^{-1}\boldsymbol{E}(x)a_{\mathsf{n}}(x). \tag{4.42}$$

Therefore, we see that the Gauss law implies that the two-form $\boldsymbol{X}_{\mathsf{n}}$ is closed outside of n since:

$$\mathrm{d}\boldsymbol{X}_{\mathsf{n}}(x) = a_{\mathsf{n}}(x)^{-1}\mathrm{d}_A\boldsymbol{E}(x)a_{\mathsf{n}}(x) = 0, \qquad \forall\, x \in c_{\mathsf{n}} - \{\mathsf{n}\}. \tag{4.43}$$

The electric field can now easily be reconstructed since we have:

$$\boldsymbol{E}(x) = a_{\mathsf{n}}(x)\boldsymbol{X}_{\mathsf{n}}(x)a_{\mathsf{n}}(x)^{-1}. \tag{4.44}$$

One can conclude that a general solution of the two constraints $\boldsymbol{F}[\boldsymbol{A}] = \mathrm{d}_A\boldsymbol{A} = 0$ and $\mathrm{d}_A\boldsymbol{E} = 0$ on c_{n} and $c_{\mathsf{n}} - \{\mathsf{n}\}$ respectively, is given in terms of a Lie algebra-valued closed two-form $\boldsymbol{X}_{\mathsf{n}}$ and a group element $a_{\mathsf{n}} : c_{\mathsf{n}} \longrightarrow \mathrm{SU}(2)$, the connection and flux fields being given by (4.40) and (4.44).

Now we can extend this solution to the whole space $\tilde{\Sigma}$ by gluing consistently the solutions on each cell. Recall that the two-dimensional cells f_ℓ are oriented, and that their orientation is reversed when we change the orientation of the link ℓ. Demanding that the connection and flux fields be continuous across the two-dimensional cells amounts to assuming that there exists, for each f_ℓ, an SU(2) element h_ℓ such that:

$$\lim_{x' \to \mathsf{e}_{c'c}} a_{\mathsf{n}'}(x') = \lim_{x \to \mathsf{e}_{cc'}} a_{\mathsf{n}}(x)h_{cc'}, \qquad \lim_{x' \to \mathsf{e}_{c'c}} \mathrm{d}a_{\mathsf{n}'}(x') = \lim_{x \to \mathsf{e}_{cc'}} \mathrm{d}a_{\mathsf{n}}(x)h_{cc'}, \tag{4.45}$$

$$\lim_{x' \to \mathsf{e}_{c'c}} \boldsymbol{X}_{\mathsf{n}'}(x') = \lim_{x \to \mathsf{e}_{cc'}} h_{cc'}^{-1}\boldsymbol{X}_{\mathsf{n}}(x)h_{cc'}, \tag{4.46}$$

for $x \in \mathsf{f}_{cc'}$ and $x' = s_{cc'}(x) \in \mathsf{f}_{c'c}$. The limits are required in the definition since the connection and fields are defined piecewise by the a_c and $\boldsymbol{X}_{\mathsf{n}}$ fields in each cell. Notice that the first equality can be written as:

$$h_\ell[\boldsymbol{A}] = a_{s(\ell)}(x)^{-1}a_{t(\ell)}(s_{cc'}(x)) = \overrightarrow{\exp}\int_\ell \boldsymbol{A}, \tag{4.47}$$

where x is any point on the two-cell $\mathsf{f}_{cc'}$, and once again the definition does not depend on x because the connection is flat. By construction, one can see that under an orientation reversal we have $h_{\ell^{-1}} = h_\ell^{-1}$.

This construction shows that the constrained space $\mathcal{C}$ is isomorphic to the data $(a_{\mathsf{n}}, \boldsymbol{X}_{\mathsf{n}}, h_\ell)$, subject to the conditions (4.45, 4.46). We are now interested in the quotient of this constrained space by the gauge group $\mathcal{F}_{\Gamma^*} \times G_\Gamma$. Elements of this gauge group are pairs $\big(\boldsymbol{\phi}(x), g_o(x)\big)$, where $\boldsymbol{\phi}$ is a Lie algebra-valued one-form which vanishes on Γ^*, and g_o is an element of SU(2) (obtained by exponentiation of $\boldsymbol{\lambda}$) fixed to the identity of the group at the nodes n_Γ. The action of $\mathcal{F}_{\Gamma^*} \times G_\Gamma$ on the pair $(\boldsymbol{A}, \boldsymbol{E}) \in \mathcal{P}$ translates on the constraint surface $\mathcal{C}$ into an action on the data $(a_{\mathsf{n}}, \boldsymbol{X}_{\mathsf{n}}, h_\ell)$ given by:

$$a_{\mathsf{n}}(x) \longrightarrow g_o(x) a_{\mathsf{n}}(x), \qquad \boldsymbol{X}_{\mathsf{n}}(x) \longrightarrow \boldsymbol{X}_{\mathsf{n}}(x) + \mathrm{d}\left(a_{\mathsf{n}}(x)^{-1} \boldsymbol{\phi}(x) a_{\mathsf{n}}(x)\right), \qquad h_\ell \longrightarrow h_\ell. \tag{4.48}$$

Following (4.16), let us compute the flux $\boldsymbol{X}_\ell$ across a surface dual to an link ℓ which is such that $s(\ell) = \mathsf{n}$. It is given by:

$$\boldsymbol{X}_\ell = \int_{\mathsf{f}_\ell} h_{\pi_\ell}(x) \boldsymbol{E}(x) h_{\pi_\ell}(x)^{-1} = \int_{\mathsf{f}_\ell} a_{\mathsf{n}}(v) a_{\mathsf{n}}(x)^{-1} \boldsymbol{E}(x) a_{\mathsf{n}}(x) a_{\mathsf{n}}(v)^{-1} = \int_{\mathsf{f}_\ell} \boldsymbol{X}_{\mathsf{n}}, \tag{4.49}$$

where we have used the fact that $a_{\mathsf{n}}(v) = 1$. We see that the observables which are invariant under this gauge transformation are simply given by the holonomies h_ℓ and the fluxes $\boldsymbol{X}_\ell$.

4.3.3 The symplectomorphism between $\mathcal{P}_{\Gamma,\Gamma^*}$ and P_Γ

Now we come to our main result, which is the symplectomorphism between the continuous phase space $\mathcal{P}_{\Gamma,\Gamma^*}$ and the discrete spin network phase space P_Γ. Let us construct a map between the constrained continuous data in $\mathcal{C}$ (see (4.37)) and discrete data on the spin network phase space P_Γ, and denote it by

$$\begin{array}{rccc} \mathcal{I}: & \mathcal{C} & \longrightarrow & P_\Gamma \\ & (\boldsymbol{A}, \boldsymbol{E}) & \longmapsto & \big(h_\ell[\boldsymbol{A}], \boldsymbol{X}_\ell(\boldsymbol{A}, \boldsymbol{E})\big). \end{array} \tag{4.50}$$

For this, we define for every three-cell c_{n} a group-valued map $a_{\mathsf{n}} : c_{\mathsf{n}} \longrightarrow \mathrm{SU}(2)$ such that $a_{\mathsf{n}}(v) = \mathrm{id}$ and a Lie algebra-valued two-form $X_{\mathsf{n}} : c_{\mathsf{n}} \longrightarrow \Omega^2\big(c_{\mathsf{n}}, \mathfrak{su}(2)\big)$ closed outside of the nodes of Γ. Given these fields, we can reconstruct on c_{n} the connection and the two-form field using:

$$\boldsymbol{A}(x) = a_{\mathsf{n}}(x) \mathrm{d} a_{\mathsf{n}}(x)^{-1}, \qquad \boldsymbol{E}(x) = a_{\mathsf{n}}(x) \boldsymbol{X}_{\mathsf{n}}(x) a_{\mathsf{n}}(x)^{-1}. \tag{4.51}$$

The map $\mathcal{I}$ is then defined by:

$$h_\ell[\boldsymbol{A}] \equiv \overrightarrow{\exp} \int_\ell \boldsymbol{A} = a_{s(\ell)}(x)^{-1} a_{t(\ell)}(x), \tag{4.52a}$$

$$\boldsymbol{X}_\ell(\boldsymbol{A}, \boldsymbol{E}) \equiv \int_{\mathsf{f}_\ell} h_{\pi_\ell}(x) \boldsymbol{E}(x) h_{\pi_\ell}(x)^{-1} = \int_{\mathsf{f}_\ell} \boldsymbol{X}_{s(\ell)}(x), \tag{4.52b}$$

where in the definition of h_ℓ, x is any point on the two-cell f_ℓ, and once again the definition does not depend on x because the connection is flat. To compute the holonomy h_ℓ, we have used the group elements $a_{s(\ell)}(x)$ and $a_{t(\ell)}(x)$ to define the connection on the two cells dual to the nodes $s(\ell)$ and $t(\ell)$ respectively.

It is possible to use equation (4.52b) to write down the relationship between the discrete and continuous Gauss laws. We already know from (4.43) that the Gauss law is equivalent to the requirement that the two-form $\boldsymbol{X}_{\mathsf{n}}$ be closed outside of the node n. We can now write that

$$\int_{c_{\mathsf{n}}} a_{\mathsf{n}}(x)^{-1}\mathrm{d}_A\boldsymbol{E}(x)a_{\mathsf{n}}(x) = \int_{c_{\mathsf{n}}} \mathrm{d}\boldsymbol{X}_{\mathsf{n}} = \int_{\cup_\ell \mathsf{f}_\ell = \partial c_{\mathsf{n}}} \boldsymbol{X}_{s(\ell)} = \sum_{\ell | s(\ell)=\mathsf{n}} \boldsymbol{X}_\ell = \boldsymbol{G}_{\mathsf{n}}, \tag{4.53}$$

which relates the continuous and discrete constraints. This shows that the violation of the continuous Gauss constraint is located at the nodes of Γ, and given by a distribution determined by the discrete Gauss constraint introduced in Chapter 3:

$$\mathrm{d}_A\boldsymbol{E}(x) = \sum_{\mathsf{n}\in\mathsf{n}_\Gamma} \boldsymbol{G}_{\mathsf{n}}\delta(x-\mathsf{n}). \tag{4.54}$$

Since the map $\mathcal{I}$ is invariant under the gauge transformations $\mathcal{F}_{\Gamma^*}\times G_\Gamma$ we can write it as a map

$$[\mathcal{I}] : \mathcal{P}_{\Gamma,\Gamma^*} \longrightarrow P_\Gamma.$$

We will now show that this map is not only invertible, but also a symplectomorphism.

Proposition 4.3.4. *The map $[\mathcal{I}] : \mathcal{P}_{\Gamma,\Gamma^*} \longrightarrow P_\Gamma$ defined by (4.52) is a symplectomorphism, and is invariant under the action of diffeomorphisms connected to the identity preserving Γ^* and the set n_Γ of nodes of Γ.*

We are going to prove this proposition in the remainder of this work. Before doing so, let us stress that this result implies the existence of an inverse map which allows one to reconstruct from the discrete data an equivalence class $[\boldsymbol{A}(h_\ell), E(h_\ell, \boldsymbol{X}_\ell)]$ of continuous configurations satisfying the curvature and Gauss constraints (i.e. configurations in the constrained space $\mathcal{C}$). Explicitly, this equivalence class is defined with respect to the equivalence relation:

$$(\boldsymbol{A},\boldsymbol{E}) \sim \big(g_o \triangleright \boldsymbol{A}, g_o^{-1}(\boldsymbol{E}+\mathrm{d}_A\boldsymbol{\phi})g_o\big)\,, \tag{4.55}$$

where once again $\boldsymbol{\phi}$ is a Lie algebra-valued one-form vanishing on Γ^*, and g_o is an element of SU(2) fixed to the identity of the group at the nodes n_Γ.

Evidently, Proposition 4.3.4 implies a similar proposition for the gauge-invariant phase spaces. Indeed, if one defines:

$$\mathcal{P}^G_{\Gamma^*} \equiv T^*\mathcal{A}/\!\!/\big(\mathcal{F}_{\Gamma^*}\times G\big) = \mathcal{C}^G/\big(\mathcal{F}_{\Gamma^*}\times G\big), \tag{4.56}$$

where:

$$\mathcal{C}^G \equiv \big\{(\boldsymbol{A},\boldsymbol{E})\in T^*\mathcal{A} | \boldsymbol{F}[\boldsymbol{A}](x) = \mathrm{d}_A\boldsymbol{E}(y) = 0,\ \forall\, x\in\Sigma\backslash\Gamma^*,\ \forall\, y\in\Sigma\big\}, \tag{4.57}$$

and $G = C^\infty\big(\Sigma, \mathrm{SU}(2)\big)$ is the group of full SU(2) gauge transformations, we have the symplectomorphism $\mathcal{P}^G_{\Gamma^*} = P^G_\Gamma$ between the continuous and discrete gauge-invariant phase spaces. This follows directly from Proposition 4.3.4, and the fact that $G = G_\Gamma \times G_{\mathsf{n}_\Gamma}$, where G_{n_Γ} is the group of discrete gauge transformations acting at the nodes $\mathsf{n}\in\mathsf{n}_\Gamma$ only.

Notice that when we act with the full group G of SU(2) transformations, the holonomies h_ℓ and the fluxes $\boldsymbol{X}_\ell$ clearly become gauge-covariant, i.e. satisfies $\mathcal{I}(g \triangleright \boldsymbol{A}, g \triangleright \boldsymbol{E}) = g \triangleright \mathcal{I}(\boldsymbol{A}, \boldsymbol{E})$. Indeed, since the group element g is not fixed to the identity at the nodes n anymore, we have $g \triangleright a_\mathsf{n}(x) = g(x) a_\mathsf{n}(x) g(v)^{-1}$, and therefore the definition (4.45,4.46) tells us that we have $g \triangleright h_\ell = g_{\mathsf{n}_1} h_\ell g_{\mathsf{n}_2}^{-1}$, where ℓ is an link of Γ connecting the nodes n_1 and n_2.

4.3.4 The symplectic structures

In this subsection we use the map (4.52) to prove the equivalence of the symplectic structures on the continuous and discrete spaces $\mathcal{P}_{\Gamma,\Gamma^*}$ and P_Γ. We know that the spaces $\mathcal{P}$ and P_Γ are symplectic manifolds, their symplectic structures being given by (4.2) and (3.58) respectively. Since the space $\mathcal{P}_{\Gamma,\Gamma^*}$ has been obtained from $\mathcal{P}$ by symplectic reduction, the Marsden-Weinstein theorem ensures that it also carries a symplectic structure. We are now going to show that the symplectic structures on the spaces $\mathcal{P}_{\Gamma,\Gamma^*}$ and P_Γ are in fact identical.

Let us start with the symplectic potential coming from the first order formulation of gravity. It is given by

$$\Omega = \frac{1}{2} \int_\Sigma \mathrm{Tr}\left(\star(\boldsymbol{e} \wedge \boldsymbol{e}) \wedge \delta \boldsymbol{A}\right) = \int_\Sigma \mathrm{Tr}\left(\boldsymbol{E} \wedge \delta \boldsymbol{A}\right), \tag{4.58}$$

where $\star$ denotes the Hodge duality map in the Lie algebra $\mathfrak{su}(2)$. We first use the cellular space Δ to evaluate this symplectic potential on the set of partially flat connections and write:

$$\begin{aligned}
\Omega &= \sum_\mathsf{n} \int_{c_\mathsf{n}} \mathrm{Tr}\left(\boldsymbol{E} \wedge \delta\left(a_\mathsf{n} \mathrm{d} a_\mathsf{n}^{-1}\right)\right) && \text{(4.59a)}\\
&= \sum_\mathsf{n} \int_{c_\mathsf{n}} \mathrm{Tr}\left(\boldsymbol{X}_\mathsf{n} \wedge \mathrm{d}\left(\delta a_\mathsf{n}^{-1} a_\mathsf{n}\right)\right) && \text{(4.59b)}\\
&= \sum_\mathsf{n} \int_{\partial c_\mathsf{n}} \mathrm{Tr}\left(\boldsymbol{X}_\mathsf{n} \delta a_\mathsf{n}^{-1} a_\mathsf{n}\right) - \sum_\mathsf{n} \boldsymbol{G}_\mathsf{n} \delta a_\mathsf{n}^{-1} a_\mathsf{n}(\mathsf{n}) && \text{(4.59c)}\\
&= \sum_\mathsf{n} \int_{\partial c_\mathsf{n}} \mathrm{Tr}\left(\boldsymbol{X}_\mathsf{n} \delta a_\mathsf{n}^{-1} a_\mathsf{n}\right), && \text{(4.59d)}
\end{aligned}$$

where we have used the identity $\delta\left(a_\mathsf{n} \mathrm{d} a_\mathsf{n}^{-1}\right) = a_\mathsf{n} \mathrm{d}\left(\delta a_\mathsf{n}^{-1} a_\mathsf{n}\right) a_\mathsf{n}^{-1}$, the definition (4.42) of the two-form field $\boldsymbol{X}_\mathsf{n}$, and the fact that $\mathrm{d}\boldsymbol{X}_\mathsf{n} = \boldsymbol{G}_\mathsf{n} \delta(x - \mathsf{n})$ (see equation(4.54)). The last equality follows from the condition $a_\mathsf{n}(\mathsf{n}) = \mathrm{id}$, which implies $\delta a_\mathsf{n}(\mathsf{n}) = 0$. The summation over three-cells dual to the nodes n can be rearranged as a sum over two-cells dual to the links ℓ, which gives:

$$\Omega = \sum_\ell \int_{\mathsf{f}_\ell} \left[\mathrm{Tr}\left(\boldsymbol{X}_{s(\ell)} \delta a_{s(\ell)}^{-1} a_{s(\ell)}\right) - \mathrm{Tr}\left(\boldsymbol{X}_{t(\ell)} \delta a_{t(\ell)}^{-1} a_{t(\ell)}\right)\right]. \tag{4.60}$$

Now we can use the conditions (4.45, 4.46) of compatibility of the group elements a_n across the links to rewrite the second term and obtain:

$$\Omega = \sum_\ell \int_{\mathsf{f}_\ell} \left[\mathrm{Tr}\left(\boldsymbol{X}_{s(\ell)} \delta a_{s(\ell)}^{-1} a_{s(\ell)}\right) - \mathrm{Tr}\left(h_\ell^{-1} \boldsymbol{X}_{s(\ell)} h_\ell \delta\left(h_\ell^{-1} a_{s(\ell)}^{-1}\right) a_{s(\ell)} h_\ell\right)\right]. \tag{4.61}$$

Finally, we can expand the last term to find the result:

$$\Omega = -\sum_{\ell} \int_{\mathsf{f}_\ell} \mathrm{Tr}\left(h_\ell^{-1} \boldsymbol{X}_{s(\ell)} h_\ell \delta h_\ell^{-1} h_\ell\right) = \sum_{\ell} \mathrm{Tr}\left(\boldsymbol{X}_\ell \delta h_\ell h_\ell^{-1}\right). \tag{4.62}$$

This is exactly the symplectic potential associated to $|\ell_\Gamma|$ copies of the cotangent bundle $T^*\mathrm{SU}(2)$. It shows that the symplectic structure of the spin network phase space is equivalent to that of first order gravity evaluated on the set of partially flat connections. In particular, since the symplectic forms are invertible by definition, this proves that the continuous phase space $\mathcal{P}_{\Gamma,\Gamma^*}$ is indeed finite-dimensional and isomorphic to P_Γ.

4.3.5 Action of diffeomorphisms

Now we prove the second point of Proposition 4.3.4, which concerns the invariance of the symplectomorphism under a certain class of diffeomorphisms. The isomorphism $\mathcal{I} : \mathcal{P}_{\Gamma,\Gamma^*} \longrightarrow P_\Gamma$ depends on a choice of cellular space Δ dual to Γ with one-skeleton $\Delta_1 = \Gamma^*$. Diffeomorphisms $\Phi \in \mathrm{Diff}(\Sigma)$ act naturally on the continuous phase space $\mathcal{P}_{\Gamma,\Gamma^*}$ by $\boldsymbol{A} \longmapsto \Phi^*\boldsymbol{A}$ and $\boldsymbol{E} \longmapsto \Phi^*\boldsymbol{E}$.

Let us start by choosing a particular diffeomorphism Φ_o which preserves the graph Γ^* and the nodes n_Γ inside the cells c_n, and is connected to the identity[3]. Because the connection is flat on $\tilde{\Sigma}$, the holonomy $h_\ell[\boldsymbol{A}]$ is independent of the choice of path between $s(\ell)$ and $t(\ell)$ as long as any two paths are in the same homotopy class of $\tilde{\Sigma}$. The links ℓ and $\Phi_o^{-1}(\ell)$ are in the same homotopy class if Φ_o is connected to the identity and not moving Γ^*. Then it is clear that we have:

$$h_\ell(\Phi_o^*\boldsymbol{A}) = h_{\Phi_o^{-1}(\ell)}[\boldsymbol{A}] = h_\ell[\boldsymbol{A}]. \tag{4.63}$$

Similarly, the action of Φ_o on the group element $a_\mathsf{n}(x)$ maps it to $a_\mathsf{n}\big(\Phi_o(x)\big)$. This implies that the two-form $\boldsymbol{X}_\mathsf{n}$ defined by (4.42) satisfies $\boldsymbol{X}_\mathsf{n}\big(\Phi_o(x)\big) = \Phi_o^*\boldsymbol{X}_\mathsf{n}(x)$. Recall from the definitions of the cellular space that each face f_ℓ is bounded by links in the one-skeleton Γ^*. Now, since Φ_o does not move the graph Γ^*, we have that $\partial\mathsf{f}_\ell = \partial\big(\Phi_o(\mathsf{f}_\ell)\big) \in \Gamma^*$, and therefore $\mathsf{f}_\ell \cup \Phi_o(\mathsf{f}_\ell)$ encloses a volume, which furthermore does not contain any nodes of Γ. Thus, by virtue of (4.26) and (4.49), we have that:

$$\boldsymbol{X}_\ell(\Phi_o^*\boldsymbol{A}, \Phi_o^*\boldsymbol{E}) = \boldsymbol{X}_\ell(\boldsymbol{A}, \boldsymbol{E}). \tag{4.64}$$

Relations (4.63) and (4.64) together show that $\mathcal{I} \circ \Phi_o = \mathcal{I}$.

We can give another very elegant proof of the invariance of the map $\mathcal{I}$ under the diffeomorphisms Φ_o. For this, recall that given a vector field ξ^a, a diffeomorphism acts on the connection like:

$$\mathcal{L}_\xi \boldsymbol{A} = \mathrm{d}(\iota_\xi \boldsymbol{A}) + \iota_\xi \mathrm{d}\boldsymbol{A} = \iota_\xi \boldsymbol{F} + \mathrm{d}_A(\iota_\xi \boldsymbol{A}), \tag{4.65}$$

and on the electric field like:

$$\mathcal{L}_\xi \boldsymbol{E} = \mathrm{d}(\iota_\xi \boldsymbol{E}) + \iota_\xi \mathrm{d}\boldsymbol{E} = \iota_\xi \mathrm{d}_A \boldsymbol{E} + \mathrm{d}_A(\iota_\xi \boldsymbol{E}) + [\boldsymbol{E}, \iota_\xi \boldsymbol{A}], \tag{4.66}$$

[3]This means that there exists a smooth one-parameter family of diffeomorphism Φ_t such that $\Phi_{t=0} = \mathrm{id}$ and $\Phi_{t=1} = \Phi_o$.

where ι denotes the interior product. Now, if the data $(\boldsymbol{A}, \boldsymbol{E})$ is on the constraint surface $\mathcal{C}$, the curvature vanishes outside of Γ^*, while $\mathrm{d}_A\boldsymbol{E}$ vanishes outside of the set n_Γ of nodes. Therefore, if we consider a vector field ξ^a which vanishes on Γ^* and on n_Γ, we see that the action of diffeomorphisms is a combination of flat transformations (4.31) and gauge transformations (4.34) with field-dependent parameters of transformation, i.e.

$$\mathcal{L}_\xi \boldsymbol{A} = \delta^{\mathcal{F}_{\Gamma^*}}_{\iota_\xi \boldsymbol{E}} \boldsymbol{A} + \delta^{G_\Gamma}_{\iota_\xi \boldsymbol{A}} \boldsymbol{A}, \qquad\qquad \mathcal{L}_\xi \boldsymbol{E} = \delta^{\mathcal{F}_{\Gamma^*}}_{\iota_\xi \boldsymbol{E}} \boldsymbol{E} + \delta^{G_\Gamma}_{\iota_\xi \boldsymbol{A}} \boldsymbol{E}. \tag{4.67}$$

We can write this more succinctly as simply:

$$\mathcal{L}_\xi = \delta^{\mathcal{F}_{\Gamma^*}}_{\iota_\xi \boldsymbol{E}} + \delta^{G_\Gamma}_{\iota_\xi \boldsymbol{A}}. \tag{4.68}$$

Now, since the holonomy and flux variables are invariant under the flatness and gauge transformations, such diffeomorphisms vanish on the variables $(h_\ell, \boldsymbol{X}_\ell)$.

4.4 Gauge choices for the electric field

Now that we have established the isomorphism between P_Γ and the continuous phase space $\mathcal{P}_{\Gamma,\Gamma^*}$, we have a correspondence between discrete geometries and an equivalence class of continuous geometries related according to (4.55) by group gauge transformations and translations. Up to group gauge transformations, the holonomy uniquely determines a choice of connection. For the electric field, however, the story is different since even after we have performed a group gauge transformation, there is still a huge ambiguity coming from the transformation $\boldsymbol{E} \to \boldsymbol{E} + \mathrm{d}_A\boldsymbol{\phi}$ on the continuous electric field determined by the fluxes. It is clear that in order to construct a continuous field configuration starting from the discrete data, one has to specify which continuous field representative to pick in the particular equivalence class determined by the discrete data. In other words, a choice of a representative in this equivalence class is a choice of gauge. More precisely, we have the following definition:

Definition 4.4.1. A choice of gauge is a map from the discrete data to the continuous phase space,

$$\begin{array}{rccc} \mathcal{T}: & P_\Gamma & \longrightarrow & \mathcal{C} \\ & (h_\ell, \boldsymbol{X}_\ell) & \longmapsto & (\boldsymbol{A}, \boldsymbol{E}), \end{array} \tag{4.69}$$

which is the inverse of $\mathcal{I}$ in the sense that

$$\mathcal{I} \circ \mathcal{T} = \mathrm{id}. \tag{4.70}$$

We say that a gauge fixing is diffeomorphism-covariant if $\Phi^*\mathcal{T}$ is equal to the map $\mathcal{T}$ defined on the graphs $\Phi^{-1}(\Gamma)$ and $\Phi^{-1}(\Gamma^*)$, for any diffeomorphism $\Phi : \Sigma \longrightarrow \Sigma$.

In other words, choosing a gauge amounts to giving a prescription for reconstructing continuous fields $\boldsymbol{A}(h_\ell)$ and $\boldsymbol{E}(\boldsymbol{X}_\ell, h_\ell)$ starting from the discrete data, such that (4.70) holds, i.e.

$$h_\ell\big(A(h_\ell)\big) = h_\ell, \qquad\qquad \boldsymbol{X}_\ell\big(A(h_\ell), E(\boldsymbol{X}_\ell, h_\ell)\big) = \boldsymbol{X}_\ell. \tag{4.71}$$

Note that a gauge fixing $\mathcal{T}$ is a right inverse for $\mathcal{I}$, while the reverse is not true. The map $\mathcal{T} \circ \mathcal{I}$ is not the identity, it just maps a continuous configuration $(\boldsymbol{A}, \boldsymbol{E})$ that solves the Gauss and curvature constraints into another gauge-equivalent configuration which satisfies the gauge choice.

As we have already seen, at the continuous level a flat connection on $\tilde{\Sigma}$ is determined on every cell c_{n} by a group element $a_{\mathsf{n}}(x)$. Locally, it is always possible to perform a gauge transformation that sends this element to the identity of the group, and thereby construct a trivial connection. If we pick two neighboring cells c_{n_1} and c_{n_2} such that the nodes n_1 and n_2 bound the link dual to the face $\mathsf{f}_\ell = \overline{c_{\mathsf{n}_1}} \cap \overline{c_{\mathsf{n}_2}}$, the relevant gauge-invariant information about the connection is encoded in the transition group element h_ℓ.

For the electric field, there is more gauge freedom since the variable $\boldsymbol{E}$ can be acted upon by both $\mathcal{F}_{\Gamma^*}$ and G_Γ. Therefore, there is a priori a huge ambiguity in the choice of gauges that one can choose to reconstruct the continuous data. This means that knowledge of the fluxes does not accurately determine the geometry of space, but only a family of geometries that are gauge-equivalent under translations of the type $\boldsymbol{E} \longmapsto \boldsymbol{E} + \mathrm{d}_A \boldsymbol{\phi}$.

However, there is a powerful way in which we can restrict the gauge choices that are available. This can be done by asking that a gauge choice transforms covariantly under the action of diffeomorphisms. A diffeomorphism Φ of Σ acts on the continuous data in the usual manner $(\boldsymbol{A}, \boldsymbol{E}) \longmapsto \big(\Phi^* \boldsymbol{A}, \Phi^* \boldsymbol{E}\big)$. The same diffeomorphism also acts on the discrete data $(h_\ell, \boldsymbol{X}_{\mathsf{f}_\ell})$ as $\big(h_{\Phi^{-1}(\ell)}, \boldsymbol{X}_{\Phi^{-1}(\mathsf{f}_\ell)}\big)$. Note that here we have made explicit the fact that the flux field $\boldsymbol{X}_\ell$ depends on Γ^* via the choice of a surface f_ℓ whose boundary is supported on Γ^*. A gauge choice is said to be covariant if this action of the diffeomorphisms commutes with the gauge map $\mathcal{T}$.

If we restrict ourselves to gauge choices that are covariant under the action of diffeomorphisms, the ambiguity in the gauge choices is dramatically resolved, and there are only a few choices available. In the following we present two such gauge choices[4]. First, the singular gauge choice in which the electric field $\boldsymbol{E}$ vanishes outside of Γ, and then the flat gauge in which $\boldsymbol{E}$ is flat outside of Γ^*. It is remarkable that these two gauge choices correspond to the two main interpretations of the fluxes used in the literature. In loop quantum gravity one usually interprets the $\boldsymbol{E}$ field as having support only on Γ since the corresponding operator acting on a spin network state gives $\hat{\boldsymbol{E}}(x)\,|\psi\rangle = 0$ for $x \notin \Gamma$. On the other hand, the spin foam literature usually interprets the $\boldsymbol{E}$ field as being flat outside of Γ^*. Our analysis shows that these two pictures are not contradictory, but that they correspond to two different covariant gauge choices underlying the same discrete data!

Now we want to emphasize that the restriction on the gauge choices coming from the requirement of covariance under diffeomorphisms is the analog of the so-called uniqueness theorem of the quantum representation of the holonomy-flux algebra [72]. This theorem states that there is a unique diffeomorphism-covariant gauge choice, which corresponds to the singular gauge in which $\boldsymbol{E}$ has support on the graph Γ only and vanishes on Γ^*. In this singular gauge, which we refer to as the LQG gauge, the electric field $\boldsymbol{E}$ vanishes outside of the graph Γ dual to the triangulation Δ. This can be written as $\hat{\boldsymbol{E}}|0\rangle = 0$, where the vacuum state $|0\rangle$ is the state of no geometry. Indeed, in LQG excitations of quantum geometry have support on the graph Γ only. Therefore, in all the regions of Σ outside of Γ, there is simply no geometry, and the electric

[4] We conjecture these are the only two possible gauge choices, but a detailed investigation of this is still needed.

field vanishes. We are going to give below an explicit construction of the continuous singular electric field.

The key observation is that there is another legitimate choice of representative configuration in the equivalence class (4.55) of continuous geometries which respects the diffeomorphism symmetry. As we already said, it is given by the flat gauge. At the quantum level, this corresponds to a choice of a vacuum state $|0_{\mathrm{R}}\rangle$ in which the intrinsic $\boldsymbol{R}(\boldsymbol{E})$ curvature vanishes. This corresponds to the flat, or spin foam gauge, in which we have vanishing intrinsic curvature $\hat{\boldsymbol{R}}[\boldsymbol{E}]|0_{\mathrm{R}}\rangle = 0$. This diffeomorphism-invariant vacuum is different from the one singled out by the LOST theorem [72] (which obviously corresponds to the singular gauge) and it would be interesting to investigate further its properties. What should be noted is that such a vacuum state appears naturally in our context and that it corresponds to the spin foam description. It can be seen as the dual of the singular gauge, in the sense that it defines a flat geometry within the cells c_{n}, with a non-vanishing electric field $\boldsymbol{E}$ on the dual graph Γ^*. As we will see in more detail, the availability of this gauge clearly shows that it is possible to define a locally flat geometry without necessarily having a triangulation with straight links and flat faces. In Regge geometries [42], the extrinsic curvature is concentrated along the one-skeleton Δ_1 of the triangulation, but in the present construction, the links of Γ^* are not necessarily straight.

Here we have drawn a parallel between a choice of gauge at the classical level and a choice of a vacuum state at the quantum level. It would be interesting to develop this analogy further. Notice that what we are calling a 'gauge choice', is a choice amoung an equivalence class of geometries which are related by gauge transformations generated by the flatness constraint. Usually when one refers to a gauge choice, one is referring to a choice which solves the constraints within the theory, but this flatness constraint is not part of the Hamiltonian theory, having been introduced to allow for the symplectomorphism between the continuous and discrete phase spaces. The vacuum state must be invariant under the gauge transformations generated by constraints within the Hamiltonian theory, but the choice we make here does not have to be invariant under the transformations generated by the flatness constraint.

In the remainder of this section, we are going to study in more detail the singular and flat gauges for the electric field. Our goal is to study the gauge freedom for the basic variables on the continuous phase space, and to construct explicitly the electric field as a functional of the discrete variables h_ℓ and $\boldsymbol{X}_\ell$.

4.4.1 Singular gauge

The singular gauge is a gauge in which the electric field $\boldsymbol{E}$ vanishes outside of the graph Γ. Since the spatial metric is a function of $\boldsymbol{E}$, this implies that there is no geometry outside the graph in this gauge. In this section, we show by an explicit construction that it always possible to make such a gauge choice. More precisely, we construct explicitly continuous fields $\boldsymbol{A}(h_\ell)$ and $\boldsymbol{E}_{\mathrm{S}}(h_\ell, \boldsymbol{X}_\ell)$ which are such that $\boldsymbol{E}_{\mathrm{S}}(x) = 0$ if $x \notin \Gamma$, and which satisfy the property $\mathcal{I}(A, E_{\mathrm{S}}) = (h_\ell, \boldsymbol{X}_\ell)$ under the action of the map (4.52).

In order to prove this, let us first introduce the following form:

$$\omega(x,y) \equiv \omega^i(x-y)\epsilon_{ijk}\mathrm{d}x^j \wedge \mathrm{d}y^k, \qquad \text{with} \qquad \omega^i(x) \equiv \frac{1}{4\pi}\frac{x^i}{|x|^3}. \tag{4.72}$$

This object is a (1,1)-form, i.e. a one-form in x, and a one-form in y. This form satisfies a key property, which is summarized in the following lemma.

Lemma 4.4.2. *There exists an $\alpha(x,y)$ which is a (2,0)-form (i.e. a two-form in x and a zero-form in y), such that*

$$\mathrm{d}_x\omega(x,y) + \mathrm{d}_y\alpha(x,y) = \delta(x,y), \tag{4.73}$$

where $\mathrm{d}_x \equiv \mathrm{d}x^i\partial_{x^i}$, and $\delta(x,y)$ is the distributional (2,1)-form

$$\delta(x,y) = \delta(x-y)\epsilon_{ijk}\mathrm{d}x^i \wedge \mathrm{d}x^j \wedge \mathrm{d}y^k \tag{4.74}$$

vanishing outside of $x = y$.

Proof. First, it is straightforward to show that $\partial_i\omega^i(x) = 0$ for $x \neq 0$. Moreover, it is possible to show by a direct computation in spherical coordinates that:

$$\int_{S_\varepsilon} \omega^i(x)\epsilon_{ijk}\mathrm{d}x^j \wedge \mathrm{d}x^k = 2, \tag{4.75}$$

where S_ε is a sphere of radius ε. Since this integral is also equal to:

$$2\int_{B_\varepsilon} \partial_i\omega^i(x)\mathrm{d}^3x, \tag{4.76}$$

where B_ε is the ball of radius ε, we obtain that $\partial_i\omega^i(x) = \delta(x)$. By a direct computation we can now get that:

$$\mathrm{d}_x\omega(x,y) = s_k \wedge \mathrm{d}y^k \left(\partial_i\omega^i\right)(x-y) - s_j \wedge \mathrm{d}y^k \left(\partial_k\omega^j\right)(x-y), \tag{4.77}$$

with:

$$s_i = \frac{1}{8\pi}\epsilon_{ijk}\mathrm{d}x^j \wedge \mathrm{d}x^k. \tag{4.78}$$

The lemma is therefore established by introducing $\alpha(x,y) \equiv \omega^i(x-y)s_i$. □

Given this lemma, it is now a straightforward task to construct a singular flux field. For this, we first construct a flat connection $\boldsymbol{A}$ on $\tilde{\Sigma}$ following the construction of subsection 4.3.2, and then we define the singular flux field as:

$$\boldsymbol{E}_{\mathrm{S}}(x) \equiv \mathrm{d}_A\left(\sum_{\ell\in\Gamma} h_{\pi_\ell}(x)^{-1}\boldsymbol{X}_\ell h_{\pi_\ell}(x)\int_{\ell(y)}\omega(x,y)\right). \tag{4.79}$$

The integral entering this definition is a one-dimensional integral over the link ℓ parametrized by the variable y, which implies that the term inside the parenthesis is a one-form in x.

The proof that this flux satisfies all the desired requirements is straightforward. First, it is obvious that the Gauss law $\mathrm{d}_A\boldsymbol{E}_{\mathrm{S}} = 0$ is satisfied on $\Sigma\backslash\Gamma^*$ since $\mathrm{d}_A^2 = \boldsymbol{F}[\boldsymbol{A}] = 0$ on this

space. Moreover, using the previous lemma and the definition of the holonomy, we can compute explicitly the covariant derivative:

$$\boldsymbol{E}_{\mathrm{S}}(x) = \sum_{\ell} h_{\pi_\ell}(x)^{-1} \boldsymbol{X}_\ell h_{\pi_\ell}(x) \Big(\delta_\ell(x) - \alpha\big(x, s(\ell)\big) + \alpha\big(x, t(\ell)\big) \Big), \tag{4.80}$$

where:

$$\delta_\ell(x) \equiv \int_{\ell(y)} \delta(x, y). \tag{4.81}$$

The last two terms in (4.80) can be reorganized in terms associated with the nodes to find:

$$\begin{aligned} \boldsymbol{E}_{\mathrm{S}}(x) = \quad & \sum_{\ell} h_{\pi_\ell}(x)^{-1} \boldsymbol{X}_\ell h_{\pi_\ell}(x) \delta_\ell(x) \\ & - \sum_{\mathsf{n}} \alpha(x, \mathsf{n}) h_{\mathsf{n}}(x)^{-1} \left(\sum_{\ell | s(\ell) = \mathsf{n}} \boldsymbol{X}_\ell - \sum_{\ell | t(\ell) = \mathsf{n}} h_\ell^{-1} \boldsymbol{X}_\ell h_\ell \right) h_{\mathsf{n}}(x), \end{aligned} \tag{4.82}$$

where $h_{\mathsf{n}}(x)$ is the holonomy going from the node n to the point x. Now the last term vanishes due to the discrete Gauss law (3.60). Therefore, we finally find that the singular electric field is:

$$\boldsymbol{E}_{\mathrm{S}}(x) = \sum_{\ell} h_{\pi_\ell}(x)^{-1} \boldsymbol{X}_\ell h_{\pi_\ell}(x) \delta_\ell(x). \tag{4.83}$$

This electric field is obviously vanishing outside of Γ, and is such that $\boldsymbol{X}_\ell(\boldsymbol{A}, \boldsymbol{E}_{\mathrm{S}}) = \boldsymbol{X}_\ell$. It is interesting to note that the integral of the two-form $\alpha(x, y)$ along S,

$$\int_S \alpha(x, y) = \frac{1}{8\pi} \int_S \omega^i(x - y) \epsilon_{ijk} \mathrm{d}x^j \wedge \mathrm{d}x^k, \tag{4.84}$$

is simply the solid angle of S as viewed from y divided by 4π.

4.4.2 Flat cell gauge

The flat cell gauge is a choice of electric field with vanishing intrinsic and extrinsic curvature within the cells, i.e. with the Ricci curvature $\boldsymbol{R} \equiv \mathrm{d}_\Gamma \boldsymbol{\Gamma} = 0$ (where here $\boldsymbol{\Gamma}$ is the spin connection) and the extrinsic curvature $\boldsymbol{K} = 0$ in each cell c_{n}. This gauge choice requires that we be within the SU(2)-gauge invariant phase space since we use fields which solve the Gauss constraint.

We are about to prove that it is always possible to find a gauge transformation, generated by the flatness constraint, which takes an arbitrary electric field $\boldsymbol{E} \in \mathcal{P}^G_{\Gamma^*}$ to a flat electric field $\bar{\boldsymbol{E}}$. In the following we assume the frame field $\boldsymbol{e}$ is invertible.

Let us begin with two lemmas:

Lemma 4.4.3. *Extrinsic curvature is zero if and only if the frame field is torsion-free.*

Proof. Torsion is given by:

$$\mathrm{d}_A \boldsymbol{e} = \mathrm{d}\boldsymbol{e} + [\Gamma + \gamma \boldsymbol{K}, \boldsymbol{e}] = \gamma\,[\boldsymbol{K}, \boldsymbol{e}]\,, \tag{4.85}$$

where by definition, the spin connection $\boldsymbol{\Gamma}$ is the solution to $\mathrm{d}\boldsymbol{e} + [\boldsymbol{\Gamma}, \boldsymbol{e}] = 0$. This equation shows that $\boldsymbol{K} = 0$ implies $\mathrm{d}_A \boldsymbol{e} = 0$. To show that the reverse is also true, we use (4.85) in index-form to write:

$$\frac{1}{\gamma}\epsilon^{abc} D_b e_{ic} = \epsilon^{abc}\epsilon_{ijk} K_b^j e_c^k = (\det e) K_b^j (e_i^a e_j^b - e_j^a e_i^b), \tag{4.86}$$

where D_a is the covariant exterior derivative in index notation and we used the identity $\epsilon^{abc}\epsilon_{ijk} e_c^k \equiv (\det e)(e_i^a e_j^b - e_j^a e_i^b)$ in the second equality. Contracting both sides of this equation with e_a^i leads to an equation on the trace of the extrinsic curvature:

$$K_a^a = \frac{1}{2\gamma(\det e)} \epsilon^{abc} e_a^i D_b e_{ci}. \tag{4.87}$$

Now using (4.87) in (4.86), we find

$$K_a^i = \frac{1}{\gamma(\det e)} \left(\frac{1}{2} e_a^i e_d^j - e_d^i e_a^j \right) \epsilon^{dbc} D_b e_{cj}. \tag{4.88}$$

This shows that $\mathrm{d}_A \boldsymbol{e} = 0$ implies $\boldsymbol{K} = 0$ and establishes the proof. □

Lemma 4.4.4. *A flat connection, together with vanishing extrinsic curvature, imply that intrinsic curvature is zero.*

Proof. Using the definition $\boldsymbol{A} \equiv \boldsymbol{\Gamma} + \gamma \boldsymbol{K}$ of the Ashtekar-Barbero connection, we can write its curvature as:

$$\boldsymbol{F}[\boldsymbol{A}] = \boldsymbol{R} + \gamma \mathrm{d}_\Gamma \boldsymbol{K} + \frac{\gamma^2}{2}[\boldsymbol{K}, \boldsymbol{K}]. \tag{4.89}$$

Setting $\boldsymbol{F}[\boldsymbol{A}] = 0$ and $\boldsymbol{K} = 0$ implies that $\boldsymbol{R} = 0$. □

We showed previously (see (4.40) and (4.44)) that the gauge-invariant fields $(\boldsymbol{A}, \boldsymbol{E})$ are written in each cell c_{n} in general as

$$\boldsymbol{A} = a_{\mathsf{n}} \mathrm{d} a_{\mathsf{n}}^{-1}, \qquad\qquad \boldsymbol{E} = a_{\mathsf{n}} \mathrm{d} \boldsymbol{Z}_{\mathsf{n}} a_{\mathsf{n}}^{-1}, \tag{4.90}$$

where we have used a Lie algebra-valued one-form $\boldsymbol{Z}_{\mathsf{n}} \in \Omega^1\big(c_{\mathsf{n}}, \mathfrak{su}(2)\big)$ to write $\boldsymbol{X}_{\mathsf{n}}(x) = \mathrm{d} Z_{\mathsf{n}}(x)$. Since a flat triad must be torsion-free by the above lemmas, we can similarly write a flat triad in general as:

$$\bar{\boldsymbol{e}} = a_{\mathsf{n}} \mathrm{d} \boldsymbol{z}_{\mathsf{n}} a_{\mathsf{n}}^{-1}, \tag{4.91}$$

for some Lie algebra-valued function $\boldsymbol{z}_{\mathsf{n}} \in \Omega^0\big(c_{\mathsf{n}}, \mathfrak{su}(2)\big)$. The function $\boldsymbol{z}_{\mathsf{n}}$ provides a set of flat coordinates in c_{n}. Requiring the triad to be invertible places the following condition on $\boldsymbol{z}_{\mathsf{n}}$:

$$\epsilon^{abc}\epsilon_{ijk} \partial_a z_{\mathsf{n}}^i \partial_b z_{\mathsf{n}}^j \partial_c z_{\mathsf{n}}^k > 0. \tag{4.92}$$

The electric field constructed from this triad is given by:

$$\bar{\boldsymbol{E}} = a_{\mathsf{n}} \left[\mathrm{d}\boldsymbol{z}_{\mathsf{n}}, \mathrm{d}\boldsymbol{z}_{\mathsf{n}}\right] a_{\mathsf{n}}^{-1}. \tag{4.93}$$

Consider that we are given a pair $(a_{\mathsf{n}}, \boldsymbol{Z}_{\mathsf{n}})$ defining an electric field $\boldsymbol{E}$ within a cell c_{n}. Looking at (4.31), we seek a gauge field $\boldsymbol{\phi}_{\mathsf{n}} \in \Omega^1\big(c_{\mathsf{n}}, \mathfrak{su}(2)\big)$ such that:

$$\mathrm{d}_A \boldsymbol{\phi}_{\mathsf{n}} = \bar{\boldsymbol{E}} - \boldsymbol{E} = a_{\mathsf{n}} \left(\left[\mathrm{d}\boldsymbol{z}_{\mathsf{n}}, \mathrm{d}\boldsymbol{z}_{\mathsf{n}}\right] - \mathrm{d}\boldsymbol{Z}_{\mathsf{n}}\right) a_{\mathsf{n}}^{-1}. \tag{4.94}$$

Using $a_{\mathsf{n}}^{-1}\mathrm{d}_A\boldsymbol{\phi}_{\mathsf{n}}a_{\mathsf{n}} = \mathrm{d}(a_{\mathsf{n}}^{-1}\boldsymbol{\phi}_{\mathsf{n}}a_{\mathsf{n}})$, we can solve for $\boldsymbol{\phi}_{\mathsf{n}}$ to obtain:

$$\boldsymbol{\phi}_{\mathsf{n}} = a_{\mathsf{n}} \left(\left[\boldsymbol{z}_{\mathsf{n}}, \mathrm{d}\boldsymbol{z}_{\mathsf{n}}\right] - \boldsymbol{Z}_{\mathsf{n}} + \mathrm{d}g_{\mathsf{n}}\right) a_{\mathsf{n}}^{-1}, \tag{4.95}$$

for $g_{\mathsf{n}} \in \Omega^0\big(c_{\mathsf{n}}, \mathfrak{su}(2)\big)$. For $x \in \Gamma^*$ the value of $g_{\mathsf{n}}(x)$ is fixed up to an overall constant by the condition $\boldsymbol{\phi}_{\mathsf{n}}(x) = 0$:

$$g_{\mathsf{n}}(x) = \int_{s(\mathsf{e})}^{x} \left(\boldsymbol{Z}_{\mathsf{n}} - \left[\boldsymbol{z}_{\mathsf{n}}, \mathrm{d}\boldsymbol{z}_{\mathsf{n}}\right]\right), \tag{4.96}$$

where the integration is along an edge e in the boundary $\partial\mathsf{f}_\ell$ of the face f_ℓ.

We have shown the existence of a gauge field $\boldsymbol{\phi}_{\mathsf{n}}$ taking us from an arbitrary electric field $\boldsymbol{E} \in \mathcal{P}^G_{\Gamma^*}$ to a flat electric field with vanishing intrinsic and extrinsic curvature in a cell. The next question to ask is whether this choice unique. Since g_{n} is fixed only on Γ^* (and even there only up to a constant), and it is not fixed in c_{n} or the faces f_ℓ, there are many choice of $\boldsymbol{\phi}_{\mathsf{n}}$ which give the transformation $\boldsymbol{E} \to \bar{\boldsymbol{E}}$. Moreover, any $\boldsymbol{z}_{\mathsf{n}}$ satisfying (4.92) gives a flat, invertible triad, so there is not even a unique choice of flat electric field. Therefore the transformation to the flat cell gauge is not unique.

Having found a gauge transformation to a flat electric field in a single cell, we now consider how this transformation affects the geometry at cell boundaries when performing this transformation in all cells of the cellular space. The requirement of continuity of $\boldsymbol{E}$ and $\bar{\boldsymbol{e}}$ at the face $\mathsf{f}_{cc'}$ gives conditions at the face:

$$\lim_{x' \to \mathsf{e}_{c'c}} \mathrm{d}\boldsymbol{z}_{c'}(x') = \lim_{x \to \mathsf{e}_{cc'}} h_{cc'}^{-1}\mathrm{d}\boldsymbol{z}_c(x)h_{cc'}, \qquad \lim_{x' \to \mathsf{e}_{c'c}} \mathrm{d}\boldsymbol{Z}_{c'}(x') = \lim_{x \to \mathsf{e}_{cc'}} h_{cc'}^{-1}\mathrm{d}\boldsymbol{Z}_c(x)h_{cc'}, \tag{4.97}$$

for $x \in \mathsf{f}_{cc'}$ and $x' \in \mathsf{f}_{c'c}$. Using these relations and requiring $\boldsymbol{\phi}_{c'}(x')$ to vanish on the boundary of the face adds another condition:

$$\lim_{x' \to \mathsf{e}_{c'c}} \mathrm{d}g_{c'}(x') = \lim_{x \to \mathsf{e}_{cc'}} h_{cc'}^{-1}\mathrm{d}g_c(x)h_{cc'}. \tag{4.98}$$

Together, these relations imply that $\lim_{x' \to \mathsf{e}_{c'c}} \phi_{c'}(x') = \lim_{x \to \mathsf{e}_{cc'}} \phi_c(x)$, so that the gauge field is continuous across faces.

Finally, we close this section with a reconstruction of the flux elements $\boldsymbol{X}_\ell$ starting from the flat frame field $\bar{e}$. The flux elements in this gauge are given by the simple form:

$$X^i_\ell = \frac{1}{2}\epsilon^i{}_{jk} \int_{\mathsf{f}_\ell} h_{\pi_\ell}\bar{e}^j \wedge \bar{e}^k h_{\pi_\ell}^{-1} = \frac{1}{2}\epsilon^i{}_{jk} \int_{\mathsf{f}_\ell} \mathrm{d}z^j_{\mathsf{n}} \wedge \mathrm{d}z^k_{\mathsf{n}} = \frac{1}{2}\epsilon^i{}_{jk} \int_{\partial\mathsf{f}_\ell} z^j_{\mathsf{n}}\mathrm{d}z^k_{\mathsf{n}}, \tag{4.99}$$

where we have used the fact that $h_{\pi_\ell} = a_{\mathsf{n}}^{-1}$.

4.4.3 Regge geometries

The previous calculation shows that we can think of the phase space P_Γ as the phase space of piecewise (metric) flat geometries on $\Sigma\backslash\Gamma^*$. Such geometries possess an invertible locally flat metric, with curvature concentrated on the edges of the cellular space. This description is reminiscent of Regge geometries. However, it is known that the phase space of loop gravity is bigger than the phase space of Regge geometry [73]; Regge geometries appear only as a constrained subset. This fact has triggered the search for the proper geometrical interpretation of the loop gravity phase space, for instance in terms of twisted geometries [52].

We can now clearly understand the key difference between the phase space of loop gravity and that of Regge geometries. In the flat gauge, the loop gravity phase space corresponds to a cellular space of the spatial manifold Σ where the extrinsic curvature is zero within each three-cell c_n but non-zero on the faces e_ℓ. The faces do not need to be flat two-surfaces, and may be arbitrarily curved so long as they do not self-intersect and only intersect with other faces along common boundaries. The difference between this setting and a Regge geometry is the arbitrariness in the shape of the faces; the faces are all flat in a Regge geometry.

In order to see how the loop gravity phase space (in the flat gauge) may be reduced to a Regge geometry, we must ask how can the faces be made flat? A necessary condition for a face f_ℓ to be flat is that the boundary $\partial\mathsf{f}_\ell$ is composed of flat links. Since Γ^* is the union of all face boundaries, Γ^* must consist entirely of flat links in order to obtain a Regge geometry.

Let us go back to the formula for the fluxes that we have derived in the previous subsection:

$$X^i_\ell = \frac{1}{2}\epsilon^i{}_{jk}\int_{\partial\mathsf{f}_\ell} z^j_\mathsf{n}\wedge \mathrm{d}z^k_\mathsf{n}, \tag{4.100}$$

where $\boldsymbol{z}_\mathsf{n}$ is the flat coordinate in the cell c_n. One sees that if the links $\ell\in\partial\mathsf{f}_\ell$ are chosen to be flat, then $\boldsymbol{z}_\mathsf{n}$ is linear and $\mathrm{d}\boldsymbol{z}_\mathsf{n}$ is constant over $\partial\mathsf{f}_\ell$. This simplifies the expression drastically. Recall that due to the Gauss law, the fluxes are independent of the choice of faces (4.26) for fixed Γ^*. This means that (4.100) is independent of the choice of face, so that we obtain the same flux whether the face is chosen curved or flat, so long as the boundary of the face is composed of flat links. Indeed, a Regge geometry is given by a unique set of link lengths which can be reconstructed from the fluxes and dihedral angles between links, independently from the choice of faces. Imposing that Γ^* be composed entirely of flat links implies that the fluxes can be constructed, using (4.100), entirely in terms of a discrete piecewise flat geometry à la Regge.

In the twisted geometries construction [52] the geometry is seen as flat polyhedra glued together along faces. While two faces that are glued together have the same area, they may generally have different shapes. This means the metric is discontinuous across faces, although it is still possible to define a spin connection [56]. The reduction to a Regge geometry is done using gluing constraints [73]. These constraints impose that the shapes match by enforcing that corresponding dihedral angles on the face boundaries agree.

In our cellular space there is only one face between neighboring cells, so there is no notion of pairs of faces that must be made to fit together. Once the links of Γ^* are made flat, the gluing constraints are automatically satisfied by construction. This means that the set of holonomies and fluxes on a graph can be implemented as a piecewise flat geometry on $\Sigma\backslash\Gamma^*$ by making a particular gauge choice, and corresponds to a Regge geometry if we impose the additional

constraint that the links of Γ^* are straight with respect to the flat structure[5]. The phase space of full loop gravity then corresponds to piecewise geometries where this additional restriction is not imposed. In other words, the links of Γ^* do not have to be flat when mapping from the loop gravity phase space to the continuous phase space using the flat cell gauge.

4.4.4 Cotangent bundle

The result of our construction is that after a choice of gauge, we can express the elements of P_Γ as a connection $\boldsymbol{A}$ and an $\mathfrak{su}(2)$-valued frame field $\boldsymbol{e}$, which are solutions to:

$$\boldsymbol{F}[\boldsymbol{A}](x) = 0, \qquad \mathrm{d}_A \boldsymbol{e}(x) = 0, \qquad \forall\, x \in \Sigma \backslash \Gamma^*. \tag{4.101}$$

Since $\delta \boldsymbol{F}[\boldsymbol{A}] = \mathrm{d}_A \delta \boldsymbol{A}$, this is nothing but the cotangent bundle of the space of flat SU(2) connections on $\Sigma \backslash \Gamma^*$. That is:

$$P_\Gamma = T^* \mathcal{M}_{\Gamma^*}, \tag{4.102}$$

where $\mathcal{M}_{\Gamma^*}$ denotes the moduli space of flat connections modulo gauge transformations. This means that at the quantum level we can represent the quantization of holonomies and fluxes in terms of operators acting on holonomies of flat connections. This interpretation has already proposed by Bianchi in [59]. It is interesting to note that this is reminiscent of the geometry considered by Hitchin in [74].

4.4.5 Diffeomorphisms and gauge choices

We have seen in subsection 4.3.5 that diffeomorphisms Φ_o connected to the identity that do not move Γ^* or the nodes of Γ leave the construction of the holonomy-flux algebra invariant. We have also seen in the beginning of this section that the singular gauge and the flat gauge are diffeomorphism covariant. In general, the construction of h_ℓ and $\boldsymbol{X}_\ell$ depends both on Γ via the choice of ℓ, and on Γ^* via the choice of a two-cell f_ℓ. Now, because of the flatness of the connection, the holonomy does not really depend on the choice of link ℓ, but solely on the choice of the homotopy class of ℓ, which itself is left unchanged by diffeomorphisms that are connected to the identity. For the isomorphism between $\mathcal{P}^G_{\Gamma^*}$ and P^G_Γ, it is interesting to note that the choice of the singular gauge is invariant under a diffeomorphism that does not move Γ, whereas the choice of the flat gauge is invariant under diffeomorphisms that do not move Γ^*. Indeed, in the singular gauge the frame field depends on the choice of an link $\ell \in \Gamma$, and we have $\Phi^* \boldsymbol{E} = \boldsymbol{E}$ if $\Phi^{-1}(\Gamma) = \Gamma$. Moreover, under an infinitesimal diffeomorphism ξ, the flux becomes:

$$\delta_\xi \boldsymbol{X}_\ell = \int_{\partial \mathsf{f}_\ell} \iota_\xi \left(h_{\pi_\ell}(x) \boldsymbol{E}(x) h_{\pi_\ell}(x)^{-1} \right), \tag{4.103}$$

where $h_{\pi_\ell}(x)$ is again the holonomy going from the source node of the link ℓ to the point x in f_ℓ. We clearly see that this expression vanishes for all ξ when the electric field is in the singular

[5] This means that $\mathrm{d}z_\mathsf{n}$ is constant on the links of Γ^*.

gauge. In the flat gauge, the flux does not depend on Γ, and the construction is therefore invariant under diffeomorphisms leaving Γ^* invariant. This shows that there is an interesting duality between the two gauges. While the singular gauge respects diffeomorphism invariance with respect to Γ, the flat one respects diffeomorphism invariance with respect to Γ^*.

4.5 Cylindrical consistency

Recall from Chapter 3 that an important property of operators in LQG is that of cylindrical consistency associated with a projective family of graphs [24]. In a projective family of graphs we have an ordering such that we may write for any two graphs in the family that $\Gamma < \Gamma'$ if Γ' contains all the links of Γ in addition to other links. A cylindrically consistent function is such that the pull-back from P_Γ to $P_{\Gamma'}$ is identified with the function on P_Γ.

In this section we give a proposal for extending the notion of cylindrical consistency to functionals $\mathcal{O}[\boldsymbol{A}, \boldsymbol{E}]$ of the continuous fields. We analyze to what extent the knowledge of a collection of functions on P_Γ for all Γ determines a continuous functional. Given a collection of functions $\mathcal{O}_\Gamma \in P_\Gamma$, we now propose an extension of cylindrical consistency to continuous functionals.

Definition 4.5.1. Suppose that we are given a collection of functions $\mathcal{O}_\Gamma \in P_\Gamma$. We say that such a collection of functions is cylindrically consistent if there exists a continuous functional $\mathcal{O}[\boldsymbol{A}, \boldsymbol{E}]$ such that its restriction on the constraint surface $\mathcal{C}$ is equal to $\mathcal{O}_\Gamma$. That is

$$\mathcal{O}|_{\mathcal{C}}\,[\boldsymbol{A}, \boldsymbol{E}] = \mathcal{O}_\Gamma\big[h_\ell[\boldsymbol{A}], \boldsymbol{X}_\ell(\boldsymbol{A}, \boldsymbol{E})\big]. \tag{4.104}$$

The results presented in the previous sections show that such a continuous functional $\mathcal{O}[A, E]$ is characterized by the following property:

Proposition 4.5.2. *$\mathcal{O}[\boldsymbol{A}, \boldsymbol{E}]$ is a cylindrical functional if and only if its restriction to the constraint surface $\mathcal{C}$ is invariant under the gauge group $\mathcal{F}_{\Gamma^*} \times G_\Gamma$ for every pair of dual graphs (Γ, Γ^*).*

Indeed, suppose that we have a functional $\mathcal{O}[\boldsymbol{A}, \boldsymbol{E}]$ defined on the phase space $\mathcal{P}$ such that its restriction to the constraint surface $\mathcal{C}$ is then $\mathcal{O}|_{\mathcal{C}}[\boldsymbol{A}, \boldsymbol{E}]$, where the field configurations now satisfy $\boldsymbol{F}(\boldsymbol{A}) = 0$ outside of the dual graph Γ^*, and $\mathrm{d}_A \boldsymbol{E} = 0$ outside of the nodes n_Γ. $\mathcal{O}[\boldsymbol{A}, \boldsymbol{E}]$ is a cylindrically consistent functional if and only if:

$$\mathcal{O}|_{\mathcal{C}}\big[g \triangleright \boldsymbol{A}, (\phi, g) \triangleright \boldsymbol{E}\big] = \mathcal{O}|_{\mathcal{C}}\,[\boldsymbol{A}, \boldsymbol{E}], \tag{4.105}$$

which necessarily implies that $\mathcal{O}[\boldsymbol{A}, \boldsymbol{E}] = \mathcal{O}\big[h_\ell[\boldsymbol{A}], \boldsymbol{X}_\ell(\boldsymbol{A}, \boldsymbol{E})\big]$.

This proposition gives us a powerful criterion to check wether a continuous functional can be represented as a collection of functions associated with P_Γ. For instance, we can analyze the status of geometrical functionals such as area and volume. We know that the continuous expression for the area functional is:

$$A(S) = \int_S \sqrt{\tilde{E}^i_a \tilde{E}^a_i}. \tag{4.106}$$

One can easily see that even when we restrict this functional to the constraint surface $\boldsymbol{F}(\boldsymbol{A}) = 0$ outside Γ^* and $\mathrm{d}_A\boldsymbol{E} = 0$ outside of n_Γ, this functional is *not* invariant under the translations $\boldsymbol{E} \longmapsto \boldsymbol{E} + \mathrm{d}_A\boldsymbol{\phi}$. Therefore, this functional is *not* expressible purely in terms of holonomies and fluxes associated with the graph Γ. However, in loop quantum gravity, the area operator is expressed as an operator acting on the graph Γ, and is the quantum version of a function of the fluxes[6]:

$$A_{\mathrm{LQG}}(S) = \sum_{\ell|\ell\cap S\neq 0} \sqrt{X^i_\ell X_{\ell i}}. \tag{4.107}$$

Our proposition therefore shows that the LQG area operator does not come from the continuous area functional. This means that we have

$$A(S)|_{\mathcal{C}} - A_{\mathrm{LQG}}(S) \neq 0. \tag{4.108}$$

So in that sense, the LQG operator is not a proper approximation of the continuous area functional.

This is puzzling since the LQG area operator has been used extensively and derived in many ways. This result thus raises the question of the exact relationship between these two objects. To what extend does the LQG operator capture information about the continuous area functional? Now, since we have the exact relationship between the discrete and continuous phase spaces, we can investigate this question a bit further.

First, let us recall that the continuous and LQG areas are not unrelated. In fact, for any product h_Γ of holonomies supported on the graph Γ, they satisfy

$$\big\{A(S)|_{\mathcal{C}} - A_{\mathrm{LQG}}(S), h_\Gamma\big\} = 0. \tag{4.109}$$

So even if $A|_{\mathcal{C}} - A_{\mathrm{LQG}}$ does not vanish, it belongs to the commutant of the holonomy algebra.

The second key remark is that if we have a non-gauge-invariant functional like $A(S)$, we can promote it to a gauge-invariant functional under $\mathcal{F}_{\Gamma^*}$ by picking up a gauge. This can be done by working with $A^{\mathcal{T}}(S) \equiv A(S)\big(\boldsymbol{E}(\boldsymbol{X}_\ell)\big)$ instead of $A(S)(\boldsymbol{E})$, where $\mathcal{T}$ is a gauge choice as described in section 4.4. Such a functional is by construction invariant under $\mathcal{F}_{\Gamma^*}$, since it depends only on the fluxes. Moreover, the difference between two functionals that differ by a choice of gauge belongs to the commutant of the holonomy algebra:

$$\big\{A^{\mathcal{T}}(S) - A^{\mathcal{T}'}(S), h_\Gamma\big\} = 0. \tag{4.110}$$

This implies that the LQG area operator is the quantization of the continuous area functional written in a particular gauge, and as described in section 4.4, the interpretation of geometry in LQG is given by the singular gauge. This explains why it can be expressed purely in terms of fluxes.

So far in (4.107) we have considered the covariant flux (4.16) rather than the usual definition (4.13). Does this analysis hold for an area operator defined from the traditional definition of

[6]For the moment we shall use the covariant fluxes (4.16) in this definition, even though the traditional LQG area operator descends from a functional defined using (4.13). We shall comment more on this below.

flux? In the singular gauge the electric field is given by (4.83), and the integral defining the covariant flux (4.16) receives a contribution only at the point of intersection between the surface S and the link ℓ. The dependence on h_π is traced out in the definition (4.107) so that in the singular gauge, the area functional is the same whether one uses the covariant flux or the usual definition. Therefore, the above analysis is valid for either form of the flux.

Now, what is unclear is to what extent the knowledge of a function in a given gauge allows reconstruction of the continuous functional. Also, if one chooses another gauge, like the flat gauge of spin foam models, we are going to construct a different family of area functions associated with graphs, which will differ from A_{LQG} by an element of the commutant of the holonomy algebra. It is not clear which family of operators (if any) we should use to capture in the most efficient way information about the continuous volume operator.

4.6 Discussion

In this chapter, we have shown that the discrete phase space P_Γ of loop gravity associated with a graph Γ can be interpreted as the symplectic reduction of the continuous phase space of gravity $\mathcal{P}$ with respect to a constraint imposing the flatness of the connection everywhere outside of the dual graph Γ^*. This allows us to give a clear interpretation of the discrete flux variables as labeling an equivalence class of continuous geometries. The point of view that the discrete data represents a set of continuous geometries has already been advocated in [43]. Our approach gives a precise understanding of which set or equivalence class of continuous geometries is represented by the discrete geometrical data $(h_\ell, \boldsymbol{X}_\ell)$ on a graph. It provides a classical understanding of the work by Bianchi [59], who showed that the spin network states can be understood as states of a topological field theory living on the complement of the dual graph. It also allows us to reconcile the tension between the loop quantum gravity picture, in which geometry is thought to be singular, and the spin foam picture, in which the geometry is understood as being locally flat. We now see that both interpretations are valid and correspond to different gauge choices in the equivalence class of geometries represented by the fluxes. It gives us a new understanding of the geometrical operators used in loop quantum gravity as gauged fixed operators, and allows us to investigate further the relationship between these operators and the continuous ones. Finally, it opens the way to a classical formulation of loop gravity. We can now face the question of whether the dynamics of classical general relativity can be formulated in terms of these variables.

Chapter 5

Spinning Geometries

In the previous chapter, we established an isomorphism between the discrete phase space P_Γ parameterized by holonomies and fluxes on a graph, and a reduction of the continuous phase space $\mathcal{P}_{\Gamma,\Gamma^*}$ parameterized by fields $(\boldsymbol{A}, \boldsymbol{E})$ subject to certain constraints. If we impose the Gauss constraint everywhere on Σ, then we also obtain an isomorphism between gauge invariant phase spaces $P^G_\Gamma \approx \mathcal{P}^G_{\Gamma^*}$. This tells us that an equivalence class of continuous geometries corresponds with a single point in P^G_Γ. What we would like to do now, is to select a member of the equivalence class of continuous geometries which is convenient for working with, i.e. to make a gauge choice for the fields $(\boldsymbol{A}, \boldsymbol{E})$ which corresponds to some data $(h_\ell, \boldsymbol{X}_\ell)$ for all $\ell \in \Gamma$. We would like to make a choice which simplifies the scalar constraint and allows us to rewrite the continuous Hamiltonian in terms of holonomies and fluxes. There are two such choices that we presented which satisfy the condition of gauge covariance, meaning that choosing this gauge and then performing a diffeomorphism yields the same geometry as first doing the diffeomorphism and then choosing the gauge. The singular gauge has support only on the graph Γ, and the distributional nature of the geometry make it difficult to apply to the continuous Hamiltonian. The flat cell gauge on the other hand has support on all of $\bar{\Sigma}$ so that it is a good candidate for a continuous representation of the discrete phase space. The flat cells have the nice properties of vanishing extrinsic $\boldsymbol{K} = 0$ and intrinsic $\boldsymbol{F} = 0$ curvature. Notice that this already leads to a great simplification in the scalar constraint:

$$S(N) = \int_\Sigma N \frac{E^a_i E^b_j}{\sqrt{|E|}} \left(\epsilon^{ij}{}_k F^k_{ab} - 2(1+\gamma^2) K^i_{[a} K^j_{b]} \right). \tag{5.1}$$

Since the scalar constraint vanishes within each cell and on each face, the dynamics is generated solely by terms associated to the edges in the one-skeleton! This is very promising for being able to write this in terms of holonomies and fluxes, since fluxes are defined on the faces and holonomies give the curvature of loops which circle the edges.

This chapter presents the work of [75], which goes deeper into the flat cell gauge to learn more about it. So far we know that the intrinsic and extrinsic curvature vanish within cells, as is the case for Regge geometries [42] and twisted geometries [54]. A Regge geometry is a set of polyhedron-shaped cells which are glued together along faces in a continuous manner, while a twisted geometry is a set of polyhedron-shaped cells glued together in a *dis*continuous

Geometry	3-metric	faces	edges
Regge	continuous	flat	torsionless
Twisted	discontinuous	flat	torsionless
Spinning	continuous	curved	torsionfull

Table 5.1: Regge, twisted and spinning geometries are cellular spaces composed of flat, torsionless three-cells. This table contrasts their differences.

manner. For the flat cell gauge, we have a continuous gluing of the cells, but we do not know anything about the cell shapes. In this chapter we shall address this ambiguity, and discover that edges in the flat cell gauge must take the form of helices. Moreover, we shall find that these edges carry an angular momentum, which motivates the name 'spinning geometries' for a cellular space composed of cells defined by the flat cell gauge choice.

In this chapter we also want to make clear the relationship between spinning, twisted and Regge geometries. All three of these geometries are composed by the gluing of flat cells with curvature being present on the cell boundaries. We can understand their differences by considering the continuity and torsion of each type of geometry. A twisted geometry is the most general cellular space composed of flat cells that admits a torsionless connection but is discontinuous. Each cell is itself continuous so that the discontinuities arise only at the faces where cells are glued together. Conversely, the spinning geometries that we shall introduce are a piecewise-flat cellular space that is continuous, but carries torsion. Each cell is itself torsionless, and torsion is supported only on the edges in the cell boundaries. A Regge geometry is at the intersection of a twisted and spinning geometry, being a flat cellular space that is both continuous *and* torsionless. In that sense both spinning and twisted geometries are natural generalizations of Regge geometries. The obvious advantage of the spinning geometries is that they are continuous and do not require an extension of what we demand geometries to be in gravity.

We can now appreciate the differences between spinning geometries and twisted geometries: one is continuous while the other is *dis*continuous; one is piecewise-flat, the other is piecewise-*linear*-flat, one is torsion*full*, the other is torsion*less*. A summary of this comparison is presented in table 5.1. One of the key differences that explains the existence of spinning geometries is the relaxation of the demand that the geometry be linear. This extension is possible since we allow torsion to be non-vanishing along the edges within cell boundaries. If we have a linear geometry it is then necessarily flat, but the converse is not true. There exist flat geometries that are not obtained by linear gluing. An example of such a space as we will see is an helicoidal space obtained by gluing a wedge supported on an helix with a general Poincaré transformation admitting a translational component along the wedge. The main result presented in this paper is the equivalence between the truncated loop gravity phase space P^G_Γ and the spinning geometries. Now, since twisted geometries also represent points in the P^G_Γ phase space, this implies an equivalence between spinning geometries and twisted geometries. They represent the same holonomy-flux data, and we can therefore think of a twisted geometry as a regular, continuous spinning geometry.

We begin in the next section by recalling the definitions of twisted and flat-cell geometries,

using this context to discuss how these relate to Regge geometries. Following this, we look more closely at the gluing rules for the coordinate functions $\boldsymbol{z}^c$ associated to cells in the flat-cell geometry, and discover that these gluing rule imply that each edge of the one-skeleton is a helix. The axis of each helix is determined by the holonomies around each edge. In order to see what role the fluxes play, we trade the fluxes associated to faces for angular momenta associated to edges, an extension made possible by the Gauss law. Using these variables, we write an action composed of a sum over the edge lengths with a constraint to hold edge momenta fixed. Studying deformations of this action shows us that helices arise naturally as the minimum length edges for a given set of edge momenta. Using an action allows us to derive equations of motion which parameterize the helices, and reveal how fluxes come into play for determining the shapes of helices.

5.1 Definitions

In this section we provide definitions of the twisted, flat-cell and Regge geometries. This discussion is relevant for the calculations which follow, but also serves to explain the relationship between these geometries.

This chapter is essentially an exercise in the geometry of cellular complexes, and with the isomorphism established in Chapter 4, we can work entirely within this context and leave behind the notion of graphs. We use the correspondence between faces f of the two-complex and links ℓ in the dual graph to label each face with a holonomy and flux. We denote in bold letters an element $\boldsymbol{A} \in \mathfrak{su}(2)$, which can be identified with a vector in $\mathbb{R}^3$ through $A^i = -2\mathrm{Tr}(\boldsymbol{A}\boldsymbol{\tau}^i)$, where $\boldsymbol{\tau}^i$ is an $\mathfrak{su}(2)$ basis given by $-i/2$ times the Pauli matrices. This basis satisfies the algebra $[\tau_i, \tau_j] = \epsilon_{ijk}\tau^k$. We will use also the vector notation of a dot-product for a trace $\boldsymbol{A} \cdot \boldsymbol{B} \equiv -2\mathrm{Tr}(\boldsymbol{A}\boldsymbol{B})$, and a cross-product for an $\mathfrak{su}(2)$ commutator $\boldsymbol{A} \times \boldsymbol{B} \equiv [\boldsymbol{A}, \boldsymbol{B}]$. A magnitude is denoted by dropping the bold font $A \equiv |\boldsymbol{A}|$, and a unit vector is denoted by a hat $\hat{\boldsymbol{A}} \equiv \boldsymbol{A}/A$.

5.1.1 Twisted geometry

A twisted geometry is a set of polyhedra-shaped three-cells c which are 'glued' together along faces f according to certain rules. To each face oriented outwardly with respect to the cell c, we attribute an $\mathfrak{su}(2)$-valued flux $\boldsymbol{X}_\mathsf{f}$ and an SU(2)-valued holonomy h_f (see [47, 67] for a related discussion). The face areas are given by the magnitudes X_f and the orientations are given by outward pointing unit vectors $\hat{\boldsymbol{X}}_\mathsf{f}$ which are normal to the faces. In order that each polyhedron is closed, the fluxes satisfy a closure relation:

$$\sum_{\mathsf{f}} \boldsymbol{X}_\mathsf{f} = 0, \tag{5.2}$$

where the sum is over all the faces of the polyhedron. By a classical theorem of Minkowski [76], the reverse is true: A set of flux operators satisfying the closure condition defines a polyhedra.

A face $\mathsf{f}_{cc'}$ on a cell c is glued to a face $\mathsf{f}_{c'c}$ on a neighbouring cell c'. Each face possesses an orientation such that $\mathsf{f}_{cc'}$ is oriented oppositely to $\mathsf{f}_{c'c}$. Holonomies come into play for gluing

polyhedra together. For faces that are glued together the areas are the same, i.e. $X_{cc'} = X_{c'c}$, however the orientation is generally different. A consistent gluing requires that:

$$\boldsymbol{X}_{c'c} = -h_{cc'}^{-1} \boldsymbol{X}_{cc'} h_{cc'}. \tag{5.3}$$

The non-zero extrinsic curvature at the intersections between cells is manifest in these gluing conditions.

A twisted geometry does not form a continuous geometry. This is because the shape of a face $\mathsf{f}_{cc'}$ that comes from the polyhedral geometry of c, is in general different than the shape of $\mathsf{f}_{c'c}$ which it is glued to. For example, $\mathsf{f}_{cc'}$ may have three sides while $\mathsf{f}_{c'c}$ can have four. Even if each face possesses the same number of sides, the faces still have different shapes in general, so that the boundary edges of each face do not match. In order to form a continuous geometry, one may impose conditions [58] which force the shapes of faces to match when they are glued together. These extra conditions restrict the degrees of freedom in the loop gravity phase space and reduce a twisted geometry to a Regge geometry. We now explore another option which provides continuous geometries without having to reduce the number of degrees of freedom.

5.1.2 Flat cell geometry

A *Regge geometry* is a *piecewise-linear-flat* cellular complex [42]. This means that it is obtained by gluing together polyhedra along their faces with piecewise-linear maps [77]. We define a *spinning geometry* as a generalization to a *piecewise-flat*, regular cellular complex. This is a geometry which is obtained by gluing cells homeomorphic to polyhedra, but we relax the condition of the gluing maps to be piecewise-linear (see fig. 5.1. We demand instead that the resulting geometry is flat. A spinning geometry is the same as the flat-cell geometry defined in Chapter 4, but we give it a more appropriate name here due to the results we uncover[1].

First of all, recall from Section 4.3.1 our definition of a regular cellular space, composed of cells c, with faces that are glued together in a continuous manner by maps $s_{cc'}$. These maps are such that the boundaries of each face $\partial\mathsf{f}_{cc'}$ is glued to the boundary of the face of a neighbouring cell $\partial\mathsf{f}_{c'c}$. We give the following definition:

Definition 5.1.1. A spinning geometry is a regular cellular space Δ together with a (not necessarily piecewise-linear) embedding of c into $\mathbb{R}^3$. That is we have a set of injective maps:

$$\boldsymbol{z}^c : \bar{c} \to \mathbb{R}^3. \tag{5.4}$$

These maps define a flat metric $(g^c)_{\mu\nu} := \partial_\mu \boldsymbol{z}^c \cdot \partial_\nu \boldsymbol{z}^c$ on each cell c. We demand these metrics to be compatible with the gluing maps:

$$(s_{cc'})^* g_{c'}(x) = g_c(x), \qquad \forall x \in \bar{\mathsf{f}}_c. \tag{5.5}$$

[1] Our initial thoughts were that spinning geometries were a subclass of flat-cell geometries for a given choice of edge shapes, but we shall find below that in fact the helix is the only choice that satisfies the gluing maps around an edge!

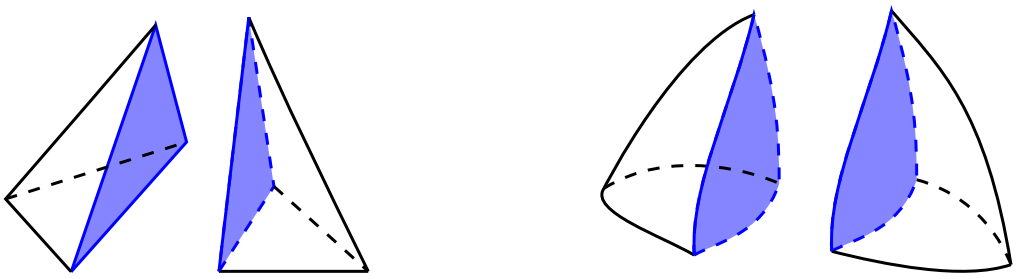

(a) Twisted geometry (b) Flat cell geometry

Figure 5.1: On the left are two cells of a twisted geometry with the shared face shown filled in blue — notice that each cell is a polyhedron, and that the blue face on one cell is a different shape than the corresponding face on the other cell, even though the areas are the same. On the right we have two cells of a flat cell geometry — notice that each cell here is a deformed polyhedron, and that the shape of the face on one cell matches the corresponding face shape on the other cell. The illustration does not show that each edge of the flat cell (or 'spinning') geometry is actually a helix, which follows from the analysis presented in this chapter.

The key point to appreciate here is that even if $\bar{c}$ is equipped with a flat metric, it does not have to coincide with the polyhedral metric on $\psi_c(\bar{c}) = P_c$. In particular we *do not* assume that the induced metric on the faces of $\bar{c}$ is flat. That is we allow an arbitrary value of the (2d) extrinsic curvature tensor on the faces of $\bar{c}$.

The condition of compatibility (5.5) of the metric with the gluing maps can be expressed more explicitly in terms of the flat coordinates $\boldsymbol{z}^c$. Indeed it implies that the coordinates $\boldsymbol{z}^c$ and $\boldsymbol{z}^{c'}$ are related by a Poincaré transformation when evaluated on the boundary of the cell.

Consider two neighbouring cells c and c'. From now on we will denote by $\mathsf{f}_{cc'}$ the face shared by c and c' viewed from c, and by $\mathsf{f}_{c'c} = s_{cc'}(\mathsf{f}_{cc'})$ the same face as seen from c'. We assign to each face their outward orientation so that $\mathsf{f}_{cc'}$ and $\mathsf{f}_{c'c}$ have opposite orientations. Under the gluing maps we obtain a continuous metric on cell faces with the requirement:

$$\lim_{x' \to \mathsf{f}_{c'c}} \mathrm{d}\boldsymbol{z}_{c'}(x') = \lim_{x \to \mathsf{f}_{cc'}} h_{cc'}^{-1} \mathrm{d}\boldsymbol{z}_c(x) h_{cc'}, \qquad \forall\ x \in c,\ x' \in c', \tag{5.6}$$

where $h_{cc'} \in \mathrm{SU}(2)$ is a group element associated to the face $\mathsf{f}_{cc'}$ such that $h_{c'c} = h_{cc'}^{-1}$. This implies that the coordinate functions are related by a Poincaré transformation:

$$\lim_{x' \to \mathsf{f}_{c'c}} \boldsymbol{z}_{c'}(x') \ = \lim_{x \to \mathsf{f}_{cc'}} h_{cc'}^{-1} \left(\boldsymbol{z}_c(x) + \boldsymbol{b}_{cc'}\right) h_{cc'}, \qquad \forall\ x \in c,\ x' \in c', \tag{5.7}$$

where $\boldsymbol{b}_{cc'} \in \mathfrak{su}(2)$ is an algebra element corresponding to a translation. While (5.6) implies (5.7), notice that the reverse is not true[2]. This suggests the following definitions:

[2]If $\boldsymbol{z}^c$ and $\boldsymbol{z}^{c'}$ are related by a Poincaré transformation, only the differential tangential to the face satisfies (5.6). This equation also expresses that the derivative normal to the face has to be continuous. This condition gives us information about the shape of the faces as embedded in the three-cells. We will postpone the detailed study of these conditions, since here we focus on the shapes of the edges.

Definition 5.1.2. A Regge geometry is a piecewise-flat cellular space such that the induced metric on all of the faces is flat. A spinning geometry is a piecewise-flat cellular space such that the image of edges of $\bar{c}$ by z^c are helices.

We will study in the following sections how the helical shape of the edges in a spinning geometry arise from the definitions we have given.

The spinning geometry is continuous; the shape of a face $\mathsf{f}_{cc'}$ is the same according to the local coordinates in c and c'. As for twisted geometries, one can define a holonomy and flux pair $(\boldsymbol{X}_\mathsf{f}, h_\mathsf{f})$ assigned to each face, and these variables satisfy the closure (5.2) and gluing (5.3) relations. As with Regge geometries, curvature is non-zero only at intersections between cells of the spinning geometry, i.e. on faces and edges.

Note that twisted and spinning geometries are each isomorphic to the SU(2) gauge invariant loop gravity phase space P_Γ. This implies an isomorphism between twisted and spinning geometries, which we can see by looking at each cell separately. Each cell of both geometries has vanishing intrinsic and extrinsic curvature, so the only difference is in the cell shape. Each of the faces in a spinning geometry has an associated flux, and these fluxes satisfy the closure constraint (5.2). A theorem by Minkowski [76] proves that a set of fluxes satisfying the closure constraint is isomorphic to a unique polyhedron. This means that one can obtain a twisted geometry from a spinning geometry by taking the spinning geometry apart cell by cell, then deforming each cell into the associated polyhedron. Turning this argument around, one can view a spinning geometry as a way to form a continuous three-geometry from a twisted geometry.

We have two isomorphic interpretations of the loop gravity phase space which possess different attributes of a Regge geometry. On the one hand, the spinning geometry is a continuous three-geometry which can represent a spatial hypersurface of spacetime. However, the cell boundaries take curved shapes rather than the neat form of polyhedra. On the other hand, cells of the twisted geometry interpretation do take the form of polyhedra, but we lose the ability to describe a continuous three-geometry.

5.2 Edge shapes

Twisted geometries rely on the Minkowski theorem [76], which states that any set of fluxes satisfying the closure condition represents a unique polyhedron (up to translations). Because of this theorem, we know that it is always possible to choose only straight edges for a single cell. However this is no longer possible when we start to glue the cells together in a continuous manner. The question is then, under what conditions on compatible holonomy-flux data can we consistently glue cells together, and what is the form of the gluing maps $s_{cc'}$?

We have seen that consistency of gluing requires that the coordinate functions satisfy the relations (5.7). Let us now consider an edge e which is common to all the cells $c_1, \cdots c_n$, that is we assume that $\mathsf{e} \equiv \mathsf{f}_{c_1} \cap \cdots \cap \mathsf{f}_{c_n}$ under the gluing maps. This means that for $x \in \mathsf{e}_{c_1}$ we have a map $S_{c_1 c_i}(x) \equiv s_{c_1 c_2} \cdots s_{c_{i-1} c_i}(x) \in \mathsf{e}_{c_i}$ for $i = 2, \cdots, n$ which maps a point in e_{c_1} to a point in e_{c_i}, and these two edges are identified under the gluing maps. We can then use repeatedly the previous identity along a path $\gamma = (c_1 c_2 \cdots c_n)$. If we define $H^\mathsf{e}_{c_1 c_i} \equiv h_{c_1 c_2} \cdots h_{c_{i-1} c_i}$, $H^\mathsf{e}_{c_i c_1}$

its inverse and $\boldsymbol{B}^{\mathsf{e}}_{c_1c_i} \equiv \sum_{k=2}^{i} H^{\mathsf{e}}_{c_kc_1} a_{c_{k-1}c_k} H^{\mathsf{e}}_{c_1c_k}$ we get:

$$\boldsymbol{z}^{c_i}(S_{c_1c_i}(x)) = H^{\mathsf{e}}_{c_ic_1} \boldsymbol{z}^{c_1}(x) H^{\mathsf{e}}_{c_1c_i} + \boldsymbol{B}^{\mathsf{e}}_{c_1c_i}. \tag{5.8}$$

If we take the path to form a closed loop ($c_1 = c_i$), we get that for any edge e_c and every point $x \in \mathsf{e}_c$ there exist gluing maps S^{e}_c, holonomies H^{e}_c and translations A^c_{e} such that:

$$\boldsymbol{z}^{c}(S^{\mathsf{e}}_c(x)) = H^{\mathsf{e}}_c \boldsymbol{z}^{c}(x) H^{\mathsf{e}}_c + \boldsymbol{B}^{\mathsf{e}}_c. \tag{5.9}$$

Let us first choose a parametrization of the edge e_c in terms of a parameter ϕ proportional to the length from a given point. Now, for some constant of proportionality ω, the induced metric on the edge is given by $\mathrm{d}s^2 = (\mathrm{d}\boldsymbol{z}^{\boldsymbol{c}})^2 = (\omega^{\mathsf{e}})^2\,\mathrm{d}\phi^2$. Since $S^{\mathsf{e}}_c(\phi)$ takes a point on the edge to another point on the same edge, this map has to be an isometry of the edge is therefore necessarily a translation in the length parametrization: $S^{\mathsf{e}}_c(\phi) = \phi + \theta^{\mathsf{e}}_c$, where θ^{e}_c is a constant associate to the edge e as seen from cell c.

What is remarkable is that the helix is a solution of (5.9). The holonomy around the edge H^{e}_c is a rotation of angle θ^{e} around some fixed axis $\hat{\boldsymbol{\omega}}^c_{\mathsf{e}}$, and the translational component is given by $\boldsymbol{B}^{\mathsf{e}}_c = K^{\mathsf{e}}\theta^{\mathsf{e}}\hat{\boldsymbol{\omega}}^c_{\mathsf{e}}$ for some constant K^{e}. Note that since the angle of rotation is the same[3] for any holonomy H^{e}_c which loops once around the edge e (and only that edge), we do not need a cell-label on the angle θ^{e}. The proportionality constant K^{e} in the translation gives a measure of the 'pitch' of the helix, i.e. how far along the axis one travels when going around the axis by an angle θ^{e}_c.

From the analysis done in three-dimensional gravity [78] we know that we can interpret H^{e}_c as the discrete curvature, while $\boldsymbol{B}^{\mathsf{e}}_c$ represents a discrete torsion. We see that if the geometry is non-Regge then the torsion does not vanish. This was already conjectured in [52, 60].

Looking carefully at the gluing maps around an edge shows us that each edge of a spinning geometry must be in the form of a helix. This implies that a given set of twisted geometry data $(\boldsymbol{X}_{cc'}, h_{cc'})$ can be represented in terms of a spinning geometry by twisted together the to form helices. Holonomies determine the axis $\hat{\boldsymbol{\omega}}^c_\ell$ of each helix, given by the axis of rotation defined by the composition of holonomies around the edge H^{e}_c. We have found how the holonomies help to determine the edge shapes, but to understand the role that fluxes play, we will need to attack this problem from a different angle.

5.3 Angular momentum

We would like to determine how the fluxes in P_Γ help to fix a spinning geometry. In loop gravity, fluxes measure the areas of surfaces and play an important role in determining local geometry. In the quantum theory, length [36], area [34] and volume [35] operators are constructed from flux operators. In twisted geometries, the flux variables completely determine the shape of cells, but in spinning geometries, fluxes only partially fix the cell shapes. Fluxes are associated to

[3]The holonomy H^{e}_c which loops around the edge e with base-point in the cell c and the holonomy $H^{\mathsf{e}}_{c'}$ looping around that edge with base-point in cell c' are related by $H^{\mathsf{e}}_{c'} = h_{cc'} H^{\mathsf{e}}_c h^{-1}_{cc'}$. The angle of rotation comes out in the trace $\mathrm{Tr}H^{\mathsf{e}}_{c'} = \mathrm{Tr}H^{\mathsf{e}}_c = 2\cos\theta^{\mathsf{e}}$ and is the same for both loop holonomies. Note however that the axes are different: $\hat{\boldsymbol{\omega}}^{\mathsf{e}}_{c'} = h_{cc'}\hat{\boldsymbol{\omega}}^{\mathsf{e}}_c h^{-1}_{cc'}$.

cell faces, but we want to know in particular how they determine the helices which make up the boundaries of these faces. To help us with this task, we now introduce angular momentum variables on each edge which can be mapped to a set of fluxes. The precise role that fluxes play in fixing a spinning geometry will be more clear at the end of the next section.

In addition to the relationship between fluxes and the areas of surfaces, these parameters are also closely related to angular momenta. This is because they satisfy the angular momentum Poisson algebra:

$$\left\{ \boldsymbol{X}^i_{\mathsf{f}}, \boldsymbol{X}^j_{\mathsf{f}} \right\} = \epsilon^{ij}{}_k \boldsymbol{X}^k_{\mathsf{f}}. \tag{5.10}$$

In this section we uncover another way in which flux is related to angular momentum.

Recall that each cell within a spinning geometry is assigned a set of flat coordinates $\boldsymbol{z}^c \in \mathfrak{su}(2)$. In terms of these coordinate functions, the flux is given by:

$$\boldsymbol{X}_{cc'} = \frac{1}{2} \int_{\mathsf{f}_{cc'}} [\mathrm{d}\boldsymbol{z}^c, \mathrm{d}\boldsymbol{z}^c], \tag{5.11}$$

where the direction of integration is clockwise as seen from inside the cell c, and the bracket on the right hand side implies taking both the wedge product and $\mathfrak{su}(2)$ commutator between elements[4].

Recall that each face possesses two orientations so that the flux appears to have a different orientation from each of the two cells which share the face. The flux $\boldsymbol{X}_{c'c}$ determined by $\boldsymbol{z}^{c'}$ is given by:

$$\boldsymbol{X}_{c'c} = -\frac{1}{2} \int_{\mathsf{f}_{c'c}} [\mathrm{d}\boldsymbol{z}^{c'}, \mathrm{d}\boldsymbol{z}^{c'}] = -h^{-1}_{cc'} \boldsymbol{X}_{cc'} h_{cc'}, \tag{5.12}$$

in agreement with (5.3) above. The negative sign comes from reversing the direction of integration.

In the case when the edges bounding the face are straight, $\boldsymbol{z}^c$ is linear along each edge and $\boldsymbol{\xi}^c_{\mathsf{e}} \equiv \dot{z}^c(x)$ for all $x \in \mathsf{e}$ is a constant vector associated to each edge in the boundary of c. For a closed face these vectors span a plane, the face is flat and we are in the Regge case. In general this is not true, but we can still assign a vector to each edge in the boundary of c. This follows from a very simple but extremely important remark: If we integrate by parts in (5.11) we can write the flux as:

$$\boldsymbol{X}_{cc'} = \sum_{\mathsf{e}_c \in \partial \mathsf{f}_{cc'}} \boldsymbol{J}^c_{\mathsf{e}}, \qquad\qquad \boldsymbol{J}^c_{\mathsf{e}} := \frac{1}{2} \int_{\mathsf{e}_c} [\boldsymbol{z}^c, \mathrm{d}\boldsymbol{z}^c], \tag{5.13}$$

which shows that we get a contribution $\boldsymbol{J}^c_{\mathsf{e}}$ from each edge $\mathsf{e}_c \in \partial \mathsf{f}_{cc'}$. This means that we can in fact decompose the flux in terms of a sum of contributions associated with each edge of the face.

Let us parameterize an edge $\mathsf{e}(s)$ by the proper length s to write:

$$\boldsymbol{J}^c_{\mathsf{e}} = \frac{1}{2} \int_{\mathsf{e}_c} \mathrm{d}s [\boldsymbol{z}^c, \dot{\boldsymbol{z}}^c], \tag{5.14}$$

[4]In coordinates this means $X^i_{cc'} = \frac{1}{2}\epsilon^{ijk} \int_{\mathsf{f}_{cc'}} \boldsymbol{z}^c_j \wedge \mathrm{d}\boldsymbol{z}^c_k$

where $\dot{\boldsymbol{z}}^c \equiv \partial_s \boldsymbol{z}^c$. If we interpret s as a time coordinate, then the integrand is a cross product between position and velocity, i.e. an angular momentum. Each $\boldsymbol{J}^c_{\mathsf{e}}$ is the angular momentum of a point particle in a 3d Riemannian 'spacetime', integrated over the 'worldline' given by the edge e. We shall refer to each $\boldsymbol{J}^c_{\mathsf{e}}$ as a *edge momentum*. In light of this, the flux associated to a face is given by the sum of the edge momenta around its boundary.

In order to maintain agreement with (5.3), the momentum associated to an edge as seen in cell c' is related to the momentum seen in cell c via:

$$\boldsymbol{J}^{c'}_{\mathsf{e}} = -h^{-1}_{cc'}(\boldsymbol{J}^c_{\mathsf{e}} + [\boldsymbol{b}_{cc'}, \boldsymbol{D}^c_{\mathsf{e}}])h_{cc'}. \tag{5.15}$$

where $\boldsymbol{D}^c_{\mathsf{e}} \equiv \boldsymbol{z}^c_{t(\mathsf{e})} - \boldsymbol{z}^c_{s(\mathsf{e})}$ is the difference between the coordinate function evaluated at the terminal $t(\mathsf{e})$ and starting $s(\mathsf{e})$ endpoints of the edge.

As with the fluxes, edge momenta are related to the oriented area of a two surface. When an edge is straight one can perform the integral in (5.14) to obtain:

$$\boldsymbol{J}^c_{\mathsf{e}} = \frac{1}{2}[\boldsymbol{z}^c_{s(\mathsf{e})}, \boldsymbol{D}^c_{\mathsf{e}}]. \tag{5.16}$$

In this case we see that $\boldsymbol{J}^c_{\mathsf{e}}$ is the oriented area of a two-surface bounded by the edge e and two straight edges joining the endpoints of e with the origin of the coordinate function $\boldsymbol{z}^c_{\mathsf{e}}$. Since this is the edge momentum when the edge is straight, this is the value one obtains for an edge in a Regge geometry.

If the edge is not straight it is no longer true that we can express simply $\boldsymbol{J}^c_{\mathsf{e}}$ as a cross product with $\boldsymbol{D}^c_{\mathsf{e}}$. If one thinks of $\boldsymbol{D}^c_{\mathsf{e}}$ as a total displacement vector, we see that the Regge contribution is analogous to the expression for the orbital angular momenta. If one pushes this analogy further, it is natural to interpret the case where the edge momenta is not Regge as being similar to the case where the total angular momenta contains a spin contribution. That is, in general we can decompose $\boldsymbol{J}$ into an orbital or Regge component $\boldsymbol{L}$, and a spin contribution $\boldsymbol{S}$:

$$\boldsymbol{J}^c_{\mathsf{e}} = \boldsymbol{L}^c_{\mathsf{e}} + \boldsymbol{S}^c_{\mathsf{e}}, \qquad \boldsymbol{L}^c_{\mathsf{e}} = \frac{1}{2}[\boldsymbol{z}^c_{s(\mathsf{e})}, \boldsymbol{D}^c_{\mathsf{e}}]. \tag{5.17}$$

The spin contribution measure the deviation from Regge and vanishes when the edge is straight. We will see that the spin contribution literally corresponds to a spinning trajectory.

The decomposition of the fluxes $\boldsymbol{X}_{cc'}$ in terms of edge angular momenta correspond to a general solution of the Gauss relation. We can interpret the Gauss law $\sum_{c'} \boldsymbol{X}_{cc'} = 0$ as a discrete differential identity $(\delta \boldsymbol{X})_c = 0$ whose solution is given by $\boldsymbol{X}_{cc'} = (\delta \boldsymbol{J})_{cc'}$ or $\boldsymbol{X}_{cc'} = \sum_{\ell \in \partial \mathsf{f}_{cc'}} \boldsymbol{J}^c_{\mathsf{e}}$. This solution follows from the fact that the discrete operation δ acts as a differential, i.e. $\delta^2 = 0$.

This solution is however a local solution valid around every cell. Moreover, a priori the number of faces differs from the number of edges, so it is not obvious that we can always trade face fluxes for edge momenta. For instance in a triangulation we generically have more edges than faces. Let us do an analysis to help understand this better. If we take the three-geometry to be homeomorphic to S^3, the number of edges $|\mathsf{e}_\Delta|$, vertices $|\mathsf{v}_\Delta|$, faces $|\mathsf{f}_\Delta|$ and cells $|c_\Delta|$ satisfy the relation:

$$|c_\Delta| - |\mathsf{f}_\Delta| + |\mathsf{e}_\Delta| - |\mathsf{v}_\Delta| = 0. \tag{5.18}$$

Recall that the fluxes satisfy a closure relation (5.2). This constraint is applied in each cell except one, since the last one is redundant. Therefore the total number of degrees of freedom in the fluxes of a spinning geometry is $|X_\Delta| = 3 \times (|\mathsf{f}_\Delta| - |c_\Delta| + 1)$.

There are $|J_\Delta| = 3 \times |\mathsf{e}_\Delta|$ degrees of freedom in a set of edge momenta. The counting of extra degrees of freedom in edge momenta versus fluxes is $|J_\Delta| - |X_\Delta| = 3 \times (|\mathsf{v}_\Delta| - 1)$. These extra degrees of freedom are accounted for in the kernel of the map (5.13) which is invariant when each of the edge momenta undergoes the transformation:

$$\boldsymbol{J}^c_{\mathsf{e}} \longrightarrow \boldsymbol{J}^c_{\mathsf{e}} + \boldsymbol{\zeta}^c_{t(\mathsf{e})} - \boldsymbol{\zeta}^c_{s(\mathsf{e})}, \tag{5.19}$$

where $\boldsymbol{\zeta}^c_{t(\mathsf{e})}$ is a vector at the terminal vertex of the edge and $\boldsymbol{\zeta}^c_{s(\mathsf{e})}$ is a vector at the starting vertex of the edge. Over the entire cellular decomposition there is one such independent vector at each vertex, which accounts for the remaining $3 \times (|\mathsf{v}_\Delta| - 1)$ degrees of freedom. The -1 here comes from the fact that one of these shifts can be accounted for by an overall translation. This analysis shows that there are as may degrees of freedom in a set of fluxes subject to the Gauss constraints as there are in the edge momenta, modulo an invariance related to the translation of vertices. Indeed, The transformation in (5.19) is defining an equivalence class of edge momenta, where each member of the class maps to the same set of flux data. If we specify a particular set of edge momenta we are choosing one member of this equivalence class.

Note finally that the kernel of the map in (5.13) is related to shifts in the coordinate functions. Looking at (5.14), if we translate the coordinates $\boldsymbol{z}^c \longrightarrow \boldsymbol{z}^c + \boldsymbol{b}$ the edge momenta transform as:

$$\boldsymbol{J}^c_{\mathsf{e}} \longrightarrow \boldsymbol{J}^c_{\mathsf{e}} + \frac{1}{2}[\boldsymbol{b}, \boldsymbol{z}^c_{t(\mathsf{e})}] - \frac{1}{2}[\boldsymbol{b}, \boldsymbol{z}^c_{s(\mathsf{e})}]. \tag{5.20}$$

This implies that the vectors transforming the edge momenta in (5.19) are given at each vertex n by $\boldsymbol{\zeta}^c_n = \frac{1}{2}[\boldsymbol{b}, \boldsymbol{z}^c_n]$.

5.4 Minimizing edge lengths

With the edge momenta, we can now address the question of how fluxes determine edge shapes. In Chapter 4 we showed that any piecewise flat geometry is isomorphic to an equivalence class of holonomy-flux data which represents a single point in the SU(2)-gauge invariant loop gravity phase space P^G_Γ. We now know that each edge of the flat-cell gauge, which we are now calling a spinning geometry, must in fact be a helix. But let us now forget about each edge being a helix and return to the perspective of Chapter 4 where the edge shapes were unknown. This will allow us to consider arbitrary deformations of the edges. From this perspective it is possible to deform the geometry of each individual cell without altering the edge momenta. Notice that if we make deformations which leave the edge momenta unchanged, then the fluxes remain fixed as well. Any two geometries related by such a deformation correspond to the same point in P^G_Γ. Our main goal is to explore this freedom and study the extent to which the edge shapes can be fixed by extra geometrical requirements. Is there a way to unambiguously fix the cell shapes to select a unique geometry to represent a point in P^G_Γ?

The Gauss law of loop gravity implies that the flux associated to a face depends only the edges on the boundary, i.e. if one fixes the edges on the boundary, any choice of face bounded by these edges will yield the same flux. This is shown explicitly in the expression of the flux given in (5.13). What this means is that we need only consider deformations of edges in the one-skeleton, and can ignore what is happening to the faces as long as we do not examine the continuity of the normal component of the frame field across faces

Now, the one-skeleton of a Regge geometry is composed of straight edges, so that each edge is the shortest path between the vertices at its endpoints. Let us use this idea to try to reduce the ambiguity in the choice of one-skeleton for a spinning geometry by minimizing the length of each edge while keeping the vertices fixed. At the same time, let us impose a constraint which keeps the edge momenta fixed so that we maintain a correspondence with the same point in the phase space P_Γ^G. This can be achieved by introducing the following action which sums over all of the edge lengths and includes a constraint to fix each edge momentum:

$$\mathcal{A} = \sum_{\mathsf{e}} \mathcal{A}_{\mathsf{e}}, \qquad \mathcal{A}_{\mathsf{e}} = \int_{\mathsf{e}} |\dot{\boldsymbol{z}}^c_{\mathsf{e}}| \mathrm{d}s + \boldsymbol{\omega}^c_{\mathsf{e}} \cdot \left(\boldsymbol{J}^c_{\mathsf{e}} - \frac{1}{2} \int_{\mathsf{e}} (\boldsymbol{z}^c_{\mathsf{e}} \times \dot{\boldsymbol{z}}^c_{\mathsf{e}}) \mathrm{d}s \right), \tag{5.21}$$

where $\boldsymbol{\omega}^c_{\mathsf{e}} \in \mathfrak{su}(2)$ is a Lagrange multiplier implementing the constraint which fixes $\boldsymbol{J}^c_{\mathsf{e}}$. In section 5.2 we used ω^c_{e} as a proportionality constant and $\hat{\boldsymbol{\omega}}^c_{\mathsf{e}}$ as a unit vector along the axis of the helix. We will see below why we are again using this notation. Notice there is only one term per edge although each edge e is attached to several cells. This is why we introduce a subscript on the coordinate functions $\boldsymbol{z}^c_{\mathsf{e}}$ to denote a choice of which coordinates are to be used for each term. Using the relations (5.7, 5.15), this action does not depend upon this choice, so long as we identify that the Lagrange multiplier defined in one cell is related to that of a neighbouring cell by:

$$\boldsymbol{\omega}^{c'}_{\mathsf{e}} = -h^{-1}_{cc'} \boldsymbol{\omega}^c_{\mathsf{e}} h_{cc'}. \tag{5.22}$$

Varying the action we find:

$$\delta\mathcal{A} = \sum_{\mathsf{e}} \int_{\mathsf{e}} \delta \boldsymbol{z}^c_{\mathsf{e}} \cdot (\dot{\boldsymbol{v}}^c_{\mathsf{e}} - \boldsymbol{\omega}^c_{\mathsf{e}} \times \dot{\boldsymbol{z}}^c_{\mathsf{e}}) \, \mathrm{d}s \tag{5.23}$$

where $\boldsymbol{v}^c_{\mathsf{e}} \equiv \frac{\dot{\boldsymbol{z}}^c_{\mathsf{e}}}{|\dot{\boldsymbol{z}}^c_{\mathsf{e}}|}$ is the 'proper velocity', treating s as the proper time and drawing upon our analogy with 3d point particles. Setting this variation to zero provides an equation of motion for each edge:

$$\dot{\boldsymbol{v}}^c_{\mathsf{e}} = \boldsymbol{\omega}^c_{\mathsf{e}} \times \dot{\boldsymbol{z}}^c_{\mathsf{e}}. \tag{5.24}$$

Let us now study the equation for a single edge.

5.4.1 Analysis of a single edge

Since we are analyzing a single edge for some choice of coordinate function $\boldsymbol{z}^c_{\mathsf{e}}$, we drop the super- and sub-scripts c and e for simplicity. Let us first assume that $\omega \neq 0$. If this is not

satisfied the equation of motion simply tells us that the edge has to be a straight line and we are back to the Regge case. When $\omega \neq 0$ it will be convenient for us to chose a parametrization of the curve $s = \phi$ where ϕ is ω times the proper length, that is:

$$\dot{z}_\phi = \omega^{-1}. \tag{5.25}$$

In this parametrization the equation of motion is simply:

$$\ddot{\boldsymbol{z}}_\phi = \hat{\boldsymbol{\omega}} \times \dot{\boldsymbol{z}}_\phi. \tag{5.26}$$

This equation can be easily solved. First of all, it implies that we have the following three conserved quantities:

$$K \equiv \hat{\boldsymbol{\omega}} \cdot \dot{\boldsymbol{z}}_\phi, \qquad \omega \equiv \dot{z}_\phi^{-1}, \qquad r \equiv \ddot{z}_\phi. \tag{5.27}$$

Moreover $\boldsymbol{r}_\phi \equiv -\ddot{\boldsymbol{z}}_\phi$ is a vector orthogonal to $\hat{\boldsymbol{\omega}}$ and a solution of the equation $\dot{\boldsymbol{r}}_\phi = \hat{\boldsymbol{\omega}} \times \boldsymbol{r}_\phi$. Since this implies that $\ddot{\boldsymbol{r}}_\phi = \hat{\boldsymbol{\omega}} \times \dot{\mathsf{r}}_\phi = -\boldsymbol{r}_\phi$, we have:

$$\mathsf{r}_\phi = \cos\phi\, \boldsymbol{r}_0 + \sin\phi\, (\hat{\boldsymbol{\omega}} \times \boldsymbol{r}_0). \tag{5.28}$$

The solution to (5.26) is therefore given by:

$$\boldsymbol{z}_\phi = \boldsymbol{c} + K\phi\hat{\boldsymbol{\omega}} + \boldsymbol{r}_\phi, \tag{5.29}$$

where $\boldsymbol{c} \in \mathfrak{su}(2)$ is a constant. This is the parametric equation for a helix! This alternative approach of minimizing the edge lengths is also telling us that each edge is a helix, separately from the analysis of gluing maps around an edge done in section 5.2.

In order to visualize the situation and understand the meaning of the different parameters, let us recall that a helix can be drawn on the boundary of a cylinder, wrapping around it. This cylinder possesses an axis given by the direction $\hat{\boldsymbol{\omega}}$, and a radius given by r. The parameter ϕ is the angle, counterclockwise about $\hat{\boldsymbol{\omega}}$, elapsed from the initial point $\boldsymbol{z}_0$ to the point $\boldsymbol{z}_\phi$. The radial vector $\boldsymbol{r}_\phi$ is the position of the point on a circle perpendicular to the axis of the cylinder. The parameter K is related to the height H of the cylinder by $H = |K\phi|$. Finally, the point $\boldsymbol{c}$ is on the axis at the 'bottom' of the cylinder. See fig. 5.2 for an illustration.

The normalization condition (5.25) implies a relation between ω, K and r:

$$1 = (K\omega)^2 + (r\omega)^2. \tag{5.30}$$

$K\omega$ represents the linear velocity along the cylinder axis and $r\omega$ the angular velocity.

There is a redundancy in allowing ϕ and K to take either sign. First of all, notice from (5.29) that K is positive when the axial component of the velocity is directed along $\hat{\boldsymbol{\omega}}$, and negative when it runs opposite to $\hat{\boldsymbol{\omega}}$. Now, the helix generated by a positive angle ϕ is different than the one generated by a negative angle. However, since ϕ is defined to be counterclockwise about $\hat{\boldsymbol{\omega}}$, the transformation $\phi \to -\phi$ is equivalent to $\boldsymbol{\omega} \to -\boldsymbol{\omega}$ with $K \to -K$. We eliminate this redundancy by taking $\phi > 0$ while allowing the axis $\hat{\boldsymbol{\omega}}$ to point in any direction.

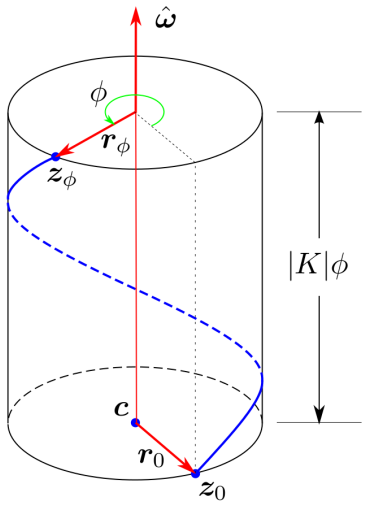

Figure 5.2: A helix (in blue) wrapping around a cylinder. The various parameters are labeled to show their geometric meaning.

We can express the displacement vector $\boldsymbol{D}_\phi \equiv \boldsymbol{z}_\phi - \boldsymbol{z}_0$ which is connecting the start of the helix to the point $\boldsymbol{z}_\phi$ along a straight line in terms of the helix parameters:

$$\boldsymbol{D}_\phi = K\phi\hat{\boldsymbol{\omega}} + \boldsymbol{r}_\phi - \boldsymbol{r}_0. \tag{5.31}$$

This allows us to express the position and velocity as:

$$\boldsymbol{z}_\phi = \boldsymbol{z}_0 + \boldsymbol{D}_\phi \qquad\qquad \dot{\boldsymbol{z}}_\phi = \dot{\boldsymbol{D}}_\phi. \tag{5.32}$$

These equations allow for a simple calculation of the edge momentum in terms of a minimal set of helix parameters.

5.4.2 Helix parameters

We are now in a position to give the parameters of the helix. In order to do this, we first develop an expression for the edge momentum in terms of the quantities introduced above. Recall that the edge momentum is given by: $\boldsymbol{J} = \frac{1}{2}\int_{\mathsf{e}}(\boldsymbol{z}\times\dot{\boldsymbol{z}})\mathrm{d}\phi$. Using $\Phi > 0$ to denote the total angle elapsed from the start to the end of the helix, i.e. $\phi \in [0, \Phi]$, a direct evaluation gives:

$$\begin{aligned}
\boldsymbol{J} &= \frac{1}{2}\int_0^\Phi \mathrm{d}\phi \left(\boldsymbol{z}_0 \times \dot{\boldsymbol{D}}_\phi + \boldsymbol{D}_\phi \times \dot{\boldsymbol{D}}_\phi\right) \\
&= \frac{1}{2}\int_0^\Phi \mathrm{d}\phi \left(\boldsymbol{z}_0 \times \dot{\boldsymbol{D}}_\phi + K\phi\ddot{\mathsf{r}}_\phi - K\dot{r}_\phi + K\hat{\boldsymbol{\omega}}\times \mathsf{r}_0 + (\mathsf{r}_\phi - \mathsf{r}_0)\times\dot{\mathsf{r}}_\phi\right) \\
&= \frac{1}{2}\int_0^\Phi \mathrm{d}\phi \left(\boldsymbol{z}_0 \times \dot{\boldsymbol{D}}_\phi + \partial_\phi(K\phi\dot{\mathsf{r}}_\phi) + K(\hat{\boldsymbol{\omega}}\times\mathsf{r}_0 - 2\dot{\mathsf{r}}_\phi) + r^2\hat{\boldsymbol{\omega}} - \mathsf{r}_0\times\dot{\mathsf{r}}_\phi\right).
\end{aligned} \tag{5.33}$$

Now, performing the integral and using the above expression (5.28) for r_Φ, we obtain:

$$\begin{aligned}\boldsymbol{J} &= \frac{1}{2}\boldsymbol{z}_0 \times \boldsymbol{D}_\Phi + \frac{1}{2}\left(K\Phi\dot{\mathsf{r}}_\Phi + K\Phi\hat{\boldsymbol{\omega}} \times \mathsf{r}_0 - 2K(\mathsf{r}_\Phi - \mathsf{r}_0) + r^2\Phi\hat{\boldsymbol{\omega}} - \mathsf{r}_0 \times \mathsf{r}_\Phi\right), \\ &= \frac{1}{2}\boldsymbol{z}_0 \times \boldsymbol{D}_\Phi + \frac{1}{2}r^2\left(\Phi - \sin\Phi\right)\boldsymbol{\sigma}_0 \\ &\quad + rK\left(1 - \cos\Phi - \frac{\Phi}{2}\sin\Phi\right)\boldsymbol{\sigma}_1 + rK\left(\frac{\Phi}{2} + \frac{\Phi}{2}\cos\Phi - \sin\Phi\right)\boldsymbol{\sigma}_2, \end{aligned} \tag{5.34}$$

where we have introduced a shorthand notation for the orthonormal 'helix basis':

$$\boldsymbol{\sigma}_i \equiv (\hat{\boldsymbol{\omega}}, \hat{\mathsf{r}}_0, \hat{\boldsymbol{\omega}} \times \hat{\mathsf{r}}_0)\,. \tag{5.35}$$

With the help of some trigonometric identities we can write the above expression in a more simple form:

$$\boldsymbol{J} = \boldsymbol{L} + \boldsymbol{S}, \qquad \boldsymbol{L} = \frac{1}{2}\boldsymbol{z}_0 \times \boldsymbol{D}_\Phi, \tag{5.36}$$

$$\boldsymbol{S} = r^2 f_\varphi \boldsymbol{\sigma}_0 + 2rK\varphi g_\varphi \boldsymbol{\sigma}_\varphi, \tag{5.37}$$

where $\varphi \equiv \Phi/2$ is half of the total angle, $\boldsymbol{\sigma}_\varphi \equiv (-\sin\varphi\boldsymbol{\sigma}_1 + \cos\varphi\boldsymbol{\sigma}_2)$ and we have defined two functions of this angle:

$$f_\varphi \equiv \varphi - \cos\varphi\sin\varphi, \qquad g_\varphi \equiv \cos\varphi - \frac{\sin\varphi}{\varphi}. \tag{5.38}$$

The Regge contribution $\boldsymbol{L}$ is the edge momentum one would obtain for a straight edge as in (5.16), and the non-Regge contribution $\boldsymbol{S}$ is giving the deviation from this value. The non-Regge contribution is invariant under translation $\boldsymbol{z} \to \boldsymbol{z} + \boldsymbol{b}$ while the Regge contribution is not.

Note that we can express the displacement vector in the helix basis:

$$\boldsymbol{D}_\Phi \equiv 2K\varphi\boldsymbol{\sigma}_0 + 2r\sin\varphi\boldsymbol{\sigma}_\varphi. \tag{5.39}$$

From the above equations (5.36–5.39), it is apparent that a minimal set of parameters for determining $\boldsymbol{J}$ is given by $(\boldsymbol{z}_0, r, K, \varphi)$ and the helix basis $\boldsymbol{\sigma}_i$, which is given by a pair of orthogonal unit vectors $(\hat{\boldsymbol{\omega}}, \hat{\mathsf{r}}_0)$.

Following Penrose and Rindler [79] we call the pairs $(\hat{\boldsymbol{\omega}}, \hat{\mathsf{r}}_0)$ a *flag*, where $\hat{\boldsymbol{\omega}}$ is the pole of the flag and $\hat{\mathsf{r}}_0$ the direction of the flag. Using the Hopf fibration, a flag is equivalent to a point in $S^3/\mathbb{Z}_2$ where the $\mathbb{Z}_2$ action is the inversion. This can be seen as follows. We can label a point in S^3 by a pair of complex numbers $|x\rangle = (x_0, x_1)$ satisfying the normalization condition $|x_0|^2 + |x_1|^2 = 1$. We can label a point in S^2 by a vector $|y) = (y_0, y = y_1 + iy_2) \in S^2$ where $y_0 \in \mathbb{R}$ and $y \in \mathbb{C}$ satisfy the condition $y_0^2 + |y|^2 = 1$. The Hopf fibration is a many-to-one map which sends circles in S^3 to points in S^2. It is given by $\pi(|x\rangle) = (|x_0|^2 - |x_1|^2, 2x_0\bar{x}_1)$. We can extend this map to a map from S^3 to a flag $(\hat{\boldsymbol{\omega}}, \hat{r}_0)$. The kernel of this map is the $\mathbb{Z}_2$ inversion and it is given by:

$$\hat{\boldsymbol{\omega}} = (|x_0|^2 - |x_1|^2, 2x_0\bar{x}_1), \qquad \hat{\mathsf{r}}_0 = (x_0x_1 + \bar{x}_0\bar{x}_1, \bar{x}_1^2 - x_0^2). \tag{5.40}$$

It can be checked explicitly that $\hat{\boldsymbol{\omega}}^2 = \hat{\mathsf{r}}_0^2 = 1$ and $\hat{\mathsf{r}}_0 \cdot \hat{\boldsymbol{\omega}} = 0$ as required. The knowledge of a flag $(\hat{\boldsymbol{\omega}}, \hat{\mathsf{r}}_0)$ determines (x_0, x_1) only up to a global sign, accounting for the $\mathbb{Z}_2$ symmetry noted above. Notice that there are three degrees of freedom in a flag.

We can also write a flag in term of three angles θ^i that are relative to a fixed basis $\boldsymbol{\tau}_i$ as shown in fig. 5.3. The first of these is the angle $0 \leq \theta^0 < \pi$ between $\hat{\boldsymbol{\omega}}$ and $\boldsymbol{\tau}_0$; the second $0 \leq \theta^1 < 2\pi$ is the angle between $\boldsymbol{\tau}_1$ and the projection of $\hat{\boldsymbol{\omega}}$ onto the $(\boldsymbol{\tau}_1, \boldsymbol{\tau}_2)$ plane; the third angle $0 \leq \theta^2 < 2\pi$ gives the orientation of $\hat{\mathsf{r}}_0$ in the plane perpendicular to $\hat{\boldsymbol{\omega}}$. With these angles the flag can be written as:

$$\begin{aligned} \hat{\boldsymbol{\omega}} &= \cos\theta^0 \boldsymbol{\tau}_0 + \sin\theta^0 \cos\theta^1 \boldsymbol{\tau}_1 + \sin\theta^0 \sin\theta^1 \boldsymbol{\tau}_2; \\ \hat{\mathsf{r}}_0 &= \sin\theta^0 \cos\theta^2 \boldsymbol{\tau}_0 + (\sin\theta^1 \sin\theta^2 - \cos\theta^0 \cos\theta^1 \cos\theta^2)\boldsymbol{\tau}_1 \\ &\quad -(\cos\theta^0 \sin\theta^1 \cos\theta^2 + \cos\theta^1 \sin\theta^2)\boldsymbol{\tau}_2. \end{aligned} \tag{5.41}$$

These angles are related to the complex parameters above via:

$$x_0 = \pm\left(\cos\frac{\theta^0}{2}\right)\exp\left(\frac{i}{2}(\theta^1+\theta^2)\right), \qquad x_1 = \pm\left(\sin\frac{\theta^0}{2}\right)\exp\left(\frac{i}{2}(\theta^2-\theta^1)\right). \tag{5.42}$$

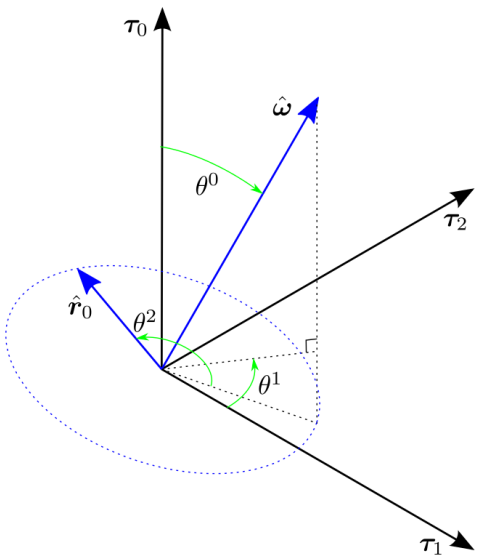

Figure 5.3: The flag $(\hat{\boldsymbol{\omega}}, \hat{\mathsf{r}}_0)$ (in blue) with respect to a fixed basis $\boldsymbol{\tau}_i$. To measure θ^2, one projects $\hat{\boldsymbol{\omega}}$ down the direction of $\boldsymbol{\tau}_0$ into a plane perpendicular to $\hat{\boldsymbol{\omega}}$. θ^2 is the angle from this projection to $\hat{\mathsf{r}}_0$, measured within the plane perpendicular to $\hat{\boldsymbol{\omega}}$.

There is yet a third way to represent the flag data. Notice that the angles θ^i are giving the helix basis $\boldsymbol{\sigma}_i$ in terms of the fixed basis $\boldsymbol{\tau}_i$. The two bases are related by a (passive) rotation, i.e. $\boldsymbol{\tau}_i = e_i{}^j \boldsymbol{\sigma}_j$ where $e_i{}^j = \boldsymbol{\tau}_i \cdot \boldsymbol{\sigma}^j$. The transpose $(e^T)_j{}^i = \boldsymbol{\tau}^i \cdot \boldsymbol{\sigma}_j = e^i{}_j$ is the inverse rotation

and satisfies $(e^T)_k{}^j e_j{}^i = e_k{}^j (e^T)_j{}^i = \delta^i_k$. Knowledge of this flag matrix allows one to determine the angles θ^i, implying that $e_i{}^j$ is equivalent to the flag data.

The passive rotation of a basis is equivalent to an active inverse rotation of the vector components. Given the six helix parameters $(r, K, \varphi, \theta^i)$ one can determine the fixed-basis components $\boldsymbol{D}_\Phi \cdot \boldsymbol{\tau}^i$ and $\boldsymbol{S} \cdot \boldsymbol{\tau}^i$ using the flag matrix and equations (5.36–5.39):

$$\boldsymbol{S} \cdot \boldsymbol{\tau}^i = e^i{}_j (\boldsymbol{S} \cdot \boldsymbol{\sigma}^j), \tag{5.43}$$

$$\boldsymbol{D}_\Phi \cdot \boldsymbol{\tau}^i = e^i{}_j (\boldsymbol{D}_\Phi \cdot \boldsymbol{\sigma}^j). \tag{5.44}$$

We have shown that there are nine degrees of freedom $(\boldsymbol{z}_0, r, K, \varphi, \theta^i)$ in the edge momentum $\boldsymbol{J}$. We call this data the helix parameters since they define a unique helix via equation (5.32). Using the six equations (5.43, 5.44) along with (5.36–5.39), we can determine $\boldsymbol{J}$ from the helix parameters. In other words, these equations provide a map:

$$(\boldsymbol{z}_0, r, K, \varphi, \theta^i) \to (\boldsymbol{z}_0, \boldsymbol{D}_\Phi, \boldsymbol{S}), \tag{5.45}$$

where the data on the right hand side determines the edge momentum $\boldsymbol{J}$. But to what extent does knowledge of $\boldsymbol{D}_\Phi$ and $\boldsymbol{S}$ in a fixed basis allow us to determine the helix parameters? Given $(\boldsymbol{z}_0, \boldsymbol{D}_\Phi, \boldsymbol{S})$, can we invert this map to find a corresponding helix? This question is at the heart of what we hope to accomplish, and we address it in the next subsection.

5.4.3 Determining the helix parameters

Let us now take take $(\boldsymbol{z}_0, \boldsymbol{D}, \boldsymbol{S})$ as given for a single edge (dropping the subscript from $\boldsymbol{D}_\Phi$), and from this data determine the helix parameters.

First of all, we remark that if $\boldsymbol{S} = 0$, then the edge is straight (a trivial helix) and the edge momentum is given entirely by the Regge contribution $\boldsymbol{J} = \boldsymbol{L} = \frac{1}{2}\boldsymbol{z}_0 \times \boldsymbol{D}$. The parameters (r, K, φ) no longer play any role so that the data defining the edge is simply the position of the vertices $(\boldsymbol{z}_0, \boldsymbol{D})$. In this way the inverse mapping is trivial for a straight edge.

The interesting analysis is for $\boldsymbol{S} \neq 0$. In this case, we can choose a convenient fixed basis: $\boldsymbol{\tau}_0 = \hat{\boldsymbol{D}}, \boldsymbol{\tau}_1 = \widehat{\boldsymbol{D} \times \boldsymbol{S}}, \boldsymbol{\tau}_2 = \boldsymbol{\tau}_0 \times \boldsymbol{\tau}_1$. In this basis we have:

$$\boldsymbol{D} \cdot \boldsymbol{\tau}^i = (D, 0, 0), \qquad \boldsymbol{S} \cdot \boldsymbol{\tau}^i = (S\cos\delta, 0, -S\sin\delta). \tag{5.46}$$

Here S is the modulus of $\boldsymbol{S}$, $S\cos\delta$ is the portion of the edge momentum which is parallel to $\boldsymbol{D}$ while $S\sin\delta = |\hat{\boldsymbol{D}} \times \boldsymbol{S}|$ is the perpendicular component. Squaring (5.37) and (5.39) gives the following equations for K and r in terms of D, S and φ:

$$D^2 = 4K^2\varphi^2 + 4r^2 \sin\varphi^2, \tag{5.47}$$

$$S^2 = f_\varphi^2 r^4 + 4K^2\varphi^2 r^2 g_\varphi^2. \tag{5.48}$$

Solving the first equation determines K only up to a sign[5] which we shall determine below. Substituting the value for K in the second equation we obtain a quadratic equation for r^2.

[5] Explicitly $K^2 = \left(\frac{D^2 - 4r^2\sin^2\varphi}{4\varphi^2}\right)$.

Only one of the solutions yields a real positive value. This gives us the expressions of r and K as functions of φ:

$$r_\varphi^2 = D^2 \left(\frac{-g_\varphi^2 + \sqrt{g_\varphi^4 + 4s^2\Delta_\varphi}}{2\Delta_\varphi} \right), \tag{5.49}$$

$$K_\varphi^2 = D^2 \left(\frac{f_\varphi^2 - 2\sin^2\varphi \left(g_\varphi^2 + \sqrt{g_\varphi^4 + 4s^2\Delta_\varphi} \right)}{4\varphi^2\Delta_\varphi} \right), \tag{5.50}$$

where we have introduced a dimensionless parameter $s \equiv S/D^2$ and the function $\Delta_\varphi \equiv (f_\varphi^2 - 4g_\varphi^2 \sin^2\varphi)$. Note that since $(f_\varphi^2 - 4g_\varphi^2 \sin^2\varphi) > 0$ for all $\varphi > 0$ the right hand side is always real and well-defined. See fig. 5.4 for a plot of this function. Note that for small s we have:

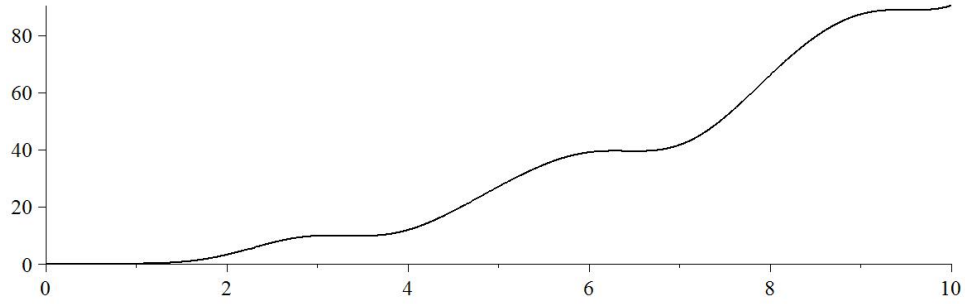

Figure 5.4: A plot of $\Delta_\varphi = (f_\varphi^2 - 4g_\varphi^2 \sin^2\varphi)$, which is positive for all $\varphi > 0$.

$$r_\varphi^2 \approx \frac{S^2}{g_\varphi^2 D^2}, \qquad K^2\varphi^2 \approx \frac{D^2}{4}. \tag{5.51}$$

This leaves us to solve for the angle φ and the flag matrix. In order to do so we introduce the following angles $(\alpha_\varphi, \beta_\varphi)$, solutions of[6]:

$$\tan\alpha = \left(\frac{r_\varphi}{K_\varphi \varphi} \right) \sin\varphi, \qquad \tan\beta = \left(\frac{K_\varphi \varphi}{r_\varphi} \right) \frac{2g_\varphi}{\mathsf{f}_\varphi}. \tag{5.52}$$

These angles give us the decomposition of the edge momentum and displacement vector in terms of the helix basis from (5.43, 5.44) along with (5.37, 5.39):

$$\boldsymbol{D} = D(\cos\alpha \boldsymbol{\sigma}_0 + \sin\alpha \boldsymbol{\sigma}_\varphi), \qquad \boldsymbol{S} = S(\cos\beta \boldsymbol{\sigma}_0 + \sin\beta \boldsymbol{\sigma}_\varphi). \tag{5.53}$$

Let us denote by $R(\boldsymbol{\tau}, \alpha)$ a rotation about the $\boldsymbol{\tau}$ axis by an angle of α. It is defined by $\partial_\alpha R(\boldsymbol{\tau}, \alpha)(\boldsymbol{\sigma}) = [\tau, R(\boldsymbol{\tau}, \alpha)(\boldsymbol{\sigma})]$. We can express the previous relations as:

$$\boldsymbol{D} = DR(\boldsymbol{\sigma}_0, \varphi)R(\boldsymbol{\sigma}_1, \alpha)(\boldsymbol{\sigma}_0), \qquad \boldsymbol{S} = SR(\boldsymbol{\sigma}_0, \varphi)R(\boldsymbol{\sigma}_1, \beta)(\boldsymbol{\sigma}_0). \tag{5.54}$$

[6] More precisely we demand that $\cos\alpha_\varphi = \frac{2K_\varphi\varphi}{D}$, $\sin\alpha = \frac{2r_\varphi \sin\varphi}{D}$ and that $\cos\beta_\varphi = \frac{r_\varphi^2 \mathsf{f}_\varphi}{\mathcal{J}}$, $\sin\beta = \frac{2r_\varphi K_\varphi \varphi g_\varphi}{\mathcal{J}}$.

This shows that the rotation $R \equiv R(\boldsymbol{\sigma}_0, \varphi)R(\boldsymbol{\sigma}_1, \alpha)$ maps the helix basis onto the fixed basis (5.46).

Now that we have determined (K, r) and the flag in terms of φ and $(\boldsymbol{D}, \boldsymbol{S})$, the only task left is to determine φ in terms of $(\boldsymbol{D}, \boldsymbol{S})$. This follows from the equation $\delta = \alpha - \beta$ where $\boldsymbol{S} \cdot \boldsymbol{D} = SD\cos\delta$ which gives us the final constraint:

$$\boldsymbol{S} \cdot \boldsymbol{D} = 2(r_\varphi^2 K_\varphi \varphi)(f_\varphi + 2g_\varphi \sin\varphi). \tag{5.55}$$

This equation gives us φ in terms of $(\boldsymbol{D}, \boldsymbol{S})$. We have checked that $f_\varphi + 2g_\varphi \sin\varphi > 0$ for $\varphi > 0$ (see fig. 5.5 for a plot), which allows us to determine that the sign of K is $\mathrm{sgn}(K) = \mathrm{sgn}(\boldsymbol{S} \cdot \boldsymbol{D})$.

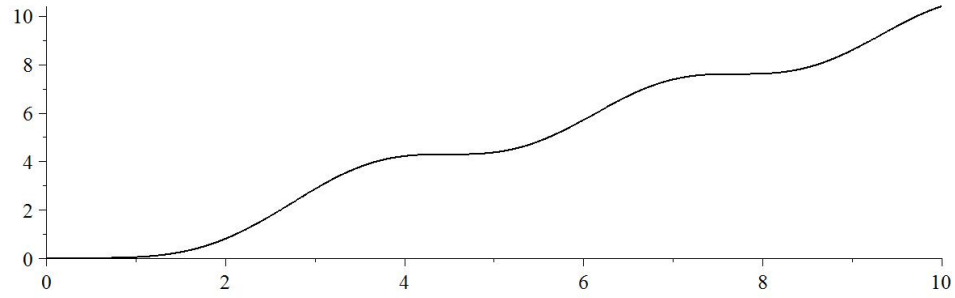

Figure 5.5: A plot of $f_\varphi + 2g_\varphi \sin\varphi$, which is positive for all $\varphi > 0$.

We checked numerically for solutions to this equation of a range of values for the parameters $-1000 \leq s\cos\delta \leq 1000$ (excluding $s\cos\delta = 0$ since this is inconsistent with $\varphi > 0$ in (5.37), as required for a non-trivial helix) and $0 \leq s\sin\delta \leq 1000$. We find in all cases that there is at least one intersection, and in general there actually many possible values of φ which solve this equation. See fig. (5.6) for a typical plot of (5.55). In minimizing the action, we have in fact found multiple local minima rather than a single global minimum.

This analysis shows that we can always invert the equations (5.43, 5.44); given $(\boldsymbol{z}_0, \boldsymbol{D}, \boldsymbol{S})$, or equivalently $(\boldsymbol{z}_0, \boldsymbol{D}, \boldsymbol{J})$ since $\boldsymbol{J} = \boldsymbol{D} + \boldsymbol{S}$, there always exists a discrete set of helix parameters $(r, K, \varphi, \theta^i)$. The inversion is not one-to-one since there are usually multiple helices which correspond to a given $(\boldsymbol{z}_0, \boldsymbol{D}, \boldsymbol{S})$. We can fix the ambiguity by always choosing the helix with the minimal length. This means that once the end points are given, there exists a one-to-one correspondence between a choice of edge momentum and a choice of helix stretching between these end points. In other words, if we fix two vertices and specify an edge momentum $\boldsymbol{J}$, we can always take the edge to be in the form of a helix whose total angular momentum $\frac{1}{2}\int(z \times \dot{z})$ is $\boldsymbol{J}$.

5.4.4 Fluxes and helices

Now that we have completed our analysis of a single edge, let us extend this analysis over the entire one-skeleton of a spinning geometry to examine the role that fluxes play in determining

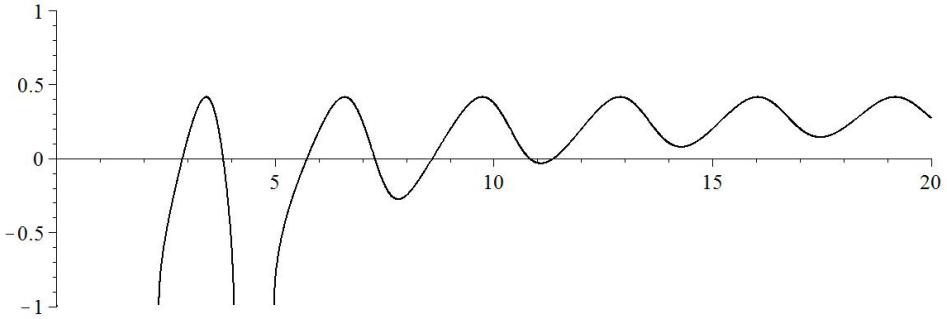

Figure 5.6: A typical plot of $2(r_\varphi^2 K_\varphi \varphi)(\mathsf{f}_\varphi + 2g_\varphi \sin\varphi) - \boldsymbol{S}\cdot\boldsymbol{D}$ where $s\cos\delta = s\sin\delta = 1$. Notice there are seven solutions for φ.

the helix parameters. The analysis of a single edge presented above applies independently to each $\mathsf{e} \in \Gamma^*$, and shows that one can deform each edge of the one-skeleton into a helix without changing the edge momenta. Recall that such deformations also leave the holonomies and fluxes unchanged, so that the resulting geometry where each edge is now a helix corresponds to the same point in P_Γ^G. Again we have found that these spinning geometries can be seen as a way to join the polyhedral cells of a twisted geometry into a continuous three-geometry, achieved by twisting the edges of polyhedra into helices.

Let us now restore the edge e and cell c super- and sub-scripts. The quantities that were labeled $(\boldsymbol{D}, \boldsymbol{J})$ above shall here be denoted $(\boldsymbol{D}^c_\mathsf{e}, \boldsymbol{J}^c_\mathsf{e})$, where e denotes the edge and c denotes the reference frame attached to the cell c. Now, since $\boldsymbol{D}^c_\mathsf{e} = \boldsymbol{z}(t(\mathsf{e})) - \boldsymbol{z}(s(\mathsf{e}))$ is the difference between the start and terminal vertices of the edge, the data (up to an overall translation) associated to a network of connected helices is a pair $(\boldsymbol{D}^c_\mathsf{e}, \boldsymbol{J}^c_\mathsf{e})$ for each edge $\mathsf{e} \in \Gamma^*$. We have seen that given $(\boldsymbol{D}^\mathsf{e}_c, \boldsymbol{J}^\mathsf{e}_c)$ compatible with the fluxes such that $\sum_{\mathsf{e}\in\partial\mathsf{f}_{cc'}} \boldsymbol{J}^\mathsf{e}_c = \boldsymbol{X}_{cc'}$ on each face of cell c, we can construct for every edge $\mathsf{e} \subset c$ a helix that is compatible with this data. This means that we can construct a map $\boldsymbol{z}^c : c \to \mathbb{R}^3$ for every cell c. This map is such that the one-skeleton of its boundary consists of helices, while the shape of the faces are undetermined at this stage. In fact, there are many possible choices of boundary helices which are compatible with a given sets of fluxes. Once we choose an origin for each map $\boldsymbol{z}^c$ we have a one-to-one correspondence between a set of fluxes $\boldsymbol{X}_\mathsf{f}$ attributed to faces, and a set of edge momenta $\boldsymbol{J}_\mathsf{e}$ associated to edges.

The role that fluxes play in determining the helices is now becoming clear. The set of fluxes gives the set of edge momenta $\boldsymbol{J}^c_\mathsf{e}$ up to some arbitrary choice of origins for the coordinate functions $\boldsymbol{z}^c$ and modulo the relations:

$$\boldsymbol{J}^c_\mathsf{e} = -h_{c'c}\boldsymbol{J}^c_e dh_{cc'}. \tag{5.56}$$

The edge momenta J^c_e fixes three of the six degrees of freedom $(r, K, \varphi, \theta^i)$ defining the helix on the edge e as seen from the cell c. However, the displacement $\boldsymbol{D}^c_\mathsf{e}$ also plays a role, and the helix is fixed by a combination of the data $(\boldsymbol{D}^c_\mathsf{e}, \boldsymbol{J}^c_\mathsf{e})$. The map from this data to a set of helix

parameters is complicated and we can so far not separate what is fixed by $\boldsymbol{J}^c_{\mathsf{e}}$ from what is fixed by $\boldsymbol{D}^c_{\mathsf{e}}$.

5.5 Discussion

The SU(2)-gauge-invariant phase space of loop gravity P^G_Γ can be represented by either twisted geometries or spinning geometries, which are both generalizations of Regge geometries. Twisted geometries have the advantage that each cell takes the form of a flat polyhedron, but the disadvantage that they do not form continuous geometries. Spinning geometries are continuous at the price of having cells with curved boundaries.

As we have seen, the loop gravity data consists of a set $(\boldsymbol{X}_{cc'}, h_{cc'}) \in \mathfrak{su}(2) \times \mathrm{SU}(2)$ for each pair of cells. We studied spinning geometries in order to learn how this data fixes the shape of cells. We first found that helices appear necessarily from the consistency of the gluing determined by the holonomies. The axis of the product of holonomies which loop around an edge e is parallel to the axis of the helix, and there is an angle θ^c_{e} encoded into the composition of gluing maps along the edge. Each loop of holonomies on the dual graph Γ then parameterizes two degrees of freedom[7] for each edge $\mathsf{e} \in \Gamma^*$.

We performed a longer analysis to see what role the fluxes play. Noticing that straight edges, as in a Regge geometry, are the shortest paths between a set of vertices, we looked at minimizing the (*a priori* arbitrarily shaped) edge lengths of a spinning geometry while keeping the vertices fixed. We found again that this results in each edge taking the form of a helix. The fluxes determine a set of edge momenta $\boldsymbol{J}^c_{\mathsf{e}}$ which, together with the $\boldsymbol{D}^c_{\mathsf{e}}$, fix a helix. (There were actually several choices of helices corresponding to this data, but we can select the one of minimum length for concreteness.) Of the six degrees of freedom in each helix, the fluxes fix three of them.

From this analysis we learned that the cells of spinning geometries are similar to polyhedra, except that the edges are helical rather than straight. Allowing for the edges to be helical accounts for the extra degrees of freedom in the loop gravity phase space which are not present in a Regge geometry. Each helical edge has six degrees of freedom; two are fixed by the holonomies and three are fixed by the fluxes. The question that we haven't resolved yet is whether we can always construct a closed network of helices for arbitrary holonomy-flux data. Since we still have one degree of freedom per helical edge to play with, we believe this to be very likely but a proof is necessary.

Another question that needs a deeper understanding is whether we can reconstruct the geometry of the faces from the requirement that the boundary edges are helices and that the normal components of the frame fields are continuous. One natural conjecture is that the shapes of the faces have to be minimal surfaces. This is what happens for bubbles separating two domains of equal pressure due to the Laplace equation [80].

An interesting outcome of this analysis is the appearance of non-trivial torsion along the edges of the cells. The connection $\boldsymbol{A}$ in question is the Ashtekar-Barbero connection, related

[7] Although there are several $\hat{\boldsymbol{\omega}}^c_{\mathsf{e}}$ attached to each edge, these are related by $\hat{\boldsymbol{\omega}}^c_{\mathsf{e}} = -h_{c'c}\hat{\boldsymbol{\omega}}^c_{\mathsf{e}}h_{cc'}$ so that only two degrees of freedom are associated to the axis on an edge.

to the spin connection[8] by $\boldsymbol{A} = \boldsymbol{\Gamma} + \boldsymbol{K}$ where $\boldsymbol{K}$ is the extrinsic curvature. The torsion of $\boldsymbol{A}$ is therefore a measure of $\boldsymbol{K}$. However, one usually expects this torsion to be supported on the faces and come entirely from the holonomies. Here we see that on top of the holonomy contribution we have an additional contribution supported on the edges. This seems to be an intrinsic property of the three-geometry stemming from the gluing rules. A deeper understanding of this is clearly needed.

Finally one of the most exciting outcomes of this work is that it may give new insights into how to formulate a consistent dynamics on the discrete geometry of loop gravity. If we could assign a continuous connection and triad to a given set of loop gravity data, we would be able to write the continuous scalar constraint in terms of these fields. Spinning geometries provide these continuous fields and provide an attractive choice for the representation of holonomy-flux data within the continuous phase space. We can take these as the continuous kinemtical solutions, but the question we need to address is: does the dynamics of a spinning geometry represent the dynamics of the corresponding holonomy-flux data? Since these geometries are both piecewise-flat and piecewise-torsionless with curvature and torsion being present only on the one-skeleton of the cellular space, we anticipate that the continuous dynamics will become drastically simplified in this gauge. If we can find a discrete dynamics on P^G_Γ that agrees with the continuous dynamics of a spinning geometry, we would have for the first time an anomaly-free way to relate the dynamics of loop gravity with the dynamics of general relativity. We shall look further into this in the next two chapters.

[8]The spin connection $\boldsymbol{\Gamma}$ is the metric-compatible connection determined entirely from the metric.

Chapter 6

Truncated dynamics

With the developments we have made on the kinematical side, we can now begin to address the most challenging problem of loop gravity: dynamics. We have established that each $P^G_\Gamma \cong \mathcal{P}^G_{\Gamma_*}$ is a truncation of the continuous phase space $\mathcal{P}^G$, and we understand the equivalence class of geometries represented by this truncation. The main issue we must now face, is that P_Γ has a finite number of degrees of freedom while the continuous phase space has infinite degrees of freedom. Obviously the dynamics for a finite dimensional phase space cannot reproduce that of a continuous theory. In order to have a discrete[1] dynamics consistent with general relativity, we will need to use the full projective family of phase spaces associated to graphs. The advantage of this approach for quantization is that we can work separately on each graph phase space to formulate a dynamics in terms of holonomies and fluxes, and these are the basic building blocks for the quantum theory. We would then have a dynamical theory of gravity suitable for quantization using the already well-established methods of loop quantum gravity. The key idea that allows this to work is that each P^G_Γ is a *truncation* of $\mathcal{P}^G$, as opposed to an approximation or discretization, meaning that the holonomy-flux data represents exactly the degrees of freedom in a certain class of geometries; one needs to consider the entire projective family of graph phase spaces P^G_Γ in order to describe arbitrary spatial geometries. This is in contrast to taking the holonomy-flux data as a discretization of the continuous fields, which gives an approximate representation of arbitrary fields $(\boldsymbol{A}, \boldsymbol{E})$, and only becomes precise in the continuous limit where the discretization scale vanishes.

The holonomies and fluxes defining a point in P^G_Γ correspond to an equivalence class of geometries defined by the relations $\boldsymbol{A} \sim g\boldsymbol{A}g^{-1} + g\mathrm{d}g$ and $\boldsymbol{E} \sim g(\boldsymbol{E} + \mathrm{d}\phi)g^{-1}$ for some $g \in \mathrm{SU}(2)$ and $\phi \in \mathfrak{su}(2)$. A point p in P^G_Γ is mapped to a unique equivalence class of geometries, and each member of this class gives a precise representation of p as a continuous geometry. To study the dynamics we need to select a single member of the class $(\bar{\boldsymbol{A}}, \bar{\boldsymbol{E}})$, and we are free to use a criteria of convenient properties to make the selection. On the kinematical side, we would like the gauge map to be diffeomorphism covariant so the choice of fields behaves appropriately under the action generated by the vector constraint. On the dynamical side, we want the choice of $(\bar{\boldsymbol{A}}, \bar{\boldsymbol{E}})$ to allow us to write the scalar constraint (with this gauge choice) in terms of

[1] By 'discrete', we mean that the phase space has a countable set of variables, as opposed to the infinite-dimensional continuous phase space.

holonomies and fluxes, so that we may formulate a discrete dynamics that is consistent with the evolution $(\dot{\bar{\boldsymbol{A}}}, \dot{\bar{\boldsymbol{E}}})$ generated by the continuous scalar constraint. Let us explain this point in more detail. Consider a set of $(h_\ell, \boldsymbol{X}_\ell)$ data on a graph Γ defining the point $p \in P^G_\Gamma$, and take this as initial data. Let us then map this to a gauge choice $(\bar{\boldsymbol{A}}, \bar{\boldsymbol{E}})$. Now, we have a continuous scalar constraint in terms of the shift function and field variables $S[N, \bar{\boldsymbol{A}}, \bar{\boldsymbol{E}}]$, and we want to find a scalar constraint $S_\Gamma[N_\ell, h_\ell, \boldsymbol{X}_\ell]$ associated to the graph which acts on the phase space P^G_Γ. The choice of gauge is key to this program, and we require it to be such that the holonomy-flux dynamics agrees precisely with the evolution of the gauge choice, i.e.:

$$\dot{h}_\ell = \{h_\ell, S_\Gamma[N_\ell, h_\ell, \boldsymbol{X}_\ell]\} = \left\{ \overrightarrow{\exp} \int_\ell \bar{\boldsymbol{A}}, S[N, \bar{\boldsymbol{A}}, \bar{\boldsymbol{E}}] \right\}, \tag{6.1}$$

$$\dot{\boldsymbol{X}}_\ell = \{\boldsymbol{X}_\ell, S_\Gamma[N_\ell, h_\ell, \boldsymbol{X}_\ell]\} = \left\{ \int_{\mathsf{f}_\ell} h_\pi[\boldsymbol{A}] \boldsymbol{E} h^{-1}_\pi[\boldsymbol{A}], S[N, \bar{\boldsymbol{A}}, \bar{\boldsymbol{E}}] \right\}. \tag{6.2}$$

This ensures that the map from the holonomy-flux data to the gauge choice of continuous fields is consistent with the equations of motion for both the discrete and continuous variables. Note that this consistency is only for an instant of time as the continuous data will evolve away from the gauge choice so that it no longer corresponds to the point $p \in P^G_\Gamma$, but rather a point in some other phase space $p' \in P^G_{\Gamma'}$. In order to handle this behaviour, we will need to address the evolution between phase spaces supported on different graphs. This is somewhat expected and welcome, since in a theory of pure gravity the dynamics we describe will be for the propagation of gravitational waves, and one expects this to be manifest in graph changes [40]. The formulation of dynamics between phase spaces of different dimension presents an interesting challenge that has not been addressed in the literature. See however [81] for related work in this direction which provides a consistent set of rules for stepwise evolution between phase spaces of different dimension.

We have established that spinning geometries satisfy the kinematical requirement for a gauge choice, providing a diffeomorphism-covariant mapping of points in P^G_Γ to continuous geometries. The key properties of this gauge choice are that intrinsic and extrinsic curvature are supported only on the one-skeleton dual Γ^* to the graph. This implies that the dynamics is concentrated on Γ^*, which greatly simplifies the evolution equations for these geometries. Let us take a closer look at this. Spinning geometries are defined as a pair of fields $(\bar{\boldsymbol{A}}, \bar{\boldsymbol{E}})$ which have a vanishing curvature of the Ashtekar connection $\mathrm{d}_A \bar{\boldsymbol{A}}(x) = 0$ and a vanishing extrinsic curvature $\boldsymbol{K}(x) = 0$ for all $x \notin \Gamma^*$. The scalar constraint (2.67) is the generator of dynamics, and we can write this using differential form notation as:

$$S[N] = \int N \boldsymbol{e} \wedge \boldsymbol{F}(\boldsymbol{A}) + (1+\gamma^2) \epsilon_{ijk} \boldsymbol{e}^i \wedge K^j \wedge K^k, \tag{6.3}$$

where the frame-field $\boldsymbol{e}$ is a function (2.58) of the electric field $\boldsymbol{E}$, and the extrinsic curvature is given in terms of the phase space by $\boldsymbol{K} = \frac{1}{\gamma}(\Gamma - \boldsymbol{A})$, recalling that $\Gamma(\boldsymbol{E})$ is the spin connection (2.83). The second term in the scalar constraint is difficult to handle, but we note that having $\boldsymbol{K} = 0$ within cells will help to simplify the picture. For now, let us look at the complex Ashtekar variables and consider the self-dual case where $\gamma = i$[2]. This choice simplifies the

[2]One can also consider Riemannian gravity with a choice of $\gamma = 1$ to obtain this simplified form of scalar

scalar constraint by eliminating the second term. In this case, the dynamics generated on the fields of a spinning geometry *inside* the cells is:

$$\big\{\bar{\boldsymbol{A}}(x), S[N]\big\} = 0, \qquad \big\{\bar{\boldsymbol{E}}(x), S[N]\big\} = \mathrm{d}_A(N\boldsymbol{e})(x), \qquad \forall x \ni \Gamma^*, \tag{6.4}$$

where we used that $\boldsymbol{F}(\bar{\boldsymbol{A}}) = 0$ for a spinning geometry. Now, what does this mean for the holonomy-flux variables? From the above equations we find:

$$\dot{h}_\ell = \left\{\overrightarrow{\exp}\int_\ell \bar{\boldsymbol{A}}, S[N]\right\} = 0, \tag{6.5}$$

$$\dot{\boldsymbol{X}}_\ell = \left\{\int_{\mathsf{f}} h_\pi \bar{\boldsymbol{E}} h_\pi^{-1}, S[N]\right\} = \int_{\partial \mathsf{f}} N\boldsymbol{e}, \tag{6.6}$$

This is an exciting result! While the holonomies stay constant, the fluxes evolve according to a motion only on their boundaries, i.e. the edges in the one-skeleton $\mathsf{e} \in \Gamma^*$. The evolution of these fields is supported on a finite number of edges, suggesting we may be able to rewrite the continuous Hamiltonian (for this particular gauge) in terms of holonomies and fluxes, so that the continuous dynamics of a spinning geometry $(\bar{\boldsymbol{A}}, \bar{\boldsymbol{E}})$ agrees with the dynamics of the holonomy-flux variables on a graph in the manner described in equations (6.1, 6.2).

Let us now consider a model which mimics the situation we have just described within a simple model using a pair of fields on the real line. We shall use a notation which makes the analogy clear. The model is that of a continuous phase space $(A, E) \in \mathcal{P}$ and a Hamiltonian H which generates dynamics. On top of this, we consider a class of smeared 'flatness' constraints which reduce the continuous phase space to one of finite dimension P_Γ, as we have done for full gravity to find the spinning geometries. The reduced phase space is parameterized by a discrete set $(h_{\mathsf{n}}, X_{\mathsf{n}})$ of variables. We show that there is a gauge choice for a representative pair of fields in the constrained space $(\bar{A}, \bar{E}) \in \mathcal{C}_{\Gamma^*}$, such that the dynamics in P_Γ agrees with continuous dynamics in $\mathcal{C}_{\Gamma^*}$. With this consistency established, we use the dynamics to study how we can evolve data from one reduced phase space P_Γ to a different phase space P_{Γ^*} of different dimension. To help us understand this better, it is useful to understand the geometrical structure underlying the classical dynamics between phase spaces. There is a nice way to characterize classical dynamics in terms of geometrical structures associated to phase spaces. We begin in the next section by reviewing these ideas before moving on to study the truncated dynamics of our model in this context.

6.1 Definitions

Dynamics within a phase space is a canonical transformation from a point (a set of phase space variables) at one time, to a point at another time. There is a geometrical representation of dynamics as a subspace embedded within a symplectic manifold that is built out of a pair of phase spaces. This is a useful framework for constructing the dynamics between phase spaces of different dimension. In this section we provide the necessary definitions to build up to a description of the geometry underlying phase space dynamics, and using this we propose a definition for truncated dynamics.

constraint.

6.1.1 Symplectic vector spaces and their distinguished subspaces

We begin by defining a *Lagrangian* subspace within a vector space. Let V be a $2n$-dimensional vector space, and ω a symplectic structure on V. Now, for a subspace $W \subset V$ the symplectic orthogonal (or symplectic complement) W^ω of W is defined by:

$$W^\omega = \big\{x \in V \mid \omega(x, y) = 0,\ \forall\, y \in W\big\}.$$

Then we have the following situations defining the distinguished subspaces:

- If $W \subseteq W^\omega$, then W is an isotropic subspace of V, and $\dim W \leq n$. W is an isotropic subspace if and only if $\omega|_W = 0$ identically.
- If $W \supseteq W^\omega$, then W is a co-isotropic subspace of V.
- If $W \cap W^\omega = \{0\}$, then W is a symplectic subspace of V, and $V = W \oplus W^\omega$. W is a symplectic subspace if and only if $\omega|_W$ is non-degenerate.
- If $W = W^\omega$, i.e. if the subspace is self-orthogonal, then W is a Lagrangian subspace of V. A Lagrangian subspace is therefore at the same time isotropic and co-isotropic.

Because ω is non-degenerate, we have $(W^\omega)^\omega = W$ and:

$$\dim W + \dim W^\omega = \dim V = 2n.$$

We see therefore that a Lagrangian subspace is an isotropic subspace of dimension $(\dim V)/2 = n$, i.e. of maximal dimension.

6.1.2 Canonical transformations as Lagrangian submanifolds

We are interested in the characterization of Lagrangian submanifolds. Let us consider a symplectic manifold $M \equiv (M, \omega)$, that is, a $2n$-dimensional manifold M together with a non-degenerate closed ($\mathrm{d}\omega = 0$) two-form ω. For a submanifold $N \subset M$, we have the following situations:

- If each tangent space T_xN of N is an isotropic subspace of T_xM, then N is an isotropic submanifold. Equivalently, we say that N is isotropic if the symplectic two-form vanishes in all the tangent spaces T_xN, i.e. if $\omega(u, v) = 0$ for all $u, v \in T_xN$ and all $x \in N$.
- If each tangent space T_xN of N is a co-isotropic subspace of T_xM, then N is a co-isotropic submanifold.
- If N is an isotropic or co-isotropic submanifold of M of maximal dimension, i.e. $\dim N = n$, then N is a Lagrangian submanifold.

An embedding (immersion) $\imath : N \longrightarrow M$ is said to be Lagrangian if $\imath^*\omega = \omega|_N = 0$ and $\dim N = n$.

We call $\overline{M} \equiv (M, -\omega)$ the symplectic dual of the symplectic manifold $M \equiv (M, \omega)$. Evidently, a symplectic manifold and its dual share the same distinguished submanifolds. The

product of a symplectic manifold together with its dual defines a new symplectic manifold $M \times \overline{M} \equiv (M \times M, \omega \ominus \omega)$. Let us denote by:

$$\begin{array}{rccc} \pi_i : & M \times M & \longrightarrow & M \\ & (x_1, x_2) & \longmapsto & x_i, \end{array}$$

for $i = 1, 2$ the projection maps from the product manifold to M. The symplectic structure $\varpi \equiv \omega \ominus \omega$ on the double manifold $M \times \overline{M}$ is then given by

$$\varpi = \pi_1^* \omega - \pi_2^* \omega.$$

A canonical transformation is a map $\phi : M \longrightarrow M$ that preserves the symplectic structure $\phi^* \omega = \omega$. We now have a nice way to describe this within the double manifold.

Lemma 6.1.1. *A map $\phi : M \longrightarrow M$ is a canonical transformation if and only if its graph $L \equiv \big\{ \big(x, \phi(x)\big) \mid x \in M \big\}$ is a Lagrangian submanifold of $(M \times M, \varpi)$.*

It is indeed easy to see that the submanifold L is isotropic and of maximal dimension, i.e. $\dim L = 2n$. Isotropy can be checked by computing the induced symplectic structure. The restriction of the symplectic structure on the product manifold:

$$\omega \ominus \omega = \frac{1}{2} \omega_{\mu\nu}(x_1) \mathrm{d}x_1^\mu \wedge \mathrm{d}x_1^\nu - \frac{1}{2} \omega_{\mu\nu}(x_2) \mathrm{d}x_2^\mu \wedge \mathrm{d}x_2^\nu,$$

to the submanifold L, is given by:

$$\omega \ominus \omega|_L = \frac{1}{2} \omega_{\mu\nu}(x_1) \mathrm{d}x_1^\mu \wedge \mathrm{d}x_1^\nu - \frac{1}{2} \omega_{\mu\nu}\big(\phi(x_1)\big) \frac{\partial \phi^\mu}{\partial x_1^\rho} \frac{\partial \phi^\nu}{\partial x_1^\sigma} \mathrm{d}x_1^\rho \wedge \mathrm{d}x_1^\sigma,$$

and is therefore vanishing if $\phi : x_1 \longmapsto x_2 = \phi(x_1)$ is a canonical transformation. The Lagrangian submanifold L has the property that $\pi_1(L)$ and $\pi_2(L)$ are of maximal dimension. They are therefore isomorphic to M, i.e. $\pi_i(L) \simeq M$.

The advantage of using this definition in terms of Lagrangian submanifolds is that it allows us to define generalized canonical transformations that map between symplectic manifolds of different dimension. Let (M_1, ω_1) and (M_2, ω_2) be two symplectic manifolds of dimension $2n_1$ and $2n_2$ respectively, with the associated projection maps:

$$\begin{array}{rccc} \pi_i : & M_1 \times M_2 & \longrightarrow & M_i \\ & (x_1, x_2) & \longmapsto & x_i, \end{array}$$

and symplectic structure:

$$\varpi \equiv \omega_1 \ominus \omega_2 = \pi_1^* \omega_1 - \pi_2^* \omega_2.$$

A canonical relation between two symplectic manifolds M_1 and M_2 of different dimension is a Lagrangian submanifold of $(M_1 \times M_2, \varpi)$. We define a generalized canonical transformation as a Lagrangian subspace that satisfies certain conditions on the projections of this subspace.

Definition 6.1.2. A generalized canonical transformation ϕ between (M_1, ω_1) and (M_2, ω_2) is defined as a Lagrangian submanifold $L_{12} \subset M_1 \times \overline{M_2} \equiv (M_1 \times M_2, \varpi)$ which satisfies the irreducibility condition that $\pi_1(L_{12}) \simeq M_1$ and $\pi_2(L_{12}) \simeq M_2$. If the Lagrangian submanifold does not satisfy the irreducibility condition, we call it simply a canonical relation between M_1 and M_2.

Now given two canonical relations $L_{12} \subset D_{12} \equiv (M_1 \times M_2, \omega_1 \ominus \omega_2)$ and $L_{23} \subset D_{23} \equiv (M_2 \times M_3, \omega_2 \ominus \omega_3)$, we can use their composition to define a new canonical relation, denoted $L_{12} \circ L_{23}$, which is a Lagrangian subset of $D_{13} \equiv (M_1 \times M_3, \omega_1 \ominus \omega_3)$. It is defined as the set of points $(x_1, x_3) \in M_1 \times M_3$ such that there exist $x_2 \in M_2$ satisfying $(x_1, x_2) \in L_{12}$ and $(x_2, x_3) \in L_{23}$. In other words,

$$L_{12} \circ L_{23} \equiv \big\{(x_1, x_3) \in M_1 \times M_3 \mid \exists\, x_2 \in M_2 \text{ such that } (x_1, x_2) \in L_{12} \text{ and } (x_2, x_3) \in L_{23}\big\}.$$

Another way to characterize this composition is to first define the intersection:

$$L_{12} \times_{M_2} L_{23} \equiv L_{12} \times L_{23} \cap (M_1 \times \Delta_2 \times M_3),$$

where Δ_2 is the diagonal of M_2, that is the subset of $M_2 \times M_2$ defined by $(x_2, y_2 = x_2)$. It is easy to see that this relation is first class, or in other words that the subset $(M_1 \times \Delta_2 \times M_3) \subset D_{12} \times D_{23}$ is co-isotropic. We can therefore define the symplectic quotient $D_{13} \equiv (D_{12} \times D_{23}) /\!\!/ \Delta_2$. The composition is then defined as the projection:

$$L_{12} \circ L_{23} = \pi_2 \left(L_{12} \times_{M_2} L_{23} \right),$$

where π_2 is the projection from $D_{12} \times D_{23}$ to D_{13}. In general however, this projection is not a manifold, unless some additional transversality conditions are satisfied. Indeed, we know from the theory of symplectic reduction that if $P /\!\!/ C$ is a manifold and if L is a Lagrangian submanifold of P which intersects C transversally, then $\imath : L \cap C \longrightarrow P /\!\!/ C$ is a local embedding (an immersion) which is Lagrangian. This shows that if $L_{12} \times_{M_2} L_{23}$ and $(M_1 \times \Delta_2 \times M_3)$ intersect transversally, then $L_{12} \circ L_{23}$ is a Lagrangian immersion in D_{13}.

6.1.3 Reduction

Suppose that a Hamiltonian dynamics is defined on a symplectic manifold which is the phase space (P, ω) of some theory. According to our discussion in the previous section, we know that we can characterize this dynamics by a one-parameter family of Lagrangian submanifolds $L_t \subset (P \times P, \omega \ominus \omega)$. Now let us suppose that we have a collection of first class constraints $c_i \in \mathcal{C}$. We denote by $C_i \subset P$ the subset of P defined by the constraint $c_i = 0$. The fact that the constraints are first class means that the constraint subspaces are co-isotropic, that is $C_i^\omega \subseteq C_i$. These constraints are such that the symplectic reduction $P_i \equiv P /\!\!/ C_i$ is a finite dimensional phase space. We also suppose that the set of constraints is complete under union, that is, if $C_i, C_j \in \mathcal{C}$, then $C_i \cup C_j \in \mathcal{C}$ and $C_i \cap C_j \in \mathcal{C}$. The set $\mathcal{C}$ of constraints is then a partially ordered set (a poset) under inclusion, i.e. we say that $i < j$ if $C_i \subset C_j$.

Let us suppose that L_t intersects each C_i transversally. This condition of transversality is the condition that the constraints c_i are not preserved by the Hamiltonian evolution, i.e. $\partial_t c_i(t) \neq 0$. In this case, we know that:

$$L_t^{ij} \equiv L_t \cap C_i \times C_j \subset P_i \times \overline{P_j}, \tag{6.7}$$

is a Lagrangian immersion of $P_i \times \overline{P_j} \to P \times \overline{P}$. In this way, we can always use L_t to define a dynamics between constrained subspaces, so that the full dynamics of the theory can be encoded in a collection of truncated dynamics, provided the set $\mathcal{C}$ of constraints is large enough. By this we mean that there is a sequence of constraints $C_{i+1} > C_i$ such that a continuous theory is recovered in the projective limit $\lim_{i\to\infty} P_i$. The question which we would like to answer is: when is the reverse true? That is, given a collection L_t^{ij} of Lagrangian submanifolds in $P_i \times \overline{P_j}$, under which conditions can we reconstruct the full dynamics, i.e. a Lagrangian submanifold of $P \times \overline{P}$?

6.2 An example

We now study a toy model which mimics the situation in full gravity. Consider a pair of conjugate fields $\{A(x), E(y)\} = \delta(x-y)$ defined upon a one-dimensions space Σ that is homeomorphic to the circle S^1. These fields parametrize an infinite-dimensional, continuous phase space $\mathcal{P}$. The continuous dynamics is generated by a Hamiltonian:

$$H = \int_\Sigma \mathrm{d}x E(x,t) A'(x,t), \tag{6.8}$$

where $A'(x) \equiv \partial_x A(x)$. This Hamiltonian will play the role of the scalar constraint for gravity. The equations of motion are:

$$\dot{A} = \{A, H\} = A', \qquad \dot{E} = \{E, H\} = E', \tag{6.9}$$

and these are solved by:

$$A(x,t) = A(x+t,0) \qquad E(x,t) = E(x+t,0). \tag{6.10}$$

Given any initial data $(A(x,0), E(x,0))$, the system simply moves around the circle in a counterclockwise manner without any change of profile. Notice that both fields satisfy the same equation of motion.

Within this simple Hamiltonian system, let us study the effects of truncation on the dynamics. To define a set of truncated phase spaces, we now introduce a set of 'flatness' constraints. Consider a set Γ^* of points $\mathsf{v} \in \Sigma$ which define the smeared flatness constraint:

$$\mathcal{F}_{\Gamma^*}[\phi] := \int_\Sigma \mathrm{d}x \phi(x) A'(x), \qquad \phi(x) = 0, \qquad \forall\ x \in \Gamma^*, \tag{6.11}$$

which sets the 'curvature' A' to be zero everywhere except the points in Γ^*. These constraints generate gauge transformations on the field variables:

$$\delta A(x) = \big\{A(x), \mathcal{F}_{\Gamma^*}[\phi]\big\} = 0, \qquad \delta E(x) = \big\{E(x), \mathcal{F}_{\Gamma^*}[\phi]\big\} = \phi'(x). \tag{6.12}$$

As with gravity, these transformations leave the 'connection' A invariant while generating a wide class of 'electric fields' E.

We define a constrained subspace as:

$$\mathcal{C}_{\Gamma^*} = \left\{(A,E) \in \mathcal{P} \mid A'(x) = 0 \quad \forall x \in \Gamma^*\right\}. \tag{6.13}$$

Notice that the constraint does not Poisson commute with the Hamiltonian:

$$\mathcal{F}_{\Gamma^*}[\phi] = \{\mathcal{F}_{\Gamma^*}[\phi], H\} = \int_\Sigma \mathrm{d}x \phi'(x) A'(x), \tag{6.14}$$

so that the constrained subspace $\mathcal{C}_{\Gamma^*}$ intersections the full dynamics L_t transversally. This implies that the dynamics leads to a violation of the constraints at the points $\mathsf{v} \in \Gamma^*$. This violation is in some sense mild, since it does not occur everywhere in Σ but only a finite number of points. This is a feature that will allow us to find a dynamics that is consistent between the full and truncated phase spaces. This is analogous to the truncation of the continuous phase space for gravity by a flatness constraint. Here the constraints also do not Poisson-commute with the generator of dynamics, which is related to the discussion above where we argued that the evolution of a spinning geometry is dictated by what happens along the edges of the one-skeleton.

There is a set Γ of points $\mathsf{n} \in \Sigma$ that we can define as 'dual' to Γ^*. We select the points n such that each is at the midpoint of the edge $\mathsf{e}_{\mathsf{v},\mathsf{v}'} \equiv \mathsf{e}_\mathsf{n}$ between neighbouring points v and v' in Γ^*. We say that the point n is dual to this edge. If there are N points in Γ^* then there are also N points in Γ. Within the constrained space $\mathcal{C}_{\Gamma^*}$, the A-field is constant along each edge so that we have N distinct values given by $A(\mathsf{n})$ for each $\mathsf{n} \in \Gamma$.

If we now form equivalence classes by identifying E-fields that are related by gauge transformations (6.12) generated by $\mathcal{F}_{\Gamma^*}$, we obtain the truncated phase space:

$$P_\Gamma = C_{\Gamma^*}/\mathcal{F}_{\Gamma^*} = \mathcal{P}/\!\!/\mathcal{F}_{\Gamma^*}. \tag{6.15}$$

A set of variables parameterizing the truncated phase space must be invariant under the gauge transformations. We introduce a pair of 'holonomy' and 'flux' variables on each edge e_n defined by averaging the fields:

$$h_\mathsf{n} := \frac{1}{\mu_\mathsf{n}} \int_{\mathsf{e}_\mathsf{n}} \mathrm{d}x A(x), \tag{6.16}$$

$$X_\mathsf{n} := \frac{1}{\mu_\mathsf{n}} \int_{\mathsf{e}_\mathsf{n}} \mathrm{d}x E(x), \tag{6.17}$$

where μ_n is the length of the dual edge e_n. Using that the smearing function $\phi(x)$ vanish for $x \in \Gamma^*$, one can check that the 'fluxes' X_n are invariant under the gauge transformations generated by the flatness constraint, while the 'holonomies' h_n are trivially invariant. For the Poisson algebra we find trivially that:

$$\{X_\mathsf{m}, X_\mathsf{n}\} = \{h_\mathsf{m}, h_\mathsf{n}\} = 0, \tag{6.18}$$

and for the last bracket:

$$\{h_{\mathsf{m}}, X_{\mathsf{n}}\} = \left\{ \frac{1}{\mu_{\mathsf{m}}} \int_{\mathsf{e}_{\mathsf{m}}} \mathrm{d}x A(x), \frac{1}{\mu_{\mathsf{n}}} \int_{\mathsf{e}_{\mathsf{n}}} \mathrm{d}y E(y) \right\} = \frac{1}{\mu_{\mathsf{n}}} \delta_{\mathsf{mn}}. \tag{6.19}$$

These variable parameterize a phase space $(h_{\mathsf{n}}, X_{\mathsf{n}}) \in P_\Gamma$ which is symplectomorphic to the truncated phase space $\mathcal{P}_\Gamma$. We can see this as follows. Each point in $\mathcal{P}_\Gamma$ is given by a pair (modulo gauge transformations) (A, E) $(A, E + \partial_x \phi)$ which satisfy the constraint $\mathcal{F}_{\Gamma^*}[\phi]$. The equations (6.16, 6.17) provide a map:

$$\begin{array}{rccc} \mathcal{I}_\Gamma : & \mathcal{C}_\Gamma & \longrightarrow & P_\Gamma \\ & (\bar{A}, \bar{E}) & \longmapsto & (h_{\mathsf{n}}, X_{\mathsf{n}}), \end{array} \tag{6.20}$$

This map is invariant under gauge transformations and also defines a map $[\mathcal{I}]_\Gamma : \mathcal{P}_{\Gamma^*} \longrightarrow P_\Gamma$. Now, we can show that the symplectic structure of the discrete phase space is equivalent to that of the continuous phase space evaluated on piecewise-constant A-fields. Beginning from the symplectic potential for the continuous phase space:

$$\begin{aligned} \Omega &= \int_\Sigma \mathrm{d}x E \delta A \\ &= \sum_{\mathsf{n}} \int_{\mathsf{e}_{\mathsf{n}}} \mathrm{d}x E \delta A, \\ &= \sum_{\mathsf{n}} \mu_{\mathsf{n}} X_{\mathsf{n}} \mathrm{d} h_{\mathsf{n}}, \end{aligned} \tag{6.21}$$

where we used that δA is constant over each edge e_{n}, and that the A-field is equal to its average along each edge, i.e. $A(x) = h_{\mathsf{n}}$ for all $x \in \mathsf{e}_{\mathsf{n}}$. The last line is the symplectic potential which generates the Poisson algebra in (6.18, 6.19). Since symplectic forms are invertible by definition, we have shown that the map $[\mathcal{I}]_\Gamma$ is invertible, and therefore $P_\Gamma \cong \mathcal{P}_{\Gamma^*}$.

We have shown that each P_Γ is symplectomorphic to a truncation of the continuous phase space $\mathcal{P}_{\Gamma^*}$ as we have for full gravity, but the analogy does not end here. We can also recover the continuous theory from the truncated phase spaces in the projective limit. In other words, if we increase in a prescribed way the number N of points $\mathsf{v} \in \Gamma^*$ used to define the truncation, we obtain the continuous functions (A, E) and the symplectic potential. Let us define this limit as follows. Consider a set of points Γ_1^* consisting of a single point v. If we add another point v' at the midpoint of the edge (from v to v around the circle), we obtain the set $\Gamma_2^* = \mathsf{v} \cup \Gamma_1^*$, which is greater than Γ_1^* in the partial order. Γ_3^* is obtained by adding points at the midpoint of edges defined by Γ_2^*, and so on. In the limit $N \to \infty$, we obtain an infinite refinement of the real line given by the Bohr compactification. Notice that since our variables $(h_{\mathsf{n}}, X_{\mathsf{n}})$ are the average values of the fields over the edges between vertices, we have:

$$\lim_{N \to \infty} h_{\mathsf{n}} = A(\mathsf{n}), \qquad \lim_{N \to \infty} X_{\mathsf{n}} = E(\mathsf{n}), \tag{6.22}$$

so that the continuous fields are recovered. We also regain the continuous symplectic potential in this limit,

$$\lim_{N \to \infty} \sum_{\mathsf{n}} \mu_{\mathsf{n}} X_{\mathsf{n}} \mathrm{d} h_{\mathsf{n}} = \int_\Sigma \mathrm{d}x E \delta A, \tag{6.23}$$

since in the limit, the sum becomes an integral with the μ_{n} becoming $\mathrm{d}x$. We have just shown that $(\mathcal{P}, \omega)$ is recovered in the projective limit of graph phase spaces P_Γ. Notice that the phase space obtained in the projective limit is bigger than the continuous phase space, since there is no restriction on how much fields can change over any 'small' neighbourhood of a point on the compactified line. In particular, the projective phase space permits the fields to be given by step-functions.

6.2.1 Gauge choice

We now have a continuous phase space $\mathcal{P}$ of infinite dimension and a discrete phase space P_Γ of dimension $2N$, along with a map $\mathcal{I} : \mathcal{C}_{\Gamma^*} \to P_\Gamma$. This map sends all of the continuous field configurations (A, E) which have the same average value of E over the edges to a single point in P_Γ. We need to choose a single configuration $(\bar{A}, \bar{E})$ in the equivalence class in order to represent the discrete data in the continuous equations, i.e. we need to make a gauge choice:

$$\begin{array}{rccc} \mathcal{T}_\Gamma : & P_\Gamma & \longrightarrow & \mathcal{C}_{\Gamma^*} \\ & (h_{\mathsf{n}}, X_{\mathsf{n}}) & \longmapsto & (\bar{A}, \bar{E}), \end{array} \tag{6.24}$$

The gauge choice is a right inverse of $\mathcal{I}_\Gamma$, i.e. $\mathcal{I}_\Gamma \mathcal{T}_\Gamma = \mathrm{id}$, but not a left inverse. Placing the gauge choice after the truncation map takes a pair of functions (A, E) whose averages over the edges are $(h_{\mathsf{n}}, X_{\mathsf{n}})$, to a different pair of functions $(\bar{A}, \bar{E})$.

We want to make this gauge choice in a way that is diffeomorphism-covariant and allows us to formulate a discrete dynamics that is consistent with the continuous dynamics in that gauge. A choice satisfying these conditions, as we will see below, is given on each edge by:

$$\bar{A}(x) = h_{\mathsf{n}}, \qquad \bar{E}(x) = X_{\mathsf{n}}, \qquad \forall x \in \mathsf{e}_{\mathsf{n}}. \tag{6.25}$$

In this gauge choice, both fields are flat along the edges, and make discrete jumps at the points $x_{\mathsf{v}} \in \Gamma^*$. That is:

$$\bar{A}(x) = h_{\mathsf{n}_N} + \sum_i \Theta(x - \mathsf{v}_i)(h_{\mathsf{n}_{i+1}} - h_{\mathsf{n}_i}), \tag{6.26}$$

$$\bar{E}(x) = X_{\mathsf{n}_N} + \sum_i \Theta(x - \mathsf{v}_i)(X_{\mathsf{n}_{i+1}} - X_{\mathsf{n}_i}), \tag{6.27}$$

where the point $\mathsf{v}_i \in \Gamma^*$ is between the points n_i and n_{i+1} in Γ. Here we are using a step function $\Theta(x)$ defined to be centred on the origin such that $\Theta(0) = \frac{1}{2}$, $\Theta(\epsilon) = 1$, and $\Theta(-\epsilon) = 0$ for any $\epsilon > 0$.

Now, diffeomorphism-covariance implies that for any diffeomorphism $\Phi : \Sigma \longrightarrow \Sigma$ connected to the identity, if we first shift the points of Σ and then make the gauge choice, we get the same result that we would get for doing these operations in reverse order, i.e. $\big(\Phi^* \bar{A}(x), \Phi^* \bar{E}(x)\big) = \big(\bar{A}(\Phi(x)), \bar{E}(\Phi(x))\big)$. We can see that our gauge choice is diffeomorphism-covariant as follows. If we choose a gauge according to the set of points Γ^*, we then have fields that are constant along the edges between these points. A diffeomorphism will shift these fields around so that they are constant between a different set of points Γ'^*. Since the new set of points is related to the original set by a diffeomorphism $\Gamma'^* = \Phi(\Gamma^*)$, we could have alternatively arrived at this

field configuration by making the gauge choice according to the set of points Γ'^*. This shows that the gauge choice is diffeomorphism-covariant.

Let us now look for a consistent dynamics. Keeping track of the different lattice spacings μ_{n} quickly becomes cumbersome, so let us work on a fixed lattice $\mu_{\mathsf{n}} = \mu$. The results we obtain will generalize to arbitrary lattice spacings. The evolution equations are $\dot{A}(x) = A'(x)$ and $\dot{E}(x) = E'(x)$, and from the gauge map given in (6.26, 6.27) we have that:

$$\dot{\bar{A}}(x) = \sum_i \delta(x - \mathsf{v}_i)(h_{\mathsf{n}_{i+1}} - h_{\mathsf{n}_i}), \tag{6.28}$$

$$\dot{\bar{E}}(x) = \sum_i \delta(x - \mathsf{v}_i)(X_{\mathsf{n}_{i+1}} - X_{\mathsf{n}_i}), \tag{6.29}$$

where we used that the derivative of the step function is a delta function $\partial_x \Theta(x) = \delta(x)$. For consistency with our definition of the step function defined above, we have a delta function that is symmetric about the origin:

$$\int_0^\infty \mathrm{d}x \delta(x) = \int_{-\infty}^0 \mathrm{d}x \delta(x) = \frac{1}{2}. \tag{6.30}$$

Using this definition we find from the continuous equations of motion that:

$$\dot{h}_{\mathsf{n}_i} = \frac{1}{\mu} \int_{\mathsf{e}_{\mathsf{n}}} \mathrm{d}x \dot{\bar{A}}(x) = \frac{1}{2\mu}(h_{\mathsf{n}_{i+1}} - h_{\mathsf{n}_{i-1}}) =: \Delta h_{\mathsf{n}_i}, \tag{6.31}$$

$$\dot{X}_{\mathsf{n}_i} = \frac{1}{\mu} \int_{\mathsf{e}_{\mathsf{n}}} \mathrm{d}x \dot{\bar{E}}(x) = \frac{1}{2\mu}(X_{\mathsf{n}_{i+1}} - X_{\mathsf{n}_{i-1}}) =: \Delta X_{\mathsf{n}_i}. \tag{6.32}$$

As for the continuous fields, the discrete variables h_{n} and X_{n} satisfy the same equation of motion.

What we seek now is a discrete Hamiltonian in terms of the $(h_{\mathsf{n}}, X_{\mathsf{n}})$ variables which generates this dynamics via the Poisson brackets in (6.18, 6.19). Because we know the continuous gauge choice in terms of the discrete variables $(\bar{A}(h_{\mathsf{n}}), \bar{E}(X_{\mathsf{n}}))$, we can *derive* the discrete Hamiltonian by writing the continuous Hamiltonian (6.8) in terms of the fields defined in (6.26, 6.27):

$$H_\Gamma = \int_\Sigma \mathrm{d}x \bar{E}(x)\bar{A}'(x) = \int_\Sigma \sum_i \bar{E}(x)\delta(x - \mathsf{v}_i)(h_{\mathsf{n}_{i+1}} - h_{\mathsf{n}_i}). \tag{6.33}$$

Now, with our definition of the Θ function at the origin, we have $\bar{E}(\mathsf{v}_i) = \frac{1}{2}\left(X_{\mathsf{n}_{i+1}} + X_{\mathsf{n}_i}\right)$ at each point $\mathsf{v} = \mathsf{e}_{\mathsf{n}_i} \cap \mathsf{e}_{\mathsf{n}_{i+1}}$. This yields the result:

$$H_\Gamma = \mu \sum_{\mathsf{n}} X_{\mathsf{n}} \Delta h_{\mathsf{n}}. \tag{6.34}$$

With this Hamiltonian, the discrete equations of motion are:

$$\dot{h}_{\mathsf{n}} = \{h_{\mathsf{n}}, H_\Gamma\} = \Delta h_{\mathsf{n}}, \qquad \dot{X}_{\mathsf{n}} = \{X_{\mathsf{n}}, H_\Gamma\} = \Delta X_{\mathsf{n}}. \tag{6.35}$$

These are the same equations we found using the continuous Hamiltonian on our gauge choice of fields (6.31, 6.32). This shows that the gauge choice we have made provides a dynamics that is consistent between the discrete and continuous frameworks. Note that if we consider a non-uniform lattice, the result can be written as a modification to the definition of Δ.

6.2.2 Discrete dynamics

The discrete equations of motion (6.35) are solved by exponentiating the action of the Hamiltonian:

$$\dot{h}_{\mathsf{n}}(t) = e^{t\Delta} h_{\mathsf{n}}(0), \qquad \dot{X}_{\mathsf{n}}(t) = e^{t\Delta} X_{\mathsf{n}}(0). \tag{6.36}$$

Now, we can use a fourier transformation to write the equation in a form that does not depend on the difference operator Δ. Since both variables satisfy the same equation of motion, we solve for only the $h_{\mathsf{n}}(t)$ variables as the $X_{\mathsf{n}}(t)$ equations are solved identically. Using θ as the continuous transform variable of the discrete index n, we have the transformation:

$$h_{\mathsf{n}}(t) = \frac{1}{2\pi} \int_{-\pi}^{\pi} \mathrm{d}\theta e^{-i\mathsf{n}\theta} f(\theta, t), \tag{6.37}$$

and the inverse transform:

$$f(\theta, t) = \sum_{\mathsf{n}=-\infty}^{\infty} e^{i\mathsf{n}\theta} h_{\mathsf{n}}(t), \tag{6.38}$$

where we use the identification $h_{\mathsf{n}} = h_{\mathsf{n}+N}$. Using the fourier transform, let us calculate the action of Δ:

$$\begin{aligned} \Delta h_{\mathsf{n}}(0) &= \frac{1}{2\pi} \int_{-\pi}^{\pi} \mathrm{d}\theta e^{-i\mathsf{n}\theta} \left(\frac{1}{2\mu}\right) \left(e^{-i\theta} - e^{i\theta}\right) f(\theta, 0) \\ &= \frac{1}{2\pi} \int_{-\pi}^{\pi} \mathrm{d}\theta e^{-i\mathsf{n}\theta} \big(-i\bar{t} \sin\theta \big) f(\theta, 0), \end{aligned} \tag{6.39}$$

where $\bar{t} \equiv t/\mu$. Comparing (6.36) and (6.39), we write the equation of motion as:

$$\begin{aligned} h_{\mathsf{n}}(t) &= \frac{1}{2\pi} \int_{-\pi}^{\pi} \mathrm{d}\theta e^{-i(\mathsf{n}\theta + \bar{t}\sin\theta)} f(\theta, 0) \\ &= \frac{1}{2\pi} \sum_{\mathsf{m}=-\infty}^{\infty} h_{\mathsf{m}}(0) \int_{-\pi}^{\pi} \mathrm{d}\theta e^{-i(\theta(\mathsf{n}-\mathsf{m}) + \bar{t}\sin\theta)} \\ &= \sum_{\mathsf{m}=-\infty}^{\infty} J_{\mathsf{m}-\mathsf{n}}(\bar{t}) h_{\mathsf{m}}(0), \end{aligned} \tag{6.40}$$

where we substituted the fourier transform of $f(\theta, 0)$ to get to the second line, and $J_{\mathsf{m}-\mathsf{n}}(\bar{t})$ is a Bessel function of the first kind. This same equation holds also for $X_{\mathsf{n}}(\bar{t})$. From this equation we can define a propagator $G_{\mathsf{mn}}(t) = J_{\mathsf{m}-\mathsf{n}}(\bar{t})$ taking data from point m at time $\bar{t} = 0$ to point n at time $\bar{t}$. The time $\bar{t} = t/\mu$ is scaled properly so that the velocity of propagation is constant as one increases the number of points on a circle of fixed circumference.

We showed above that the discrete equations of motion for $(h_{\mathsf{n}}, X_{\mathsf{n}})$ agree with the continuous equations of motion for the gauge choice $(\bar{A}, \bar{E})$ at a particular value of $\bar{t}$. It is difficult to see this from the discrete solution written in terms of Bessel functions, but never-the-less the

correspondence holds as demonstrated in the video file A.1. This file shows an animation generated by Maple of the discrete data h_{n} evolving according to the discrete equations of motion. Note that the endpoints of the abscissa are to be identified. The animation demonstrates that while the initial dynamics corresponds exactly, as time evolves errors creep into the discrete dynamics as the profile of points h_{n} changes, indicating a disagreement with the continuous evolution of the gauge choice $\bar{A}$, which does not change profile dynamically. Note that these errors are mostly due to the discrete evolution equations rather than coming from errors in the numerics. If enough points N are used the errors become suppressed and the discrete and continuous dynamics will continue to coincide for arbitrarily long times, up to small errors. However, maintaining the dynamical correspondence between discrete and classical evolutions *up to small errors* is the idea of an approximation, which *is not* what we are considering in this chapter. What we want is to find a way to use the discrete phase space for finite N to describe the *exact* evolution of certain classes of continuous data. This is the topic of the next section.

6.2.3 Truncated dynamics

Let us now generalize to consider arbitrary lattices. As mentioned above, this results in a redefinition of the difference operator Δ in the discrete equations of motion, and the solutions are no longer given in terms of Bessel functions. However, the idea that the discrete dynamics is consistent with the continuous dynamics at an instant of time still holds.

Now, consider two different constraints $\mathcal{F}_{\Gamma^*}$ and $\mathcal{F}_{\Gamma'^*}$. We can apply these to the full phase space $\mathcal{P}$ to obtain two different constrained phase spaces $\mathcal{C}_{\Gamma^*}$ and $\mathcal{C}_{\Gamma'^*}$. From these spaces, we can mod out the gauge transformations to obtain truncated phase spaces $\Pi_\Gamma : \mathcal{C}_{\Gamma^*} \to P_\Gamma$, and likewise for Γ'. We would like to develop a truncated dynamics $U_{\Gamma\Gamma'}(t) : P_\Gamma \to P_{\Gamma'}$ from one reduced phase space to the other. If we label the full dynamics $U(t) : \mathcal{P} \to \mathcal{P}$, we can draw the following diagram:

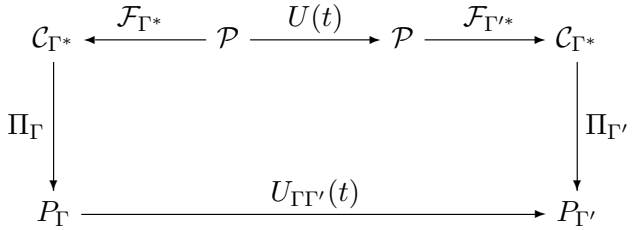

This suggests a form of dynamics from one reduced phase space to another reduced phase space can be obtained by mapping to the constrained phase space with the gauge choice $\mathcal{T}_\Gamma$, placing the constrained fields in the full phase space using the inclusion map (denote by $\mathcal{F}_{\Gamma^*}^{-1}$), using the full dynamics, and then reducing again with a new constraint $\mathcal{F}_{\Gamma^*}^{-1}$ and the projection $\Pi_{\Gamma'}$, i.e.:

$$U_{\Gamma\Gamma'}(t) := \Pi_{\Gamma'}\ \mathcal{F}_{\Gamma'^*}\ U(t)\ \mathcal{F}_{\Gamma^*}^{-1}\ \mathcal{T}_\Gamma. \tag{6.41}$$

Let us apply this dynamics to our model. We begin with some initial data $(h_{\mathsf{n}}(0), X_{\mathsf{n}}(0)$ for all $\mathsf{n} \in \Gamma_i$. Our definition of truncated dynamics allows us to evolve this data into any other discrete phase space. The first step is to use our gauge choice to define the fields $(\bar{A}(x,0), \bar{E}(x,0))$

according to equations (6.26, 6.27). These fields are within the constrained phase space $\mathcal{C}_{\Gamma^*_0}$, defined as the continuous phase space restricted to data which satisfies $\mathcal{F}_{\Gamma^*_0} = 0$. The continuous dynamics governed by $U(t)$ will take these fields and shift them counterclockwise around the circle to obtain $(\bar{A}(x,t), \bar{E}(x,t)) = (\bar{A}(x+t,0), \bar{E}(x+t,0))$. Notice this is the same as acting on the initial data with a diffeomorphism that satisfies $\Phi_t(x) = x + t$, i.e. shifting the fields counterclockwise is equivalent to shifting the points clockwise. This dynamics takes the fields out of the constrained space $\mathcal{C}_{\Gamma^*_0}$, since we no longer have $\mathrm{d}A = 0$ along the edges $\mathsf{e_n} \in \Gamma^*_0$. At this point we can project down to any truncated phase space we like using the constraint $\mathcal{F}_{\Gamma'^*}$ and the projection $\Pi_{\Gamma'}$. Notice however, that the continuous data at time t is sitting within the constrained space $\mathcal{C}_{\Gamma^*_t}$ defined by the points $\mathsf{v} + t \in \Gamma^*_t$ for all $\mathsf{v} \in \Gamma^*_0$. This is a preferred truncation. If this truncation is used, the stepwise profile of $(\bar{A}, \bar{E})$ is maintained under this map, and no data is lost or reorganized when we project down after the continuous evolution to P_{Γ_t}. Since this dynamics is given by a diffeomorphism of the points, and our gauge map is diffeomorphism-covariant, we have for this model the nice property that:

$$U_{\Gamma_{t_1}\Gamma_{t_2}}(t_2 - t_1) U_{\Gamma_{t_0}\Gamma_{t_1}}(t_1) = U_{\Gamma_{t_0}\Gamma_{t_2}}(t_2). \tag{6.42}$$

There are other choices which allow for this property, namely, any choice of 'larger' graphs in the partially ordered sense so that $\Gamma_{t_1} \geq \Phi_{t_1}\Gamma_0$ and $\Gamma_{t_2} \geq \Phi_{t_2-t_1}\Gamma_{t_1}$. With any such preferred Γ_t, the gauge choice $\mathcal{T}_{\Gamma_t}$ is an inverse of the truncation: $\mathcal{T}_{\Gamma_t}\mathcal{I}_{\Gamma_t} = \mathcal{I}_{\Gamma_t}\mathcal{T}_{\Gamma_t} = \mathrm{id}$. However, this is an artifact of the simplicity of the model, as a more complex dynamics which changes the field profiles would not allow for these preferred choices of truncation.

What will happen for other choices of Γ'^* used to project down to the continuous phase space from the data $(\bar{A}(x,t), \bar{E}(x,t))$? For an arbitrary set of points Γ'^* enforcing the flatness constraint, we will project down to the truncated phase space $P_{\Gamma'}$ by averaging the fields over the edges $\mathsf{e_n}$ between the points in Γ'^*. In this general case the gauge choice is not the inverse of the truncation map $\mathcal{T}_\Gamma\mathcal{I}_\Gamma \neq \mathcal{I}_\Gamma\mathcal{T}_\Gamma$. Wherever a point $\mathsf{v} \in \Gamma^*$ lies on an edge $\mathsf{e_{n'}}$ between points $\mathsf{v'} \in \Gamma'^*$, we get a reorganizing of the data, i.e. different level values of $(\bar{A}(x,t), \bar{E}(x,t))$ are combined in the averaging used for the map $\mathcal{I}_{\Gamma'}$ as defined in (6.16, 6.17). Evidently, the 'nice' evolution property (6.42) no longer applies when the gauge map $\mathcal{T}_\Gamma$ is not the inverse of the truncation $\mathcal{I}_\Gamma$.

6.2.4 Geometrical picture

Now what does this mean in terms of the geometric structures underlying Hamiltonian dynamics? The Poisson algebra $\{A(x), E(y)\} = \delta(x-y)$ defines a symplectic two-form ω, and the 'doubled' symplectic manifold in question is $\mathcal{P} \times \overline{\mathcal{P}} \equiv (\mathcal{P} \times \mathcal{P}, \omega \ominus \omega)$. Dynamics within this symplectic manifold is a Lagrangian subspace L_t, and we would like to construct this subspace from a collection of truncated dynamics.

The truncated dynamics $U_{\Gamma\Gamma'}(t)$ as we have defined it is the full dynamics restricted to constrained subspaces. We showed above that any constraint $\mathcal{F}_{\Gamma^*}$ is not preserved by the dynamics, so that we have L_t intersecting each constrained subspace $\mathcal{C}_\Gamma$ transversely. The truncated dynamics define a Lagrangian submanifold within the symplectic manifold defined

from two truncated phase spaces:

$$L_t^{\Gamma\Gamma'} = L_t \cap (\mathcal{C}_{\Gamma^*} \times \mathcal{C}_{\Gamma'^*}) \subset P_\Gamma \times P_{\Gamma'}. \tag{6.43}$$

In this way, the continuous dynamics L_t is allowing us to define a set of truncated dynamics for any initial and final phase spaces P_Γ and $P_{\Gamma'}$. Each $L_t^{\Gamma\Gamma'}$ covers a portion of the full Lagrangian subspace L_t. The question then is, can we reconstruct the full dynamics from the set of all such truncated dynamics?

We showed above (6.22, 6.23) that the continuous phase space is contained within the projective limit of truncated P_Γ phase spaces. These same arguments apply also to the projective limit of constrained phase spaces $\mathcal{C}_{\Gamma^*}$, that is:

$$\mathcal{P} \subset \lim_{\Gamma\to\infty} \mathcal{C}_{\Gamma^*}. \tag{6.44}$$

Using the projective limit, we can consider the entire projective family of constraints to formally reconstruct the full dynamics:

$$\lim_{\Gamma\to\infty}\lim_{\Gamma'\to\infty} L_t^{\Gamma\Gamma'} = L_t \cap \left(\lim_{\Gamma\to\infty} \mathcal{C}_{\Gamma^*} \times \lim_{\Gamma'\to\infty} \mathcal{C}_{\Gamma'^*}\right) = L_t. \tag{6.45}$$

This suggests that the projective limit is key to defining the dynamics for a continuous theory in terms of truncated phase spaces.

6.3 Conclusion

The phase spaces P_Γ of loop gravity are finite-dimensional truncations of the continuous phase space defined by a connection and electric field $(\boldsymbol{A}, \boldsymbol{E})$. The full phase space is obtained in the projective limit of these graph phase spaces, and we would like to use these phase spaces to describe the full dynamics of general relativity. Since the phase spaces P_Γ are each defined on a different graph, and generally have a different number of holonomy-flux pairs, this will require a formulation of dynamics that is capable of describing an evolution between phase spaces of different dimension, i.e. a truncated dynamics. Within the gauge of a spinning geometry, the scalar constraint is supported only on the one-skeleton dual to a cellular decomposition. This generates a dynamics on the fluxes defined on the boundary of each face, which is a promising sign for the development of dynamics in the discrete phase space that is consistent with the continuous dynamics.

In order to better understand truncated dynamics, we make use of the geometrical picture underlying dynamics within a phase space. We reviewed how one can construct a double manifold from two copies of a symplectic manifold $(M \times M, \varpi)$, within which dynamics takes the form of a Lagrangian submanifold. This provides the framework for a generalization to a dynamics between symplectic manifolds of different dimension $(M_1 \times M_2, \varpi)$.

We studied truncated dynamics using a simple model that mimics the case of full gravity. Here a continuous phase space (A, E) was defined upon S^1, and the dynamics was found to shift the fields counterclockwise around the circle without change of profile, equivalent to a diffeomorphism Φ_t which shifts each point $x \to x + t$. We imposed a set of flatness constraints

and found a reduced phase space $(h_{\mathsf{n}}, X_{\mathsf{n}}) \in P_\Gamma$, which contains the continuous phase space in the projective limit. We defined a truncated dynamics for initial data $(h_{\mathsf{n}}, X_{\mathsf{n}}) \in P_\Gamma$ by using a gauge choice to represent this data within the continuous phase space. Then the continuous Hamiltonian was used to evolve this data for some time, before truncating down to the final phase space $P_{\Gamma'}$. If the zero-skeleton Γ'^* imposing the final truncation by $\mathcal{F}_{\Gamma'^*}$ was chosen to be a diffeomorphism of the initial zero-skeleton $\Phi_t\Gamma^*$, then this definition reproduces the continuous dynamics exactly for the subclass of data that exists in the constrained space $\mathcal{C}_{\Gamma*}$. Using an arbitrary truncation generally leads to a change in the profile of the fields. Nevertheless, we showed formally that the full dynamics L_t is obtained in the projective limit of truncated dynamics $L_t^{\Gamma\Gamma'}$.

In 4d gravity, we do not expect a preferred truncation such as we had for this model. The gauge choice we propose is that of a spinning geometry, where curvature is concentrated along the edges of the one-skeleton. The continuous dynamics leads to a dispersion of this curvature, but the hope is that the localization will make this problem manageable so that we can construct a set of truncated dynamics $L_t^{\Gamma\Gamma'}$. Notice that since the full theory of loop gravity has a projective limit, the formal construction given in equation (6.45) applies here as well. The framework of loop quantum gravity is built upon spin network states which satisfy the condition of cylindrical consistency, so that a state defined on a graph Γ is also well defined in a larger graph Γ' and has the same behaviour under the action of operators in both Hilbert spaces. A truncated dynamics for loop gravity will need to take this into account. We conjecture that this is possible as long as we have the relation $L_t^{\Gamma_1\Gamma_3} \subset L_t^{\Gamma_2\Gamma_3}$ if $\mathcal{C}_{\Gamma_1^*} \subset \mathcal{C}_{\Gamma_1^*}$, so that the dynamics between two constrained subspaces agrees with the inclusion of the initial data into a larger constrained subspace.

Chapter 7

Point particles in 3d gravity

In the previous chapters we have gone a long way toward developing a theory of classical loop gravity. We began by developing a Hamiltonian theory in terms of a continuous phase space $\mathcal{P}$. We showed that a certain symplectic reduction (truncation) of this phase space by a flatness constraint $\mathcal{F}_\Gamma$ is isomorphic to the loop gravity phase space associated to an embedded graph P_Γ, and we showed also that the SU(2)-gauge invariant phase spaces are also isomorphic $\mathcal{P}^G_{\Gamma,\Gamma^*} \cong P^G_\Gamma$. We looked in particular at a spinning geometries as a candidate to represent the discrete data as a continuous spatial geometry. With this gauge choice, we hope to recover the full dynamics of gravity in terms of a collection of truncated dynamics $U_{\Gamma\Gamma'}(t)$ between truncated phase spaces. Let us now consider a model of 3d gravity which encompasses all of this and demonstrates what we would like to accomplish in four dimensions.

Three-dimensional gravity has often served as a useful testing ground for the 4d theory. Without matter, the model does not possess local degrees of freedom and would be too simple for our purposes. We add complexity to the model by including a number of point particles which give rise to a finite number of topological degrees of freedom associated to the particle positions. The study of point particles in 3d gravity has a rich history. Static solutions for one- and two-body models were first found by Staruszkiewicz in 1963 [82]. Over twenty years later, interest in the field began to grow after the seminal work by Deser, Jackiw and 't Hooft [83]. This work presents a clear understanding of dynamical point particles as conical singularities, described on a flat hypersurface by cutting out 'wedges' of space and identifying sides of the wedges. More recently there have been models [84, 85, 86] which divide space into polygons in order to describe the system. This is closely related to the approach we take here.

We consider 3d gravity coupled to a number of spinless point particles[1]. We start from the first order action which parameterizes the continuous phase space in terms of a connection $\boldsymbol{A}$ and a frame-field (or dreibein) $\boldsymbol{e}$. As in the 4d theory, the Hamiltonian formalism yields a Gauss constraint, but here this constraint implies that the connection is piecewise-torsionless. We also find a flatness constraint which imposes that the connection is flat everywhere except at the particle locations. In addition to these constraints, we impose a constraint on the holonomy around each particle in order to fix the curvature associated to particles. We fix a gauge $(\bar{\boldsymbol{A}}, \bar{\boldsymbol{e}})$, choosing a particular geometry from the equivalence class of fields which satisfy the flatness

[1] See [87] for a precursor to this work.

and Gauss constraints, and are related by the gauge transformations which these constraints generate. This gauge is the 3d analog of a spinning geometry, and is chosen by defining the spatial manifold as a 2d-cellular complex with particles sitting at the vertices. This leads naturally to a description of the theory in terms of the discrete phase space associated to a dual graph Γ. In both the continuous and discrete theories, particle mass and momenta are described by the holonomies around the particle locations. We find a discrete dynamics in terms of holonomies and fluxes, and show that it is consistent with the continuous dynamics. The theory can be described exactly in terms of P_Γ phase spaces, with dynamics appearing as a time-dependent embedding of a graphs, similarly to the model of Chapter 6, but here we have the additional feature of discrete graph changes. These occur whenever one of the 2d-cells collapses to zero area, and causes an adjacent triangle to split into two, along with the corresponding changes in the dual graph and its associated phase space. This work sets the stage for a quantization using the well-established framework of loop quantum gravity, making an interesting toy model for the full four-dimensional theory. This model has been quantized according to the path integral approach of spin foams (see the papers by Freidel and Louapre in [78]), and it would be very interesting to compare results between the Lagrangian and Hamiltonian quantization techniques.

7.1 Hamiltonian analysis

The first order formalism of general relativity parameterizes the gravitational field in terms of a connection $\boldsymbol{A}$ and a frame-field $\boldsymbol{e}$. We write the spacetime manifold as $M = \mathbb{R} \times \Sigma$ where Σ is a spacelike surface homeomorphic to S^3. Recall that in a 4d Lorentzian spacetime the field variables take values in the $\mathfrak{su}(2)$ algebra. In this three-dimensional setting, we choose to work with a Riemannian rather than a Lorentzian spacetime since the field variables are then $\mathfrak{su}(2)$-valued as in the 4d Lorentzian case[2], providing a theory that bears more similarity to the case of full gravity.

We use $\mathfrak{su}(2)$ basis elements $\boldsymbol{\tau}^i$ (for $i = 0, 1, 2$) which are given by $-i/2$ times the Pauli matrices. Our notation is such that elements of $\mathfrak{su}(2)$ are written as $\boldsymbol{A} \equiv A^i \boldsymbol{\tau}^i$, for example, and all internal indices are written as superscripts. Where coordinate indices are explicitly shown, we shall use Greek letters $\mu = 0, 1, 2$ to label spacetime indices and Latin letters $a = 1, 2$ to label space indices. We work in units such that $8\pi G = c = 1$.

7.1.1 Pure gravity

The singular nature of point particles requires some special treatment, so we shall begin with an analysis of pure gravity before bringing matter into the picture. We postpone an analysis of boundary terms and conditions until after we have introduced particles.

The first order action for pure gravity is:

$$S = \frac{1}{2} \int_M \mathrm{d}^3x \epsilon^{\mu\nu\rho} e^i_\mu F^i_{\nu\rho}, \tag{7.1}$$

[2]In a 3d Lorentzian spacetime the field variables take values in the $\mathfrak{so}(1,2)$ algebra.

where $F^i_{\mu\nu} = \partial_\mu A^i_\nu - \partial_\nu A^i_\mu + \epsilon^{ijk} A^j_\mu A^k_\nu$ is the curvature of the connection. By splitting the coordinate indices into 0 and a, the action is decomposed into time and space components as follows:

$$\begin{aligned} S &= \frac{1}{2}\int dt \int_\Sigma \mathrm{d}^2x \left(\epsilon^{0ab} e^i_0 F^i_{ab} + 2\epsilon^{ab0} e^i_a F^i_{b0}\right) \\ &= \frac{1}{2}\int dt \int_\Sigma \mathrm{d}^2x \epsilon^{ab} \left[e^i_0 F^i_{ab} + 2e^i_a \left(\partial_b A^i_0 - \partial_0 A^i_b + \epsilon^{ijk} A^j_b A^k_0\right)\right] \\ &= \int dt \int_\Sigma \mathrm{d}^2x \epsilon^{ab} \left[e^i_b \dot{A}^i_a + \frac{1}{2} e^i_0 F^i_{ab} + A^i_0 \left(\partial_a e^i_b + \epsilon^{ijk} A^j_a e^k_b\right)\right] \\ &= \int dt \int_\Sigma \mathrm{d}^2x \epsilon^{ab} \left[e^i_b \dot{A}^i_a + \frac{1}{2} N^i F^i_{ab} + \frac{1}{2}\lambda^i G^i_{ab}\right] \end{aligned} \tag{7.2}$$

where the over-dot denotes a derivative with respect to the arbitrary time parameter t, $\epsilon^{\mu\nu\rho}$ is the completely antisymmetric, metric-independent tensor density and $\epsilon^{ab} \equiv \epsilon^{0ab}$. The boundary terms arising in this decomposition will be discussed in section 7.1.3. The time components of the fields are Lagrange multipliers, written in the last line as $N^i := e^i_0$ and $\lambda^i := A^i_0$ corresponding respectively to the flatness constraint:

$$F^i_{ab} := \partial_a A^i_b - \partial_b A^i_a + \epsilon^{ijk} A^j_a A^k_b, \tag{7.3}$$

and the Gauss constraint:

$$G^i_{ab} := \partial_a e^i_b - \partial_b e^i_a + \epsilon^{ijk}(A^j_a e^k_b - A^j_b e^k_a). \tag{7.4}$$

Notice that the Gauss constraint in 3d is equivalent to a zero-torsion constraint. The flatness and Gauss constraint have the same form, setting the covariant derivatives of both the connection and the triad to zero, and putting these variables on the same footing.

We choose A^i_a as the configuration variable and find that the canonical momentum is e^i_a. The Poisson brackets are:

$$\left\{A^i_a(x), A^j_b(y)\right\} = \left\{e^i_a(x), e^j_b(y)\right\} = 0, \qquad \left\{A^i_a(x), e^j_b(y)\right\} = \epsilon_{ab}\delta^{ij}\delta^2(x-y). \tag{7.5}$$

These variables parameterize a continuous phase space $(\boldsymbol{A}, \boldsymbol{e}) \in \mathcal{P}$ for general relativity. There are $2 \times 3 \times 2 = 12$ degrees of freedom per point, and the two constraints completely constrain these variables leaving no degrees of freedom in the case of pure gravity.

We write the smeared constraints as:

$$\mathcal{F}(N) := \frac{1}{2}\int_\Sigma \mathrm{d}^2x \epsilon^{ab} N^i F^i_{ab} = \int_\Sigma N^i F^i, \tag{7.6}$$

$$\mathcal{G}(\lambda) := \frac{1}{2}\int_\Sigma \mathrm{d}^2x \epsilon^{ab} \lambda^i G^i_{ab} = \int_\Sigma \lambda^i G^i, \tag{7.7}$$

where we have used differential form notation to write the curvature and torsion without coordinate indices, e.g. $F^i \equiv F^i_{ab}\mathrm{d}x^a \wedge \mathrm{d}x^b$. If we also use our notation for elements of $\mathfrak{su}(2)$, e.g. $\boldsymbol{F} \equiv F^i\tau^i$, the curvature is written simply as $\boldsymbol{F} = \mathrm{d}_A\boldsymbol{A} = \mathrm{d}\boldsymbol{A} + \frac{1}{2}[\boldsymbol{A}, \boldsymbol{A}]$, and the torsion as

$\boldsymbol{G} = \mathrm{d}_A \boldsymbol{e} = \mathrm{d}\boldsymbol{e} + [\boldsymbol{A}, \boldsymbol{e}]$. Here the notation $[\cdot,\cdot]$ implies taking the $\mathfrak{su}(2)$ commutator *and* the wedge product between the elements within the bracket.

With appropriate boundary terms and conditions, the constraints form a first class algebra:

$$\begin{aligned} \left\{\mathcal{F}(\boldsymbol{N}), \mathcal{F}(\tilde{\boldsymbol{N}})\right\} &= 0, \\ \{\mathcal{F}(\boldsymbol{N}), \mathcal{G}(\boldsymbol{\lambda})\} &= \mathcal{F}(]\boldsymbol{N}, \boldsymbol{\lambda}]), \\ \left\{\mathcal{G}(\boldsymbol{\lambda}), \mathcal{G}(\tilde{\boldsymbol{\lambda}})\right\} &= \mathcal{G}([\boldsymbol{\lambda}, \tilde{\boldsymbol{\lambda}}]), \end{aligned} \tag{7.8}$$

Again we leave a discussion of the boundary terms and conditions for after we have included particles in the system.

The Gauss constraint generates SU(2)-gauge transformations. The infinitesimal transformations are:

$$\delta_{\mathcal{G}} A^i = \left\{A^i, \mathcal{G}(\boldsymbol{\lambda})\right\} = -\mathrm{d}_A \lambda^i, \qquad \delta_{\mathcal{G}} e^i = \left\{e^i, \mathcal{G}(\boldsymbol{\lambda})\right\} = \epsilon^{ijk} e^j \lambda^k. \tag{7.9}$$

For a function $g(x) \in \mathrm{SU}(2)$, the finite transformations are:

$$\boldsymbol{A} \to g\boldsymbol{A}g^{-1} + g\mathrm{d}g^{-1}, \qquad \boldsymbol{e} \to g\boldsymbol{e}g^{-1}. \tag{7.10}$$

These are the Riemannian analog of Lorentz boosts and rotations.

The flatness constraint generates the following infinitesimal transformations:

$$\delta_{\mathcal{F}} A^i = \left\{A^i, \mathcal{F}(\boldsymbol{N})\right\} = 0, \qquad \delta_{\mathcal{F}} e^i = \left\{e^i, \mathcal{F}(\boldsymbol{N})\right\} = \mathrm{d}_A N^i. \tag{7.11}$$

Notice these transformations do not affect the connection. For an $\mathfrak{su}(2)$-valued one-form $\boldsymbol{\phi} \in \Omega^1(\mathfrak{su}(2))$, the finite gauge transformations are:

$$\boldsymbol{A} \to \boldsymbol{A}, \qquad \boldsymbol{e} \to \boldsymbol{e} + \mathrm{d}_A \boldsymbol{\phi}. \tag{7.12}$$

This shift of the triad is equivalent to a translation.

From the action (7.2) we read off the Hamiltonian to be a sum of constraints:

$$H_0 = -\int_\Sigma \left(N^i F^i + \lambda^i G^i\right). \tag{7.13}$$

Up to possible boundary terms, this is the Hamiltonian for pure 3d Riemannian gravity parameterized by a connection and frame-field $(\boldsymbol{A}, \boldsymbol{e}) \in \mathcal{P}$.

7.1.2 Gravity with particles

It is well-known that point particles manifest themselves as conical singularities on spatial hypersurfaces of a 3d spacetime [83]. This makes defining the field variables problematic at these locations. We handle this problem by excising the particle worldlines from the spacetime following the method used in [85, 88]. Let us now bring a number $|\mathsf{v}_\Delta|$ of point particles into the picture. Excising the particle worldlines from the spacetime corresponds to treating each particle location on Σ_t as a puncture, topologically equivalent to an open disc. The closure of

an open disc is a circle, which can be parameterized by a radius r and an angle φ. In the limit $r \to 0$ the boundary $\mathcal{B}_{\mathsf{v}}$ of the disc shrinks to have a vanishing circumference, but here we shall not identify points on this boundary with different values of φ. The only identification we make is $\varphi = \varphi + 2\pi$ so that the boundary maintains its S^1 properties in the limit of vanishing radius. We associate such a boundary $\mathcal{B}_{\mathsf{v}}$ to each particle on Σ_t.

A spatial hypersurface Σ_t is then homeomorphic to S^2 with $|\mathsf{v}_\Delta|$ punctures. The boundary of Σ_t is the union of a boundary $\mathcal{B}_{\mathsf{v}}$ for each particle:

$$\partial\Sigma_t = \bigsqcup_v \mathcal{B}_{\mathsf{v}}. \tag{7.14}$$

As is commonly done, we shall adopt a slight abuse of notation and drop the subscript t labeling spatial hypersurfaces.

In order that a particle boundary $\mathcal{B}_{\mathsf{v}}$ appears point-like in a hypersurface Σ, the component of the frame-field that is tangent to $\mathcal{B}_{\mathsf{v}}$ must be zero [85, 88] so that its circumference vanishes. We can use a variable $s = [0, 1]$ to parameterize the loop $\mathcal{B}_{\mathsf{v}}(s)$ such that a vector tangent to the boundary is given by $(\dot{\mathcal{B}}_{\mathsf{v}})^a$, where the over-dot represents a derivative with respect to s. We ensure that each particle boundary appears point-like by introducing a boundary condition at each $\mathcal{B}_{\mathsf{v}}$:

$$(\dot{\mathcal{B}}_{\mathsf{v}})^a e^i_a = 0. \tag{7.15}$$

Notice this condition also sets to zero any variation of the tangential frame-field component, i.e. $(\dot{\mathcal{B}}_{\mathsf{v}})^a \delta e^i_a = 0$.

In this treatment particles do not have independent degrees of freedom, but rather are defined as singular configurations of the gravitational field. Properties of the particles are seen in the field variables $(\boldsymbol{A}, \boldsymbol{e})$ outside of the particle locations. Since the particle positions $\boldsymbol{q}_{\mathsf{v}}$ are $\mathfrak{su}(2)$-valued, the momenta $\boldsymbol{p}_{\mathsf{v}}$ are also $\mathfrak{su}(2)$-valued. Up to SU(2)-gauge transformations, the momentum of a particle determines the value of a holonomy around a loop encircling the particle (and only that particle). The holonomy defined on a path γ is given by the path-ordered exponential of the connection:

$$h_\gamma := \overrightarrow{\exp}_\gamma \boldsymbol{A}. \tag{7.16}$$

Calculating the holonomy around a loop requires the specification of a base-point b where the path integral begins and ends. If we choose the path around the particle to be the boundary $\mathcal{B}_{\mathsf{v}}$ we have:

$$h_{\mathcal{B}_{\mathsf{v}},b} = \mathbb{1} \cos \frac{m_{\mathsf{v}}}{2} - 2 g_b \boldsymbol{u}_{\mathsf{v}} g_b^{-1} \sin \frac{m_{\mathsf{v}}}{2}, \tag{7.17}$$

for some $g(x) \in \mathrm{SU}(2)$ that depends upon the gauge choice. See appendix A.2 for details. Taking the trace of this equation defines a Wilson loop associated to the particle $|\mathsf{v}_\Delta|$:

$$W_{\mathsf{v}} = \mathrm{Tr} h_{\mathcal{B}_{\mathsf{v}},b} = 2 \cos \frac{m_{\mathsf{v}}}{2}, \tag{7.18}$$

where the dependance on the base-point via has been traced out, i.e. W_{v} is the same for any choice of base point.

We now use Wilson loops to introduce mass-shell constraints[3] for each particle, written in terms of the trace of the holonomies $h_{\mathcal{B}_\mathsf{v}}$:

$$\psi_\mathsf{v} := 2\cos^{-1}\frac{W_\mathsf{v}}{2} - m_\mathsf{v}. \tag{7.19}$$

These constraints are the covariant analog of $|p_\mathsf{v}|^2 = |m_\mathsf{v}|^2$, imposing that the connection $\boldsymbol{A}$ encodes the deficit angle m_v associated with the mass of each particle. Through these constraints, each particle adds a point of curvature to the spatial hypersurface giving it the geometry of a polyhedron, which implies that the total mass of all particles must be equal to 4π [83]. Note that the upper limit on the deficit angle for any single vertex of a polyhedron implies that each mass $m_\mathsf{v} < 2\pi$, which leaves no ambiguity in the inverse cosine in the definition of the mass shell constraint.

We close this section by stating the Hamiltonian for gravity and a number of point particles with masses m_v:

$$H_0 = \sum_\mathsf{v} \alpha_\mathsf{v}\psi_\mathsf{v} - \mathcal{F}(\boldsymbol{N}) - \mathcal{G}(\boldsymbol{\lambda}), \tag{7.20}$$

where α_v is the Lagrange multiplier associated to the mass shell constraint ψ_v. This is a sum of constraints as is the case for pure gravity. The phase space is given by $(\boldsymbol{A}, \boldsymbol{e}) \in \mathcal{P}$, but now these fields are defined on a sphere with punctures $\Sigma \cong S^2 \setminus \{\boldsymbol{q}_\mathsf{v}\}$. The mass shell constraints impose conditions on the fields, imparting them with topological information associated to the particles. Note that the mass shell constraints are not first class with the Gauss constraint, so we shall need to do some additional work to obtain a first class constraint algebra. We discuss this in detail in the next section.

7.1.3 Boundary terms and conditions

In calculating the various Poisson brackets and variations of the fields in order to find a consistent Hamiltonian theory, one generally finds that boundary terms appear which must be properly dealt with in order to avoid an ill-defined variational principal and/or a second class constraint algebra. There are two ways in which such anomalous boundary terms can be dealt with: 1) add cancelation terms to the Hamiltonian; 2) place boundary conditions on the field variables and Lagrange multipliers which set the anomalous terms to zero. There is generally some freedom in this process. We shall make a particular choice and stick with this choice for the remainder of the chapter. We point the interested reader to similar calculations done for the case of a bounded region of 4d Lorentzian gravity in terms of the Ashtekar variables [89].

Preserving the variational principal

We begin by looking at the boundary terms and conditions necessary to preserve the variational principal. Variation of the Hamiltonian (7.20) results in a boundary term associated to each

[3] We borrow this name from [85, 88] although our constraints are written slightly differently.

particle:

$$\delta H|_{\mathcal{B}_\mathsf{v}} = \oint_{\mathcal{B}_\mathsf{v}} \left(\frac{\alpha_\mathsf{v}}{\sin(\frac{m_\mathsf{v}}{2})} \mathrm{Tr}\left(h_{\mathcal{B}_\mathsf{v},x} \boldsymbol{\tau}^i \right) + N(x)^i \right) \delta A(x)^i + \oint_{\mathcal{B}_\mathsf{v}} \lambda(x)^i \delta e(x)^i, \tag{7.21}$$

where $h_{\mathcal{B}_\mathsf{v},x}$ is the holonomy around the loop $\mathcal{B}_\mathsf{v}$ with base-point[4] at the point of integration x. The second term vanishes due to the condition (7.15), which also sets to zero the variation of the frame field in a direction tangent to the boundary. In order to eliminate the first term, we impose a condition at each particle boundary:

$$N(x)^i = -\frac{\alpha_\mathsf{v}}{\sin(\frac{m_\mathsf{v}}{2})} \mathrm{Tr}\left(h_{\mathcal{B}_\mathsf{v},x} \boldsymbol{\tau}^i \right), \qquad \forall x \in \mathcal{B}_\mathsf{v}. \tag{7.22}$$

Using the equation (A.17) we can write this as:

$$\boldsymbol{N}(x) = -\alpha_\mathsf{v} \boldsymbol{u}_{\mathsf{v},x}, \qquad \forall x \in \mathcal{B}_\mathsf{v}, \tag{7.23}$$

where $\boldsymbol{u}_x$ is the axis of rotation for $h_{\mathcal{B}_\mathsf{v},x}$. As we move around the boundary $\mathcal{B}_\mathsf{v}$, the vector $\boldsymbol{N}(x)$ will point in different directions although its magnitude $|\alpha_\mathsf{v}|^2$ remains constant. Recall that $N^i := e^i_0$ is the time component of the frame-field so that the choice of α_v has implications on the evolution of hypersurfaces. We shall make an appropriate choice once we have derived the equations of motion.

Obtaining a first class constraint algebra

Next we study the constraint algebra to determine which boundary conditions and/or additional boundary terms are required so that the constraints are first class. Since the mass shell constraints and the flatness constraint do not contain the frame-field, the following Poisson brackets vanish trivially without need for additional boundary conditions:

$$\{\psi_\mathsf{v}, \psi_v\} = \{\psi_\mathsf{v}, \mathcal{F}(\boldsymbol{N})\} = \left\{ \mathcal{F}(\boldsymbol{N}), \mathcal{F}(\tilde{\boldsymbol{N}}) \right\} = 0. \tag{7.24}$$

As mentioned above, the Gauss constraint has a non-trivial Poisson bracket with the mass-shell constraints:

$$\{\mathcal{G}(\lambda), \psi_\mathsf{v}\} = 2 \oint_{\mathcal{B}_\mathsf{v}} \mathrm{Tr}\left(g(x) \boldsymbol{u}_\mathsf{v}(x) g(x)^{-1} \tau^i \right) (\mathrm{d}_A \lambda(x)^i), \tag{7.25}$$

where $g(x) \in \mathrm{SU}(2)$ and $\boldsymbol{u}_\mathsf{v} \in \mathfrak{su}(2)$ is a unit vector which points in the direction of particle momentum. Details of this calculation are given in appendix A.3. In order to obtain a first class constraint algebra, we set the right hand side of the above equation to zero by imposing a condition at each particle boundary:

$$(\dot{\mathcal{B}}_\mathsf{v})^a (\partial_a \lambda^i + \epsilon^{ijk} A^j_a \lambda^k) = 0, \tag{7.26}$$

[4]Note that variation of a holonomy along a path γ splits the path into two, i.e. $\delta h_\gamma = h_{\gamma_1} \delta \boldsymbol{A} h_{\gamma_2}$ where γ_1 is the part of the path before the variation, and γ_2 is the part of the path after the variation.

where $(\dot{\mathcal{B}}_{\mathsf{v}})^a$ is the vector tangent to the boundary. This condition imposes that the covariant external derivative of the Lagrange multiplier $\boldsymbol{\lambda}$, in a direction tangent to the particle boundary, vanishes at each boundary. In other words, $\boldsymbol{\lambda}$ is covariantly constant around each boundary $\mathcal{B}_{\mathsf{v}}$.

There are still two more Poisson brackets to check. Using the condition (7.26) along with the flatness and Gauss constraints, we find as desired that:

$$\{\mathcal{F}(\boldsymbol{N}), \mathcal{G}(\boldsymbol{\lambda})\} = \left\{\mathcal{G}(\boldsymbol{\lambda}), \mathcal{G}(\tilde{\boldsymbol{\lambda}})\right\} = 0. \tag{7.27}$$

We can now summarize the results of our analysis. The full Hamiltonian with boundary terms is parameterized by the fields $(\boldsymbol{A}, \boldsymbol{e}) \in \mathcal{P}$ defined upon a sphere with punctures $\Sigma = S^2 \setminus \{\boldsymbol{q}_v\}$, and is given by:

$$H_f \;=\; \sum_{\mathsf{v}} \alpha_{\mathsf{v}} \psi_{\mathsf{v}} - \mathcal{F}(\boldsymbol{N}) - \mathcal{G}(\boldsymbol{\lambda}), \tag{7.28}$$

where we restate the constraints for convenience:

$$\psi_{\mathsf{v}} \;=\; 2\cos^{-1}\frac{W_{\mathsf{v}}}{2} - m_{\mathsf{v}}, \qquad \text{where} \qquad W_{\mathsf{v}} := \mathrm{Tr}\left(\overrightarrow{\exp}\oint_{B_{\mathsf{v}}} \boldsymbol{A}\right), \tag{7.29}$$

$$\mathcal{F}(\boldsymbol{N}) \;=\; \int_\Sigma N^i \left(\mathrm{d}A^i + \frac{1}{2}\epsilon^{ijk} A^j \wedge A^k\right), \tag{7.30}$$

$$\mathcal{G}(\boldsymbol{\lambda}) \;=\; \int_\Sigma \lambda^i \left(\mathrm{d}e^i + \epsilon^{ijk} A^j \wedge e^k\right). \tag{7.31}$$

The field variables $(\boldsymbol{A}, \boldsymbol{e})$ and Lagrange multipliers $\boldsymbol{N}$ and $\boldsymbol{\lambda}$ are subject to conditions at each particle boundary:

$$N(x)^i = -\alpha_{\mathsf{v}} \boldsymbol{u}_{\mathsf{v},x} \tag{7.32}$$

$$\dot{\mathcal{B}}_{\mathsf{v}}(x)^a (\partial_a \lambda(x)^i + \epsilon^{ijk} A(x)^j_a \lambda(x)^k) = 0, \tag{7.33}$$

$$\dot{\mathcal{B}}_{\mathsf{v}}(x)^a e(x)^i_a = 0, \tag{7.34}$$

for all points around the boundary $x \in \mathcal{B}_{\mathsf{v}}$. With the boundary terms and these conditions, the variational principal is well defined and the constraint algebra is first class. Having established a consistent Hamiltonian, we move on to the next task: fixing a gauge for the field variables.

7.2 Gauge fixing

In this section we choose a gauge for the field variables, i.e. we specify a pair of fields $(\bar{\boldsymbol{A}}, \bar{\boldsymbol{e}})$ such that $\boldsymbol{F}(x) = \boldsymbol{G}(x) = 0$ for all $x \in \Sigma$. Note that this is a gauge fixing in the usual sense, since both of these constraints are derived from the action, and the physical behaviour of the theory is independent of this choice. In developing spinning geometries for the 4d theory, we also applied a gauge choice of a representative three-geometry, selected amoung an equivalence class of geometries related by a constraints $\boldsymbol{F} = 0$. But in this case the flatness constraint was not derived from the action, and the dynamics of theory is affected by this choice.

In choosing a guage, we will eliminate the kinematical constraints from the Hamiltonian leaving only the mass shell constraints. These remaining constraints are the generators of dynamics. The gauge is fixed by defining Σ as a two-dimensional cellular space such that the particles reside at vertices of the zero-skeleton. This will allow us to give a piecewise definition of the field variables within each cell, which can be glued together in a continuous manner.

Consider a two-dimensional cellular space $\Sigma \cong S^2 \setminus \{\boldsymbol{q}_{\mathsf{v}}\}$ as defined in Section (4.3.1), which we take to be the spatial hypersurface corresponding to a level value of the time parameter t. Each two-cell c is taken to be a triangle equipped with a coordinate function $\boldsymbol{z}_c$. Generally in d-dimensions, one cannot assume the $d-1$ cells to be flat, but $d=2$ is a special case where the flatness of space between vertices permits the use of straight edges and linear gluing maps between cells. The boundary ∂c is composed of three vertices v_c and three straight edges e^c which connect the vertices. The number of cells is fixed by the number of particles $|\mathsf{v}_\Delta|$ to be $2(V-2)$ via the Euler characteristic for polyhedra. There is ambiguity in the choice of triangulation, since there are different ways of connecting a set of vertices with edges. Since the number of triangles is fixed, the different choices are related by bistellar flips[5] Different triangulations generally lead to different configurations of the field variables, i.e. different gauge choices.

Recall that on each particle boundary $\mathcal{B}_{\mathsf{v}}$, the component of the frame-field tangent to $\mathcal{B}_{\mathsf{v}}$ must vanish (7.15). This translates into a boundary condition on $\boldsymbol{z}_c$:

$$\dot{\mathcal{B}}_{\mathsf{v}}(x)^a \partial_a \boldsymbol{z}_c(x) = 0 \qquad \forall x \in \mathcal{B}_{\mathsf{v}} \cap c. \tag{7.35}$$

We require the functions $\boldsymbol{z}_c$ to be single valued in c so that the metric is non-degenerate, except at the particle boundaries, where this condition is telling us that $\boldsymbol{z}_c$ must be constant on the boundary $\mathcal{B}_{\mathsf{v}}$. This means that the functions $\boldsymbol{z}_c$ can serve as local coordinates within each triangle since each point receives a unique value. Degeneracy at $\mathcal{B}_{\mathsf{v}}$ means that the vertex v_c receives a single coordinate value $\boldsymbol{z}_c(\mathsf{v}_c)$ within a cell even though the boundary is smeared.

The gluing maps between cells are such that vertices are identified:

$$\mathsf{v}_{c'} = s_{cc'}(\mathsf{v}_c). \tag{7.36}$$

This implies that the point $\boldsymbol{q}_{\mathsf{v}} \in \Sigma$ is given a different coordinate $\boldsymbol{z}_c(\mathsf{v}_c)$ depending upon which frame c one uses to describe it, as is to be expected in a general relativistic theory. The maps along edges are linear, taking the interior of the edge $\mathsf{e}_{cc'} \in \partial c$ between cells c and c' to the interior of the corresponding edge $\mathsf{e}_{c'c} \in \partial c'$:

$$x' = s_{cc'}(x), \qquad \forall\, x \in \mathsf{e}_{cc'}, \quad x' \in \mathsf{e}_{c'c}. \tag{7.37}$$

Within each triangle c, we must find $(\bar{\boldsymbol{A}}_c(x), \bar{\boldsymbol{e}}_c(x))$ such that $\boldsymbol{F}(x) = \boldsymbol{G}(x) = 0$ for all $x \in c$. The general solution is given by a pair of functions, a 'rotation' function $a_c(x) \in \mathrm{SU}(2)$ and 'coordinate' function $\boldsymbol{z}_c(x) \in \mathfrak{su}(2)$:

$$\bar{\boldsymbol{A}}_c = a_c \mathrm{d} a_c^{-1}, \qquad \bar{\boldsymbol{e}}_c = a_c \left(\mathrm{d}\boldsymbol{z}_c\right) a_c^{-1}, \tag{7.38}$$

[5]Bistellar flips change two triangles into a new pair with a different adjacency relationship.

where the subscript c denotes a field restricted to the cell c. We use a piecewise definition to give the fields over all of Σ: $\boldsymbol{A}(x) \equiv \cup_c \boldsymbol{A}_c$ and $\boldsymbol{e}(x) \equiv \cup_c \boldsymbol{e}_c(x)$ for all $c \in \Sigma$. The continuity of these piecewise fields must be defined by a limiting procedure, where one ensures that the value of $(\bar{\boldsymbol{A}}_c, \bar{\boldsymbol{e}}_c)$ agrees with the value of $(\bar{\boldsymbol{A}}_{c'}, \bar{\boldsymbol{e}}_{c'})$ as one approaches the edge $\mathsf{e}_{cc'}$ from either side. This condition is satisfied so long as there exists a constant gluing element $h_{cc'} \in \mathrm{SU}(2)$ associated to the edge such that:

$$\lim_{x' \to \mathsf{e}_{c'c}} a_{c'}(x') = \lim_{x \to \mathsf{e}_{cc'}} a_c(x) h_{cc'}, \qquad \lim_{x' \to \mathsf{e}_{c'c}} \mathrm{d}a_{c'}(x') = \lim_{x \to \mathsf{e}_{cc'}} \mathrm{d}a_c(x) h_{cc'}, \quad (7.39)$$

$$\lim_{x' \to \mathsf{e}_{c'c}} \boldsymbol{z}_{c'}(x') = \lim_{x \to \mathsf{e}_{cc'}} h_{cc'}^{-1} \left(\boldsymbol{z}_c(x) + \boldsymbol{b}_{cc'} \right) h_{cc'}, \quad \lim_{x' \to \mathsf{e}_{c'c}} \mathrm{d}\boldsymbol{z}_{c'}(x') = \lim_{x \to \mathsf{e}_{cc'}} h_{cc'}^{-1} \mathrm{d}\boldsymbol{z}_c(x) h_{cc'}, \quad (7.40)$$

where the constant $\boldsymbol{b}_{cc'} \in \mathfrak{su}(2)$ is a translation. Notice the first equation gives an expression for the constant gluing elements $h_{cc'} = a_c(x)^{-1} a_{c'}(x)$ which is constant for all $x \in \mathsf{e}_{cc'}$.

7.2.1 Preliminary definitions

In order to define suitable $(a_c, \boldsymbol{z}_c)$ functions capable of parameterizing fields $(\bar{\boldsymbol{A}}, \bar{\boldsymbol{e}})$ in the presence of conical singularities, we subdivide each triangle into three *regions* defined by edges joining the centroid n_c to the vertices v_c as shown in fig. 7.1. Consider one such triangular region r that has v_c, v'_c, and the centroid n_c in its boundary. We drop the subscript c for the moment since we are now going to look at this single region. We assign a pair of cartesian coordinates (x, y) to the region and place the origin at the midpoint of the edge $\mathsf{e}_{\mathsf{v}\mathsf{v}'}$ between vertices v and v'. In these coordinates, the centroid is at some $\mathsf{n} = (x_\mathsf{n}, y_\mathsf{n})$, and the vertices are at $(0, \pm\frac{L}{2})$ where $L := 2y_\mathsf{v} = -2y_{\mathsf{v}'}$ is the coordinate length of $\mathsf{e}_{\mathsf{v}\mathsf{v}'}$. See fig. (7.1) for an illustration.

Now, we define a function:

$$\theta(x, y) = \tanh\left(\tanh^{-1}(\theta^+) + \tanh^{-1}(\theta^-) \right), \qquad \theta^\pm = \frac{x}{x_\mathsf{n}} \pm 2\left(\frac{y}{L} - \frac{x y_\mathsf{n}}{x_\mathsf{n} L} \right). \quad (7.41)$$

Over the range of values $\theta = [0, 1]$, lines of constant θ provide a family of curves connecting the endpoints of the edge. The line of $\theta = 0$ is the edge contained in r, and the line $\theta = 1$ connects the vertices with the centroid.

Let us recall the vector notation we can use for elements of $\mathfrak{su}(2)$. We denote in bold letters an element $\boldsymbol{A} \in \mathfrak{su}(2)$, which can be identified with a vector in $\mathbb{R}^3$ through $A^i = -2\mathrm{Tr}(\boldsymbol{A}\boldsymbol{\tau}^i)$, where $\boldsymbol{\tau}^i$ is an $\mathfrak{su}(2)$ basis given by $-i/2$ times the Pauli matrices. This basis satisfies the algebra $[\tau_i, \tau_j] = \epsilon_{ijk}\tau^k$. We will use also the vector notation of a dot-product for a trace $\boldsymbol{A} \cdot \boldsymbol{B} \equiv -2\mathrm{Tr}(\boldsymbol{A}\boldsymbol{B})$, and a cross-product for an $\mathfrak{su}(2)$ commutator $\boldsymbol{A} \times \boldsymbol{B} \equiv [\boldsymbol{A}, \boldsymbol{B}]$. A magnitude is denoted by dropping the bold font $A \equiv |\boldsymbol{A}|$, and a unit vector is denoted by a hat $\hat{\boldsymbol{A}} \equiv \boldsymbol{A}/A$.

From the function $\theta(x, y)$, one can define a function $\rho(x, y)$ within r such that lines of constant ρ are orthogonal to lines of constant θ. The unit vectors which point along these lines are:

$$\widehat{\boldsymbol{\theta}} = \frac{1}{\sqrt{U^2 + V^2}} \left(U\boldsymbol{\tau}^1 + V\boldsymbol{\tau}^2 \right), \qquad \widehat{\boldsymbol{\rho}} = \frac{1}{\sqrt{U^2 + V^2}} \left(-V\boldsymbol{\tau}^1 + U\boldsymbol{\tau}^2 \right), \quad (7.42)$$

where $\boldsymbol{\tau}^1, \boldsymbol{\tau}^2 \in \mathfrak{su}(2)$ represent orthogonal ($\mathrm{Tr}(\boldsymbol{\tau}^1\boldsymbol{\tau}^2) = 0$) unit vectors corresponding to the x, y coordinates of the region, and we have defined the functions:

$$U := x^2\left(y_{\mathsf{n}}^2 - \left(\frac{L}{2}\right)^2\right) - x_{\mathsf{n}}^2\left(y^2 - \left(\frac{L}{2}\right)^2\right), \qquad V := 2xx_{\mathsf{n}}(x_{\mathsf{n}}y - y_{\mathsf{n}}x). \tag{7.43}$$

See fig. 7.1 for an illustration. The function ρ is a solution to:

$$U\partial_x\rho + V\partial_y\rho = 0. \tag{7.44}$$

In general the solution to this equation must be found numerically, however, when the centroid is positioned on the x-axis so that $y_{\mathsf{n}} = 0$, we can find an analytical solution:

$$\rho = C_1 y^{\frac{L^2}{4x_{\mathsf{n}}^2}}\left((x - x_{\mathsf{n}})(x + x_{\mathsf{n}}) + \frac{4x_{\mathsf{n}}^2y^2}{8x_{\mathsf{n}}^2 + L^2}\right) + C_2, \tag{7.45}$$

where C_1, C_2 are arbitrary constants. In the general case, we note that the line of constant $\rho = \rho_{\mathsf{n}}$ connecting the midpoint of the edge with the centroid is always straight in terms of (x, y). We shall denote as ρ_{v} the value of ρ along the particle boundary where $\mathcal{B}_{\mathsf{v}} \bigcap \mathsf{r}$.

Recall that particle boundaries are smeared in a polar coordinate system (r, ϕ) by not identifying points with different ϕ-values in the limit $r \to 0$, except for the identification $\phi = \phi + 2\pi$. In terms of (ρ, θ) coordinates, the smearing implies that we do not identify points with different θ-values when $\rho = \rho_{\mathsf{v}}$.

We are now ready to define the fields $(a_{\mathsf{r}}, \boldsymbol{z}_{\mathsf{r}})$ in the region. In the following we should include r subscripts on the functions (θ, ρ) as well, but this leads to a cumbersome notation so we shall not include these subscripts when the relevant region is apparent from the context. We define the group-valued field in a region as:

$$a_{\mathsf{r}}(x) = a_{\mathsf{r}}(\theta) = \exp\left(-\boldsymbol{P}_{\mathsf{r}}\int_1^\theta f(\tilde{\theta})\mathrm{d}\tilde{\theta}\right), \tag{7.46}$$

where we have introduced a bump function $f(\theta)$ which satisfies $\int_0^1 f(\theta)\mathrm{d}\theta = 1$ and goes to zero smoothly as $\theta \to 0$ and as $\theta \to 1$. An example of such a bump function is:

$$f(\theta) = \begin{cases} Ce^{\frac{1}{(2\theta-1)^2-1}}, & 0 \le \theta \le 1 \\ 0, & \text{otherwise} \end{cases}, \tag{7.47}$$

where $C^{-1} = \int_0^1 e^{\frac{1}{(2\theta-1)^2-1}}\mathrm{d}\theta$, although any function which satisfies these properties will suffice.

When $\theta_{\mathsf{r}} = 0$, the group function a_{r} defines a rotation about a direction $-\boldsymbol{P}_{\mathsf{r}}/|P_{\mathsf{r}}|$ by an angle of $|P_{\mathsf{r}}|$. Because the bump function goes to zero smoothly as $\theta \to 0$, we have that $a_{\mathsf{r}}(x) \to e^{-\boldsymbol{P}_{\mathsf{r}}}$ and $\mathrm{d}a_{\mathsf{r}}(x) \to 0$ smoothly as one approaches the edge associated to r. Since the definition (7.46) depends only on θ_{r}, we have that $a_{\mathsf{r}}(x) = a_{\mathsf{r}}(x')$ whenever x and x' are both on the same line of constant θ_{r}, and in particular a_{r} is constant along the edge where $\theta = 0$.

Consider two neighbouring triangles c and c', and let us label the regions of these triangles which include the shared edge $\mathsf{e}_{cc'}$ as r and r' respectively. Since a_{r} and $a_{\mathsf{r}'}$ are each constant along $\mathsf{e}_{cc'}$, the gluing conditions (7.39) are satisfied by a constant group element $h_{cc'}$, as required.

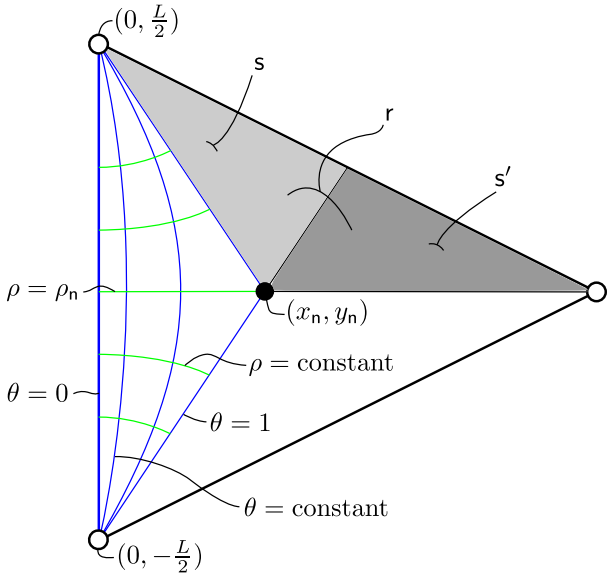

Figure 7.1: A single triangle split into three regions by lines from the vertices (open circles) to the centroid (filled black circle). The (θ, ρ) coordinates are shown within one of the regions, with lines of constant θ shown in blue, and lines of constant ρ in green. The line $\theta = 0$ runs between the two vertices at $(0, \pm\frac{L}{2})$, and the line $\theta = 1$ connects the centroid at $(x_{\mathsf{n}}, y_{\mathsf{n}})$ to both of these vertices. A straight line $\rho = \rho_{\mathsf{n}}$ connects the midpoint of the edge to the centroid. In another region, the line from the midpoint of the edge to the centroid is shown splitting the region $\mathsf{r} = \mathsf{s} \cup \mathsf{s}'$ into two sections, with each section shown in a different shade of grey.

Now, the three regions $\mathsf{r}_1, \mathsf{r}_2, \mathsf{r}_3$ of c intersect along portions of their boundaries $\theta_r = 1$ for all $\mathsf{r} \in c$, i.e. the intersection $\mathsf{r}_1 \bigcap \mathsf{r}_2 \bigcap \mathsf{r}_2$ is formed by lines joining the centroid with the three vertices of the triangle c. Since a bump function goes smoothly to zero as $\theta \to 1$, we have each $a_{\mathsf{r}}(x) \to \mathbb{1}$ smoothly as one approaches this intersection for all $\mathsf{r} \in c$. This property ensures that within all of c, the function $a_c = \bigcup_{\mathsf{r}} a_{\mathsf{r}}$ is smooth. Using (7.46) the connection in a region is found to be:

$$\bar{\boldsymbol{A}}_{\mathsf{r}} = -\boldsymbol{P}_{\mathsf{r}} f(\theta) \mathrm{d}\theta. \tag{7.48}$$

We give a piecewise definition of the connection within the cell $\boldsymbol{A}_c = \cup_{\mathsf{r} \in c} A_{\mathsf{r}}$, which is smooth due to the properties of the bump function.

The group valued fields can be written as a holonomy from some point $x \in \mathsf{r}$ to any point on the line $\theta_{\mathsf{r}} = 1$, i.e.:

$$a_{\mathsf{r}}(x) = \overrightarrow{\exp} \int_x^{\theta=1} \bar{\boldsymbol{A}}, \tag{7.49}$$

where the choice of path does not matter since the connection is flat. The gluing elements h_{e} can now be seen as holonomies written in terms of the connection $\bar{\boldsymbol{A}}$ defined piecewise in each

region. Using (7.46) and (7.48), the holonomy associated to the edge $\mathsf{e}_{cc'}$ can be written as:

$$h_{cc'} = h_{c'c}^{-1} = a_{\mathsf{r}}^{-1}(0)a_{\mathsf{r}'}(0), \tag{7.50}$$

where $h_{cc'}$ is the parallel transport from any point on the line $\theta_{\mathsf{r}} = 1$ on the boundary of $\mathsf{r} \in c$ to any point on the line $\theta_{\mathsf{r}'} = 1$ on the boundary of $\mathsf{r}' \in c'$. Since each holonomy possesses an orientation, we label the parallel transport along a reverse path as $h_{c'c}$.

Let us now work toward a definition of the coordinate functions. In order to satisfy the condition (7.15), we make a further subdivision of the triangle by splitting each region into two *sections* divided by the $\rho = \rho_{\mathsf{n}}$ line which joins the centroid n to the midpoint of the edge e, as shown in fig. (7.1. We label these sections $\mathsf{s} \ni \mathsf{v}$ and $\mathsf{s}' \ni \mathsf{v}'$ according to which vertex is contained within the section. In each section we define:

$$\boldsymbol{z}_{\mathsf{s}} = (x - x_{\mathsf{v}})\hat{\boldsymbol{x}} + (y - y_{\mathsf{v}})\hat{\boldsymbol{y}}, \qquad \hat{\boldsymbol{x}} \equiv a_{\mathsf{r}}\boldsymbol{\tau}^1 a_{\mathsf{r}}^{-1}, \qquad \hat{\boldsymbol{y}} \equiv a_{\mathsf{r}}\boldsymbol{\tau}^1 a_{\mathsf{r}}^{-1}. \tag{7.51}$$

This places the origin at the particle position, and causes the function to vanish everywhere on the smeared boundary $\mathcal{B}_v \cap \mathsf{s}$, which also sets the derivative tangential to the boundary to zero as required by (7.15). One can check that this definition satisfies the gluing rules (7.40), and maps to itself under the composition of maps going around the vertex, as discussed in section 5.2. Notice the same pair of basis vectors $(\hat{\boldsymbol{x}}, \hat{\boldsymbol{y}})$ span each section of the region, and that they rotate as one approaches the edge giving each region a curved geometry. Never-the-less, since our definitions of (a_{r}) and $\boldsymbol{z}_{\mathsf{s}}$ satisfy (7.38) the resulting connection is flat and the frame-field is torsion-free.

Defining $\boldsymbol{z}_{\mathsf{r}} = \bigcup_{\mathsf{s}\in\mathsf{r}} \boldsymbol{z}_{\mathsf{s}}$, the frame-field for $x \in \mathsf{r}$ is given by $\boldsymbol{e}_{\mathsf{r}}(x) = a_{\mathsf{r}}^{-1}\mathrm{d}z_{\mathsf{r}}a_{\mathsf{r}}$. We need to make sure that the frame-field $\boldsymbol{e}_c$ is continuous within each triangle. Our definition (7.51) yields a smooth frame-field within each of the six sections in c, but we need to check what happens at the intersections between sections. Notice that both sections share the same (x, y) coordinates, and a single a_{r} function is defined across both sections. Between the two sections of a region, the definition (7.51) introduces a translation:

$$\lim_{\rho\to\rho_{\mathsf{n}}^-} \boldsymbol{z}_{\mathsf{s}'}(x, y) = \lim_{\rho\to\rho_{\mathsf{n}}^+} \left(\boldsymbol{z}_{\mathsf{s}}(x, y) + \boldsymbol{b}_{\mathsf{ss}'} L\hat{\boldsymbol{y}}\right), \tag{7.52}$$

where $\boldsymbol{b}_{\mathsf{ss}'} = \boldsymbol{z}_{\mathsf{s}}(\mathsf{v}) - \boldsymbol{z}_{\mathsf{s}}(\mathsf{v}') = L\hat{\boldsymbol{y}}$ is given the edge vecto, and the limits $\rho \to \rho_{\mathsf{n}}^{\pm}$ imply that the point x approaches the intersection at $\rho = \rho_{\mathsf{n}}$ from the relevant section s or s'. The frame-field however will be smooth at the intersection $\mathsf{s} \cap \mathsf{s}'$ so long as all of the derivatives of $\boldsymbol{z}_{\mathsf{s}'}$ agree $\boldsymbol{z}_{\mathsf{s}}$ in the limit given above. Since the function a_{r} is smooth over the region, it follows that the derivatives do agree, and we have a smooth frame-field throughout the region r. The nice properties of the bump functions used to define the a_{r} fields also ensure that the frame-field is continuous at the centroid of the triangle where the three regions intersect. In the case that $a_c(x) = \mathbb{1}$ for all $x \in c$, the connection vanishes everywhere within the cell and we regain the geometry of flat triangle. In this sense, our definition is a generalization of the flat case, giving a 'covariant triangle' for some choice of a_c. These covariant triangles $(a_c(x), \boldsymbol{z}_c(x))$ are the building blocks of the geometry $(\bar{\boldsymbol{A}}(x), \bar{\boldsymbol{e}}(x))$ for all $x \in \Sigma$.

With our definition of the coordinate functions, we can now look more closely at the gluing maps $s_{cc'}$ between cells. Consider two regions r and r' which belong to different cells c and c'.

Let us take each region to have its own cartesian coordinate system (x, y) and (x', y') adapted to the edge as done above. On the edge $\mathsf{e}_{cc'}$ we have $x = x' = 0$, and find the map:

$$s_{cc'} : (0, y) \to (0, y') = (0, y). \tag{7.53}$$

Looking at the gluing map for coordinate functions:

$$\lim_{x' \to \mathsf{e}_{c'c}} \boldsymbol{z}_{c'}(x', y') = \lim_{x \to \mathsf{e}_{cc'}} h_{cc'}^{-1} \left(\boldsymbol{z}_c(x, y) + \boldsymbol{b}_{cc'} \right) h_{cc'}, \tag{7.54}$$

where $(x', y') = s_{cc'}(x, y)$. With our definition (7.51), we have that $\boldsymbol{b}_{cc'} = 0$ so that there are no translations associated to edges, only rotations. These rotations relate the bases of the cells on either side of the edge:

$$\hat{\boldsymbol{x}}_{c'}(x') = h_{cc'}^{-1} \hat{\boldsymbol{x}}_c(x) h_{cc'}, \qquad \hat{\boldsymbol{y}}_{c'}(x') = h_{cc'}^{-1} \hat{\boldsymbol{y}}_c(x) h_{cc'}, \qquad x \in \mathsf{e}_{cc'} \tag{7.55}$$

We have a cellular space Σ defined as a collection of triangles in $\mathbb{R}^2$, connected by gluing rules $s_{cc'}$ which identify the edges of neighbouring cells. The resulting topology is that of a sphere with punctures. On top of this space, we have defined coordinate functions $\boldsymbol{z}_c$ and rotation functions a_c which yield a continuous geometry, where by 'geometry' we mean a connection and frame-field $(\bar{\boldsymbol{A}}, \bar{\boldsymbol{e}}) \in \Sigma$. It is important to distinguish between topology and geometry; our choice of triangulation and fields $(\bar{\boldsymbol{A}}, \bar{\boldsymbol{e}})$ is a single member of a class of topologically equivalent geometries. The fields $(a_c, \boldsymbol{z}_c)$ defined upon each cell are glued together along edges by SU(2) rotations, here being the analog of Lorentz transformations. This geometry bears some resemblance to the picture presented by Deser, Jackiw and 't Hooft [83], where they study a system of spinless point particles in $\mathbb{R} \times \mathbb{R}^2$.The spatial geometry is a flat plane, with the deficit angles associated to particle masses being accounted for by a single wedge or 'tail' for each particle. Each particle lies at the vertex of a wedge running to infinity, and the sides of each wedge are identified. With the sides identified, the wedges appear as one-dimensional defects (tails) along an edge that spans a half-line to infinity. This leads to conditions for matching points on either side of the tail, which in the article are calculated for a single particle, and a pair where one particle moves relative to the other with the tails on top of each other. In our description, the gluing conditions on $(a_c, \boldsymbol{z}_c)$ are the analog of these matching conditions.

In order to check that our theory reproduces the matching conditions, we can consider certain choices of holonomies $h_{cc'}$ to create the scenarios relevant for these equations. Although the tails defined in [83] extend to infinity, the edges of our triangulation mimic these in the neighbourhood of the particles in question. For instance, the tail stemming from a single particle at rest looks in our case like a vertex v that has a non-trivial holonomy $h_{cc'} = e^{m_{\mathsf{v}} \boldsymbol{\tau}^0}$ on only one edge $\mathsf{e}_{cc'} \ni \mathsf{v}$:

$$\boldsymbol{z}^{c'}(s_{cc'}(x)) = e^{-m_{\mathsf{v}} \boldsymbol{\tau}^0} \boldsymbol{z}^c(x) e^{m_{\mathsf{v}} \boldsymbol{\tau}^t}, \tag{7.56}$$

which is the SU(2) equivalent of the rotation in equation (5.1) of [83]. For the case of one particle moving relative to another, with one tail on top of the other, we consider that the edge e_{12} joins particles v and v' as in fig. 7.2, where the holonomy $h_{12} = e^{m_{\mathsf{v}} \boldsymbol{\tau}_{\mathsf{r}}^t}$ is a Lorentz rotation and $h_{34} = e^{\boldsymbol{p}_{\mathsf{v}'}} e^{m_{\mathsf{v}} \boldsymbol{\tau}_{\mathsf{r}}^t}$ is a Lorentz rotation and boost defined by some $\boldsymbol{p}_{\mathsf{v}'} \in \mathfrak{su}2$. We take all

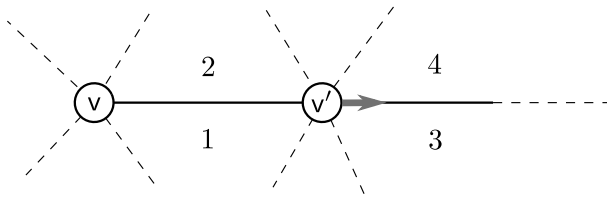

Figure 7.2: Triangulation in the neighbourhood of two vertices v and v' with holonomies chosen appropriately for the matching conditions of [83] to be applied. The holonomies are $h_{12} = e^{m_{\mathsf{v}}\boldsymbol{\tau}_{\mathsf{r}}^t}$ and $h_{34} = e^{\boldsymbol{p}_{\mathsf{v}'}} e^{m_{\mathsf{v}}\boldsymbol{\tau}_{\mathsf{r}}^t}$, while all others are set to the identity. The particle v' moves to the right along the edge e_{34}.

other holonomies on edges connected to these particles to be trivial for this setup. In this case the coordinate functions associated to the cells satisfy $\boldsymbol{z}_4 = \boldsymbol{z}_2 - \boldsymbol{X}_{21}$ and $\boldsymbol{z}_3 = \boldsymbol{z}_1 - \boldsymbol{X}_{12}$, where the translations are given by $\boldsymbol{X}_{12} = \boldsymbol{z}_1(\mathsf{v}') - \boldsymbol{z}_1(\mathsf{v})$ and $\boldsymbol{X}_{21} = \boldsymbol{z}_2(\mathsf{v}') - \boldsymbol{z}_2(\mathsf{v}) = h_{12}^{-1}\boldsymbol{X}_{12}h_{12}$. We can now check our matching condition. At some point $x \in \mathsf{e}_{34}$ which is mapped to $x' \in \mathsf{e}_{43}$ we have the gluing relation:

$$\begin{aligned}
\boldsymbol{z}_4(x') &= h_{34}^{-1}\boldsymbol{z}_3(x)h_{34} \\
\boldsymbol{z}_2(x') - \boldsymbol{X}_{21} &= h_{34}^{-1}(\boldsymbol{z}_1(x) - \boldsymbol{X}_{12})h_{34} \\
\boldsymbol{z}_2(x') &= h_{12}^{-1}\boldsymbol{X}_{12}h_{12} + h_{34}^{-1}(\boldsymbol{z}_1(x) - \boldsymbol{X}_{12})h_{34} \\
\boldsymbol{z}_2(x') &= e^{-m_{\mathsf{v}}\boldsymbol{\tau}_{\mathsf{r}}^t}(\boldsymbol{X}_{12} + e^{-\boldsymbol{p}_{\mathsf{v}'}}(\boldsymbol{z}_1(x) - \boldsymbol{X}_{12})e^{\boldsymbol{p}_{\mathsf{v}'}})e^{m_{\mathsf{v}}\boldsymbol{\tau}_{\mathsf{r}}^t}. \qquad (7.57)
\end{aligned}$$

This is the analog of equation (5.8) in [83], so we see that our model agrees with the description given by Deser, Jackiw and 't Hooft.

We have defined coordinate functions $\boldsymbol{z}_{\mathsf{s}}$ in each section of each cell, and used a piecewise definition to define the function $\boldsymbol{z}_c = \cup_{\mathsf{s}\in c}\boldsymbol{z}_{\mathsf{s}}$ for each cell. This paints the geometry as a collection of 'covariant' triangles (with rotating bases), that are glued together along edges by the holonomies $h_{cc'}$ according to (7.40). However, we also introduced gluing maps between the $\boldsymbol{z}_{\mathsf{s}}$ within each cell (7.52), along the $\rho = \rho_{\mathsf{n}}$ lines connecting the centroid to the midpoints of the edge. These maps introduce a translation $\boldsymbol{b}_{\mathsf{ss}'}$ between the functions $\boldsymbol{z}_{\mathsf{s}}$ for $\mathsf{s} \in c$, which presents an alternative way to picture the geometry. We can define a 'cone' $\mathsf{o}_{\mathsf{v}} = \cup_{\mathsf{s}\ni\mathsf{v}}\mathsf{s}$ as the collection of sections intersecting at a vertex, where each o_{v} is homeomorphic to an actual cone. With this we can define a piecewise $\boldsymbol{z}_{\mathsf{v}} = \cup_{\mathsf{s}\in c}\boldsymbol{z}_{\mathsf{s}}$ defined over the cone associated to each particle. In this light, the geometry is cast as a collection of cones which are glued together by translations. This is similar to the geometry defined in [90] which assigns a polar coordinate system locally around each particle with transition maps between them. See fig. (7.3) for an illustration of the geometry in terms of triangles as compared to the picture given by the cones.

The interpretations discussed above are about the geometry of the cellular space Σ that is given by the coordinate functions $\boldsymbol{z}_c$ and h_{e}, but there is another layer on top of this to consider. The phase space is defined by a connection and frame-field, and our gauge choice for these fields is given in terms of a_c and $\boldsymbol{z}_c$. With these definitions, we have continuous fields $(\bar{\boldsymbol{e}}_c(x), \bar{\boldsymbol{A}}_c(x)$ for $x \in c$, and the gluing conditions (5.3) extend the continuity throughout Σ.

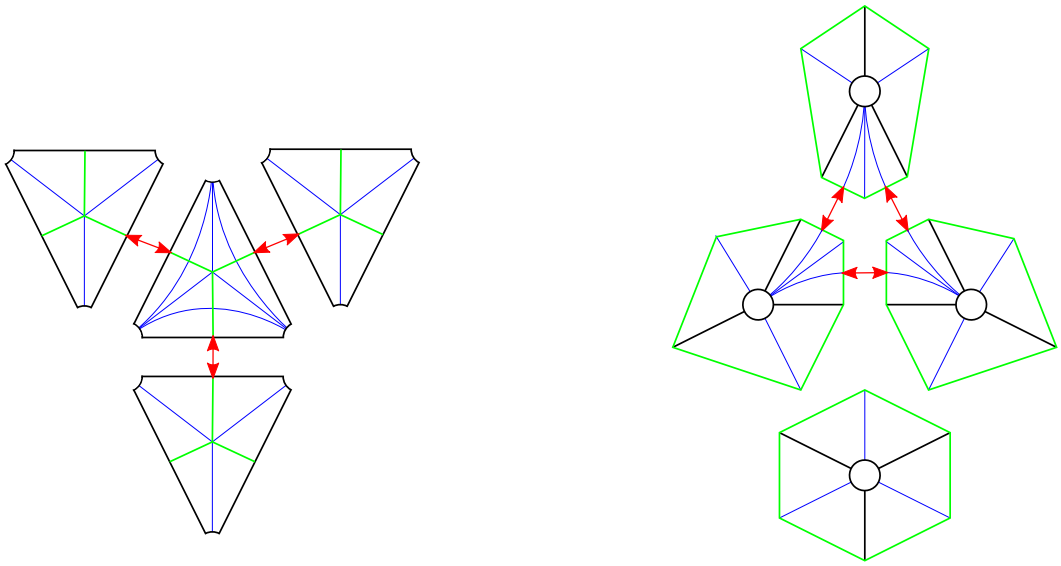

(a) Triangles $\boldsymbol{z}_c$ (b) Cones $\boldsymbol{z}_{\mathsf{v}}$

Figure 7.3: Two ways of viewing the geometry of Σ, in this case for 4 particles. Although each cell c is a flat triangle, the coordinate functions on top of these describe a different geometry, and this is the picture seen by the metric. One can view the geometry as composed of triangles using $\boldsymbol{z}_c$, or as cones using $\boldsymbol{z}_{\mathsf{v}}$. Edges are in black, some of the gluing relations are denoted by red arrows, and lines of constant θ are drawn in blue with lines of constant ρ in green. Note that the particle boundaries are shown with non-vanishing radii for illustrative purposes, but the metric sees these as points due to the boundary condition (7.35) on the coordinate functions.

These fields satisfy the flatness and Gauss constraints for all $x \in \Sigma$, and describe a geometry with a non-zero connection within cells.

We have given the definitions for describing a gauge choice of fields $(\bar{\boldsymbol{A}}, \bar{\boldsymbol{e}})$, but we have yet to implement this choice in the Hamiltonian formalism. In the next section, we apply a gauge-fixing procedure to concretely select this choice of field variables using the procedure of Dirac.

7.2.2 Dirac's gauge fixing procedure

We now employ the formalism of Dirac [19] to implement the choice of gauge within the phase space $(\boldsymbol{A}, \boldsymbol{e}) \in \mathcal{P}$. We have 6×2 degrees of freedom per point to be fixed in the variables (A_a^i, e_a^i), while each of the constraints, F^i and G^i, can be used to fix 3×2 degrees of freedom per point. We shall do this in two steps, first eliminating the Gauss constraint then the flatness constraint.

The first condition is:

$$\boldsymbol{\mathcal{C}}_1 := \boldsymbol{A}_\theta - a\partial_\theta a^{-1}. \tag{7.58}$$

This constraint is applied within each region $\mathsf{r} \in \Sigma$. A good gauge fixing condition must be second class with at least one of the constraints, and this condition is second class with the Gauss constraint. The Poisson bracket is:

$$\left\{(\mathcal{C}_1)^i, \int_\Sigma \lambda^j G^j\right\} = -\delta^{ij}\left(\partial_\theta \lambda^j + \epsilon^{jkl} A^k_\theta \lambda^l\right), \tag{7.59}$$

where we do not sum over the repeated index j so that the right hand side is a 3×3 diagonal matrix giving the Poisson brackets between each component of the gauge condition with each component of the Gauss constraint.

The condition must be preserved dynamically, which means the evolution equation provided by the Poisson bracket with the hamiltonian H_f must vanish. Calculating this we obtain:

$$\{\boldsymbol{\mathcal{C}}_1, H_f\} = \partial_\theta \boldsymbol{\lambda} + [\boldsymbol{A}_\theta, \boldsymbol{\lambda}] = 0. \tag{7.60}$$

Setting the right hand side to zero provides a condition on $\boldsymbol{\lambda}$.

Following the gauge fixing procedure, we now define Dirac brackets. In general, the Dirac bracket for two functions f and g of the phase space variables is defined as:

$$\{f, g\}_D := \{f, g\} - \{f, \Phi_m\}\,(M^{-1})^{mn}\,\{\Phi_\mathsf{n}, g\}, \tag{7.61}$$

where Φ_m are the constraints, and the antisymmetric matrix M is defined as:

$$M_{mn} := \{\Phi_m, \Phi_\mathsf{n}\}. \tag{7.62}$$

Notice that the invertibility of this matrix depends upon the set of constraints Φ_m being second class with each other.

We can set the Gauss constraint and the gauge condition $\boldsymbol{\mathcal{C}}_1$ *strongly* to zero, so long as we use Dirac brackets instead of Poisson brackets. In doing so, the gauge-fixed variable $\boldsymbol{A}_\theta$ and its complex conjugate $\boldsymbol{e}_\rho$ become non-dynamical, and we can eliminate them from the Hamiltonian since they are now fixed in terms of $\boldsymbol{z}$, a and the remaining field variables $\boldsymbol{A}_\rho, \boldsymbol{e}_\theta$ through the Gauss constraint and the gauge condition. The matrix M is easily inverted, and one can check that for the remaining phase space variables, the Dirac brackets (7.61) are equivalent to Poisson brackets.

We have now partially fixed our gauge and can continue using Poisson brackets in our analysis. The Gauss constraint has been eliminated and the Hamiltonian is given by:

$$H_{pf} = \sum_\mathsf{v} \alpha_\mathsf{v} \psi_\mathsf{v} - \mathcal{F}(\boldsymbol{N}). \tag{7.63}$$

We fix the remaining degrees of freedom with the condition:

$$\boldsymbol{\mathcal{C}}_2 := \boldsymbol{e}_\theta - a\,(\partial_\theta \boldsymbol{z})\,a^{-1}. \tag{7.64}$$

This is second class with the flatness constraint:

$$\left\{(\mathcal{C}_2)^i_\theta, \int_\Sigma N^j F^j\right\} = \delta^{ij}\left(\partial_\theta N^j + \epsilon^{jkl} A^k_\theta N^l\right). \tag{7.65}$$

The same procedure as above involving Dirac brackets can be applied again, so that we can set $(\mathcal{C}_2)^i$ and F^i strongly to zero to eliminate the remaining degrees of freedom in the field variables.

Preserving this constraint dynamically provides a condition on the Lagrange multiplier $\boldsymbol{N}$. Using the partially fixed Hamiltonian, the condition is:

$$\{\boldsymbol{\mathcal{C}}_2, H_{pf}\} = \partial_\theta \boldsymbol{N} + [\boldsymbol{A}_\theta, \boldsymbol{N}] = 0. \tag{7.66}$$

The second gauge choice removes the flatness constraint and reduces the Hamiltonian to:

$$H_R = \sum_{\mathsf{v}} \alpha_{\mathsf{v}} \psi_{\mathsf{v}} \tag{7.67}$$

The connection $\boldsymbol{A}$ and frame-field $\boldsymbol{e}$ are now completely determined by the constraints and the gauge choices (7.58, 7.64). The topological degrees of freedom associated with the particles are contained within the parameters $\boldsymbol{P}_{\mathsf{r}}$ defining the a-fields in (7.46). Notice the Hamiltonian has support at the particles so we expect some non-trivial action at these locations.

The gauge fixing procedure places conditions on the Lagrange multipliers, and we now present a solution which satisfies these conditions. We found above that $\boldsymbol{N}$ must satisfy (7.66), while also satisfying at the particle boundaries:

$$\boldsymbol{N}(x) = -\alpha_{\mathsf{v}} \boldsymbol{u}_{\mathsf{v},x} \qquad\qquad \forall x \in \mathcal{B}_{\mathsf{v}}. \tag{7.68}$$

A solution for the Lagrange multiplier within each region r is given by:

$$\boldsymbol{N}_{\mathsf{r}}(x) = a_{\mathsf{r}}(\theta) \bar{\boldsymbol{N}}_{\mathsf{r}}(\rho) a_{\mathsf{r}}(\theta)^{-1}, \qquad\qquad \forall x \in \mathsf{r}, \tag{7.69}$$

where $\bar{\boldsymbol{N}}_{\mathsf{r}}(\rho)$ is a function of ρ only. Recall that the two particles v, v' associated to a region sit at ρ_{v} and $\rho_{\mathsf{v}'}$ respectively, where $\rho_{\mathsf{v}'} < \rho_{\mathsf{v}}$, and ρ_{n} is an intermediate value defining a line from the node n to the midpoint of the edge between v and v'. We define at each particle boundary:

$$\bar{\boldsymbol{N}}_{\mathsf{r}}(\rho_{\mathsf{v}}) = -\alpha_{\mathsf{v}} \boldsymbol{u}_{\mathsf{v},b}, \qquad\qquad \bar{\boldsymbol{N}}_{\mathsf{r}}(\rho_{\mathsf{v}'}) = -\alpha_{\mathsf{v}'} \boldsymbol{u}_{\mathsf{v}',b'}, \tag{7.70}$$

where b (resp. b') is the intersection between the $\theta = 1$ line and $\mathcal{B}_{\mathsf{v}}$ (resp. $\mathcal{B}_{\mathsf{v}'}$). To specify this function over the values of ρ ranging between the particles, we again use a bump function, this time taking ρ as an argument. The function $f(\rho)$ is normalized so that:

$$\int_{\rho_{\mathsf{n}}}^{\rho_{\mathsf{v}}} f(\rho) \mathrm{d}\rho = \int_{\rho_{\mathsf{v}'}}^{\rho_{\mathsf{n}}} f(\rho) \mathrm{d}\rho = 1, \tag{7.71}$$

and goes smoothly to zero in the limits $\rho \to \rho_{\mathsf{v}}$, $\rho \to \rho_{\mathsf{v}'}$ and $\rho \to \rho_{\mathsf{n}}$. Using a vector $\hat{\boldsymbol{t}} := \hat{\boldsymbol{x}} \times \hat{\boldsymbol{y}} = a_{\mathsf{r}} \boldsymbol{\tau}^0 a_{\mathsf{r}}^{-1}$ that is normal to the region and define:

$$\bar{\boldsymbol{N}}_{\mathsf{r}}(\rho) = \hat{\boldsymbol{t}} + \begin{cases} (-\alpha_{\mathsf{v}} \boldsymbol{u}_{\mathsf{v},b} - \hat{\boldsymbol{t}}) \displaystyle\int_{\rho_{\mathsf{n}}}^{\rho} f(\tilde{\rho}) \mathrm{d}\tilde{\rho}, & \rho_{\mathsf{n}} \le \rho \le \rho_v \\ (-\alpha_{\mathsf{v}'} \boldsymbol{u}_{\mathsf{v}',b'} - \hat{\boldsymbol{t}}) \displaystyle\int_{\rho}^{\rho_{\mathsf{n}}} f(\tilde{\rho}) \mathrm{d}\tilde{\rho}, & \rho_{v'} \le \rho < \rho_{\mathsf{n}} \end{cases} \tag{7.72}$$

Values of this function vary smoothly from $-\alpha_{\mathsf{v}'}\boldsymbol{u}_{\mathsf{v}',b'}$ to $\hat{\boldsymbol{t}}$ to $-\alpha_{\mathsf{v}}\boldsymbol{u}_{\mathsf{v},b}$ as one travels from $\mathcal{B}_{\mathsf{v}'}$ to the line $\rho = \rho_{\mathsf{n}}$ and then to $\mathcal{B}_{\mathsf{v}}$. With this definition, the Lagrange multiplier in the region $\boldsymbol{N}_{\mathsf{r}} = a_{\mathsf{r}}\bar{\boldsymbol{N}}_{\mathsf{r}}a_{\mathsf{r}}^{-1}$ satisfies the boundary conditions at $\mathcal{B}_{\mathsf{v}}$ and $\mathcal{B}_{\mathsf{v}'}$. Moreover, one can check that this definition yields a smooth function defined piecewise over the triangle $\boldsymbol{N}_c = \cup_{\mathsf{r}\in c}\boldsymbol{N}_{\mathsf{r}}$ and also over all of Σ with the piecewise definition $\boldsymbol{N} = \bigcup_{c\in\Sigma}\boldsymbol{N}_c$. As for α_{v}, we shall fix this below once we have the equations of motion.

The other Lagrange multiplier $\boldsymbol{\lambda}$ must satisfy the condition (7.60) for all $x \in \Sigma$. Any function of the form $a\bar{\boldsymbol{\lambda}}a^{-1}$ for constant $\bar{\boldsymbol{\lambda}} \in \mathfrak{su}(2)$ will do the trick, but for concreteness we choose:

$$\boldsymbol{\lambda} = \cup_{\mathsf{r}} a_{\mathsf{r}}\boldsymbol{\tau}^0 a_{\mathsf{r}}^{-1} = \cup_{\mathsf{r}}\hat{\boldsymbol{t}}_{\mathsf{r}}. \tag{7.73}$$

We now summarize what we have accomplished with this gauge fixing procedure. We have triangulated Σ by placing particles at the vertices $\mathsf{v} \in \Gamma^*$ of the zero-skeleton for a cellular space Δ, and have specified the frame-field and connection everywhere on Σ by giving a definition in each section s, region r, and triangle c. The fields are specified in terms of an $\mathfrak{su}(2)$-valued coordinate function $\boldsymbol{z}(x)$ and an SU(2)-valued field $a(x)$ according to (7.38), given by a choice of bump function f_{r} and rotation parameter $\boldsymbol{P}_{\mathsf{r}}$ for each region. The solutions are glued together along each edge e of the triangulation by a constant h_{e} and the rule (5.3), as well as an additional gluing rule for the coordinate functions (7.52) between sections. In addition, we have given solutions for the Lagrange multipliers which satisfy the conditions resulting from the gauge choice (7.60, 7.66). The gauge fix depends on the choices of cellular space Δ, and the bump functions f_{r} and rotation parameters $\boldsymbol{P}_{\mathsf{r}}$ in each region. This amounts to choosing a specific point $(\bar{\boldsymbol{A}}, \bar{\boldsymbol{e}})$ in the constrained subspace

$$\mathcal{C}_{\Gamma^*} = \{(\boldsymbol{A}, \boldsymbol{e}) \in \mathcal{P} \mid \mathcal{F}_{\Gamma^*}[\boldsymbol{N}] = \mathcal{G}[\boldsymbol{\lambda}] = 0\}\,. \tag{7.74}$$

This constrained subspace contains all of the physical degrees of freedom associated to the particles.

7.3 Particle degrees of freedom

Now that we have fixed a gauge and reduced the Hamiltonian, the only remaining degrees of freedom in the phase space are the topological degrees of freedom associated to the particles. But how can we extract this information from the fields $(\bar{\boldsymbol{A}}, \bar{\boldsymbol{e}})$?

Let us first consider how to define the particle positions. In a general relativistic theory, one cannot say anything about position without specifying a frame of reference. We are working within a spatial hypersurface defined as a triangulation, where each triangle possesses its own coordinate function. We can use each triangle c, or more specifically each centroid n_c, as a point of reference for defining the location of the vertices $\mathsf{v} \in \partial c$. Since we have smeared the particle boundary, we must choose a point on $\mathcal{B}_{\mathsf{v}}$ at which to define the position. Taking this point b to be at the intersection of the boundary $\mathcal{B}_{\mathsf{v}}$ and the $\theta = 1$ line, we define the position in the frame of c as:

$$\boldsymbol{q}^c_{\mathsf{v}} := \int_{\mathsf{n}_c}^{\mathsf{v}} h_\pi^{-1}\boldsymbol{e}h_\pi = \int_{\mathsf{n}_c}^{\mathsf{v}} \mathrm{d}\boldsymbol{z} = \boldsymbol{z}(b) - \boldsymbol{z}(\mathsf{n}_c), \tag{7.75}$$

where π is a path from the centroid to the vertex, and $h_\pi = a_c^{-1}$. Using the gluing rules, one finds for neighbouring cells c and c' that:

$$\boldsymbol{q}_{\mathsf{v}}^{c'} = h_{cc'}^{-1} \boldsymbol{q}_{\mathsf{v}}^{c} h_{cc'}. \tag{7.76}$$

Next we turn to the momentum. We want something defined in terms of the connection so that it has a non-trivial Poisson bracket with $\boldsymbol{q}_{\mathsf{v}}^{c}$. The obvious choice is the holonomy around the particle:

$$\boldsymbol{p}_{\mathsf{v}}^{c} := h_{\mathcal{B}_{\mathsf{v}},b} = \overrightarrow{\exp} \int_{\mathcal{B}_{\mathsf{v}},b} \boldsymbol{A} \in \mathrm{SU}(2), \tag{7.77}$$

where we have chosen b as the base-point of the loop $\mathcal{B}_{\mathsf{v}}$. Momenta of neighbouring cells are related by:

$$\boldsymbol{p}_{\mathsf{v}}^{c'} = h_{cc'}^{-1} \boldsymbol{p}_{\mathsf{v}}^{c} h_{cc'}. \tag{7.78}$$

Only the orientation of momentum is affected by these rules, so that the particle masses are the same as seen from any cell:

$$m_{\mathsf{v}} = 2 \cos^{-1} \frac{\mathrm{Tr}(\boldsymbol{p}_{\mathsf{v}}^{c})}{2}, \tag{7.79}$$

as they should be.

The Poisson algebra of these relative position and momentum variables is given by:

$$\{\boldsymbol{q}_{\mathsf{v}}^{c}, \boldsymbol{q}_{\mathsf{v}'}^{c'}\} = \{\boldsymbol{p}_{\mathsf{v}}^{c}, \boldsymbol{p}_{\mathsf{v}'}^{c'}\} = 0, \qquad \{(q_{\mathsf{v}}^{c})^i, \boldsymbol{p}_{\mathsf{v}'}^{c'}\} = -\boldsymbol{\tau}^i \boldsymbol{p}_{\mathsf{v}}^{c} \delta_{\mathsf{v}\mathsf{v}'}, \tag{7.80}$$

where we used (7.78) to calculate the last bracket[6]. The variables $(\boldsymbol{q}_{\mathsf{v}}^{c}, \boldsymbol{p}_{\mathsf{v}}^{c})$ modulo the equivalence relations in (7.76, 7.78) parameterize the reduced phase space:

$$\mathcal{P}_{\Gamma^*}^{G} = \mathcal{P} /\!\!/ (\mathcal{F}_{\Gamma^*} \times G), \tag{7.81}$$

where Γ^* is the zero-skeleton of the cellular space. They provide a position and momentum for each particle v, in the frame associated to each cell c which contains v.

In terms of this phase space, the reduced Hamiltonian is given by:

$$H = \sum_{\mathsf{v}} \alpha_{\mathsf{v}} \psi_{\mathsf{v}}, \qquad \psi_{\mathsf{v}} = 2 \cos^{-1} \frac{\mathrm{Tr}(\boldsymbol{p}_{\mathsf{v}})}{2} - m_{\mathsf{v}}. \tag{7.82}$$

This has support on each particle boundary, and we anticipate that it will generate dynamics at the vertices of the triangulation.

[6]In defining the last bracket, we also need a precise definition of the Poisson bracket $\{\boldsymbol{e}(x), h_{\mathcal{B}_{\mathsf{v}},b}\}$ when x is at the base-point (both the start and end of the loop). Here we define this intersection to be at the start of the loop. See equation (A.22) and the footnote which follows this equation for details.

7.4 Dynamics in the triangulation

The first step in the study of dynamics is to define initial data. It should be clear from the discussion so far that one cannot assign a position and momentum $(\boldsymbol{q}_{\mathsf{v}}, \boldsymbol{p}_{\mathsf{v}})$ to each particle without specifying a frame of reference. In our approach, the particle degrees of freedom are defined from the connection and frame-field, and if we specify these fields $(\bar{\boldsymbol{A}}, \bar{\boldsymbol{e}})$, the particle degrees of freedom can be extracted as a pair $(\boldsymbol{q}^c_{\mathsf{v}}, \boldsymbol{p}^c_{\mathsf{v}})$ for each particle as seen from each cell. In order to define the cellular space Δ upon which the fields are defined, we need to give a set of triangles with adjacency relations that yield a closed manifold that is topologically equivalent to a polyhedron. Within each cell, we can assign a cartesian coordinate system as used above, so that we have the gluing maps $s_{cc'}$. Within each region of a cell, we give a rotation parameter $\boldsymbol{P}_{\mathsf{r}}$ and a bump function f_{r} which gives the rotation function a_{r} as in (7.46), and also the gluing elements between cells. With the rotation functions, we can define the coordinate function in each section $\boldsymbol{z}_{\mathsf{s}}$. With a_r in each region and $\boldsymbol{z}_{\mathsf{s}}$ in each section, we can piece together a pair $(\boldsymbol{z}_c, a_c)$ for each cell, which in turn provides a definition of $(\bar{\boldsymbol{A}}, \bar{\boldsymbol{e}})$ over all of Σ. Once we have the overall geometry, the particle degrees of freedom are given by the definitions in the previous section.

The geometry to keep in mind is that of a set of 'covariant triangles' (i.e. with non-zero connections) glued together along common edges. The dynamics will be manifest in the motion of the vertices, with the equations of motion being generated by the Hamiltonian (7.82). Evidently, the momenta are constants of motion:

$$\dot{\boldsymbol{p}^c_{\mathsf{v}}} = \{\boldsymbol{p}^c_{\mathsf{v}}, H\} = 0. \tag{7.83}$$

For the positions we calculate:

$$\begin{aligned}
\left\{(q^c_{\mathsf{v}})^i, H\right\} &= \left\{(q^c_{\mathsf{v}})^i, \alpha_{\mathsf{v}}\psi_{\mathsf{v}}\right\} \\
&= \frac{-\alpha_{\mathsf{v}}}{\sin\frac{m}{2}}\left\{(q^c_{\mathsf{v}})^i, \mathrm{Tr}(\boldsymbol{p}^c_{\mathsf{v}})\right\} \\
&= \frac{\alpha_{\mathsf{v}}}{\sin\frac{m}{2}}\mathrm{Tr}\left(\boldsymbol{\tau}^i\boldsymbol{p}^c_{\mathsf{v}}\right) \\
(\dot{\boldsymbol{q}^c_{\mathsf{v}}})^i &= \alpha_{\mathsf{v}}(u^c_{\mathsf{v}})^i.
\end{aligned} \tag{7.84}$$

where $(u^c_{\mathsf{v}})^i$ is the rotation axis associated to $\boldsymbol{p}^c_{\mathsf{v}}$. Notice that $\dot{\boldsymbol{q}}^c_{\mathsf{v}} = \boldsymbol{N}_{\mathsf{v}}(b)$, so that these equations fit with the idea that $\boldsymbol{N}$ tells us where points on the spatial hypersurface flow under time evolution.

The fact that particles have constant momentum imposes a restriction on the choices for each α_{v}. The spatial hypersurface is described as a triangulation with particles at the vertices, and in order for this to stay consistent dynamically, the vertices most move along with the particles according to the equations of motion. The gluing rules ensure that this dynamics is consistent for all cells which share a vertex. One issue that could spoil this picture is if the vertices in any given triangle evolve such that the triangle becomes inverted. We can avoid this by choosing:

$$\alpha_{\mathsf{v}} = (\boldsymbol{u}^c_{\mathsf{v}} \cdot \hat{\boldsymbol{t}})^{-1}, \tag{7.85}$$

which normalizes the velocity $\dot{\boldsymbol{q}}^c_{\mathsf{v}} \cdot \hat{\boldsymbol{t}} = 1$ of each vertex $\mathsf{v} \in \partial c$ in the direction perpendicular to the triangle. Since the rotation axes $\boldsymbol{u}^c_{\mathsf{v}}$ and basis vectors $\hat{\boldsymbol{t}}$ each satisfy a gluing rule, this choice is made consistently around each vertex and normalizes $\dot{\boldsymbol{q}}^c_{\mathsf{v}} \cdot \hat{\boldsymbol{t}} = 1$ for each particle in the frame of each cell.

Given that the vertices of the triangulation are moving, how can we describe what is happening to the fields? The dynamics is a time dependant diffeomorphism $\Phi_t(\Gamma^*)$ of the vertices $\mathsf{v} \in \Gamma^*$, and defining the edges of Δ as straight edges between the vertices, we can extend this diffeomorphism to act on the cellular space $\Phi_t(\Delta)$. We defined our initial data in terms of fields $(\bar{\boldsymbol{A}}, \bar{\boldsymbol{e}})$ using a gauge fix that depends upon an initial triangulation Δ_0, as well as a choice of bump functions f_{r} and rotation parameters $\boldsymbol{P}_{\mathsf{r}}$. Once these choices are made, we have a prescription for choosing a unique pair of fields $(\bar{\boldsymbol{A}}, \bar{\boldsymbol{e}})$. The dynamics changes the triangulation $\Delta_0 \to \Delta_t = \Phi_t(\Delta_0)$, leaving the bump functions and rotation parameters unchanged. For any initial data $(\Delta_0, f_{\mathsf{r}}, \boldsymbol{P}_{\mathsf{r}})$ defining $(\boldsymbol{q}_{\mathsf{v}}, \boldsymbol{p}_{\mathsf{v}})$, the dynamics $U(t)$ depends upon the gauge fix prescribed by a time-dependant triangulation Δ_t:

$$\begin{aligned} U(t): \qquad \mathcal{C}_{\Gamma^*} &\longrightarrow \mathcal{C}_{\Phi_t(\Gamma^*)} \\ \Delta_0 &\longrightarrow \Phi_t(\Delta_0), \\ (\bar{\boldsymbol{A}}(x,0), \bar{\boldsymbol{e}}(x,0)) &\longmapsto (\bar{\boldsymbol{A}}(x,t), \bar{\boldsymbol{e}}(x,t)) \end{aligned} \tag{7.86}$$

Because we are using the gauge-fixed Hamiltonian H_R with the constraints set strongly to zero, we have obtained a definition of dynamics between constrained phase spaces. With this definition, we can find a geometry $(\bar{\boldsymbol{A}}(x,t), \bar{\boldsymbol{e}}(x,t))$ at any time t according to the cellular space Δ_t.

7.4.1 Discrete transitions in the triangulation

We have a nice geometrical picture of particle dynamics within $\mathbb{R} \times \Sigma$. Each cell of the space Δ is a triangle with dynamical vertices, and the geometry $(\bar{\boldsymbol{A}}, \bar{\boldsymbol{e}})$ comes along for the ride. The question then is, what happens when a vertex meets an edge? This will bring a change in the triangulation, and we need to find a way to do this that is consistent with the particle data. This is a discrete transition that will affect only some of the triangles. We need the particle masses to be maintained in the transition, and we would like the particle data $(\boldsymbol{q}^c_{\mathsf{v}}, \boldsymbol{p}^c_{\mathsf{v}})$ in the unaffected triangles to be invariant under the transition so that they do not see any change. There is a consistent set of transition rules that provides this for us.

Consider the setup depicted in fig. 7.4, where the particle v has a momentum $\boldsymbol{p}^A_{\mathsf{v}}$ directed toward the edge e. When the particle reaches the edge, we define a discrete change in the triangulation as follows. The cell A is removed from the triangulation, while the cell B is split into two along a new edge $\mathsf{e}_{A'B'}$, i.e. we have a bistellar flip. After the transition, we must define new rotation fields within the cells A' and B' by an appropriate choice of the rotation parameters $\boldsymbol{P}_{\mathsf{r}}$. A consistent transition requires:

$$e^{-\boldsymbol{P}_{1'}} = e^{-\boldsymbol{P}_1} e^{\boldsymbol{P}_3} e^{-\boldsymbol{P}_4}, \qquad e^{-\boldsymbol{P}_{2'}} = e^{-\boldsymbol{P}_2} e^{\boldsymbol{P}_3} e^{-\boldsymbol{P}_4} \tag{7.87}$$

$$\boldsymbol{P}_{3'} = \boldsymbol{P}_{4'} = 0, \qquad \boldsymbol{P}_{5'} = \boldsymbol{P}_5, \qquad \boldsymbol{P}_{6'} = \boldsymbol{P}_6, \tag{7.88}$$

while none of the cells outside of these are affected by the transition. Within the new triangles A' and B' we can then define the new coordinate and rotation functions, which in turn provide

the frame-field and connection within these cells. The total number of triangles is preserved in this transition, as is the total number of particle parameters $(\boldsymbol{q}_{\mathsf{v}}^c, \boldsymbol{p}_{\mathsf{v}}^c)$. In addition, one can check that the relations (7.76, 7.78) continue to hold. After such a discrete transition, the particles again evolve according to the continuous dynamics until one of the particles meets an edge. The definition (7.86) for dynamics can be generalized to include these discrete transitions, by

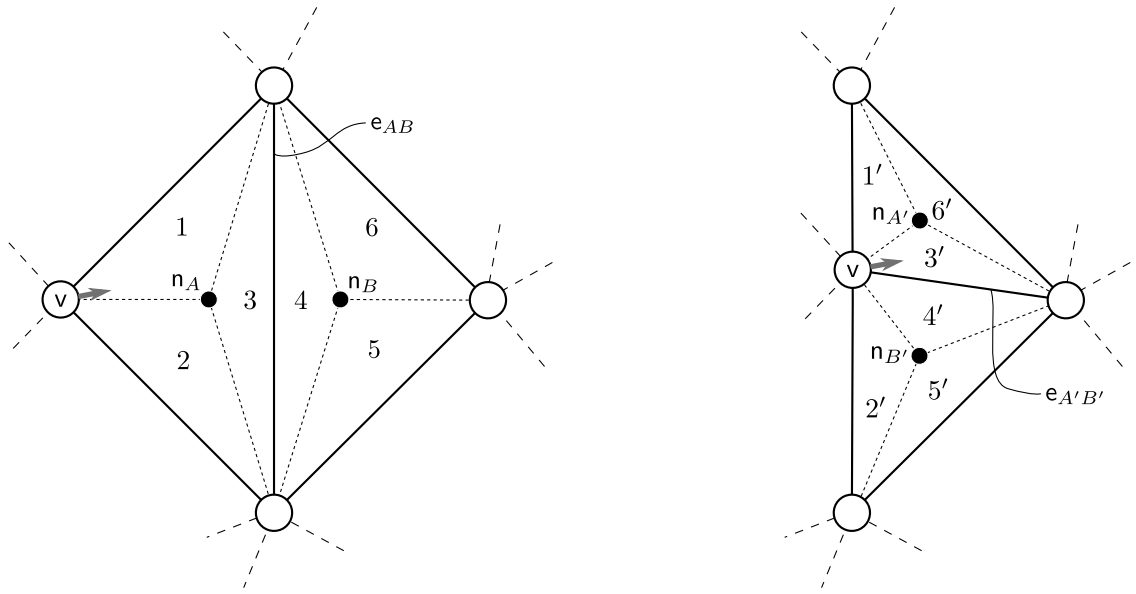

(a) Before (b) After

Figure 7.4: Before and after a discrete transition in the triangulation. This is known as a bistellar flip. The centroids and the 'flipped' edge are labeled, and the numbers labels the six regions of the two triangles.

allowing for these in the definition of the diffeomorphism $\Phi_t : \Delta_0 \to \Delta_t$.

Let us now check that our definition provides a consistent dynamics. This transition results in a redefinition for six pairs $(\boldsymbol{q}_{\mathsf{v}}^c, \boldsymbol{p}_{\mathsf{v}}^c) \to (\boldsymbol{q}_{\mathsf{v}}^{c'}, \boldsymbol{p}_{\mathsf{v}}^{c'})$, since these positions and momenta are now defined within new reference frames. Notice that this preserves the dimension of the phase space. We know that dynamics is a canonical transformation, and one can check that the Poisson algebra is preserved. As an example, let us check the Poisson bracket for one of the new pairs. The transition rules are such that:

$$\boldsymbol{q}_{\mathsf{v}}^{A'} = h_{AA'}^{-1} \boldsymbol{q}_{\mathsf{v}}^{A} h_{AA'}, \qquad \boldsymbol{p}_{\mathsf{v}}^{A'} = h_{AA'}^{-1} \boldsymbol{p}_{\mathsf{v}}^{A} h_{AA'}, \tag{7.89}$$

where $h_{AA'}$ is the holonomy from n_A to $\mathsf{n}_{A'}$ at the instant of the transition. Evaluating the Poisson bracket between these new variables using the Poisson bracket for the old ones, we find:

$$\begin{aligned} \left\{ (\boldsymbol{q}_{\mathsf{v}}^{A'})^i, \boldsymbol{p}_{\mathsf{v}}^{A'} \right\} &= R(h_{AA'})^i_j \left\{ (\boldsymbol{q}_{\mathsf{v}}^{A})^j, h_{AA'}^{-1} \boldsymbol{p}_{\mathsf{v}}^{A} h_{AA'} \right\} \\ &= -R(h_{AA'})^i_j h_{AA'}^{-1} \boldsymbol{\tau}^j \boldsymbol{p}_{\mathsf{v}}^{A} h_{AA'} \\ &= -\boldsymbol{\tau}^i \boldsymbol{p}_{\mathsf{v}}^{A'}, \end{aligned} \tag{7.90}$$

where we used that $R(h_{AA'})^i_j \boldsymbol{\tau}^j = h_{AA'} \boldsymbol{\tau}^i h^{-1}_{AA'}$ (acting inversely on the basis). We see that the Poisson algebra is indeed preserved with these rules.

7.4.2 Scattering

Scattering in three-dimensional gravity depends upon the choice of geometry [91, 92, 93]. There is freedom in choosing a geometry $(\boldsymbol{A}, \boldsymbol{e})$ to represent the topology, and different choices lead to different trajectories. Take for example a single particle with mass (deficit angle) m, at rest in $\mathbb{R}^2$. In polar coordinates this can be described by a connection $\boldsymbol{A} = -\boldsymbol{\tau}^0 \mathrm{d}\phi$ where $0 \leq \phi \leq 2\pi - m$, or alternatively by the connection $\boldsymbol{A'} = -\boldsymbol{\tau}^0(1 - m/2\pi)\mathrm{d}\phi'$ where $0 \leq \phi' \leq 2\pi$. The first connection $\boldsymbol{A}$ is for the geometry of a plane with a wedge cut out, while the second connection $\boldsymbol{A'}$ is for the geometry of a cone; both of these correspond to a topological cone.

The geometry described by Deser, Jackiw and 't Hooft in [83] is that of a flat space with wedges cut out. Both sides of each wedge are identified, which leads to a metric that is multi-valued along the tails. When one particle passes another, it is deflected if it crosses the tail, or not if it does not cross the tail. Note that the choice of where to make the cuts is arbitrary, so that the dynamics depends upon these ambiguous choices. There is no well-defined centre of mass frame as used for conventional scattering, and we are stuck with this sort of gauge dependence of particle trajectories. We note that it is possible to find geometries with trajectories that do not depend upon such choices. For instance, one can constrain the asymptotic motion of the particles by requiring the metric to be smooth and invertible outside of the particle locations [91]. This allows for an unambiguous perturbative solution of scattering up to second order in the mass parameters. Alternatively, the authors of [92] use a non-trivial map from the multi-valued flat metric to a single-valued metric which allows for a non-perturbative description of scattering.

In this paper, we have developed a specific choice of geometry that provides a clear picture in terms of evolving triangulations of S^2. This setting is not appropriate for discussing the asymptotic trajectories of particles, so we cannot use this to formulate scattering in the conventional sense. However, a gauge-invariant description is possible in terms of so called *particle exchanges*, the action of the braid group on holonomies around the particles [91, 94].

Let us consider such an exchange between two particles $\mathsf{v}_1, \mathsf{v}_2$. We fix a base-point b and choose two particle holonomies, i.e. holonomies defined on loops γ_1, γ_2 which go around the corresponding particle and only that particle. The action of the braid group is to wind these holonomies around each other. Following [91], we define a particle exchange operator σ_{12} which acts on the tensor space $\mathcal{V}_1 \otimes \mathcal{V}_2$ of SU(2) holonomies of the two particles. The action of a particle exchange is given by:

$$\sigma_{12} : \begin{cases} h_1 & \to & h_1 \\ h_2 & \to & h_1 h_2 h_1^{-1} \end{cases} \tag{7.91}$$

The full monodromy of particle v_2 around particle v_1 is gauge-invariant. This is given by the action of $\sigma_{12}\sigma_{21}$, i.e. braiding twice.

This picture generalizes to any braiding of an arbitrary number $|\mathsf{v}_\Delta|$ of particle holonomies h_{γ_v}. For a fixed base-point, we can define exchange operators $\sigma_{i,i+1}$ for $i = 1, \ldots, V-1$ which

act on the tensor space $\mathcal{V}_1 \otimes \cdots \otimes \mathcal{V}_V$ of particle holonomies to generate the braid group B_V. The braid group provides a useful tool for understanding the Jones polynomial of knot theory [95] and plays an important role in the quantization of three-dimensional gravity with point sources (see the papers by Freidel and Louapre listed in [78]). In this classical setting, the discrete changes in triangulation described above can be written in terms of the action of generators $\sigma_{i,i+1}$ on particle holonomies. One can check this by choosing a base point and writing the holonomies around particles in terms of the rotation functions a_{r} associated to regions. As particles move, one finds that these holonomies can change under the discrete changes of triangulation according to the braiding action given above. Note that whether or not a single braid appears during a discrete transition depends upon the choice of base-point. Only once a particle has gone completely around the other do we get a result that does not depend upon the choice of base-point.

This concludes our analysis within the picture of the triangulation. We have given the particle data in terms of a position and momentum $(\boldsymbol{q}^c_{\mathsf{v}}, \boldsymbol{p}^c_{\mathsf{v}})$ for each particle in the frame of each cell that contains the particle. Masses are found from the norm $m_{\mathsf{v}} = |\boldsymbol{p}_{\mathsf{v}}|$. Dynamics lead to motion of the vertices which causes the triangles to change shape. It may happen that a vertex reaches an edge and collapses a triangle and splitting another into two. A description of trajectories depends upon how one chooses the triangulation and fields $(\bar{\boldsymbol{A}}, \bar{\boldsymbol{e}})$, but a gauge invariant description of scattering is provided by the braid group. Remarkably, all of this can be described equivalently in terms of holonomy-flux data on a graph. Let us see how this works.

7.5 Point particles in the loop gravity phase space

Point particles in 3d gravity make a nice model for this thesis since they permit a description in terms of spatial geometries that are the 2d analog of spinning geometries. This allows us to use the isomorphism between the continuous phase space, reduced by the flatness and Gauss constraints, and the gauge-invariant loop gravity phase space. The flatness constraint was imposed everywhere except a set of points $\mathsf{v} \in \Gamma^*$, which is the zero-dimensional analog of the one-skeleton used in chapter 4. Within this space then, we can embed a graph Γ that is dual to Γ^*, and use this to map to an isomorphic phase space P^G_Γ that is parameterized by the holonomies and fluxes associated to the graph Γ. This provides insight into how we can describe four-dimensional gravity in these phase spaces. In this model we can look at how to embed a graph and which truncations are suitable for given data, and we can see what a gravitational dynamics looks like in terms of holonomies and fluxes. We have already seen a bistellar flip within the continuous picture of dynamics, and we can expect this to have implications on graph-changes in the discrete picture.

Let us now choose a suitable graph and embed it within the cellular space. As hinted at by the notation, we place a node n at the centroid of each triangle, and choose the links ℓ between these nodes so that there is one link in the graph intersecting each link in the triangulation. See fig. 7.5 for an illustration.

Now, with the graph and the fields $(\bar{\boldsymbol{A}}, \bar{\boldsymbol{e}})$ defined in the dual cellular space, we can map to

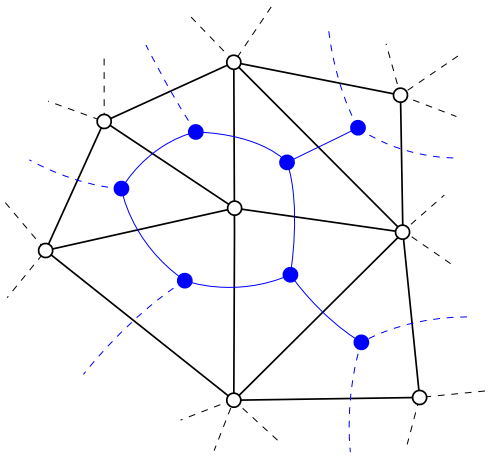

Figure 7.5: Neighbourhood of a triangulation. Edges (black lines) and vertices (open black circles) of a triangulation are shown, together with a dual embedded graph Γ consisting of links (blue curves) and nodes (filled blue circles). The vertices of the triangulation compose a one-skeleton Γ^* that is dual to the graph Γ.

the holonomies and fluxes. For a link $\ell_{cc'}$ from the node n_c to $\mathsf{n}_{c'}$ we have the holonomy:

$$h_{cc'} = \overrightarrow{\exp} \int_{\ell_{cc'}} \boldsymbol{A} = a_{\mathsf{r}}^{-1} a_{\mathsf{r}'} = e^{\boldsymbol{P}_{\mathsf{r}}} e^{-\boldsymbol{P}_{\mathsf{r}'}}, \tag{7.92}$$

where the regions $\mathsf{r} \in c$ and $\mathsf{r}' \in c'$ are on either side of the edge, and the rotation functions are evaluated at the edge. The holonomy for the reversed link $\ell_{cc'}^{-1} = \ell_{c'c}$ is given by the inverse:

$$h_{c'c} = h_{cc'}^{-1}. \tag{7.93}$$

For the fluxes, we require a little more care in handling the smeared particle boundaries. Consider two vertices v and v' with an edge $\mathsf{e}_{cc'}$ between them, and let us take the associated boundaries $\mathcal{B}_{\mathsf{v}}(\varepsilon)$ and $\mathcal{B}_{\mathsf{v}'}(\varepsilon)$ to have a finite radius ε. We define the flux associate to the link $\ell_{cc'}$ to include integrals over portions of the boundaries in addition to the integral over the edge:

$$\boldsymbol{X}_{cc'}(\varepsilon) = \int_{\mathcal{B}_{\mathsf{v}}(\varepsilon)\cap\mathsf{r}} h_\pi \boldsymbol{e} h_\pi^{-1} + \int_{\mathsf{e}_{cc'}} h_\pi \boldsymbol{e} h_\pi^{-1} + \int_{\mathcal{B}_{\mathsf{v}'}(\varepsilon)\cap\mathsf{r}} h_\pi \boldsymbol{e} h_\pi^{-1}, \tag{7.94}$$

where π is a path from n_c to the point of integration, and the edge $\mathsf{e}_{cc'}$ is given by the $\theta = 0$ line of the region r. With this definition, the fluxes satisfy the closure constraint (Gauss law):

$$\sum_{\ell \in \partial c} \boldsymbol{X}_\ell = 0, \tag{7.95}$$

since this is the integral around a closed loop. In the limit that $\varepsilon \to 0$, each boundary shrinks to a point and the frame-fields satisfy $(\mathcal{B}_{\mathsf{v}})^a \boldsymbol{e}_a = 0$ so that the flux becomes:

$$\boldsymbol{X}_{cc'} = \int_{\mathsf{e}_{cc'}} h_\pi \boldsymbol{e} h_\pi^{-1} = \int_{\mathsf{e}_{cc'}} \mathrm{d}\boldsymbol{z}^c = L_{cc'} \hat{\boldsymbol{y}}, \tag{7.96}$$

which is the length of the edge $L_{cc'}$ in the direction $\hat{\boldsymbol{y}}$ from one vertex to the other. Notice the 2d flux is the relative distance vector from one particle to the other. They satisfy the gluing relation:

$$\boldsymbol{X}_{c'c} = -\int_{\mathsf{e}_{c'c}} \mathrm{d}\boldsymbol{z}^{c'} = -h_{cc'}^{-1}\boldsymbol{X}_{cc'}h_{cc'}. \tag{7.97}$$

The definitions (7.92, 7.94) provide a map from the constrained space to the discrete phase space:

$$\begin{array}{rccc} \mathcal{I}_\Gamma: & \mathcal{C}_{\Gamma^*} & \longrightarrow & P_\Gamma \\ & (\bar{A},\bar{E}) & \longmapsto & (h_{\mathsf{n}}, X_{\mathsf{n}}), \end{array} \tag{7.98}$$

where the fields $(\bar{A},\bar{E})$ are determined by the bump functions f_{r} and rotation parameters $\boldsymbol{P}_{\mathsf{r}}$ on a cellular space Δ. If we retain this information, we have the inverse map from the discrete data back to the pair of fields $(\bar{A},\bar{E})$ in the constrained subspace:

$$\begin{array}{rccc} \mathcal{T}_{\Gamma,f_{\mathsf{r}},\boldsymbol{P}_{\mathsf{r}}}: & P_\Gamma & \longrightarrow & \mathcal{C}_{\Gamma^*} \\ & (h_{\mathsf{n}}, X_{\mathsf{n}}) & \longmapsto & (\bar{A},\bar{E}). \end{array} \tag{7.99}$$

In other words, knowing $(\Gamma, f_{\mathsf{r}}, \boldsymbol{P}_{\mathsf{r}})$ allows us to find a gauge choice such that $\mathcal{T}_{\Gamma,f_{\mathsf{r}},\boldsymbol{P}_{\mathsf{r}}}\mathcal{I}_\Gamma = \mathcal{I}_\Gamma\mathcal{T}_{\Gamma,f_{\mathsf{r}},\boldsymbol{P}_{\mathsf{r}}} = \mathbb{1}$.

Recall that these variables satisfy the Poisson algebra:

$$\{h_\ell, h_{\ell'}\} = 0, \qquad \{X^i_\ell, h_{\ell'}\} = -\tau^i h_\ell \delta_{\ell\ell'}, \qquad \{X^i_\ell, X^j_{\ell'}\} = \epsilon^{ijk}X^k_\ell\delta_{\ell\ell'}. \tag{7.100}$$

each equivalence class of holonomy-flux data under SU(2)-gauge transformations defines a point in the gauge-invariant phase space P^G_Γ. The phase space P^G_Γ is isomorphic to the reduced continuous phase space $\mathcal{P}^G_{\Gamma^*}$, and contains all of the position and momenta information of the particles. We commented above that there are different choices of triangulations for a set of points Γ^*, and that these choices are related by bistellar flips. Each choice of triangulation leads to a different embedded graph, and these different graphs are related by two-to-two Pachner moves. What these choices amount to are different fields $(\bar{\boldsymbol{A}},\bar{\boldsymbol{e}})$ on the continuous side, or different sets of $(h_\ell, \boldsymbol{X}_\ell)$ on the discrete side. These are gauge choices since any choice yields the same physical results.

The Hamiltonian H was reduced according to our gauge choice, and this is a good gauge choice since H_R is easily written in terms of holonomies in P^G_Γ. Consider a vertex at the intersection of m cells $c_1,\cdots,c_m$. Since the connection is flat everywhere outside of the vertex, we can expand the loop $\mathcal{B}_{\mathsf{v}} \to \partial\mathsf{o}_{\mathsf{v}}$ to one that runs along embedded links to take a path between nodes $\mathsf{n}_1,\cdots,\mathsf{n}_m,\mathsf{n}_1$, which defines a loop around the cone o_{v}. We then have that:

$$h_{\partial\mathsf{o}_{\mathsf{v}},\mathsf{n}_1} = h_{c_1c_2}\cdots h_{c_mc_1}, \tag{7.101}$$

With this equation we have for the Wilson loop around the particle at v:

$$W_{\mathsf{v}} = \mathrm{Tr}(\prod_{\ell\in\mathsf{o}_{\mathsf{v}}} h_\ell), \tag{7.102}$$

where the product is ordered counterclockwise around v, and the choice of base-point is washed out in trace so we need not specify it. Having the Wilson loops in terms of h_ℓ, we have also the mass shell constraints and the Hamiltonian in terms of these variables:

$$H_R = \sum_{\mathsf{v}} \alpha_{\mathsf{v}} \psi_{\mathsf{v}}, \qquad \psi_{\mathsf{v}} := 2\cos^{-1}\frac{W_{\mathsf{v}}}{2} - m_{\mathsf{v}}. \tag{7.103}$$

Each constraint ψ_{v} tells us the mass of particle v in terms of the holonomies h_ℓ. The question now is: What evolution does this Hamiltonian generate on the graph data?

7.6 Dynamics on the graph

Let us define a set of initial data for the dynamics in the loop gravity picture. We first require an initial triangulation Σ_0, so that we can define the dual embedded graph. Alternatively, we could take an unknotted graph and from this define the triangulation that it is dual to[7]. Now, upon each link of the embedded graph, we choose a consistent set of holonomies and fluxes that satisfy the relations between cells (7.93, 7.97) and the closure constraint (7.95). This is our initial data.

The holonomies are constants of motion since:

$$\dot{h}_\ell = \{h_\ell, H_R\} = 0. \tag{7.104}$$

The interesting dynamics is on the fluxes. These represent the edge vectors of the triangulation, and changes in the flux correspond to changes in the triangulation. The Hamiltonian is written in terms of a holonomy $h_{\partial \mathsf{o}_{\mathsf{v}},\mathsf{n}}$ for each particle v, around the boundary of its cone o_{v}. Where m cells meet at a particle, let us label the cells such that the loop starts at the node n_1 as in (7.101). From the holonomy-flux Poisson algebra, we have for any cells c and $c+1$ in the loop $\partial \mathsf{o}_{\mathsf{v}}$:

$$\begin{aligned}
\left\{X^i_{c,c+1}, W_{\mathsf{v}}\right\} &= \left\{X^i_{c,c+1}, \mathrm{Tr}\; h_{\partial \mathsf{o}_{\mathsf{v}},\mathsf{n}_{c'}}\right\} \\
&= \mathrm{Tr}\left(h_{12}\cdots h_{c-1,c}(-\boldsymbol{\tau}^i)h_{c,c+1}\cdots h_{m1}\right) \\
&= -\mathrm{Tr}\; h_{\boldsymbol{\tau}^i \partial \mathsf{o}_{\mathsf{v}},\mathsf{n}_{c'}} \\
&= -\sin(\frac{m_{\mathsf{v}}}{2})\,(u^c_{\mathsf{v}})^i
\end{aligned} \tag{7.105}$$

while the bracket vanishes if the link $\ell_{c,c+1}$ is not part of the loop $\partial \mathsf{o}_{\mathsf{v}}$. Recall that $(u^c_{\mathsf{v}})^i$ is a unit vector in the direction of particle momentum in the cell c. Using this bracket we can find the equation of motion for the flux associated to the edge between two vertices v and v':

$$\begin{aligned}
\left\{X^i_{c,c+1}, H_R\right\} &= \left\{X^i_{c,c+1}, \sum_{\mathsf{v}} \alpha_{\mathsf{v}} 2\cos^{-1}\frac{W_{\mathsf{v}}}{2}\right\} \\
&= \frac{-\alpha_{\mathsf{v}}}{\sin\frac{m}{2}}\left\{X^i_{c,c+1}, W_{\mathsf{v}}\right\} + \frac{\alpha_{\mathsf{v}'}}{\sin\frac{m}{2}}\left\{X^i_{c,c+1}, W_{\mathsf{v}'}\right\} \\
&= \alpha_{\mathsf{v}}\,(u^c_{\mathsf{v}})^i - \alpha_{\mathsf{v}'}\,(u^c_{\mathsf{v}'})^i\,,
\end{aligned} \tag{7.106}$$

[7]Note however that in 4d gravity where the spatial topology is S^3, an arbitrary graph generally becomes knotted when embedded, so that one should take the cellular space as fundamental.

where the α_{v} are normalization constants given by (7.85). A flux is the relative distance between two vertices, and as one might expect, the equation of motion is the difference between the equations of motion for the endpoints.

The picture of dynamics here appears here as a time dependant triangulation Δ_t within which the graph Γ has been embedded. Given some initial triangulation Δ_0, the triangulation at some later time is given by a diffeomorphism $\Delta_t = \Phi_t(\Delta_0)$. As we did for the continuous fields, we can again rely on the evolution of the triangulation to help us define a dynamics for the variables $(h_\ell, \boldsymbol{X}_\ell)$. Each set of three fluxes $\boldsymbol{X}_\ell$ for all $\ell \ni \mathsf{n}$ at the intersection of a common node define a triangle, and the equations of motion define how this cell evolves via Φ_t. Now, we have not (yet) defined the graph to be dynamical, which means that the evolution of Δ_t immediately moves nodes off of the centroids. If the graph does not evolve with the triangulation, this will eventually result in nodes of Γ crossing edges of Δ_t, and links of Γ losing their one-to-one correspondence with edges of Δ_t. What we need is dynamical embedding that preserves the duality between Γ and Δ_t. Given some initial holonomy-flux data on a Γ_0 that is dual to Δ_0 with a node at each centroid, we use the flux equations of motion to find the triangulation Δ_t at time t, and choose the dual graph with a node at the new location of each centroid $\Gamma_t = \Phi_t(\Gamma_0)$. In this way, the loop gravity dynamics $U_{\Gamma\Gamma'}(t)$ appears as a dynamical embedding of a graph within a dynamical triangulation.

$$\begin{array}{ccc} \mathcal{C}_{\Gamma^*} & \xrightarrow{U(t)} & \mathcal{C}_{\Gamma^*} \\ \Big\downarrow \mathcal{I}_\Gamma & & \Big\downarrow \mathcal{I}_{\Gamma'} \\ P_\Gamma & \xrightarrow{U_{\Gamma\Gamma'}(t)} & P_{\Gamma'} \end{array}$$

where $U(t)$ was defined above for the fields on the triangulation in (7.86). If we know the bump functions and rotation parameters on the triangulation, we can invert the maps $\mathcal{I}$ to define the dynamics between graph phase spaces::

$$U_{\Gamma\Gamma'}(t) := \mathcal{I}_{\Gamma'}\ U(t)\ \mathcal{T}_{\Gamma, f_{\mathsf{r}}, \boldsymbol{P}_{\mathsf{r}}}. \tag{7.107}$$

With this definition, the discrete dynamics agrees precisely with the continuous picture in the triangulation. As we shall soon see, we can also incorporate the discrete transitions associated to graph changes.

7.6.1 Discrete transitions of the graph

When we looked at the dynamics of the triangulation, we found that a bistellar flip occurs whenever a vertex moved onto an edge. In terms of fluxes, this happens whenever the fluxes associated to a single node become parallel ($[\boldsymbol{X}_\ell, \boldsymbol{X}_{\ell'}] = 0$). We need to find the corresponding rules which describe this transition in terms of P^G_Γ phase spaces. These follow directly from the definitions we gave for the triangulation.

A bistellar flip in the triangulation corresponds to a two-to-two Pachner move on dual the graph. Consider the holonomies as labeled in fig. 7.6, under the transition that occurs when

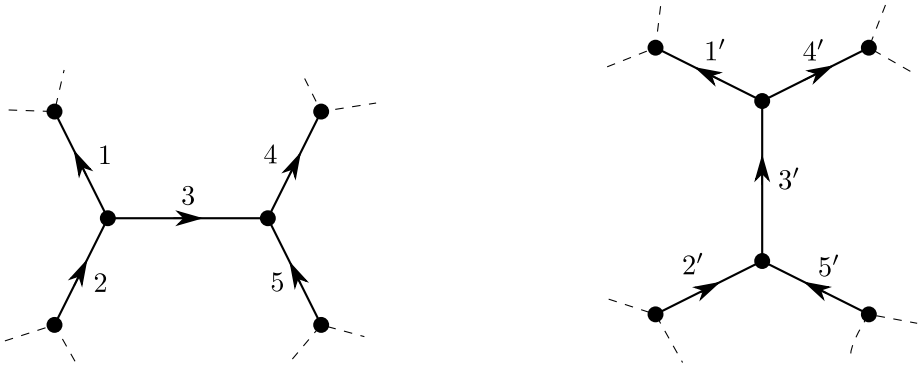

(a) Before (b) After

Figure 7.6: Before and after a discrete transition in the graph known as a two-to-two Pachner move. The links are each labeled with a number.

triangle $(\boldsymbol{X}_1, \boldsymbol{X}_2^{-1}, \boldsymbol{X}_3)$ become parallel. This is dual to the transition shown in (7.4) that we discussed above for the triangulation. In order for a consistent duality between the pictures we have for the holonomies that:

$$h_{1'} = h_3^{-1} h_1, \qquad h_{2'} = h_2 h_3, \qquad h_{3'} = \mathbb{1}, \qquad h_{4'} = h_4, \qquad h_{5'} = h_5. \tag{7.108}$$

This definition preserves the holonomies around particles $h_{\partial \mathsf{o}_\mathsf{v}, n_c}$ for each node except the two which are attached to ℓ_3. These nodes are replaced by new nodes that are dual to the new triangles. For the fluxes we have:

$$\boldsymbol{X}_{1'} = h_3^{-1} \boldsymbol{X}_1 h_3, \qquad \boldsymbol{X}_{2'}^{-1} = h_3^{-1} \boldsymbol{X}_2^{-1} h_3, \qquad \boldsymbol{X}_{4'} = \boldsymbol{X}_4, \qquad \boldsymbol{X}_{5'} = \boldsymbol{X}_5. \tag{7.109}$$

In order to determine $\boldsymbol{X}_{3'}$ we use the closure constraint, taking orientations into account:

$$\boldsymbol{X}_{3'} = -\boldsymbol{X}_{2'}^{-1} - \boldsymbol{X}_{5'}^{-1} = -h_3^{-1} \boldsymbol{X}_2^{-1} h_3 - \boldsymbol{X}_5^{-1}. \tag{7.110}$$

One can check that all of the relationships (7.93, 7.97) remain consistent under this transition.

This transition takes us from the phase space associated to the graph Γ, to a different phase space associated to a new graph Γ'. However, the number of degrees of freedom are preserved, and this transition is a canonical transformation. We can check to see that the new variables satisfy the Poisson algebra of $T^*(\mathrm{SU}(2))$. Let us check explicitly for $h_{1'}$ and $\boldsymbol{X}_{1'}$ as an example. We have trivially that:

$$\{h_{1'}, h_{1'}\} = 0. \tag{7.111}$$

For the fluxes we find:

$$\begin{aligned} \{\boldsymbol{X}_{1'}, \boldsymbol{X}_{1'}\} &= \left\{h_3^{-1} \boldsymbol{X}_1 h_3, h_3^{-1} \boldsymbol{X}_1 h_3\right\} \\ &= h_3^{-1} [\boldsymbol{X}_1, \boldsymbol{X}_1] h_3 \\ &= [\boldsymbol{X}_{1'}, \boldsymbol{X}_{1'}], \end{aligned} \tag{7.112}$$

as desired, and the final bracket also checks out:

$$\begin{aligned}\left\{X^i_{1'}, h_{1'}\right\} &= R(h_3)^i_j \left\{\boldsymbol{X}^j_1, h_3^{-1}h_1\right\} \\ &= -R(h_3)^i_j h_3^{-1}\boldsymbol{\tau}^j h_1 \\ &= -\boldsymbol{\tau}^i h_3^{-1} h_1 \\ &= -\boldsymbol{\tau}^i h_{1'} \end{aligned} \tag{7.113}$$

Note that the holonomy $h_{3'}$ is not given in terms of holonomies on the 'before' graph, but has been assigned to the identity. Because of this, we cannot use the 'before' Poisson brackets to define the 'after' Poisson brackets for this link. We must assign the $T*(SU(2))$ algebra to the variables on link $\ell_{3'}$ in order to be consistent with the mapping from the continuous fields $(\boldsymbol{A}, \boldsymbol{e})$. With this definition, we then have that this transition is a canonical transformation between the variables in P^G_Γ, to the variables parameterizing $P^G_{\Gamma'}$ on a new graph.

In the loop gravity picture, we see dynamics in terms of changes in the flux associated to the relative distances between particles. This is not amenable to a description of particle scattering in terms of trajectories. However, the action of the braid group is easily given in terms of the holonomies h_ℓ associated to the links on the graph, so the discussion of braiding given above for the continuous phase space applies here as well.

We have found a dynamics in terms of holonomies and fluxes on a graph Γ_t that is consistent with the evolution of the dual triangulation Σ_t. We define the graph Γ_t according to a dynamical embedding which keeps nodes of the graph on top of centroids in Σ_t and preserves the duality between them. The flux dynamics dictate how the triangulation moves, and tells us how the graph changes when a triangle in the dual collapses. This causes a change of phase space at the instant of the transition, as the change in the triangulation tells us how the graph changes $\Gamma_t \to \Gamma'_t$. These discrete changes are two-to-two Pachner moves which preserve the number of links on the graph, and therefore also preserves the dimension of the phase space. This is expected since the only degrees of freedom in the system are the singular configurations of the gravitational field (i.e. particle degrees of freedom), and if the number of particles do not change than the dimension of phase space should not change either.

7.7 Conclusion

Point particles in 2+1 dimensional Riemannian gravity make a nice test theory for loop classical gravity. This chapter serves an example for what we have accomplished, and would like to accomplish, within a 3+1 dimensional theory of pure gravity. The continuous phase space is given by a connection and frame-field $(\boldsymbol{A}, \boldsymbol{e}) \in \mathcal{P}$, each taking values in $\mathfrak{su}(2)$. There is a flatness constraint that arises naturally from the Hamiltonian decomposition of the action, which restricts the curvature $\boldsymbol{F}(\boldsymbol{A})(x) = 0$ for all $x \neq \Gamma^*$. Point particles reside at the locations $\mathsf{v} \in \Gamma^*$ where curvature is supported. In addition to the flatness constraint, there is a Gauss constraint, which on the 2d hypersurface is equivalent to a zero-torsion condition. We showed explicitly the gauge fixing procedure of Dirac, which selects a representative geometry $(\bar{\boldsymbol{A}}, \bar{\boldsymbol{e}})$ that obeys the constraints, and allows us to solve for the Lagrange multipliers. The geometry

defined by the gauge choice is the 2d analog of spinning geometries, which also have $\boldsymbol{F}(\boldsymbol{A}) = \mathrm{d}_A \boldsymbol{e} = 0$ everywhere within the cells.

After the gauge-fixing procedure, we are left with a reduced Hamiltonian given by a sum of mass shell constraints, determined by holonomies around the particles. The reduced Hamiltonian can be written in terms of a position and momentum $(\boldsymbol{q}^c_{\mathsf{v}}, \boldsymbol{p}^c_{\mathsf{v}})$ for each vertex v and each frame c which contains the vertex, modulo identifications for the various cells intersecting at a single vertex. This allows us to describe the dynamics in terms of an evolving triangulation, where the fields $(\bar{\boldsymbol{A}}, \bar{\boldsymbol{e}})$ move along with triangulation. We are able to define how the geometry changes even under bistellar flips in the triangulation. On the other hand, we used the isomorphism between P^G_Γ and the reduced phase space $\mathcal{P}^G_{\Gamma^*}$ to study this in terms of the holonomies and fluxes on a graph. We were able to use the holonomy-flux equations of motion to define the evolution of the triangulation, and keeping this dual picture in mind allowed us to define a dynamical embedding of the graph Γ_t. This allowed us to define discrete transitions on the graph, and using the dynamical triangulation we developed the loop gravity dynamics to correspond exactly with the continuous picture. The result is a theory in terms of holonomies and fluxes on a graph, that agrees with the continuous evolution of a finite number of degrees of freedom, and is well-suited for quantization via loop quantum gravity techniques. This is what we would like to accomplish in the full theory of gravity. A discussion of which aspects we expect to carry over will be given in the next and final chapter.

Chapter 8

Summary

The quantization of gravity has proven to be a formidable task as we have been working on this problem now for nearly a century. Early attempts along the lines of canonical quantization were pursued by Bergmann, Dirac and others. A key challenge facing this approach was the development of a Hamiltonian theory for gravity, and time is not easily separated from space in general relativity. It was a great success when Arnowitt, Deser and Misner managed this feat in the late fifties, painting gravity in terms of a spatial geometry q_{ab} and its conjugate momentum π^{ab} (closely linked with extrinsic curvature) evolving in time, This presented the opportunity to apply a canonical quantization to gravity. Wheeler and DeWitt developed a formal equation for the dynamics of quantum gravity, but unfortunately in terms of (q_{ab}, π^{ab}) this equation is intractable and little progress was made toward finding solutions.

New life was breathed into the canonical approach when Ashtekar introduced new variables for gravity in 1986. This cast general relativity as a Yang-Mills type gauge theory written in terms of a connection $\boldsymbol{A}$ and an electric field $\boldsymbol{E}$. This allowed for kinematical solutions in terms of Wilson loops, and 'loop' quantum gravity was born. In the years since, loop quantum gravity has made many advances toward the quantization of gravity and stands as one of the leading candidates for a consistent theory. Yet, difficult problems remain. Perhaps the most challenging of these is to formulate a dynamics and prove that it is consistent with general relativity in the appropriate limits.

The continuous, kinematical Hilbert space of loop quantum gravity is built upon a projective family of spaces $\mathcal{H}_\Gamma$, each associated to a different graph Γ that is embedded within a spatial geometry. The key idea behind this thesis is that there are two steps in getting to the quantum theory from the classical one: first, the embedded graphs are used to define one- and two-dimensional surfaces upon which the continuous phase space variables $(\boldsymbol{A}, \boldsymbol{E}) \in \mathcal{P}$ are integrated, giving a holonomy and a flux $(h_\ell, \boldsymbol{X}_\ell) \in P_\Gamma$ for each link $\ell \in \Gamma$; second, this phase space P_Γ is quantized to yield a finite-dimensional Hilbert space $\mathcal{H}_\Gamma$. Little is known about the intermediate, classical theory suggested by the P_Γ phase spaces, and learning more about this classical side of loop gravity would be a great help for developing the quantum theory. The previous sentence is our motivation.

Similarly to the continuous Hilbert space structure, a continuous phase space is obtained by taking the projective limit of graph phase spaces P_Γ. We want to find a way to describe gravity

in terms of holonomies and fluxes in the projective family of phase spaces associated to graphs. We want to know what kind of continuous geometry can be described by the holonomy-flux data on a graph. We want to use this geometrical description as a bridge to general relativity, and rely on this relationship to develop a classical dynamics for gravity in terms of the projective family of P_Γ phase spaces. If this can be achieved, then we will have a theory of gravity based upon a collection of finite-dimensional phase spaces, perfectly suited for quantization by the well-established methods of loop quantum gravity. And moreover, this theory would be consistent with general relativity by construction.

8.1 What we have accomplished

We began from the Einstein action, first reviewing the ADM formalism in order to set up a canonical transformation to the Ashtekar variables, demonstrating the connection between these two canonical descriptions of gravity. We defined the basic elements of loop quantum gravity, and then took a step back to introduce the classical phase space structure which underlies the Hilbert space operators and states.

With the basic framework established, we used a graph embedded within a dual cellular space to develop the connection between the kinematics of loop gravity and the kinematics of general relativity. We were able to find a symplectic reduction of the continuous phase space $\mathcal{P}$ by a family of flatness constraints $\mathcal{F}_{\Gamma^*}$ permitting curvature only on the one-skeleton Γ^* of a cellular space, and a Gauss constraint imposed everywhere except the nodes of the dual embedded graph Γ. The reduced phase space $\mathcal{P}_{\Gamma,\Gamma^*}$ was shown to be symplectomorphic to the discrete phase space P_Γ defined on the graph. What this result implies is that for any set of holonomy-flux data on a graph Γ representing a point in $p \in P_\Gamma$, there exists an equivalence class of continuous geometries defined by fields $(\boldsymbol{A}, \boldsymbol{E})$ which each map to the same point $p \in P_\Gamma$. Furthermore, the symplectomorphism applies also to the case where the continuous Gauss constraint is imposed everywhere in the continuous geometry, and the discrete Gauss constraint is imposed in the holonomy-flux phase space, i.e. $\mathcal{P}^G_{\Gamma^*} \cong P^G_\Gamma$.

We took special interest in a particular member of the equivalence class of geometries associated to a point in the SU(2)-gauge invariant phase space $\mathcal{P}^G_{\Gamma^*}$. This member is a spinning geometry, defined such that the curvature $\boldsymbol{F}(\boldsymbol{A})$ and torsion $\mathrm{d}_A \boldsymbol{e}$ both vanish within each cell, and have support only on the edges of Γ^*. We found that the edge shapes are necessarily helices, and that the holonomy-flux data serves to fix the helix parameters for each edge. Spinning geometries have the desirable feature of simplifying the scalar constraint of the continuous theory, causing it to vanish everywhere except the helical edges. Given a spinning geometry as initial data, this implies that along a dual link ℓ the curvature will remain zero for a finite time, and the holonomy along this link will remain constant for this time[1]. The flux on a face f of a spinning geometry is given entirely by the fields along the edges $\mathsf{e} \in \partial\mathsf{f}$, and having a dynamics supported on these edges is much more simple than having to consider the evolution of fields over the entire face. All of this suggests that the discrete dynamics can be formulated by relying upon the continuous evolution of spinning geometries, helping us to find a dynamics

[1] A discrete graph change would be required once the curvature becomes non-zero somewhere on the link.

for loop gravity that is consistent with that of general relativity.

In working within the projective family (recall the last paragraph of section 3.2, and see [24]) of graph phase spaces, we need to understand how to formulate a dynamics between different phase spaces P_Γ and $P_{\Gamma'}$ that may have different dimension, and how the dynamics on these finite-dimensional, truncated phase spaces relates to the continuous evolution. There is a geometrical description of phase spaces where dynamics is present as a class of subspaces within a symplectic manifold. We used this picture to help us formulate a dynamics between truncated phase spaces, and we demonstrated how this works on a simple model which mimics the case of full gravity. The continuous model is that of a conjugate pair of fields (A, E) on the circle, and the discrete picture is obtained by imposing that $\partial_x A = 0$ everywhere except a finite set of points $\mathsf{v} \in \Gamma^*$. The reduced phase space P_Γ is parameterized by a pair $(h_\mathsf{n}, X_\mathsf{n})$ on a dual set of points $\mathsf{n} \in \Gamma$ embedded between the points of Γ^*. To represent the discrete data in the continuous theory, we found a good gauge choice of fields $(\bar{A}, \bar{E})$ which satisfy $\partial_x A(x) = \partial_x E(x) = 0$ for all points $x \ni \Gamma^*$. This allowed us to formulate a dynamics $L_t^{\Gamma\Gamma'}$ between discrete phase spaces, and we showed that the full continuous dynamics L_t can be reconstructed from the truncated dynamics, at least formally, owing to the fact that the continuous phase space is contained within the projective limit $\lim_{\Gamma\to\infty} P_\Gamma$. An interesting feature here was a preferred truncation. The continuous dynamics is equivalent to a diffeomorphism Φ_t which shifts the points $x \to x+t$. Given initial data on Γ, our definition of dynamics is to map to fields $(\bar{A}(x,0), \bar{E}(x,0))$ and evolve using the continuous Hamiltonian for a time t. At this time, one truncates down again to a phase space $P_{\Gamma'}$, and if the shifted graph $\Gamma' = \Phi_t(\Gamma)$ is used, the truncation respects the profile of the data $(\bar{A}(x,t), \bar{E}(x,t))$. This preferred truncation is the inverse of the gauge choice, so one can repeatedly map back and forth between the discrete and continuous frameworks according to this choice without disturbing the data.

There is a model of gravity which naturally possesses a curvature which is non-vanishing only upon a discrete set of points Γ^* on a two-dimensional spatial hypersurface. This is the case of point particles in 3d gravity, which we studied on hypersurfaces that are topologically equivalent to S^2 with punctures, embedded within a Riemannian 'spacetime'. The Riemannian choice was made so that the relevant gauge group is SU(2) as in 4d Lorentzian gravity. This system makes an ideal model for applying the entire program of loop classical gravity. We began from an action and developed the classical Hamiltonian theory, showing that it can be described by an evolving triangulation with particles residing at the vertices. It can happen that a particle moves onto an edge so that one triangle disappears and another is split into two, a process described by a bistellar flip. The underlying spatial manifold is the 2d analog of a regular 3d cellular space as we have defined it. Using this, we gave an explicit example of the mapping between the continuous phase space $(\boldsymbol{A}, \boldsymbol{E}) \in \mathcal{P}^G_{\Gamma^*}$ and the discrete phase space $(h_\ell, \boldsymbol{X}_\ell) \in P^G_\Gamma$. Relying on this correspondence allowed us to define a dynamics that is consistent with the evolution of the triangulation. This requires us to use a dynamical embedding of the graph where the nodes of the graph stay at the centroids of the triangles as the triangles change shape. With this idea, we were able to define a discrete two-to-two transition of the graph that mirrors the bistellar flip. Particle masses are determined by holonomies which loop around them, and these are neatly described by the holonomies on a graph. The discrete transitions preserve the number of particles, and maintain the dimension of the graph phase spaces, although the graph

itself is changed. In this way we found a consistent transition between different phase spaces of the projective family. It is exciting that we have been able to achieve a description of this gravitational system using the loop gravity phase space. However, the jump up in dimension to the 4d theory is likely to introduce some difficult new and difficult challenges.

8.2 What remains to be done

On the kinematical side, spinning geometries make a promising candidate for a continuous representation of the discrete holonomy-flux data associated to a graph. We know that the edges of these geometries are helices, and we have uncovered how to map to these helices from the holonomies and fluxes. There is more work to be done here on how to consistently glue together the cells of the spinning geometry. We need to know how the entire network of helices in Γ^* is joined together, and we would like to have a better understanding of the gluing maps between faces. However, since the fluxes in this gauge are determined entirely by the edge geometry and the scalar constraint is supported only along these edges, perhaps an existence proof for the face maps is sufficient since the faces do not play a role in determining the holonomy-flux data or the dynamics.

In the point particle model, the masses are defined entirely by the holonomies on a graph. What will the holonomies tell us in 4d gravity? There is a non-Abelian Stokes theorem [96] which uses an ordered two-dimensional integral of the curvature, and relates it to the holonomy around the boundary. Using this, the fundamental loops on a graph give us a number of holonomies which will tell us about the curvature inside the loop. Perhaps this can lead to a formulation of quasilocal energy in terms of the holonomy-flux data on a graph?

For the dynamics, we have identified two main challenges and proposed a program that is capable of overcoming these hurdles. One issue is to find a suitable gauge choice which allows us to derive a discrete generator of dynamics written in terms of holonomies and fluxes. The 1d and 2d analogs of spinning geometries were applied within the models we studied to successfully achieve this goal. Since the 3d scalar constraint is drastically simplified in the spinning geometry gauge, this seems to be an achievable goal for (3+1)d gravity as well. In the models, we found that dynamics was described by an evolution in the cell shapes. There is a good indication that this feature will carry over into the 4d theory, since applying the spinning geometry gauge choice to the continuous scalar constraint gives us holonomies as constants of motion, and fluxes which evolve only at the edges. Now, in our simple models, we were able to find a preferred truncation which preserved all of the information of the evolution so that nothing is lost in the truncation. However, in 4d gravity the dynamics for one-dimensional defects will lead to a dispersion of this curvature so that we do not expect a preferred truncation to exist. We will need to find a way to describe the dynamics using multiple truncations, i.e. we will need to understand how to use a collection $\left(L_t^{\Gamma\Gamma'_1}, L_t^{\Gamma\Gamma'_2}, \cdots\right)$ to evolve the data on some initial graph Γ. We anticipate that having curvature localized around the edges will help make this a tractable problem.

Another issue we face is how to evolve between phase spaces associated to different graphs with generally different dimension, so that we can use the $L_t^{\Gamma\Gamma'}$ for any initial Γ and final Γ' to reconstruct the full dynamics L_t from a collection of truncated dynamics. We have provided a

definition of this which applies also to the case of full gravity, and we showed that this works on a simple 2d dimensional model. Since the continuous phase space is contained within the projective limit of P_Γ phase spaces, this reconstruction appears to be possible. In the 3d model of point particles, we encountered graph changes which occur whenever one of the triangular cells in the dual collapsed to zero area. Graph changes are an expected feature of 4d gravity. It seems reasonable that the dynamics of a spinning geometry will lead to situations where a face collapses and changes the topology of the cells which share this face. We may also see that cells collapse, and new cells must be created for consistency. These scenarios would lead to changes of the graph, and we can rely on the geometrical picture to help us find a consistent set of rules for how to change the graph and redefine the holonomies and fluxes.

We have established a solid foundation for the classical theory which underlies loop quantum gravity, and learning more about this will give us insight into how to approach the difficulties we face with dynamics in the quantum theory. Indeed, many of most difficult problems pertain to the truncation rather than the quantization. Studying classical loop gravity is a 'divide and conquer' approach, which allows us to tackle the truncation issues while setting aside the quantization issues. The classical kinematics is becoming clear, and we have a program for the dynamics with many hints that it can be applied to the full theory.

I find this approach to be the natural progression from general relativity toward the quantum theory. The transition from the Ashtekar formulation to loop quantum gravity has perhaps been too big of a jump, and the program we have begun to develop here aims to fill in the missing steps. If general relativity can be described in terms of the projective family of phase spaces P_Γ, then this would be an incredible result, not just for the loop community but for physics as a whole. We would have a classical theory of gravity defined in finite-dimensional phase spaces, and we already know how to quantize these! If a loop classical gravity that is consistent with general relativity can be obtained, then several of the most challenging problems facing loop quantum gravity would be addressed, and a fully consistent quantum theory of gravity may be just around the corner.

Appendix A

Appendix

A.1 Animation of 1+1 Dimensional Model

This appendix is an animation of the evolution of discrete h_{n} data in the 1+1 dimensional model discussed in chapter 6. The initial data is a Gaussian profile defined on a closed 1d lattice with 64 points. The animation was generated using Maple, and the file name is animation.gif.

If you accessed this thesis from a source other than the University of Waterloo, you may not have access to this file. You may access it by searching for this thesis at `http://uwspace.uwaterloo.ca` .

A.2 Holonomy around a particle

In this appendix we review some relevant properties of holonomies and derive an expression for the holonomy around the particle boundary $\mathcal{B}$, dropping the v subscript since we shall consider only a single particle. Recall that a particle worldline in spacetime possesses a boundary which is topologically equivalent to a cylinder; the boundary $\mathcal{B}$ as the intersection between this cylinder and the spatial hypersurface Σ.

The geometric meaning associated to a holonomy $h_\gamma \in \mathrm{SU}(2)$ is the parallel transport of a vector along a path in spacetime. Recall that an element $\boldsymbol{\xi} \in \mathfrak{su}(2)$ is associated with a vector through the identification $\xi^i = -2\mathrm{Tr}(\boldsymbol{\xi}\boldsymbol{\tau}^i)$. Under parallel transport along a curve γ, the vector transforms as:

$$\boldsymbol{\xi} \to h_\gamma \boldsymbol{\xi} h_\gamma^{-1}. \tag{A.1}$$

We may parameterize a path (that does not intersect itself) as $\gamma(s)$, where s takes values over the interval $[0,1]$:

$$\begin{aligned} \gamma : [0,1] &\to M \\ s &\mapsto x^\mu(s) \end{aligned} \tag{A.2}$$

The beginning of the curve is $\gamma(0)$ and the end of the curve is $\gamma(1)$. The holonomy along this

path is defined as:

$$\begin{aligned} h_\gamma[\boldsymbol{A}] &:= \overrightarrow{\exp}\int_0^1 \mathrm{d}s\dot{\gamma}(s)^\mu A(s)^i_\mu \boldsymbol{\tau^i} \equiv \overrightarrow{\exp}\int_\gamma \boldsymbol{A} \\ &:= \sum_{n=0}^{\infty}\int_0^1 \mathrm{d}s_1\int_0^{s_1}\mathrm{d}s_2\cdots\int_0^{s_{n-1}}\mathrm{d}s_n \boldsymbol{A}\left(\gamma(s_n)\right)\cdots\boldsymbol{A}\left(\gamma(s_1)\right), \end{aligned} \tag{A.3}$$

where $\dot{\gamma}(s)^\mu = \frac{\partial\gamma(s)^\mu}{\partial s}$ is a vector tangent to the curve. Under SU(2)-gauge transformations, the holonomy transforms as:

$$h_\gamma \to g_{\gamma(0)} h_\gamma g^{-1}_{\gamma(1)}, \tag{A.4}$$

where $g(x) \in \mathrm{SU}(2)$.

Path-ordering is required in the definition since the connection generally does not commute with itself at different points, so two choices of path, say γ and γ', will generally lead to different results ($h_\gamma \neq h_{\gamma'}$) even if the endpoints remain the same ($\gamma(0) = \gamma'(0)$ and $\gamma(1) = \gamma'(1)$). However, when the curvature is zero ($\boldsymbol{F}(\boldsymbol{A}) = 0$) the holonomy depends upon its endpoints only:

$$h_\gamma = h_{\gamma'} = g_{\gamma(0)} h_\gamma g^{-1}_{\gamma(1)}, \tag{A.5}$$

so long as γ and γ' are not closed loops, and are in the same homotopy class, i.e. one curve can be deformed smoothly into the other without crossing any topological defects in M such as particle worldlines.

Now that we have established the necessary properties of holonomies, let us look at the case of a holonomy which follows a path around a particle. Consider a single particle with mass m in the spacetime M, at rest at the origin of a cylindrical coordinate system (t, r, ϕ). The metric for this spacetime is given by [83]:

$$\mathrm{d}s^2 = \mathrm{d}t^2 + \mathrm{d}r^2 + (1 - \frac{m}{2\pi})\mathrm{d}\phi^2. \tag{A.6}$$

This can be related to (the Riemannian analog of) a Minkowski spacetime through the transformation $\theta = (1 - m/2\pi)\phi$. While the coordinate ϕ has the identification $\phi = \phi + 2\pi$, the Minkowski coordinate has the identification $\theta = \theta + 2\pi - m$. This implies that a two-surface which intersects the worldline transversely has the geometry of a cone with a deficit angle given by the particle mass.

A frame-field[1] and connection describing the above metric is given by:

$$\boldsymbol{e} = \boldsymbol{\tau}^0\mathrm{d}t + \left(\cos\phi\boldsymbol{\tau}^1 + \sin\phi\boldsymbol{\tau}^2\right)\mathrm{d}r + r\left(1 - \frac{m}{2\pi}\right)\left(\cos\phi\boldsymbol{\tau}^2 - \sin\phi\boldsymbol{\tau}^1\right)\mathrm{d}\phi, \tag{A.7}$$

$$\boldsymbol{A} = -\frac{m}{2\pi}\boldsymbol{\tau}^0\mathrm{d}\phi = -\frac{1}{2\pi}\boldsymbol{p}\mathrm{d}\phi. \tag{A.8}$$

The particle is moving in the direction $\boldsymbol{u} = \boldsymbol{\tau}^0$ and has a momentum of $\boldsymbol{p} = m\boldsymbol{\tau}^0$. One can check that these fields satisfy $\boldsymbol{F} = \boldsymbol{G} = 0$, remembering that we have excised the particle world

[1]The metric is given in terms of the frame-field by $e^i_\mu e^i_\nu$.

line[2]. From now on, we take the path γ to be a circular loop around the particle worldline at some fixed values of r and t, with a base-point at $b = \gamma(0) = \gamma(1)$. The holonomy $h_{\gamma,b}$ is easy to calculate since the frame field commutes with itself (making path-ordering irrelevant):

$$h_{\gamma,b} = \exp - \int_0^{2\pi} \frac{1}{2\pi} \boldsymbol{p} \mathrm{d}\phi = e^{-\boldsymbol{p}}. \tag{A.9}$$

Here the result does not depend on the base-point, but we include it in the notation since the general result will depend on b.

Since the connection is flat outside of the particle worldline, this result is the same for any smooth deformation of γ that leaves the base-point fixed. To find the holonomy around the particle boundary, we define a path which begins at b, goes along a path π of constant ϕ until it reaches the boundary at point b', circles the boundary $\mathcal{B}$ once, then returns from b' along π back to the base-point b. This path is a smooth deformation of γ which leaves the endpoints fixed, so we have:

$$h_{\gamma,b} = h_\pi(b,b') h_{\mathcal{B},b'} h_\pi(b,b')^{-1}. \tag{A.10}$$

Since the connection does not depend on the radial coordinate we have $h_\pi(b,b') = \mathbb{1}$, and using (A.9) we have the holonomy around the particle boundary:

$$h_{\mathcal{B},b'} = e^{-\boldsymbol{p}}. \tag{A.11}$$

We have so far considered a particle at rest in the frame defined by the $\boldsymbol{\tau}^i$ basis. We can repeat the calculation for a particle traveling in an arbitrary timelike[3] direction by rotating the direction vector $\boldsymbol{u} \to \tilde{\boldsymbol{u}} = g\boldsymbol{\tau}^0 g^{-1}$ with an element $g \in \mathrm{SU}(2)$. The connection and frame field can then be written in terms of a new basis $\tilde{\boldsymbol{\tau}}^i = g\boldsymbol{\tau}^i g^{-1}$ as:

$$\boldsymbol{e} = \tilde{\boldsymbol{\tau}}^0 \mathrm{d}\tilde{t} + \left(\cos\tilde{\phi}\tilde{\boldsymbol{\tau}}^1 + \sin\tilde{\phi}\tilde{\boldsymbol{\tau}}^2\right)\mathrm{d}\tilde{r} + \tilde{r}\left(1 - \frac{m}{2\pi}\right)\left(\cos\tilde{\phi}\tilde{\boldsymbol{\tau}}^2 - \sin\tilde{\phi}\tilde{\boldsymbol{\tau}}^1\right)\mathrm{d}\tilde{\phi}, \tag{A.12}$$

$$\boldsymbol{A} = -\frac{m}{2\pi}\tilde{\boldsymbol{\tau}}^0 \mathrm{d}\tilde{\phi} = -\frac{1}{2\pi}\tilde{\boldsymbol{p}}\mathrm{d}\tilde{\phi}. \tag{A.13}$$

The coordinate $\tilde{t}$ is associated to the $\tilde{\boldsymbol{u}}$ direction, and $(\tilde{r},\tilde{\phi})$ are polar coordinates for any plane running perpendicular to this. The holonomy associated to a circular loop $\tilde{\gamma}$ at fixed $(\tilde{t},\tilde{r})$ is given by:

$$h_{\tilde{\gamma},\tilde{b}} = e^{-\tilde{\boldsymbol{p}}}. \tag{A.14}$$

We have defined our spatial hypersurfaces Σ to be spanned by $\boldsymbol{\tau}^1$ and $\boldsymbol{\tau}^2$ in the definition of the frame-field (A.7), so the loop $\tilde{\gamma}$ is not contained within Σ, while the particle boundary $\mathcal{B} \in \Sigma$. However, since the connection does not depend on the radial or time coordinates, we

[2]There is a delta function contribution to the curvature if we do not excise the worldline. See the second reference listed in [78].

[3]Nothing in the Riemannian theory is fixing the worldlines to be timelike, however, since the purpose here is to mimic the Lorentzian case we shall adopt these notions.

can deform the curve $\tilde{\gamma}$ while keeping b fixed in a similar manner as done above to find that $h_{\mathcal{B},\tilde{b}'} = e^{-\tilde{\boldsymbol{p}}}$.

There is one further generalization required before we achieve our desired result. We have been using a connection that commutes with itself, but in general the connection may take on different $\mathfrak{su}(2)$-values around the loop encircling the particle. Such fields are related to the above via SU(2)-gauge transformations, which we recall here:

$$\boldsymbol{A} \to g\boldsymbol{A}g^{-1} + g\mathrm{d}g^{-1}, \qquad\qquad \boldsymbol{e} \to g\boldsymbol{e}g^{-1}, \tag{A.15}$$

for an element $g(x) \in \mathrm{SU}(2)$. So, any choice of SU(2)-valued field $g(x)$ will produce a new frame-field and connection also providing a geometry associated to a point particle. Suppose we have calculated in a particular SU(2) gauge that $h_{\mathcal{B},b} = e^{-\boldsymbol{p}}$. Under an SU(2)-gauge transformation (A.4) we obtain:

$$h_{\mathcal{B},b} \to g_b e^{-\boldsymbol{p}} g_b^{-1}. \tag{A.16}$$

The dependence on the choice of gauge and the base-point b is now apparent, and one sees that the particle momentum fixes the holonomy only up to SU(2)-gauge transformations. Each choice of base-point gives a momentum $\boldsymbol{p}_b = m\boldsymbol{u}_b$, where $\boldsymbol{u}_b$ is the axis of rotation for $h_{\mathcal{B},b}$. We can write this general holonomy in a useful form:

$$h_{\mathcal{B},b} = \mathbb{1}\cos\frac{m}{2} - 2\boldsymbol{u}_b \sin\frac{m}{2}. \tag{A.17}$$

A.3 Details in calculating $\{\mathcal{G}(\lambda), \psi_{\mathsf{v}}\}$

In this appendix we give a detailed calculation of the Poisson bracket $\{\mathcal{G}(\lambda), \psi\}$ between the mass shell and Gauss constraints. For notational convenience we consider the case of a single particle and drop the v subscript. The generalization to many particles follows simply.

From the constraint definitions (7.4), (7.19) we write:

$$\{\mathcal{G}(\lambda), \psi\} = \left\{ \int_\Sigma \lambda(x)^i \left(\mathrm{d}e(x)^i + \epsilon^{ijk} A^j \wedge e^k \right), 2\cos^{-1}\frac{W}{2} - m \right\}. \tag{A.18}$$

Integrating by parts on the left side of the bracket, and taking the derivative with respect to W on the right side of the bracket, we obtain:

$$\{\mathcal{G}(\lambda), \psi\} = \left\{ \int_{\mathcal{B}_o} \lambda^i e^i - \int_{\mathcal{B}} \lambda^i e^i - \int_\Sigma e^i \left(\mathrm{d}\lambda^i + \epsilon^{ijk} A^j \lambda^k \right), W \right\} \left(\frac{-1}{\sqrt{1 - \left(\frac{W}{2}\right)^2}} \right). \tag{A.19}$$

Since the Wilson loop is around the inner boundary, the Poisson bracket involving outer-boundary term vanishes. Using index notation, we write:

$$\{\mathcal{G}(\lambda), \psi\} = \frac{1}{\sin\frac{m}{2}} \left(\int_{\mathcal{B}} \mathrm{d}s \lambda^i \dot{\mathcal{B}}^b + \int_\Sigma \mathrm{d}x^2 \epsilon^{ab} \left(\partial_a \lambda^i + \epsilon^{ijk} A_a^j \lambda^k \right) \right) \{ e_b^i, \mathrm{Tr} h_{\mathcal{B},b} \} \tag{A.20}$$

where $\dot{\mathcal{B}}^b \equiv \partial \mathcal{B}^b / \partial s$ and we used that $W = \mathrm{Tr} h_{\mathcal{B},b} = 2\cos(m/2)$ as shown in (7.18).

In order to evaluate the Poisson bracket between the frame-field and the Wilson loop, we will need to know the bracket between the frame field and the holonomy around $\mathcal{B}$ with base-point b. We write this holonomy as:

$$h_{\mathcal{B},b} = \overrightarrow{\exp} \oint_{\mathcal{B}} \mathrm{d}s \dot{\mathcal{B}}(s)^c A(s)^i_c \boldsymbol{\tau}^i, \tag{A.21}$$

The Poisson bracket of $\boldsymbol{e}(x)$ with $\boldsymbol{A}(y)$ is non-zero only where $x = y$. This splits the holonomy into two:

$$\left\{ e(x)^i_b, h_{\mathcal{B},b} \right\} = h_{\mathcal{B}}(b,x) \boldsymbol{\tau}^i h_{\mathcal{B}}(x,b) \oint_{\mathcal{B}} \mathrm{d}s \epsilon_{bc} \dot{\mathcal{B}}(s)^c \delta^2 \left(\mathcal{B}(s), x \right), \tag{A.22}$$

where $h_{\mathcal{B}}(b,x)$ is the holonomy along $\mathcal{B}$ from the base point b of the loop to the point x, and $h_{\mathcal{B}}(x,b)$ is the holonomy along the remainder of the loop, from the point x to the base point b[4].

We substitute this into (A.20) to obtain:

$$\begin{aligned} \{\mathcal{G}(\lambda), \psi\} &= \frac{1}{\sin \frac{m}{2}} \left(\int_{\mathcal{B}} \mathrm{d}s \lambda^i \dot{\mathcal{B}}^b + \int_\Sigma \mathrm{d}x^2 \epsilon^{ab} \left(\partial_a \lambda^i + \epsilon^{ijk} A^j_a \lambda^k \right) \right) \\ &\quad \times \mathrm{Tr}(h_{\mathcal{B},x} \boldsymbol{\tau}^i) \oint_{\mathcal{B}} \mathrm{d}s \epsilon_{bc} \dot{\mathcal{B}}(s)^c \delta^2 \left(\mathcal{B}(s), x \right), \end{aligned} \tag{A.25}$$

where we used that $h_{\mathcal{B}}(x,b) h_{\mathcal{B}}(b,x) = h_{\mathcal{B},x}$ is a holonomy around the loop $\mathcal{B}$ with base-point x at the point of integration. The first term is zero by symmetry, and using (A.17) we finally obtain:

$$\{\mathcal{G}(\lambda), \psi\} = 2 \oint_{\mathcal{B}} \mathrm{Tr} \left(g(x) \boldsymbol{u} g(x)^{-1} \tau^i \right) (\mathrm{d}_A \lambda(x)^i). \tag{A.26}$$

[4]In the case of $x \to b$ there is ambiguity in this Poisson bracket. As x approaches the base-point at the beginning of the loop we have:

$$\lim_{x \to b^+} h_{\mathcal{B}}(b,x) = \mathbb{1}, \qquad \lim_{x \to b^+} h_{\mathcal{B}}(x,b) = h_{\mathcal{B},b}. \tag{A.23}$$

For the limit taken from the other direction we have:

$$\lim_{x \to b^+} h_{\mathcal{B}}(b,x) = h_{\mathcal{B},b}, \qquad \lim_{x \to b^+} h_{\mathcal{B}}(x,b) = \mathbb{1}. \tag{A.24}$$

By convention we make the first choice. Note that either choice gives the same result under a trace.

Bibliography

[1] C. Rovelli, "The century of the incomplete revolution", J. Math. Phys. 41, 3776 (2000).

[2] C. Kiefer, "Quantum Gravity: General Introduction and Recent Developments", Annalen der Physik, vol. 15, issue 1, 129 (2006).

[3] T. Thiemann, *Modern Canonical Quantum General Relativity*, Cambridge University Press, Cambridge, UK, 2007.

[4] A. Borde, A. H. Guth, and A. Vilenkin, "Inflationary Spacetimes Are Incomplete in Past Directions", Phys. Rev. Lett. 90, 151301 (2003).

[5] S. W. Hawking and R. Penrose, *The nature of Space and Time*, Princeton University Press, Princeton, USA, 1996.

[6] S. Hawking, "Particle Creation by Black Holes", Commun. Math. Phys. vol. 43, 199 (1975).

[7] S.B. Giddings, "Quantum Mechanics of Black Holes", arXiv:hep-th/9412138v1 (1994).

[8] J.D. Bekenstein, "Black Holes and Entropy", Phys. Review D vol. 7, no. 8, 2333 (1973).

[9] S. Hawking "Black Holes and Thermodynamics", Phys. Review D vol. 13, no. 2, 191 (1976).

[10] D. Oriti (ed.) *Approaches to Quantum Gravity: Toward a New Understanding of Space, Time and Matter*, Cambridge University Press, Cambridge, (2009).

[11] J. Polchinski, *String Theory*, Cambridge University Press, Cambridge (1998); M.B. Green, J.H. Schwarz and E. Witten, *Superstring Theory: Introduction*, Cambridge University Press, Cambridge (1988).

[12] C. Rovelli, *Loop Quantum Gravity,* Cambridge University Press, Cambridge (2004).

[13] J. Ambjorn, J. Jurkiewicz and R. Loll, "Causal Dynamical Triangulations and the Quest for Quantum Gravity", `arXiv:1004.0352 [hep-th]` (2010).

[14] R.D. Sorkin, "Causal Sets: Discrete Gravity." In A. Gomberoff and D. Marolf (eds.), *Lectures on Quantum Gravity*, Springer, New York (2005).

[15] A. Connes, *Noncommutative Geometry*, Academic Press, San Diego (1994).

[16] M. Niedermaier and M. Reuter, "The Asymptotic Safety Scenario in Quantum Gravity", Living Rev. Relativity 9, (2006), 5. URL: `http://www.livingreviews.org/lrr-2006-5.`

[17] L. Smolin, "The case for background independence", `arXiv:hep-th/0507235` (2005).

[18] A. Ashtekar, *Lectures on Non-perturbative Canonical Gravity*, World Scientific Publishing Co. Pte. Ltd., Singapore (1991).

[19] P.A.M. Dirac, *Lectures on Quantum Mechanics*, Dover Publications, New York, USA (2001).

[20] R. Arnowitt, S. Deser, C.W. Misner, "The Dynamics of General Relativity", in *Gravitation: an Introduction to Current Research* by L. Witten, ch. 7, pp. 227 (1962).

[21] A. Ashtekar, "New Variables for Classical and Quantum Gravity", Physical Review Letters **57** 18 (1986); J. F. Barbero, "Real Ashtekar variables for Lorentzian signature space-times", Phys. Rev. **D 51** 5507 (1995).

[22] C. Rovelli, "Zakopane lectures on loop gravity", (2011) `arXiv:1102.3660`.

[23] A. Ashtekar and J. Lewandowski, "Background independent quantum gravity: a status report", Class. Quant. Grav. **21** R53 (2004).

[24] A. Ashtekar and J. Lewandowski, "Differential Geometry on the Space of Connections via Graphs and Projective Limits", J. Geom. Phys. **17** (1995); "Projective Techniques and Functional Integration", J. Math. Phys. **36** (1995).

[25] R. Geroch, "The domain of dependence", Math. Phys. 11, 437 (1970).

[26] R. Wald, *General Relativity*, The University of Chicago Press, Chicago, USA (1984).

[27] A. Perez, "Introduction to Loop Quantum Gravity and Spin Foams", arXiv:gr-qc/0409061v3 (2005).

[28] T. Thiemann, "Anomaly-free formulation of non-perturbative, four-dimensional Lorentzian quantum gravity", Phys. Lett. B **380** 257 (1996).

[29] K. Wilson. "Confinement of quarks", Phys. Rev. D **10** 2445 (1974).

[30] B. Bahr, B. Dittrich, F. Hellmann and W. Kaminski, "Holonomy Spin Foam Models: Definition and Coarse Graining", Phys. Rev. D **87**, 044048 (2013).

[31] C. Rovelli and L. Smolin, "Knot Theory and Quantum Gravity", Phys. Rev. Lett. **61** 1155 (1988).

[32] C. Rovelli and L. Smolin, "Spin Networks and Quantum Gravity", Phys. Rev. D **52** 5743 (1995).

[33] A. Ashtekar and J. Lewandowski, "Representation Theory of Analytic Holonomy C* Algebras", in J.C. Baez, J.C. (ed.) *Knots and Quantum Gravity*, Oxford University Press, Oxford (1994).

[34] A. Ashtekar and J. Lewandowski, "Quantum Theory of Geometry I: Area Operators", Class. Quant. Grav. **14** A55 (1997); K. Krasnov, "The Area Spectrum in Quantum Gravity", Class. Quant. Grav. **15** L47 (1998).

[35] C. Rovelli and L. Smolin, "Discreteness of area and volume in quantum gravity", Nucl. Phys. **B442** 593 (1995); Erratum-ibid. **B456** 753 (1995); A. Ashtekar and J. Lewandowski, " Quantum Theory of Geometry II: Volume operators", Adv. Theor. Math. Phys. **1** 388 (1998).

[36] T. Thiemann, "A length operator for canonical quantum gravity", J.Math.Phys. **39** 3372 (1998); E. Bianchi, "The length operator in Loop Quantum Gravity", Nucl. Phys. B **807** 591 (2009); Y. Ma, C. Soo and J. Yang, "New length operator for loop quantum gravity", Phys. Rev. D **81** 124026 (2010).

[37] L. Kauffman, *Knots and Physics*, World Scientific, Singapore (1991).

[38] A. Alekseev, A.P. Polychronakos and M. Smedback, "On area and entropy of a black hole", Phys. Lett. B **574** 296 (2003); A.P. Polychronakos, "Area spectrum and quasinormal modes of black holes", Phys. Rev. D **69** 044010 (2004); G. Gour and V. Suneeta, "Comparison of area spectra in loop quantum gravity", Class. Quant. Grav. **21** 3405 (2004).

[39] E. Bianchi, P. Doná and S. Speziale, "Polyhedra in loop quantum gravity", Phys. Rev. D **83** 044035 (2011).

[40] L. Smolin, "The classical limit and the form of the hamiltonian constraint in nonperturbative quantum gravity", `arXiv:gr-qc/9609034` (1996).

[41] J.C. Baez, "An Introduction to Spin Foam Models of Quantum Gravity and BF Theory", Lect. Notes Phys. **543** 25 (2000); A. Perez, "Spin Foam Models for Quantum Gravity", Class.Quant.Grav. **20** R43 (2003).

[42] T. Regge, "General relativity without coordinates", Nuovo Cim. **19** 558 (1961).

[43] C. Rovelli and S. Speziale, "Geometry of loop quantum gravity on a graph", Phys. Rev. D **82** 044018 (2010).

[44] L. Freidel, K. Krasnov and E. R. Livine, "Holomorphic factorization for a quantum tetrahedron", Commun. Math. Phys. **297** 45 (2010).

[45] E. Bianchi, E. Magliaro and C. Perini, "Coherent spin-networks", Phys. Rev. D **82** 024012 (2010).

[46] L. Freidel and E. R. Livine, "U(N) coherent states for loop quantum gravity", J. Math. Phys. **52** 052502 (2011).

[47] T. Thiemann, "Quantum spin dynamics (QSD) : VII. Symplectic structures and continuum lattice formulations of gauge field theories", Class. Quant. Grav. **18** 3293 (2001).

[48] L. Freidel and D. Louapre, "Diffeomorphisms and spin foam models", Nucl. Phys. B **662**, 279 (2003).

[49] J. Fuchs and C. Schweigert, *Symmetries, Lie algebras and representations: A graduate course for physicists*, Cambridge University Press, Cambridge (1997).

[50] V. I. Arnold, *Mathematical Methods of Classical Mechanics*, Springer, New York (1989).

[51] A. Y. Alekseev and A. Z. Malkin, "Symplectic structures associated to Lie-Poisson groups", Commun. Math. Phys. **162** 147 (1994).

[52] L. Freidel and S. Speziale, "Twisted geometries: A geometric parametrisation of SU(2) phase space", Phys. Rev. D **82** 084040 (2010).

[53] L. Freidel and E. R. Livine, "The Fine Structure of SU(2) Intertwiners from U(N) Representations", J. Math. Phys. **51**, 082502 (2010).

[54] L. Freidel and S. Speziale, "From twistors to twisted geometries", Phys. Rev. D **82**, 084041 (2010).

[55] S. Speziale and W. M. Wieland, "The twistorial structure of loop-gravity transition amplitudes", Phys. Rev. D **86**, 124023 (2012).

[56] H.M. Haggard, C. Rovelli, W. Wieland and F. Vidotto, "The spin connection of twisted geometry", `arXiv:1211.2166` (2012).

[57] L. Freidel and J. Hnybida, "A Discrete and Coherent Basis of Intertwiners", `arXiv:1305.3326 [math-ph]` (2013).

[58] B. Dittrich and J. P. Ryan, "Simplicity in simplicial phase space", Phys. Rev. D **82**, 064026 (2010); "On the role of the Barbero-Immirzi parameter in discrete quantum gravity", Class. Quant. Grav. **30**, 095015 (2013).

[59] E. Bianchi, "Loop quantum gravity à la Aharonov-Bohm", `arXiv:0907.4388 [gr-qc]` (2009).

[60] L. Freidel, M. Geiller and J. Ziprick, "Continuous formulation of the Loop Quantum Gravity phase space", Class. Quantum Grav. **30** 085013 (2013).

[61] J. Marsden and A. Weinstein, "Reduction of symplectic manifolds with symmetry", Reports on Math. Phys. **5** 121 (1974).

[62] J. Butterfield, "On symplectic reduction in classical mechanics", in *Philosophy of Physics* North Holland, Amsterdam (2006).

[63] A. Weinstein, "The local structure of Poisson manifolds", J. Differential Geom. **18**(3) 523 (1983).

[64] M. Atiyah and R. Bott, "The Yang-Mills equations over Riemann surfaces", Phil. Trans. R. Soc. Lond. A **308** 523 (1983).

[65] J. C. Baez and J. Huerta, "An invitation to higher gauge theory", `arXiv:gr-qc/1003.4485` (2010).

[66] V. Husain, "Topological quantum mechanics", Phys. Rev. D **43** 1803 (1991).

[67] H. Sahlmann and T. Thiemann, "On the superselection theory of the Weyl algebra for diffeomorphism invariant quantum gauge theories", `arXiv:gr-qc/0302090` (2003).

[68] W. Wieland, "Complex Ashtekar variables and reality conditions for Holst's action", `arXiv:1012.1738v1 [gr-qc]` (2010).

[69] A. Ashtekar, A. Corichi and J. A. Zapata, "Quantum theory of geometry III: Noncommutativity of Riemannian structures", Class. Quant. Grav. **15** 2955 (1998).

[70] A. Hatcher, *Algebraic topology*, Cambridge University Press, Cambridge (2002).

[71] A. Kirillov, Jr. "On piecewise linear cell decompositions", `arXiv:1009.4227` (2010).

[72] J. Lewandowski, A. Okolow, H. Sahlmann and T. Thiemann, "Uniqueness of diffeomorphism invariant states on holonomy-flux algebras", Commun. Math. Phys. **267** 703 (2006).

[73] B. Dittrich and J. P. Ryan, "Phase space descriptions for simplicial 4d geometries", Class. Quant. Grav. **28** 065006 (2011).

[74] N. Hitchin, "The self-duality equations on a Riemann surface", Proc. London Math. Soc. 53-55(1) 59 (1987).

[75] L. Freidel and J. Ziprick, "Spinning geometries = Twisted geometries", arXiv:1308.0040 (2013).

[76] H. Minkowski, "Allgemeine Lehrsatze uber die konvexe Polyeder", Nachr. Ges. Wiss., Gottingen 198 (1897).

[77] C. Rourke and B. Sanderson, *Introduction to piecewise-linear topology*, Springer, Berlin (1972).

[78] P. de Sousa Gerbert, "On spin and (quantum) gravity in (2+1)-dimensions", Nucl. Phys. B **346**, 440 (1990); L. Freidel and D. Louapre, "Ponzano-Regge model revisited I: Gauge fixing, observables and interacting spinning particles", Class. Quant. Grav. **21**, 5685 (2004); "Ponzano-Regge model revisited II: Equivalence with Chern-Simons", `arXiv:gr-qc/0410141` (2004); K. Noui and A. Perez, "Three-dimensional loop quantum gravity: Coupling to point particles", Class. Quant. Grav. **22**, 4489 (2005); C. Meusburger and T. Schonfeld, "Gauge fixing in (2+1)-gravity with vanishing cosmological constant", PoS CORFU **2011**, 051 (2011).

[79] R. Penrose, W. Rindler, *Spinors and Spacetime*, Cambridge University press, Cambridge (1984).

[80] P.-G. de Gennes, F. Brochard-Wyart and D. Quere, *Capillarity and Wetting Phenomena: Drops, Bubbles, Pearls, Waves*, Springer-Verlag, Berlin (2004).

[81] B. Dittrich and P. Höhn, "Constraint analysis for variational discrete systems", J. Math. Phys. **54** 093505 (2013); "Canonical simplicial gravity", Class. Quant. Grav. **29**, 115009 (2012).

[82] A. Staruszkiewicz, "Gravitation Theory in Three-Dimensional Space", Acta. Phys. Polon. **24**, 734 (1963).

[83] S. Deser, R. Jackiw and G. 't Hooft, "Three-Dimensional Einstein Gravity: Dynamics of Flat Space", Annals of Physics **152**, Issue 1, 220 (1984).

[84] G. 't Hooft, "Causality in (2 + 1)-dimensional gravity", Class. Quantum Grav. **9**, 1335 (1992); "The evolution of gravitating point particles in 2+1 dimensions", Class. Quantum Grav. **10**, 1023 (1993).

[85] H.J. Matschull, "The Phase Space Structure of Multi Particle Models in 2+1 Gravity", Class. Quant. Grav. **18**, 3497 (2001).

[86] Z. Kadar, "Polygon model from first order gravity", Class. Quant. Grav. **22**, 809 (2005).

[87] J. Ziprick, "Point particles in 2+1 dimensions: toward a semiclassical loop gravity formulation", Canadian Journal of Physics **91**(6), 467 (2013).

[88] H.J. Matschull and M. Welling, "Quantum Mechanics of a Point Particle in 2+1 Dimensional Gravity", Class. Quant. Grav. **15**, 2981 (1998).

[89] V. Husain and S. Major, "Gravity and BF theory defined in bounded regions", Nucl.Phys. B **500**, 381 (1997).

[90] A. Cappelli, "Classical Dynamics of Point Particles in 2+1 Gravity", Nucl. Phys. Proc. Suppl. A **25**, 54 (1992).

[91] A. Cappelli, M. Ciafaloni and P. Valtancoli, "Classical Scattering in 2+1 Gravity with N Point Sources", Nucl. Phys. B **369**, 669 (1992).

[92] A. Bellini, M. Ciafaloni, an P. Valtancoli, "Solving the N-body problem in (2+1) gravity", Nucl. Phys. B **462**, 453 (1996); Nucl. Phys. B **369** (1992) 669; "Non-Perturbative Particle Dynamics", Phys. Lett. B **357**, 532 (1995); "(2+1)-Gravity with Moving Particles in an Instantaneous Gauge", Nucl. Phys. B **454**, 449 (1995).

[93] G. 't Hooft, "Non-Perturbative 2 Particle Scattering Amplitudes in 2 + 1 Dimensional Quantum Gravity", Commun. Math. Phys. **117**, 685 (1988).

[94] S. Carlip, "Exact quantum scattering in 2+1 dimensional gravity", Nucl. Phys. B **324**, 106 (1989).

[95] E. Witten, "Quantum Field Theory and the Jones Polynomial", Commun. Math. Phys. **121**, 351 (1989).

[96] I.Y. Aref'eva, "Non-Abelian Stokes Formula", Theor. Math. Phys. **43**, 353 (1980).